WARSAW UNIVERSITY OF TECHNOLOGY

FIELD OF SCIENCE – NATURAL SCIENCES

DISCIPLINE OF SCIENCE – BIOTECHNOLOGY

PhD Thesis

Joanna Baran, MSc.

Opracowanie metody *in vitro* do oceny immunogenności komponentów szczepionek w profilaktyce chorób infekcyjnych

Development of an *in vitro* method to assess the immunogenicity of vaccine components in the prevention of infectious diseases

Supervisor

Monika Staniszewska, PhD, Associate professor

Additional supervisor

Małgorzata Milner-Krawczyk, PhD

WARSAW 2024

Acknowledgments

I would like to express my deep gratitude and appreciation for **PhD Monika Staniszewska**, **Prof. WUT**, for her unwavering support and invaluable insights throughout the entire journey of my doctoral research.

I am also deeply thankful to **PhD Małgorzata Milner-Krawczyk**, who instilled in me a passion for microbiology and without whose support I would not consider a PhD.

I extend my gratitude to my colleagues and fellow researchers in CEZAMAT and Faculty of Chemistry who have shared their knowledge and experiences, fostering an environment of collaborative learning. Special thanks to **PhD Anna Sobiepanek**, who guided me since the first degree studies and did not let me down to the end of my PhD.

Furthermore, I wish to acknowledge the support provided by my family and friends. Their encouragement, patience, and understanding have been a constant source of strength and motivation, enabling me to overcome challenges and persevere.

Last but not least, I am grateful to all of the students I was honored to meet and guide during their journey at Warsaw University of Technology.

Streszczenie Rozprawy Doktorskiej

Opracowanie szczepionek to kosztowny i czasochłonny proces, który oparty jest w pierwszej kolejności na serii badań przedklinicznych, ze szczególnym uwzględnieniem badań *in vivo*. W kolejnym etapie, poprzedzającym rejestrację szczepionek, są oceniane w szeregu jasno określonych badań klinicznych pozwalających na ocenę ich bezpieczeństwa, immunogenności i skuteczności. Wszystkie badania kliniczne podlegają międzynarodowym zasadom etycznym i miejscowym regulacjom prawnym. Układ immunologiczny człowieka obejmuje: narządy i naczynia limfatyczne, obecne w tych narządach i krążące komórki uczestniczące w reakcjach immunologicznych oraz wydzielane przez nie przeciwciała, cytokiny i inne czynniki. Najważniejszą funkcją układu odpornościowego jest obrona przed mikroorganizmami. Badania przedkliniczne są istotnym etapem rozwoju każdego leku. Jednak wykorzystywane obecnie modele przedkliniczne *in vitro* oraz *in vivo* są modelami suboptymalnymi i nie odzwierciedlają w pełni złożoności ludzkiego układu odpornościowego, fizjologii i anatomii. Dlatego też prace nad opracowaniem nowych, bardziej reprezentacyjnych systemów umożliwiających ocenę bezpieczeństwa, efektywności i immunogenności testowanych szczepionek są wysoce pożądane.

Istnieje wiele powodów nakazujących skupić się na rozwoju modeli alternatywnych, takich jak eksplantaty tkanek, modele *in silico*, oraz kultury komórkowe. W tym przypadku trudnością jest jednak odwzorowanie złożoności oddziaływań międzykomórkowych, które zachodzą w miejscu infekcji lub szczepienia *in vivo*. Opracowanie kompleksowych modeli, zawierających różnorodne linie komórkowe ludzkie oraz innego pochodzenia, ale dobrze naśladujące ludzkie tkanki, jest ważnym kierunkiem w rozwoju badań nad odpowiedzią immunologiczną człowieka. Modele alternatywne pozwolą znacznie wzbogacić badania przesiewowe oraz ewaluację szczepionek w zakresie mechanizmu działania oraz bezpieczeństwa, przynosząc dodatkową korzyść w postaci potencjalnej redukcji ilości niezbędnych badań *in vivo* oraz badań klinicznych.

Niniejsza rozprawa przedstawia serię badań przedklinicznych skupiających się nad opracowaniem metody *in vitro* do oceny immunogenności komponentów szczepionek w profilaktyce chorób infekcyjnych. W obliczu pandemii COVID-19, moje wysiłki skoncentrowały się na opracowaniu modelu komórkowego 3D i jego ewaluacji wobec antygenów wirusa SARS-CoV-2. Głównym celem rozprawy było opracowanie strategii badawczej umożliwiającej ocenę odpowiedzi immunologicznej *ex vivo* oraz badanie bezpieczeństwa biologicznego *in vivo*. Opracowano procedurę izolacji, krioprezerwacji oraz

hodowli ludzkich komórek krwi obwodowej (PBMC, ang. *peripheral blood mononuclear cell*). PBMC pochodzą z ludzkich kożuchów leukocytarnych i zawierają różne typy komórek odpornościowych, w tym limfocyty T, limfocyty B, komórki NK (ang. *Natural Killer* – „urodzeni" zabójcy), monocyty i komórki dendrytyczne. Skład ten ściśle odzwierciedla różnorodność komórkową ludzkiego układu odpornościowego. Do opracowania modeli 2D oraz 3D użyto komórek linii Calu-3, które wykazują fenotyp zbliżony do komórek nabłonka oskrzeli dróg oddechowych. Calu-3 są zdolne do wydzielania śluzu, natomiast w warunkach ALI (ang. *air-liquid,* hodowla powietrze-ciecz) wytwarzają strukturę rzęsek imitującą nabłonek układu oddechowego. W celu wywołania efektu immunologicznego w proponowanych modelach zastosowano spektrum antygenów SARS-CoV-2, zarówno produkcji biotechnologicznej (rRBD, *recombinant receptor binding protein*), jak i komercyjnie dostępnych (Spike-S1-His i Nucleocapsid-His; InvivoGen). We współpracy z badaczami, którzy wcześniej zaprojektowali niereplikujące w zdrowych tkankach adenowirusy, w badaniach zastosowano dwa rodzaje adiuwantów. Wektor wirusowy oparty na serotypie ludzkiego adenowirusa 5, charakteryzujący się wysoką immunogennością AdV-D24-ICOSL-CD40L uzbrojony w indukowalny ko-stymulator (ICOSL) i ligand CD40 (CD40L) oraz wektor pozbawiony tych transgenów AdV5/3 służący jako adiuwant ze względu na skuteczną początkową interakcję z komórką prezentującą antygen (APC). Takie podejście zapewniło indukcję kaskady odpornościowej prowadzącej do rekrutacji komórek prezentujących antygen i rozwoju komórkowej i humoralnej odpowiedzi immunologicznej (przeciwko adiuwantowi i prezentowanym antygenom). W ramach serii kompleksowo przeprowadzonych badań oceniono oraz określono ilościowo cechy świadczące o apoptozie i zmianach w integralności błony komórkowej ludzkich komórek (test MTS, cytometria przepływowa). Analizowano mechanizmy na poziomie, których adenowirusy działają jako adiuwanty. Oceniono odpowiedź komórkową i humoralną poprzez immunofenotypowanie limfocytów CD4^{+}, CD8^{+} i CD19^{+} oraz profilowanie cytokin „*Cytometric Bead Array"*. Dzięki połączeniu antygenów i adiuwantów scharakteryzowano ścieżki prowadzące do wykształcenia odpowiedzi immunologicznej zawierające limfocyty T_{CM} (ang. *Central Memory*), T_{EM} (ang. *Effective Memory*), CD45RA T_{EMRA}(ang. *terminally differentiated effector memory cells re-expressing CD45RA*). Sprawdzono również jak zmienia się dystrybucja subpopulacji limfocytów B specyficznych dla antygenu. Analiza została wzbogacona przez badanie wpływu czynników immunogennych na ekspresję genu *CD40* (RT-qPCR), a następnie pogłębiona przez analizę danych transkryptomicznych pochodzących z komórek Calu-3 oraz PBMC (RNA-Seq).

Badania zwieńczyła analiza bezpieczeństwa biologicznego proponowanej platformy szczepionkowej przeprowadzona z udziałem myszy Balb/c w toku 30-dniowej ekspozycji.

W badaniach będących przedmiotem niniejszej pracy zaobserwowano, że stopień oczyszczenia oraz forma antygenu stosowanego do immunizacji komórek jest kluczowa dla prawidłowego przebiegu doświadczeń. Zastosowanie rRBD (z/bez adiuwantu) spowodowało toksyczny efekt wobec komórek VERO E6 oraz PBMC. Analiza z użyciem mikroskopu konfokalnego wykazała natomiast, że proponowana platforma bazująca na rRBD oraz AdV-D24-ICOSL-CD40L (AdV1) ogranicza internalizację pseudo-SARS-CoV-2 do komórek VERO E6. Dowiedziono, że zastosowanie AdV1 w połączeniu z antygenami SARS-CoV-2 może przyczyniać się do reorganizacji cytoszkieletu komórkowego, co wpływa na internalizację wirusa do komórki. Po zastosowaniu platformy o zoptymalizowanym składzie (komercyjne białka), po 24 godzinach zaobserwowano istotny wzrost w procentowej ilości subpopulacji limfocytów CD4$^+$ T$_{CM}$, CD4$^+$ T$_{EMRA}$ oraz CD4$^+$ T$_{EM}$, które są zaangażowane w wytworzenie pamięci komórkowej. Wydłużenie czasu ekspozycji do 7 dni indukowało istotny wzrost ilości limfocytów CD4$^+$ T oraz CD19$^+$B w badanych próbkach. Analiza RNA-Seq komórek PBMC w modelu 3D dowiodła nadeskpresji genów (m.in. FGFR4) powiązanych ze ścieżką Rap1 w komórkach poddanych działaniu platformy AdV1+S-His+N-His. Ponadto wykazano wpływ proponowanej platformy na różnicowanie limfocytów oraz na produkcję cytokin: IL-10, IL-12p70 oraz IL-8. Komórki poddane działaniu adiuwantu (AdV1) wykazały podwyższony poziom IFN-γ. Platforma szczepionkowa nie wpływa negatywnie na przeżywalność oraz morfologię narządów wewnętrznych myszy podczas 30-dniowej ekspozycji.

W badaniach zawartych w niniejszej rozprawie zidentyfikowano i podkreślono ograniczenia istniejących modeli *in vitro* i *in vivo* w zakresie pełnego oddania złożoności ludzkiego układu odpornościowego. Ustanowiony trójwymiarowy model *in vitro* z wykorzystaniem komórek krwi obwodowej i Calu-3 dostarczył nowych informacji na temat dynamiki odpowiedzi immunologicznej na wirusy oraz nowe platformy szczepionkowe oparte na adenowirusowych wektorach. Udowodniono, że AdV1 i AdV2 działają jako adiuwanty, wpływając na subpopulacje CD4$^+$, CD8$^+$ oraz CD19$^+$. Kluczowa rola ścieżki ICOS/ICOSL, dobrze znana i szeroko opisana w literaturze w środowisku *in vivo*, występuje również w modelu *in vitro*, co zaobserowano poprzez aktywację i różnicowanie limfocytów T. Stymulacja komórek PBMC za pomocą platformy szczepionkowej wykazała istotny wpływ na komórki CD4$^+$ i CD8$^+$, wpływając na limfocyty T$_{CM}$ (ang. *Central Memory*), T$_{EM}$ (ang. *Effective*

Memory), CD45RA T$_{EMRA}$ (ang. *terminally differentiated effector memory cells re-expressing CD45RA*). Wykazano potencjał platformy w stymulowaniu proliferacji i różnicowania limfocytów B, ze szczególnym uwzględnieniem komórek B specyficznych dla antygenu wpływających na produkcję cytokin. Wykazano, że wyposażenie adenowirusów w ligandy ko-stymulujące CD40L i ICOSL ma wysoki potencjał immunostymulacyjny. Potwierdzono również wstępnie bezpieczeństwo biologiczne platformy w badaniach *in vivo*. Badanie szlaku CD40 ujawniło jego znaczący wpływ na populacje komórek odpornościowych, co sugeruje potencjalne możliwości terapeutyczne i kierunek dla dalszych badań. Odkrycia poczynione w niniejszej rozprawie podkreślają znaczenie wydłużonego czasu hodowli i potrzebę dalszych badań nad mechanistyczną rolą szlaku CD40.

Opracowana metoda wpisuje się w nowatorski kierunek rozwoju badań przedklinicznych umożliwiający szybką analizę właściwości immunogennych i bezpieczeństwo środków prewencyjnych, na przykład szczepionek.

Słowa kluczowe: immunologia, SARS-CoV-2, szczepionki, Calu-3, model 3D, *ex vivo*, *in vivo*, limfocyty, cytokiny, immunogenność

Abstract

Vaccine development is an expensive and time-consuming process, rooted in a series of preclinical studies, with a particular emphasis on *in vivo* research. Prior to registration, vaccines undergo a series of well-defined preclinical studies to assess their safety, immunogenicity, and efficacy. All the studies adhere to international ethical principles and local legal regulations. The human immune system is a complex network of specialized cells, proteins, tissues, and organs responsible for the body's immune defense against harmful substances and pathogens that may cause infections.

Preclinical studies constitute a crucial stage in the development of any drug. Both *in vitro* and *in vivo* preclinical models are suboptimal and do not fully reflect the complexity of the human immune system, physiology, and anatomy. Therefore, efforts to develop new, more representative systems for evaluating the safety, efficacy, and immunogenicity of tested vaccines are highly desirable.

There are several reasons prompting a focus on the development of alternative models, such as tissue explants, *in silico* models, and cell cultures. However, the challenge lies in replicating the complexity of intercellular interactions occurring at the site of infection or *in vivo* vaccination. Developing comprehensive models, incorporating diverse human cell lines that closely mimic human tissues, represents a crucial direction in researching the human immune response. Alternative models will significantly enrich screening studies and vaccine evaluation concerning mechanism of action and safety, potentially reducing the need for *in vivo* and clinical studies.

This dissertation presents a series of preclinical studies focusing on the development of an *in vitro* method for assessing the immunogenicity of vaccine components in the prevention of infectious diseases. In response to the COVID-19 pandemic, my efforts concentrated on developing a 3D cellular model and its evaluation. The main objective was to devise a research strategy enabling the assessment of *ex vivo* immune responses and the investigation of *in vivo* biological safety. A procedure for isolating, cryopreserving, and culturing human peripheral blood mononuclear cells (PBMC) was developed. PBMCs, derived from human leukocyte buffy coats, containing various immune cell types, including T lymphocytes, B lymphocytes, natural killer (NK) cells, monocytes, and dendritic cells, closely mirror the cellular diversity of the human immune system. Calu-3 cell line, exhibiting a phenotype similar to bronchial epithelial cells, was used to develop 2D and 3D models. Calu-3 cells can secrete mucus and,

under air-liquid interface (ALI) conditions, form a ciliated structure mimicking the respiratory epithelium.

To induce an immunological effect in the proposed models, a spectrum of SARS-CoV-2 antigens, both biotechnologically produced (recombinant receptor binding protein - rRBD) and commercially available (Spike-S1-His and Nucleocapsid-His; InvivoGen), was applied. Collaboration with researchers who previously designed non-replicating adenoviruses in healthy tissues led to the use of two types of adjuvants. A human adenovirus 5 serotype-based viral vector, demonstrating high immunogenicity (AdV-D24-ICOSL-CD40L), armed with inducible co-stimulator (ICOSL) and CD40 ligand (CD40L), and a vector lacking these transgenes (AdV5/3) served as an adjuvant due to its effective initial interaction with antigen-presenting cells (APC). This approach ensured the induction of an immune response cascade, leading to the recruitment of antigen-presenting cells and the development of cellular and humoral immune responses (against the vector and presented antigens). A series of comprehensive studies assessed and quantified features indicative of apoptosis and changes in the cell membrane integrity of human cells (MTS assay, flow cytometry). Mechanisms at the level of which adenoviruses act as adjuvants were analyzed. Cellular and humoral responses were assessed by immunophenotyping $CD4^+$, $CD8^+$, and $CD19^+$ lymphocytes, as well as cytokine profiling using Cytometric Bead Array. By combining antigens and adjuvants, pathways leading to the development of an immune response involving central memory (T_{CM}), effective memory (T_{EM}), CD45RA T_{EMRA} (terminally differentiated effector memory cells re-expressing CD45RA) T lymphocytes were characterized. Changes in the distribution of antigen-specific B lymphocyte subpopulations were also examined. The analysis was enriched by studying the impact of immunogenic factors on the expression of the *CD40* gene (RT-qPCR), followed by an in-depth analysis of gene expression data in the RNA sequence of Calu-3 and PBMC (RNA-Seq). The studies were concluded with an analysis of the biological safety of the proposed vaccine platform conducted in mice over a 30-day exposure period.

Throughout the research, it was observed that the degree of purification and the form of the antigen used for cell immunization are crucial for the course of experiments. The application of rRBD (with/without adjuvant) resulted in a toxic effect on VERO E6 and PBMC. Moreover, excessive immunogenicity was also evident. Confocal microscopy analysis showed that the proposed platform based on rRBD and AdV-D24-ICOSL-CD40L (AdV1) limited the internalization of pseudo-SARS-CoV-2 into VERO E6 cells. It was demonstrated that the use of AdV1 in combination with SARS-CoV-2 antigens could contribute to the reorganization of

the cellular cytoskeleton, affecting virus internalization. Upon application of the optimized composition platform (commercial proteins), a significant increase in the percentage of $CD4^+$ T_{CM}, $CD4^+$ T_{EMRA}, and $CD4^+$ T_{EM} lymphocyte subpopulations involved in memory cell generation was observed after 24 hours. Prolonging the exposure time to 7 days induced a significant increase in the number of $CD4^+$ T and $CD19^+$ B lymphocytes in the tested samples. RNA-Seq analysis of PBMC cells in the 3D model demonstrated gene overexpression (including FGFR4) associated with the Rap1 pathway in the sample exposed to AdV1+S-His+N-His. The proposed platform's impact on lymphocyte differentiation was confirmed, and cytokine profile analysis in this sample revealed elevated levels of IL-10, IL-12p70, and IL-8. All samples exposed to AdV1 showed increased levels of IFN-γ. Safety studies of the vaccine platform demonstrated that a 30-day exposure did not impact the survival or organ morphology of mice.

The research resulted in the development of a method providing a reliable assessment of immunogenic factors under *in vitro* conditions using Calu-3 lung epithelial cells. It was proven that AdV1 and AdV2 act as adjuvants impacting $CD4^+$, $CD8^+$, and $CD19^+$ subpopulations. The crucial role of ICOS/ICOSL pathway well known and reported *in vivo* occurred also in *in vitro* model, due to T cell activation and differentiation. The stimulation of PBMCs with the vaccine platform has lasting effects on $CD4^+$ and $CD8^+$ T cells, affecting central memory, effector memory, and T_{EMRA} cells. The platform shows also potential in stimulating B cells development and differentiation, with the focus on antigen-specific B cells. Adenovirus-based platform influence the production of cytokines influencing effector cytotoxic T cells or B cells. It has been shown that equipping adenoviruses with CD40L and ICOSL co-stimulating ligands has a high immunostimulatory potential with initially confirmed safety and biodistribution in *in vivo* studies. Notably, the exploration of the CD40 pathway reveals its significant impact on immune cell populations, suggesting potential therapeutic avenues.

The developed method aligns with a promising direction in preclinical research, allowing for a rapid analysis of the immunogenic properties and safety of preventive measures, such as vaccines. The study identifies critical factors influencing immune reactions, including inflammation, immune cell activation, and regulatory responses, providing insights into the virus-host dynamics.

Keywords: immunology, SARS-CoV-2, vaccines, Calu-3, 3D model, ex vivo, in vivo, lymphocytes, cytokines, immunogenicity

Spis treści

Scientific achievements related to the PhD dissertation

- **Patent pending:**
  - [WIPO ST 10/C PL442478] „Vaccine composition for use in the prevention of infectious diseases" („Kompozycja szczepionki do zastosowania w profilaktyce chorób zakaźnych")

- **Research articles:**
  - **Baran, J.**, et al., (2024) Induction of an immune response by a formulation based on non-replicating adenoviruses versus a commercial pseudo-SARS-CoV-2, BioTechnologia, BTa JBCBB, accepted to be published in 3/2024 issue.
  - **Baran, J.**, et al., (2023) In vitro Immune Evaluation of Adenoviral Vector-Based Platform for Infectious Diseases. BioTechnologia, BTa JBCBB, 104(4), 403-419.
  - **Baran, J.**, et al., (2024) Development of an in vitro method to assess the immunogenicity of biologics in the prevention of infectious diseases. Immunologic Research, SPRINGER NATURE, Submission ID 28aa96b4-c9bc-4867-8db9-f9768f33841e (under revision).

- **Review articles:**
  - **Baran, J**., et al. (2023) Practical applications of peripheral blood mononuclear cells (PBMCs) in immunotherapy preclinical research. Journal of Current Science and Technology, 12(3), 1-10.

- **Conferences:**
  - **Baran, J.,** Musolf, P., Sobiepanek, A., Staniszewska, M., (2021). The role of mast cells in severe COVID-19 disease, Druga Edycja Wirtualnej Konferencji Naukowej Kampusu Ochota

Different scientific achievements in the discipline "biotechnology"

- **Research articles:**
  - Staniszewska, M., Kuryk, Ł., Gryciuk, A., Kawalec, J., Rogalska, M., **Baran, J.,** & Kowalkowska, A. (2021). The Antifungal Action Mode of N-Phenacyldibromobenzimidazoles. Molecules, 26, 1–20.
  - Staniszewska, M., Kuryk, Ł., Gryciuk, A., Kawalec, J., Rogalska, M., **Baran, J.,** Łukowska-Chojnacka, E., & Kowalkowska, A. (2021). In Vitro Anti-Candida Activity and Action Mode of Benzoxazole Derivatives. Molecules, 26, 1–19.

- Gizińska, M., Staniszewska, A., Kazek, M., Koronkiewicz, M., Kuryk, Ł., Milner-Krawczyk, M., **Baran, J.,** Borowiecki, P., & Staniszewska, M. (2020). Antifungal polybrominated proxyphylline derivative induces Candida albicans calcineurin stress response in Galleria mellonella. Bioorganic & Medicinal Chemistry Letters, 30, 127545.
- Sobiepanek, A., **Baran, J.,** Milner-Krawczyk, M., & Kobiela, T. (2020). Different Types of Surface Modification used for Improving the Adhesion and Interactions of Skin Cells. Open Access Journal of Biomedical Science, 2, 275–278.

- **Patent pending:**
  - [WIPO ST 10/C PL442234] „Method of testing the adhesion of pathogenic fungal cells to the surface of abiotic materials and its application in the study of potential adhesion inhibitors." („Sposób badania adhezji komórek grzybów patogennych do powierzchni materiałów abiotycznych oraz jego zastosowanie w badaniu potencjalnych inhibitorów adhezji.")

- **Review articles:**
  - Musolf, P., **Baran, J.,** Ścieżyńska, A., Staniszewska, M., & Sobiepanek, A. (2021). Rola mastocytów w nadzorze odpornościowym procesów fizjologicznych i patologicznych skóry. W K. Piech (red.), Zagadnienia aktualnie poruszane przez młodych naukowców (T. 19, s. 78–83). Creativetime.
  - Sobiepanek, A., Kuryk, Ł., Garofalo, M., Kumar, S., **Baran, J.**, Musolf, P., Siebenhaar, F., et al. (2022). The Multifaceted Roles of Mast Cells in Immune Homeostasis, Infections and Cancers. International Journal of Molecular Sciences, 23(4), 2249.
  - **Baran, J.**, et al. (2023). Mast cells as a target – a comprehensive review of recent therapeutic approaches. Cells. 2023; 12(8):1187.
  - Gryciuk, A., Rogalska, M., **Baran, J.**, Kuryk, L., & Staniszewska, M. (2023). Oncolytic Adenoviruses Armed with Co-Stimulatory Molecules for Cancer Treatment. Cancers, 15, 1–24.
  - Mazurkiewicz-Pisarek, A., **Baran, J.**, & Ciach, T. (2023). Antimicrobial Peptides: Challenging Journey to the Pharmaceutical, Biomedical, and Cosmeceutical Use. International Journal of Molecular Sciences, 24, 1–32.

- **Awards:**
  - MedTech-Athon award winner "Engineers for medicine" for the project of VIRITEST (*Lassa virus* biodegradable antigen test), Team leader of Scienceporium - 30 000 PLN for the project realization,
  - DemoDay winner for the presentation of the demonstrator of VIRITEST (*Lassa virus* biodegradable antigen test), Team leader of Scienceporium – 200 000 PLN for the project development.

List of abbreviations

ATF	Activating Transcription Factor
APCs	Antigen-Presenting Cells
B cells	B lymphocytes
CD (eg. CD4$^+$)	Cluster of Differentiation
COVID-19	Coronavirus Disease 2019
CoV	Coronavirus
DCs	Dendritic Cells
EBV	Epstein-Barr virus
EMA	European Medicine Agency
EMEM	Eagle's Minimum Essential Medium
HIV	Human Immunodeficiency Virus
hCoV-OC43	Human betacoronavirus OC43
IFN	Interferon
IFN-I	Type I Interferon
IL	Interleukin
INFγ	Interferon-gamma
IRF	Interferon Regulatory Factor
IIMCB	International Institute of Molecular and Cell Biology in Warsaw
JAK	Janus Kinases
MBL	Mannose-binding Lectin
MCs	Mast Cells
MEM	Minimum Essential Medium
MIX1	MIXture of AdV1, pseudo-SARS-CoV-2 and spike protein

MIX2	MIXture of AdV2, pseudo-SARS-CoV-2 and spike protein
NIPH-NIH	National Institute of Public Health-National Institute of Hygiene
NK cells	Natural Killer cells
PAMPs	Pathogen-Associated Molecular Patterns
PBMC	Peripheral Blood Mononuclear Cells
PRR	Pattern Recognition Receptors
RNA	Ribonucleic Acid
RSV	Respiratory Syncytial Virus
SARS-CoV-2	Severe Acute Respiratory Syndrome Coronavirus 2
SEM	Scanning Electron Microscope
STAT	Signal Transducers and Activators of Transcription
T_{CM}	Central Memory T cells
T_{EM}	Effector Memory T cells
T_{EMRA}	Terminally Differentiated Effector Memory Cells Re-expressing CD45RA
Tfh cells	T Follicular Helper cells
Th1 cells	T helper 1 cells
TLRs	Toll-like receptors
Tnaïve	Naïve T cells
TNFα	Tumor Necrosis Factor-alpha
Treg cells	Regulatory T cells
T_{SCM}	Stem Cell Memory T cells

1. Introduction

The pursuit of effective vaccines against emerging pathogens stands as an imperative endeavor in the realm of global health. In response to the SARS-CoV-2 pandemic, a challenge occurred to produce innovative approaches to decipher the intricacies of pathogenesis and immunoprophylaxis. This dissertation investigate the terrain of non-clinical vaccine assessment, a pivotal nexus where *in vitro* and *ex vivo* studies converge to unravel the complex dynamics of immune responses. When the new viruses like SARS-CoV-2 appear in the environment, fast and effective therapeutic approaches are crucial to limit the spread and limit the implications of it. In this study the focus was directed towards non-replicating adenoviruses and surface antigens of COVID-19. Grounded in the urgent context described, it delves into the complex field of non-clinical vaccine assessment. At the epicenter of investigation lies the *ex vivo* model, a platform offering insights into the dynamics of human immune responses.

1.1. Immune response to viruses

The human body fights viral infections through a complex immune response involving innate and adaptive immunity. The immune response depends on the virus type, as different viruses affect the body in different ways. Many viruses have properties that allow them to inhibit the activity and response of the host's immune system. Viruses such as HIV (human immunodeficiency virus) and various herpes viruses can directly destroy tissues. Weak symptoms of those infections in a long period of time (chronic infection) can lead to serious damage.

In the case of respiratory infections, such as influenza virus, coronaviruses, or respiratory syncytial virus (RSV), the picture of the disease depends on the host's condition, ranging from mild symptoms to severe cases, including fatal death. Viral infection can even lead to the development of cancer or autoimmune diseases, such as Epstein-Barr virus (EBV), which is associated with several types of cancer (e.g. Burkitt's lymphoma) and has been linked to some autoimmune diseases (e.g. multiple sclerosis) (Śliwa-Dominiak et al., 2014).

The innate immune response is the first line of host defence against pathogens. Many cells contribute to innate immunity by producing type I interferon and other cytokines. Upon infection, innate immune cells such as dendritic cells and macrophages recognize viral pathogens and activate the appropriate immune response. These cells carry Pattern Recognition Receptors (PRR), which include toll-like receptors (TLRs) that respond to PAMPs (Pathogen-Associated Molecular Patterns) (Saito and Gale, 2007). In the case of viruses, PAMPs are often

ss- and dsRNA, usually found in the viral genome and differ from normal cellular RNAs found in the human body. After recognizing PAMP, cells set off biochemical cascades that lead to further activation. Phagocytosis and cytokines secretion is activated, which induces an inflammation state. One of the critical cells in neutralizing the viral infection are natural killer cells (NK), which can recognize and kill virus-infected cells, limiting viral replication and spread. Oppose to cellular factors, an important role is held by soluble factors, such as interferons, complement proteins, and cytokines, play a critical role in defending against viral infections (Thompson et al., 2011).

Interferons are signaling molecules released by infected cells, triggering an antiviral response in neighboring cells. They are classified into three types: type I (IFN-α and INF-β), type II (IFN-γ), and type III (IFN-λ) (Sen, 2001). The context of host-virus infection in the case of the IFN system is very complex (**Figure 1**). The main trigger of the production of IFNs is dsRNA, as it can signal to the promoter of type I IFNs' genes through activating the transcription factors, such as IRF, NF-κB, and ATF. This leads to the secretion of IFN into the environment and binding it to cell surface receptors. The binding can lead to activating the JAK/STAT signaling pathway, which is crucial for the immune response. Activated Janus kinases (JAKs) phosphorylate and activate signal transducers and activators of transcription (STAT) proteins that are translocated to the nucleus. STATs can induce the transcription of interferon-stimulated genes that can directly inhibit viral replication. Some viruses, for example, hepatitis C virus, evolved strategies evading the JAK/STAT pathway, e.g. by inhibiting the phosphorylation and activation of STATs. Understanding the interplay between viruses and the JAK/STAT pathway is important for developing new antiviral drugs. The pathway inhibitors, such as Ruxolitinib, Baricitinib, and Tofacitinib were tested in clinical trials as antiviral drugs. Starker et al., (2021) implicated that they could also be used in COVID-19 therapy.
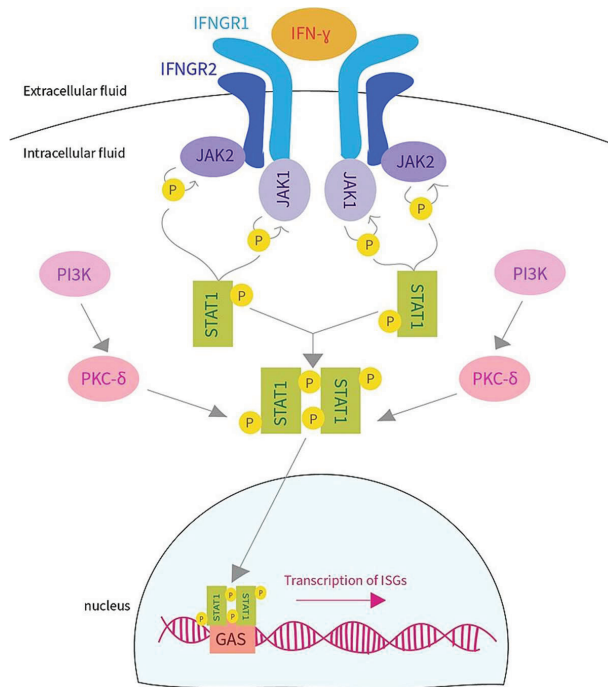
Figure 1 JAK/STAT (Janus Kinase Signal Transducer and Activator of Transcription) interferon pathway. GAS - gamma interferon activation site, PI3K - phosphatidylinositol 3-kinase, PKC-δ - protein kinase C-δ, ISGs - interferon-γ stimulated genes, IFNGR - IFN-gamma receptor. From Wikimedia Commons, the free media repository.

Type I interferons play a critical role in linking innate and adaptive immunity. For example, IFN-I promotes the maturation and activation of dendritic cells (DCs), which is critical for the induction of adaptive immune responses (Le Bon and Tough, 2002). Type I interferon enhance the proliferation and survival of activated T cells and can promote the differentiation of CD4^{+} T cells into T helper 1 cells (Th1). Th1 cells produce cytokines that activate macrophages and enhance their ability to fight pathogens. Type I interferon also play an important role in the development of B cells and their antibody responses. They can enhance the survival and proliferation of B lymphocytes, which can result in a more robust immune response. What is more, interferon I can stimulate the differentiation of B cells to the form of antibody-producing plasma cells.

Part of the innate immune response is the complement system, which helps in killing and controlling invading pathogens (Mellors et al., 2020). Complement proteins can directly or indirectly destroy viruses, e.g. by activating other immune cells. This system can be activated through three pathways:

1. the classical pathway - activated by the binding of antibodies to the surface of pathogens,
2. the alternative pathway – activated by the recognition of PAMPs,
3. the lectin pathway – activated by the binding of MBL (mannose-binging lectin to carbohydrates on the surface of pathogens.

Activation of the complement system leads to the destruction of pathogens through several mechanisms, such as opsonization, chemotaxis, and formation of membrane attach complexes. Opsonization is the coating of the virus particles' surface with opsonins, which promotes phagocytosis of the immune cells. The complement system can also induce the inflammatory response attracting immune cells to the site of the infection, which enhances the effectivity of the virus elimination. The proteins of the complement system can also directly neutralize viral particles by binding to them, which prevents infecting the cells. Some viruses learned to evade the complement immune system by hijacking the regulatory proteins of mimicking host cells (poxviruses) (Agrawal et al., 2017).

SARS-CoV-2 can activate the complement system in an excessive manner, which leads to tissue damage and inflammation (Mellors et al., 2020). It was shown that COVID-19 patients very often have elevated levels of complement proteins, which suggests a potential role of the system in the pathogenesis of the disease. Blocking complement system in animal studies resulted in the reduction of lung injury and improvement of the survivals in the COVID-19 models. Several complement inhibitors, such as eculizumab and ravulizumab, were mentioned as potential treatments for SARS-CoV-2 infection; however, more research is needed to determine their safety and efficacy. Despite the limited data available, targeting the complement system seems to be a promising therapeutic path in the treatment of COVID-19.

Adaptive immunity is highly specialized and much more complex than innate immunity. It is characterized by specificity, memory and ability to distinguish self from non-self, and is mediated by a complex network of cells and molecules. The key research technique in this doctoral thesis is cell immunophenotyping using flow cytometry. Therefore, it is crucial to precisely define their role (Burrell et al., 2017). T lymphocytes are involved in cell-mediated immunity and play a pivotal role in the immune response to viral infections. There are two main types of T cells: CD4$^+$ T cells and CD8$^+$ T cells (**Figure 2**).
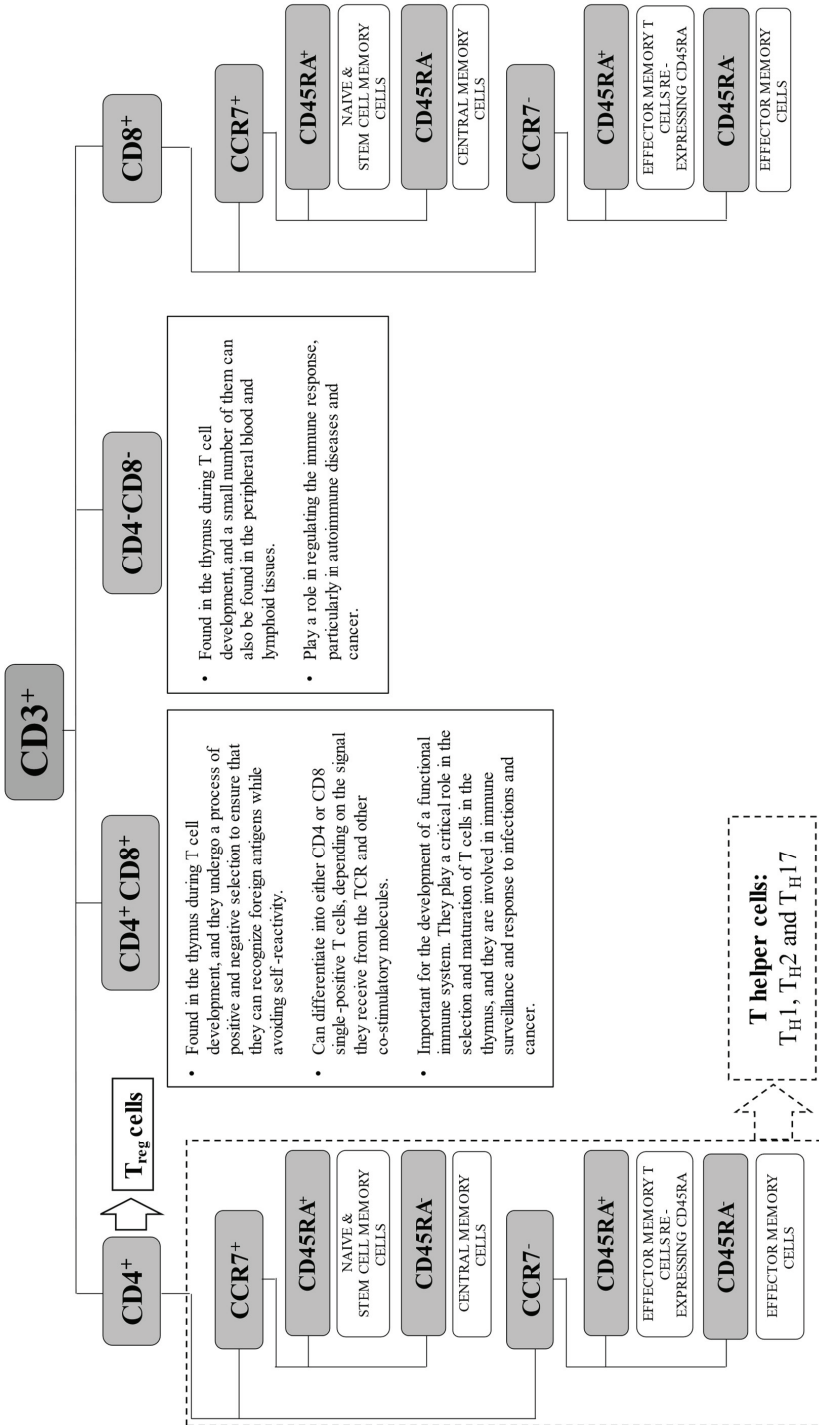
CD3$^+$

CD4$^+$

T$_{reg}$ cells

- CCR7$^+$
  - CD45RA$^+$ — NAIVE & STEM CELL MEMORY CELLS
  - CD45RA$^-$ — CENTRAL MEMORY CELLS
- CCR7$^-$
  - CD45RA$^+$ — EFFECTOR MEMORY T CELLS RE-EXPRESSING CD45RA
  - CD45RA$^-$ — EFFECTOR MEMORY CELLS

T helper cells: T$_H$1, T$_H$2 and T$_H$17

CD4$^+$ CD8$^+$

- Found in the thymus during T cell development, and they undergo a process of positive and negative selection to ensure that they can recognize foreign antigens while avoiding self-reactivity.
- Can differentiate into either CD4 or CD8 single-positive T cells, depending on the signal they receive from the TCR and other co-stimulatory molecules.
- Important for the development of a functional immune system. They play a critical role in the selection and maturation of T cells in the thymus, and they are involved in immune surveillance and response to infections and cancer.

CD4$^-$CD8$^-$

- Found in the thymus during T cell development, and a small number of them can also be found in the peripheral blood and lymphoid tissues.
- Play a role in regulating the immune response, particularly in autoimmune diseases and cancer.

CD8$^+$

- CCR7$^+$
  - CD45RA$^+$ — NAIVE & STEM CELL MEMORY CELLS
  - CD45RA$^-$ — CENTRAL MEMORY CELLS
- CCR7$^-$
  - CD45RA$^+$ — EFFECTOR MEMORY T CELLS RE-EXPRESSING CD45RA
  - CD45RA$^-$ — EFFECTOR MEMORY CELLS

Figure 2 Schematic representation of CD3+ subsets with their main clusters of differentiation (CDs). CCR stands for Chemokine Receptor CCR, CD45RA stands for Cluster of Differentiation 45 Receptor Antigen, Treg stands for regulatory T cells.

CD4^{+} T lymphocytes are known as helper T cells. They coordinate the immune response by recognizing viral antigens presented by antigen-presenting cells (APCs) and activating other immune cells, such as B cells and CD8^{+} T cells. Their "helper" function is fulfilled by secreting the cytokines. Activation of CD4^{+} T cells happens when their T cells receptor (TCR) recognizes an antigen presented by APC, along with the major histocompatibility complex class II (MHC-II) molecule. This triggers proliferation and differentiation into the effector cells (Bacchetta, 2016; Sant and McMichael, 2012).

Th1 cells produce INFγ and TNFα, both critical in the control of viral infections. IFNγ promotes macrophage activation and CD8^{+} T cells differentiation into cytotoxic T lymphocytes (CTLs). It can also promote apoptosis of the infected cells. TNFα is another pro-inflammatory cytokine with a wide range of functions. It is crucial in activating immune cells, inducing fever, and promoting the recruitment of immune cells to the sites of infection (Burrell et al., 2017; Linterman and Vinuesa, 2010).

Th2 cells produce IL-4, IL-5, IL-9, IL-13, key interleukins in activating mast cells (MCs), and CD19^{+} B cells. Most data show a strong connection between Th2 cells and parasitic infections. Although they are not as crucial as Th1 cells in the defence against viral infections, they still play a role in the immune response, especially to viruses such as respiratory syncytial virus (RSV) and some influenza virus strains. Vaccines that induce strong Th2 response, for example, due to the use of adjuvants, can lead to substantial and durable antibody response (Burrell et al., 2017; Linterman and Vinuesa, 2010).

Th17 cells are crucial for inflammation and host defence against pathogens. These cells produce IL-17 and IL-22 that activate and recruit neutrophils to the site of infection. Neutrophils can do phagocytosis, which is crucial in clearing pathogens (Burrell et al., 2017; Linterman and Vinuesa, 2010).

Tfh cells are crucial in generating high-affinity antibody responses during viral infection. Tfh cells produce IL-4 and IL-21, essential for plasma cells. B cells present viral antigens to Tfh cells that in turn produce cytokines stimulating B cell proliferation and differentiation into plasma cells producing antibodies. Tfh cells express CXCR5, a unique biomarker that reflects ongoing humoral immune response. It allows them to migrate to the B cell follicles within the lymph nodes, where they can participate in the immune response with B cells. In terms of vaccines, Tfh cells can promote the development of memory B cells, which can provide long-term protection against viruses and thus enhance the efficacy of the prophylactic approaches (Burrell et al., 2017; Linterman and Vinuesa, 2010).

Treg cells are regulatory cells specialized in maintaining immune tolerance and suppression of the immune response. They express the transcription factor Foxp3 and produce anti-inflammatory cytokines – IL-10 and TGF-β. Treg in viral infections can have a dual role – they can contribute to viral persistence by limiting the immune response, but at the same time, they can help to prevent immune-mediated tissue damage. Excessive Treg activity can also lead to chronic viral infections, as they can impair viral clearance. The role of Tregs in the immune response to viruses is very complex and depends on the context (Burrell et al., 2017; Linterman and Vinuesa, 2010).

Naïve T cells (**T$_{naïve}$**) are the cells unexposed to antigen. As shown in **Figure 3**, after virus entry to the host organism, CD4$^+$ T cells begin the differentiation to the effector T cells, which can eliminate infected cells and produce virus-specific antibodies, respectively, or memory T cells, that protect against future viral infections.
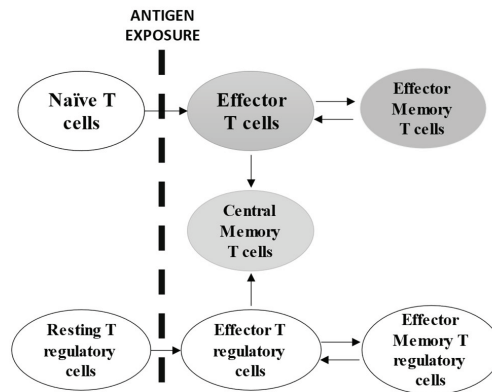
Figure 3 The differentiation of CD4+ T cells (Golubovs.kaya & Wu, 2016).

T$_{NAÏVE}$ and T$_{SCM}$ (stem cell memory) cells can differentiate into different Th subsets based on the cytokine environment and APC signals (Raeber et al., 2018; Y. Wang et al., 2021). During subsequent viral infections, memory T and B cells are rapidly activated and can provide a more robust immune response. Memory T cells consists of several subpopulations: effector memory T cells (T$_{EM}$), central memory T cells (T$_{CM}$), terminally differentiated effector memory cells re-expressing CD45RA (T$_{EMRA}$) (Tian et al., 2017). T$_{EM}$ cells have a short lifespan and are found in peripheral tissues, where they can quickly respond to antigen re-exposure by producing cytokines and performing effector functions. T$_{CM}$ cells are a subset of memory T cells that have homed to secondary lymphoid organs and can rapidly proliferate upon antigen re-exposure,

giving rise to both effector and memory T cells. T_{CM} cells are thought to be precursors to T_{EM} cells and can differentiate into different Th subsets based on the cytokine environment and antigen-presenting cell signals. T_{EMRA} are a subset of T cells that have lost CD62L and express CD45RA, which is a marker for naïve T cells. T_{EMRA} cells are found in peripheral tissues and are thought to be the end-stage of effector T cell differentiation. They have a high effector function and can quickly respond to antigen re-exposure but have a short lifespan.

It is worth emphasizing that memory T cells can rapidly expand and produce cytokines that can eliminate infected cells and limit viral replication. CD8^{+} cells are closely connected to CD4^{+} cells in the context of viral response. T helper cells are responsible for coordinating the immune response and providing help to cytotoxic CD8^{+} cells. During viral infections, CD4^{+} cells activate and differentiate CD8^{+} cells and provide them with cytokines and signal molecules that enhance their effector function (Kervevan and Chakrabarti, 2021).

CD8^{+} cells play a critical role in the body's immune response to viral infections. They are generated in the thymus gland and mature into functional cells in response to signals from other immune cells. They are characterized by a long lifespan and can be activated quickly in response to a new infection. As shown in **Figure 4**, upon antigen exposure, CD8^{+} cells undergo differentiation to become effector cells that specifically recognize and destroy virus-infected cells (Hashimoto et al., 2019). CD8^{+} cells are often called cytotoxic cells, as once they bind to a target cell, they become effector cells which release toxic molecules, as perforins or granzymes, that kill target cells. Those molecules act together effectively, as perforins form pores on the surface of the target cell, allowing granzymes to enter and trigger apoptosis. After the infection has been cleared, some of the effector CD8^{+} T cells can differentiate into memory cells providing long-lasting immunity to specific pathogens.
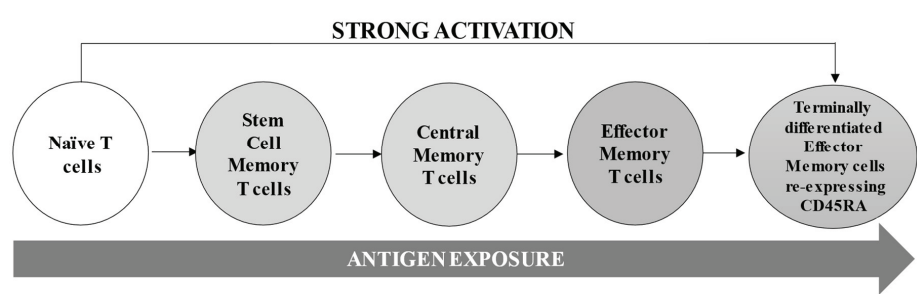
Figure 4 The differentiation of CD8^{+} T cells (Golubovskaya and Wu, 2016). CD45RA stands for Cluster of Differentiation 45 Receptor Antigen.

Besides cellular response, the humoral response provided by B cells is crucial in the adaptive immune system. The process of CD19^{+} B cell activation is regulated by a complex network of signaling molecules, cytokines, and co-stimulatory receptors (**Figure 5**) (Catalán et al., 2021). The interaction between the B cell receptor (BCR) and the antigen triggers a series of intracellular signaling pathways that activate the transcription factors NF-κB and IRF4 (Wen et al., 2019). In B cells, NF-κB promotes the expression of cytokines, such as IL-6 and IL-10, which can promote cell proliferation and differentiation. It is worth emphasizing that it also promotes the expression of co-stimulatory molecules, such as CD40, a surface protein expressed on B cells, DCs, macrophages, and some T cells. CD40 is a member of the tumor necrosis factor receptor (TNFR) family and plays a critical role in the regulation of the immune responses. Interaction of CD40 with the CD40 ligand (CD154) on activated CD4^{+} T cells leads to the recruitment of the TNF receptor-associated factors (TRAFs), activation of the JAK-STAT signaling pathway, activation of mitogen-activated protein kinase (MAPK) pathway (Kawabe et al., 2011). Overall, the engagement of CD40 by CD40L is a critical step in the activation and differentiation of B cells, but also activation and cytokine production by T cells.
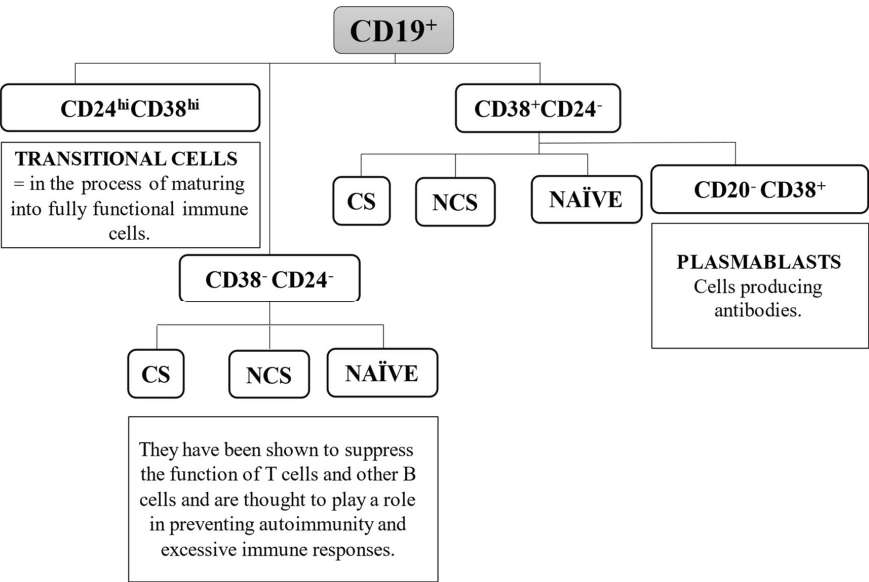
Figure 5 The differentiation of CD19+ B cells. CD stands for cluster of differentiation; CS stands for class-switched lymphocytes; NCS stands for non-class-switched lymphocytes; hi in superscript stands for high expression level of the cluster of differentiation on the surface.

1.2. SARS-CoV-2 virus

Coronaviruses (CoVs.) of the family *Coronaviridae* consists of four classes – alpha, beta, gamma and delta **Figure 6**). They are characterized by a positive-sense single stranded RNA genome which is encapsulated within a membrane envelope studded with glycoprotein spikes. Generally, coronaviruses like NL63-CoV, 229E-CoV, OC43-CoV were associated with mild respiratory infections (Aitken, 2010). SARS-CoV-2 changed the view on this family, causing the global COVID-19 pandemic.
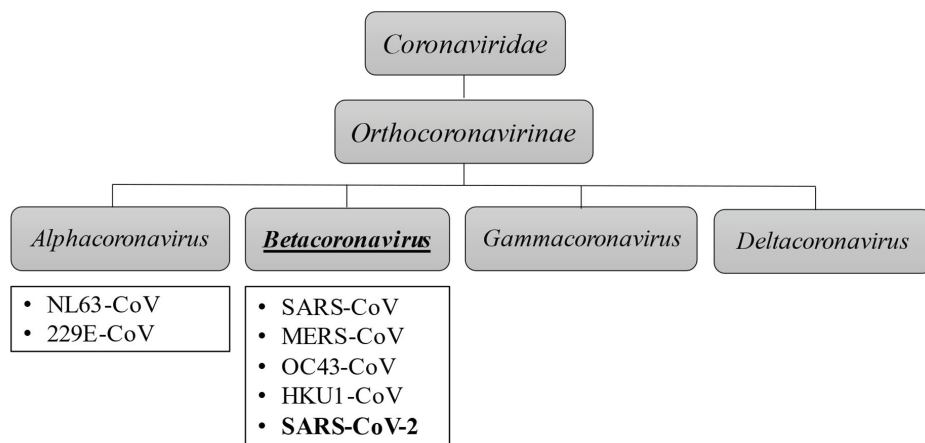
Figure 6 Taxonomy of coronaviruses (Kesheh et al., 2022).

SARS-CoV-2 cause multiorgan failure attacking the lower respiratory system, gastrointestinal system, heart, kidney, liver, central nervous system (Varghese et al., 2020). The heart, after the lungs, is the second major organ damaged by the infection (Loganathan et al., 2021). Infection of the brain can cause fatal complications such as acute respiratory syndrome or cardiac problems (Kempuraj et al., 2020).

SARS-CoV-2 virion contains four major proteins: the envelope protein (E), the transmembrane protein (M), the nucleocapsid protein (N), and the spike protein (S), which appears to be the most important during internalization of the virus (Yao et al., 2020). S protein binds to a receptor protein called angiotensin-converting enzyme 2 (ACE2) located on the surface membrane of host cells. The SARS-CoV-2 contains a proprotein convertase motif; however, as opposed to other avian viruses, it does not enhance the entry into host cells (Shang et al., 2020; Tse et al., 2014). Proteolytic modifications of the S1-ACE2 protein complex are considered a critical step in viral entry (Hoffmann et al., 2020a). Researchers considered it as the therapeutic target, as the inhibition of the protease with camostat mesylate blocks

SARS-CoV-2 entry into epithelial cells. The internalization is facilitated by lysosomal proteases and TMPRSS2, which is a serine protease priming SARS-2-S for entry (Hoffmann et al., 2020b). Other factors contributing to internalization are high human ACE-2-binding affinity by SARS-2-RBD and the pre-activation of the virus by furin (Shang et al., 2020).
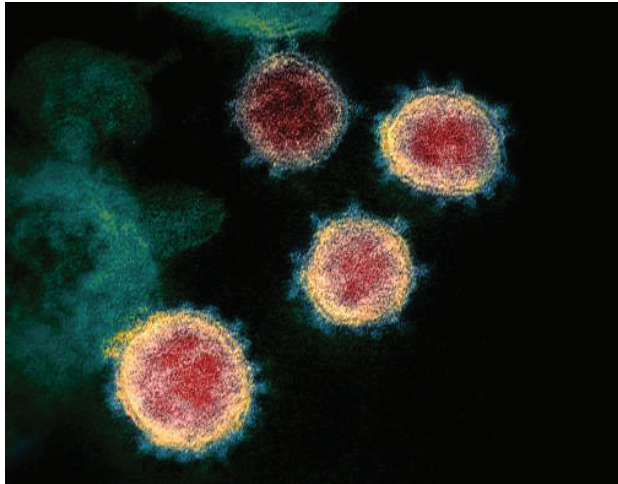
Figure 7 SARS-CoV-2 - colorized transmission electron microscope image [www.commons.wikimedia.org].

ACE2 receptor is found in up to 6% of the nasal epithelial cells, mainly the apical surface of the ciliary cells. Alveolar type 2 (AT2) cells also express this receptor and are a target for the coronavirus, which can damage the lungs, resulting in the spread to other tissues (Ortiz Bezara et al., 2020). It is worth emphasizing that some authors have suggested that despite the lack of ACE2 expression, immune cells, including T cells, monocytes and macrophages, can be infected by coronaviruses (Gu et al., 2005; Hamming et al., 2004).

SARS-CoV-2 can enter the cells expressing CD26 present in the lungs and CD147 (transmembrane protein), which is found in inflamed tissues, tumors and the brain (Masre et al., 2021). Interestingly, several studies show that some of the organs expressing the ACE2 receptor remain uninfected (Gu et al., 2005; Hamming et al., 2004). This implicates, that the ACE2 receptor is not the only factor necessary for virus internalization.

Followed by the clathrin-dependent endocytosis, a viral genome is released to the host cell's cytosol (Haque et al., 2020).
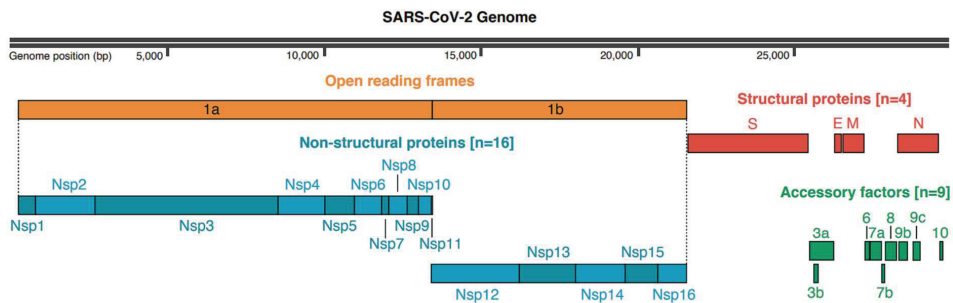
Figure 8 SARS-CoV-2 genome annotation (Gordon et al., 2020).

The SARS-CoV-2 genome (**Figure 8**) is a single-strand RNA containing 14 open reading frames (ORF). ORF1a/b are translated into the replicase poliproteins (pp) – pp1a and pp1ab. Then, the papain-like protease (PL2pro) and chemotripsin-like protease 3 (3CLpro) cut them into smaller sizes non-structural proteins (Nsp, **Figure 8**). Nsps form the replication-transcription complex, which is responsible for the duplication of the viral genetic material and the synthesis of mRNA - a template for structural protein translation. The role of non-structural proteins is described in **Table 1**.

Non-structural protein	Role in the replication cycle
Nsp1	Interferes with the synthesis of host cell proteins by binding to the 40S ribosome subunit and endonucleolytic cleavage of mRNA.
Nsp2	Modulates the survival signaling pathway of the host cell.
Nsp3	Inhibits ubiquitination. Structure transmembrane domain.
Nsp4	Modifies the membranes of the endoplasmic reticulum.
Nsp5	Participates in the process of polyprotein replication. Protease activity.
Nsp6	Works with Nsp3 and Nsp4. Transmembrane domain. Involved in autophagy.
Nsp7	Increase the efficiency of polymerase.
Nsp8	Increase the efficiency of polymerase. Primase activity.
Nsp9	Single-stranded RNA binding protein involved in virulence of the virus (in complex with Nsp8).
Nsp10	"Backbone protein", forming with Nsp14 and Nsp16 methylation complex of the mRNA cap.
Nsp12	RNA-dependent RNA polymerase (RdRp).
Nsp13	Helicase and RNA NTPase activity.
Nsp14	Two domains: exonuclease and guanine methyltransferase.
Nsp15	Endoribonuclease activity.

Table 1 Role of the non-structural proteins coded in the SARS-CoV-2 genome (Raj, 2021; Snijder et al., 2016).

1.3. Cytokine response to SARS-CoV-2

One of the most severe complications associated with COVID-19 is the cytokine storm. Cytokine storm is a severe immune response that can occur when the body's immune system overreacts to an infection or other stimulus, resulting in the release of large amounts of pro-inflammatory cytokines into the bloodstream. Cytokines play a crucial role in the immune response, but when produced in excessive amounts, they can cause damage to tissues and organs throughout the body (Kempuraj et al., 2020).

In COVID-19, SARS-CoV-2 viral components are recognized by innate immune cells, particularly monocytes and macrophages, through pattern recognition receptors (PRRs; **Table 2**) such as toll-like receptors (TLRs) and nucleotide-binding oligomerization domain-like receptors (NLRs). This recognition leads to the activation of signaling pathways, including the nuclear factor kappa B (NF-κB) and interferon regulatory factor (IRF) pathways, resulting in the production and secretion of pro-inflammatory cytokines, chemokines, and other mediators.

Pattern recognition receptor	Role in COVID-19	Reference
TLR3	Inducing the production of pro-inflammatory cytokines, such as IL-6 and TNF-α.	(Q. Zhang et al., 2020)
TLR4	Inducing the production of pro-inflammatory cytokines and chemokines, including IL-6, IL-8, and monocyte chemoattractant protein-1 (MCP-1).	(Vabret et al., 2020; Yang et al., 2014)
TLR7	Inducing the production of type I interferons (IFN-α and IFN-β) and pro-inflammatory cytokines, such as IL-6 and TNF-α.	(Hadjadj et al., 2020)

TLR8	Inducing the production of pro-inflammatory cytokines, such as IL-6 and TNF-α.	(Kuzmicki et al., 2013)
NLRP3	Leading to the production of pro-inflammatory cytokines such as IL-1β and IL-18. It may contribute to the cytokine storm and severe lung injury observed in COVID-19 patients.	(Jamilloux et al., 2020; Vabret et al., 2020; Yang et al., 2020)
NLRP4	Activated by SARS-CoV-2 nucleocapsid protein. Leading to the production of pro-inflammatory cytokines such as IL-1β and IL-18.	(Albornoz et al., 2022; Campbell et al., 2021; Pan et al., 2021)
NLRP6	Possible role in regulating the immune response to SARS-CoV-2 infection (studies on mice).	(Kozlov et al., 2021; Zhang et al., 2023)

Table 2 Pattern recognition receptors and their role in COVID-19 cytokine storm.

The activation of the NF-κB pathway is triggered by the binding of viral particles to pattern recognition receptors (PRRs) on immune cells, such as toll-like receptors (TLRs) and RIG-I-like receptors (RLRs). This activation leads to the production of pro-inflammatory cytokines and chemokines, such as interleukin-6 (IL-6), tumor necrosis factor-alpha (TNF-α), and interferons (Liu et al., 2022).

The Interferon Regulatory Factor (IRF) pathway is activated by the binding of viral RNA to cytoplasmic sensors, such as RIG-I and MDA5. This leads to the activation of the IRF3 and IRF7 transcription factors, which translocate to the nucleus and induce the expression of type I interferons (IFN-α and IFN-β) and other antiviral genes. In COVID-19, the activation of the IRF pathway leads to the production of type I interferons, which have antiviral activity. However, excessive activation of this pathway can also contribute to the cytokine storm, as type I interferons can induce the production of pro-inflammatory cytokines, such as IL-6 and TNF-α (Feng et al., 2021; Glanz et al., 2021).

Several cytokines have been identified as key players in the cytokine storm associated with COVID-19. These include:

- **Interleukin-6 (IL-6):** produced by a variety of immune cells and is known to play a critical role in inflammation and the immune response. In COVID-19 patients, high levels of IL-6 have been associated with more severe disease and poorer outcomes (Abbasifard and Khorramdelazad, 2020).

- **Tumor necrosis factor-alpha (TNF-alpha):** involved in the inflammatory response and has been shown to be elevated in COVID-19 patients with severe disease (Guo et al., 2022).

- **Interleukin-1 beta (IL-1 beta):** involved in the inflammatory response and has been shown to be elevated in COVID-19 patients, particularly those with severe disease (Makaremi et al., 2022).

- **Interferon-gamma (IFN-gamma):** produced by T cells and natural killer cells and plays a key role in the antiviral immune response. However, in COVID-19 patients, high levels of IFN-gamma have been associated with more severe disease (Gadotti et al., 2020; Todorović-Raković and Whitfield, 2021).

- **Interleukin-10 (IL-10):** anti-inflammatory properties and involved in regulating the immune response. In COVID-19 patients, low levels of IL-10 have been associated with more severe disease (Islam et al., 2021).

Other cytokines that are implicated in the cytokine storm associated with COVID-19 include IL-2, IL-4, IL-7, IL-8, IL-17, granulocyte colony-stimulating factor (G-CSF), and macrophage inflammatory protein-1 alpha (MIP-1 alpha) (Montazersaheb et al., 2022).

The direct role of the ACE-2 receptor in cytokine storm induction remains unclear. It was suggested that the ACE-2 receptor plays a role in the cytokine storm due to the regulation of the renin-angiotensin system (RAS). When SARS-CoV-2 infects cells in the lungs, it binds to the ACE-2 receptor, leading to the downregulation of ACE-2 expression and dysregulation of RAS. The dysregulation of RAS can result in a cytokine storm leading to widespread inflammation and tissue damage in multiple organs, including the lungs, heart, kidneys, and brain (H. Zhang et al., 2020).

Overall, the cytokine storm associated with COVID-19 is a complex phenomenon involving the dysregulation of multiple cytokines and other inflammatory molecules. Further research is needed to better understand the mechanisms underlying this phenomenon and to develop more effective treatments for patients with severe disease.

1.4. Treatment and prevention possibilities

Treatment for COVID-19 depends on the severity of the course of the disease. Symptomatic treatment is usually sufficient for mild infections. More severe cases may require oxygen therapy or mechanical ventilation. Antiviral drugs with a different mechanism of action are used in hospitalized patients. There are several groups of antiviral drugs, including viral RNA synthesis inhibitor, viral protein synthesis inhibitors, viral internalization inhibitors, and immunomodulators. Despite the therapeutic potential, vaccines remain the most important factor in defeating the virus.

Currently, 8 drugs are authorized for the treatment of COVID-19 in the European Union (EU), while the other two (molnupiravir and baricitinib) were applied for marketing authorization. Moreover, the EU approved two mRNA vaccines (BioNTech/Pfizer and Moderna), several adenovirus vaccines (e.g. AstraZeneca, Johnson & Johnson / Janssen Pharmaceuticals), a protein vaccine (Novavax) and inactivated virus vaccine (Valneva) (European Medicines Agency, EMA). Different strategies of the vaccine designs are shown in **Figure 9**.
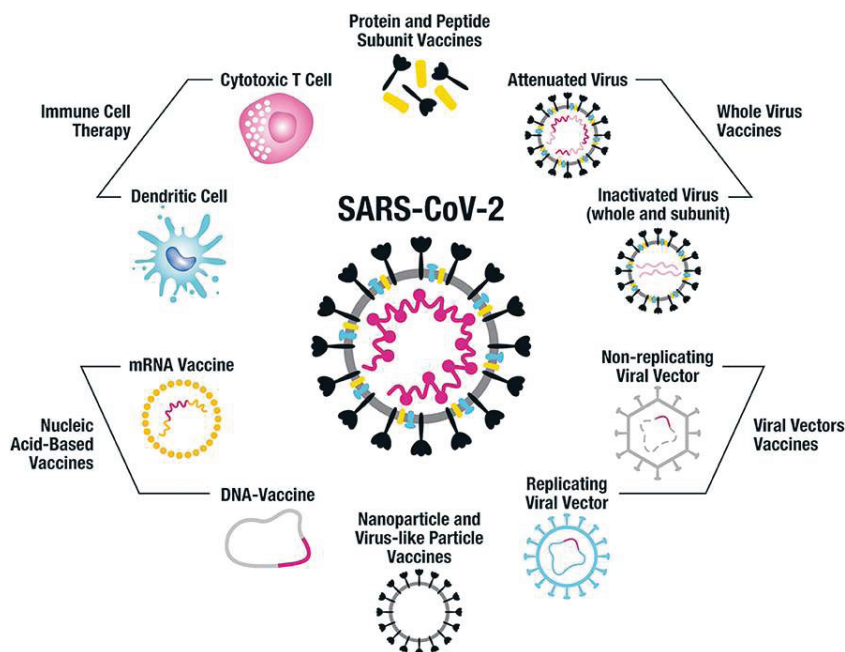
Figure 9 Vaccine platforms being employed for SARS-CoV-2 vaccines design. Credit: (Flanagan et al., 2020) (CC license).

The mRNA vaccines for COVID-19 are the first vaccines of this type authorized to the market (Dai and Gao, 2021). They have many advantages, among which the fast production time, large possibilities of changes in the designed formulation and clinically proven ability to generate humoral and cellular responses have proved to be particularly important.

The mRNA vaccines are based on the fact that mRNA can be translated into an antigen (Fiedler et al., 2016; Xu et al., 2020). The genetic material encoding the antigen in the lipid envelope is delivered to the body by intramuscular injection. This coating increases the absorption of mRNA into cells, which at the same time reduces the possibility of degradation. Once inside the muscle cell, mRNA is transported to the cytosol, where the ribosomes use it as a template for the production of the spike protein (S). This protein is subsequently released, triggering an immune response, including class I and class II MHC (major histocompatibility complex) molecules. The MHCs transport the antigen to the cellular membrane, which leads to dendritic cells (DCs) activation. DCs migrate to lymph nodes and present the antigen to B and T lymphocytes. The result of this process is an antigen-specific response, which in turn leads to the development of immunity (Batty et al., 2021).

Another approach is adenovirus (AdV) based vaccines. They have many advantages, such as an easy scale-up, the development of balanced immunity, and a fast production process. Previous research suggests that unlike lentivirus or retrovirus vectors, AdVs. are safer due to the lack of viral genome integration with the host genome (Mendonça et al., 2021). In nature, adenoviruses are responsible for mild respiratory and eye infections in humans (Lukashev and Zamyatnin, 2016). Just like mRNA, AdVs. have been used in vaccines relatively recently. For the purpose of using these vectors in immunotherapy, the genes responsible for replication (E1 and/or E3) are removed from the AdVs. genome. In place of these genes, a transgene enables translation of the protein of interest, e.g., an antigen is inserted (Holm and Poland, 2021). Further response to the antigen is similar to mRNA vaccines. The difference is that adenoviruses can play more roles in vaccines than delivering genes. Generally, two routes of adenoviral vaccines administration are practiced – intramuscular and intranasal (Chavda et al., 2023). There are six intramascular vaccines that currently have emergency use authorization (EUA) and five intranasal vaccines under the development. Between the EUA vaccines two different types of viral vectors dominate. The exception is Astra Zenecas vaccine Covishield/Vaxzevria, that has ChAdOx1 (chimpanzee adenovirus Oxford 1) as a vector. Similar to other viral vectors, ChAdOx1 is modified to deliver specific genetic material into human cells. In the case of the Oxford-AstraZeneca COVID-19 vaccine, the ChAdOx1 vector

is engineered to carry the gene that codes for the spike protein of the SARS-CoV-2 virus. Other adenoviral vaccines carry either rAdV5 (recombinant adenovirus serotype 5) or rAdV26 (recombinant adenovirus serotype 26) as vectors (Table 3). All vaccines in the tables are engineered to carry the gene that codes for the spike protein of the SARS-CoV-2 virus, which is the target for immune response.

Vector type	Name of the vaccine and phase of clinical development		
rAdV5 as a vector	GamCOVID-Vac & GamCOVID-Vac Lyo (Sputnik V) Phase III	Ad5-nCoV (Convidecia) Phase III	Gam-COVID-Vac Phase II (Phase III is ongoing)
rAdV26 as a vector		Sputnik Light Phase III	Ad26Cov2-S (JNJ-78436735) Phase III

Table 3 Adenoviral vaccines having EMA (Chavda et al., 2023).

As our team previously reported (Garofalo et al., 2020), AdVs. can be potent adjuvants due to acting as a strong immune activator, enhancing the immunogenicity of vaccine antigens, attracting antigen-presenting cells to the side of infection, enhancing T-cell priming and inducing the development of pro-inflammatory responses. Adenoviral vectors can present various types of epitopes on their surface, such as co-stimulatory ligands CD40L and ICOSL, which are involved in the activation of lymphocytes. The adenovirus itself acts as a strong adjuvant enhancing the immunogenicity of vaccine antigens, e.g. by attracting immune cells to the site of infection and inducing a pro-inflammatory response.

Protein and peptide subunit vaccines contain purified fragments of the viral epitope recognized in the course of infection. The main component of the commercially available antigen vaccine for SARS-CoV-2, Novavax, is the full-length spike protein (Wise, 2022). Due to the fact that the genetic material of coronaviruses is RNA, they are characterized by the ability to mutate very dynamically (Duffy, 2018). This means that the most effective form of prevention, which is vaccines, can quickly become obsolete. Some variants of SARS-CoV-2, such as omicron (B.1.1.529), are unlikely to correlate with vaccines and monoclonal antibody therapies approved by the EMA and the Food and Drug Administration (FDA) (Khani et al., 2022, p. 19). In order to prevent the secondary loss of epidemic control, care should be taken not only about prevention but also about the production of effective drugs. The EMA listed eight authorized treatments in the EU to treat COVID-19 (EMA). As shown in

Figure 10 and **Table 4**, other possibilities are considered too.

Trade name	Ingredients	Target	Mechanism of work	Reference
Evusheld	Tixagevimab Cilgavimab	Epitopes of S-protein	Monoclonal antibodies bind to non-overlapping epitopes of the SARS-CoV-2 virus within the RBD binding domain. They neutralize the internalization of the virion into the cell. They show high efficiency in pre-exposure administration.	(Wu et al., 2022; Yang and Du, 2022)
Regkirona	Regdanvimab	Spike protein	Regdanvimab neutralizes SARS-CoV-2 by binding to the receptor binding domain (RBD) of the virus' spike protein. This leads to the inhibition of internalization of the virus into the cell.	(Syed, 2021)
Ronapreve (REGEN-COV)	Casirivimab Imdevimab	Spike protein	Casirivimab and imdevimab are monoclonal antibodies that target the SARS-CoV-2 spike protein to reduce the risk and severity of COVID-19 in patients.	(Sidebottom and Gill, 2021; Yang and Du, 2022)
Xevudy	Sotrovimab	Spike protein	The antibody binds to the S protein ("Spike") of the SARS-CoV-2 coronavirus, preventing the internalization of the virus.	(Mungmunpuntipant ip and Wiwanitkit, 2022)

Kineret	Anakinra	IL-1 receptor	Anakinra blocks IL-1 receptors and inhibits the binding of IL-1α and IL-1β.	(Khani et al., 2022, p. 19; Kyriazopoulou et al., 2021)
Paxlovid	PF-07321332 Ritonavir	Mpro protease 3CL Protease	Ritonavir-boosted Mpro inhibitor.	(Mahase, 2021; Wen et al., 2022)
RoActemra	Tocilizumab	IL-6	Humanized IgG1 monoclonal antibody directed against the receptor for interleukin 6 – IL-6R.	(Bednarek et al.)
Veklury	Remdesivir	RNA	Remdesivir triphosphate is produced by metabolizing the prodrug veklury. It functions as an ATP analog and engages in competition with ATP for viral RNA synthesis. After RDV-TP is incorporated into the viral RNA template, the production of viral RNA can be inhibited due to read-through by the viral polymerase, which can happen at greater nucleotide concentrations. Remdesivir nucleotide interferes with the viral RNA template's ability to incorporate the complementary natural nucleotide, which prevents the creation of viral RNA.	(Pilote et al., 2021)

Table 4 Authorized treatments for COVID-19 (EMA).
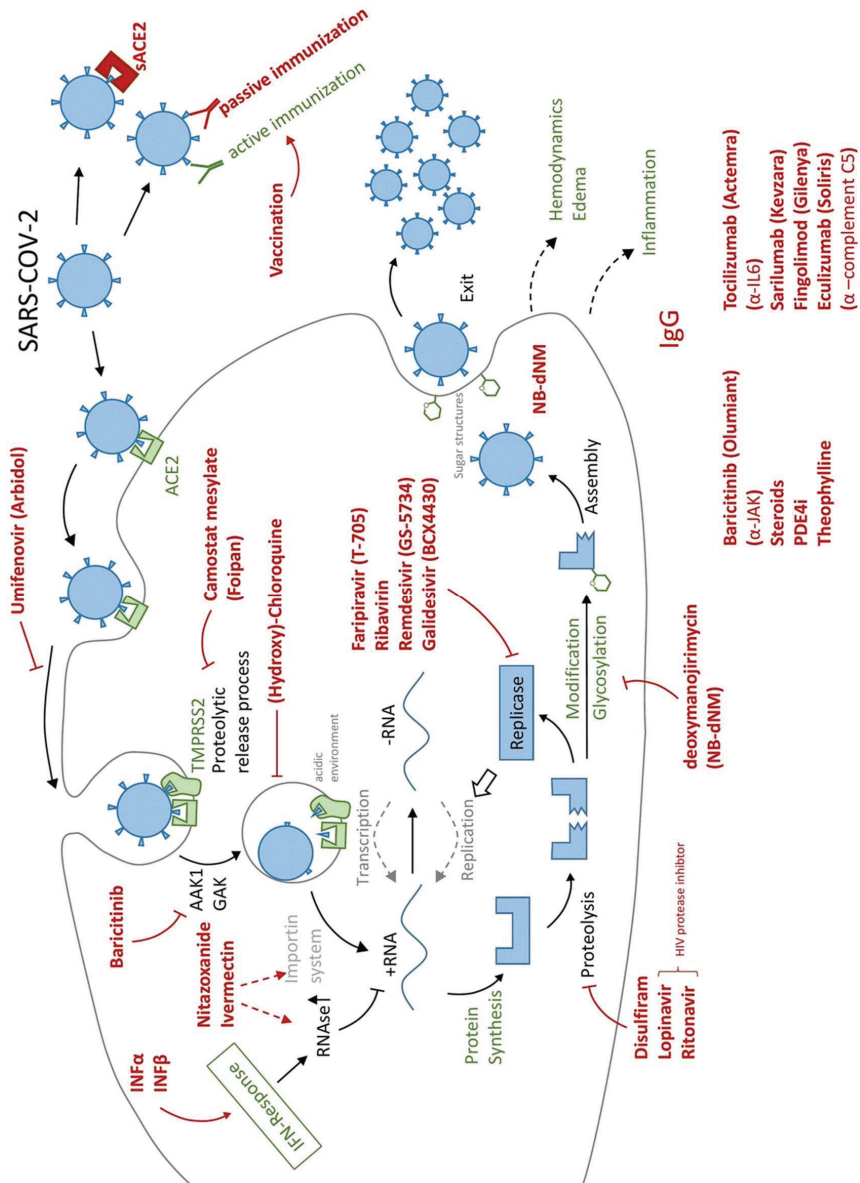
Figure 10 Therapeutic targets for COVID-19. Credits: Graphic used unchanged with permission from Marcel Leist, PhD, University of Konstanz.

1.5. Non-clinical evaluation of adjuvanted vaccines

Non-clinical testing is a crucial part of screening for new therapeutic approaches. It consists of the *in vitro* & *in vivo* laboratory evaluation, including broad characterization of the product. In preclinical studies, we prove that the first concept is true and that the proposed formula is immunogenic and safe. The evaluation concerns the toxicity of the active reagents on themselves and in the fixed combination.

In designing novel vaccines, *in silico* studies might be useful (Hagmann, 2000). Reverse vaccinology can be used to choose a protein of the particular pathogen that will be highly immunogenic and effective in boosting specific response to further infection. *In silico* vaccine design begins with a broad literature review to prepare a representative background of the topic of interest. After selecting a pathogen, the process of amino acid sequence choosing starts. It is important to consider the variety in the epitopes of different strains. With RNA viruses, the diversity of epitopes can be significant, so choosing the correct sequence to represent a pathogen is crucial. Most of the COVID-19 vaccines focus on receptor binding receptor (RBD) sequence, protein relevant in internalization of the virus (Yi et al., 2021). However, studies show that receptor-binding motif (RBM) is the most divergent region, and that's why SARS-CoV-2's variants can often evade the antibody response. Thus, tracking mutations and different variants is crucial in designing effective vaccines (Alam et al., 2021; Baum et al., 2020; Z. Liu et al., 2021; Thomson et al., 2021). In this process, viral genome sequencing is crucial (Chen et al., 2021). Through the FASTA sequence of the genome there is a possibility for epitope prediction, for instance using the Immune Epitope Database and Analysis Resource (IEDB). IEDB provides tools to predict MHC-I and MHC-II Binding Predictions. For predicting B-cell epitopes there are few methods available, such as Chou and Fasman beta-turn prediction, Emini surface accessibility scale, Karplus and Schulz flexibility scale etc.
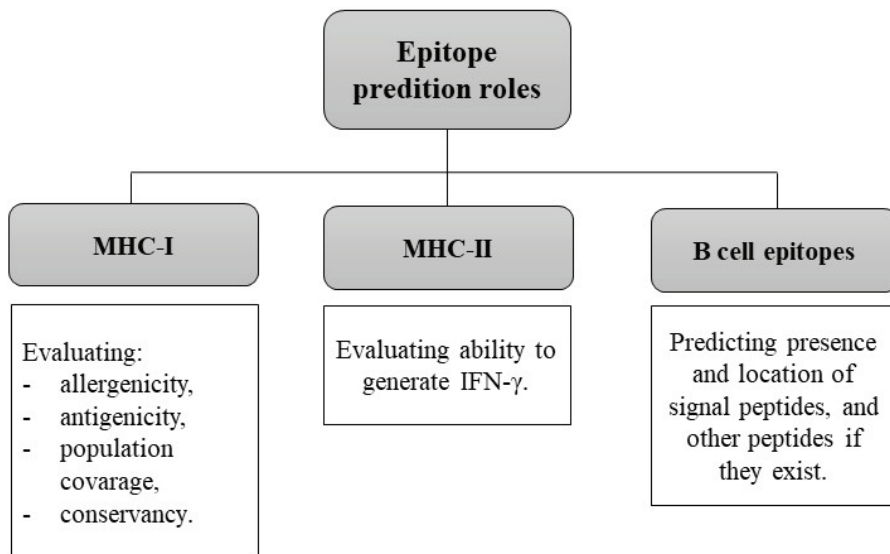
Figure 11 Role of *in silico* epitope prediction roles (Martinelli, 2022). *MHC* stands for Major Histocompatibility Complex, *IFN-γ* stands for Interferon gamma.

After selecting target pathogen, literature review, selecting target proteins and predicting the epitopes (MHC I, MHC II and B cell epitopes; **Figure 11**), the process of vaccine construction starts. Antigens can be produced in a variety of ways, such as growing the pathogen in the laboratory and extracting specific molecules from it or using genetic engineering techniques to produce recombinant proteins. The antigens used in vaccines are selected based on their ability to induce an immune response that will protect against the specific pathogen. Adjuvants are added to vaccines to enhance the immune response to the antigens. They work by activating the innate immune system, which in turn helps to stimulate the adaptive immune response. Adjuvants can be derived from various sources, such as bacterial cell walls or synthetic compounds, and are selected based on their ability to enhance the immune response without causing excessive inflammation or toxicity. Once the antigens and adjuvants have been selected, they are combined and formulated into the final vaccine product. The vaccine may be administered in various ways, such as through injection, nasal spray, or oral ingestion, depending on the type of vaccine and the target population (Cid and Bolívar, 2021).

The EMA provides for the pharmaceutical researchers a guidelines on the clinical testing of the medicines divided into 8 chapters in which are Immunogenicity, Efficacy,

Effectiveness and Safety ('Guideline on clinical evaluation of vaccines'). Immunogenicity provides guidance on the evaluation of the immune response to medicinal products, including the assessment of antibodies and cellular immune responses. The rest of them describe the requirements for demonstrating the efficacy, effectiveness, and safety of medicinal products through clinical trials. However, adequately justified deviations from them are allowed. Overall, these guidelines provide a framework for pharmaceutical researchers to follow when conducting clinical trials and developing medicinal products, with the ultimate goal of ensuring the safety and efficacy of these products for patients.

The immune response can be characterized in various biological matrixes, such as whole blood or PBMCs. This characterization involves several techniques, which include measuring functional antibodies, describing the kinetics of the response, exploring the induction of memory cells, and examining the cross-interferences of antibodies.

Measuring functional antibodies involves determining the ability of antibodies to neutralize the targeted pathogen or toxin (Gattinger et al., 2023). There are five main techniques used to evaluate the ability of the antibodies to neutralize the pathogen:

1. Neutralization assays, that can include plaque reduction test. It is used to determine the ability of an antibody or other substance to neutralize the infectivity of the virus. It involves infecting cells with the virus, then adding e.g. antibody at varying dilution to determine what concentration is required to reduce the number of the virus plaques by a certain percentage.
2. Antibody-dependent cell-mediated cytotoxicity (ADCC) assay, which is the process by which NK cells and macrophages are stimulated to kill target cells that have been coated with antibodies. The mechanism of ADCC involves multiple steps, including the binding of the FC region of the antibodies to FC receptors on immune cells, which triggers a signaling cascade leading to the release of cytotoxic granules and the killing of the target cells (Hashimoto et al., 1983).
3. Complement-dependent cytotoxicity (CDC) assay is a process involving killing of the cells by the activation of the complement system (Gazzano-Santoro et al., 1997).
4. Enzyme-linked immunosorbent assay (ELISA), which can be used to measure the binding of the antibody to its antigen.
5. Flow cytometry, that can be used to measure the binding of an antibody to cells by detecting a fluorescently labelled secondary antibody.

Examining the cross-interferences of antibodies involves evaluating the ability of antibodies to cross-react with other related pathogens or toxins. This can help to identify potential risks or benefits of vaccination or to inform the design of new vaccines.

Describing the kinetics of the immune response involves monitoring the levels of specific antibodies or immune cells over time, for example in response to vaccination or infection. This can help to determine the optimal timing for vaccination or identify potential biomarkers of immune protection. To describe the kinetics of the immune response several techniques can be used – ELISA, flow cytometry and cytokine assays. Immunophenotyping is a subset of flow cytometry that focuses on identifying and characterizing immune cells in a sample based on their surface markers (Maecker et al., 2012). This technique can be used to evaluate the immune response to vaccines by analyzing the distribution and activation of different immune cell subsets before and after stimulation. As shown in Figure 12, immunophenotyping is based on fluorescent staining of the cell suspension with antibody conjugates. Then, the optimization of the fluorescence detectors is performed. The data acquisition is based on fluorescence detection of the events appearing in the flow cell. Using different markers, cells can be differentiated into population-specific groups and gated for analysis.
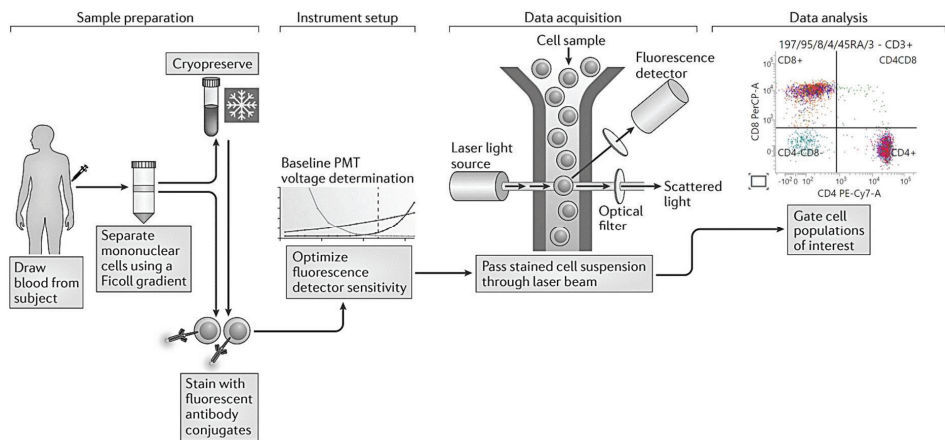
Figure 12 Schematic representation of immunophenotyping (Maecker et al., 2012).

In addition to these techniques, the correlation between cytokine or gene expression profiles can also be examined to gain insights into the mechanisms of immune response. For example, in this study, correlation between immunophenotyping, relative gene expression and RNA-sequencing analysis was performed.

Animal models are often used to evaluate the immunogenicity and protective efficacy of vaccine candidates. However, it is important to note that vaccines that appear promising in animal studies may fail in clinical trials (Tapia-Calle et al., 2017). This underscores the need for *ex vivo* human cell response studies that evaluate the qualitative and quantitative characteristics of the immune response to vaccine candidates (Watkins et al., 2008). *Ex vivo* studies involve the use of human cells or tissues outside the body, which allows for the evaluation of the immune response to vaccine candidates in a more human-relevant setting. These studies can provide valuable information on the safety and immunogenicity of vaccine candidates and can help to identify potential issues that may arise during clinical trials. *Ex vivo* studies of the immune response, although still not well established and studied, have many advantages (Tapia-Calle et al., 2019):

1. Physiological relevance: PBMCs are derived from human blood and thus provide a more relevant model for human immune responses than animal models or cell lines.

2. Diversity: PBMCs are a heterogeneous mixture of immune cells, including T cells, B cells, natural killer (NK) cells, monocytes, and dendritic cells, which allows for the evaluation of a wide range of immune responses.

3. Availability: PBMCs are readily available from blood samples, making them a convenient and cost-effective model for evaluating vaccine candidates.

4. Customizability: PBMCs can be isolated from individuals with different genetic backgrounds, ages, and health statuses, allowing for customized and personalized evaluations of vaccine candidates.

5. Ethical considerations: using human-derived models for vaccine evaluation may be more ethically justifiable than using animal models, as it avoids potential ethical concerns related to animal use in research.

Overall, using human-derived PBMC models in *in vitro/ex vivo* studies provides a more relevant and customizable model for evaluating vaccine candidates and may have ethical advantages over animal models. **That is why it is crucial to establish reliable and optimized models for immunogenic factors development.**

2. Research objectives

In the face of the SARS-COVID-2 pneumonia pandemic, my efforts have been directed towards understanding the pathogenesis of SARS-CoV-2 infection and prevention possibilities. My studies identified the role of the innate immune system in sensing the platform factors: the antigen (selected epitopes of SARS-CoV-19) and adjuvant (adenovirus). I collaborated with the scientists who previously designed the adenovirus AdV-D24-inducible co-stimulator ligand (ICOSL)-CD40L (AdV1 serotype 5/3 which does not replicate in healthy cells due to deletion in the E1 region) armed with two potent co-stimulatory molecules: the inducible co-stimulator (ICOSL) and the CD40 ligand (CD40L) (Garofalo et al. 2021a). AdV serotype 5 or 3 binds to the human CAR (coxsackie and adenovirus receptor) or desmoglein 2 (DSG2) receptor (Garofalo et al. 2021a). The chimeric AdV5/3 vector was served as an adjuvant due to its effective initial interaction with APC (Garofalo et al., 2021a). ICOSL-mediated immune stimulation involves the activation of CD8^{+} cytotoxic T cells through ICOS expressed on activated T cells and its ligand ICOSL on antigen-presenting cells, supporting robust anti-tumor immune responses. CD40L-mediated immune activation, engaging CD40 on B cells, macrophages, and DCs. The synergistic effect of combining ICOSL and CD40L within the AdV-D24 oncolytic adenovirus enhances the local activation of CD8^{+} cytotoxic T cells, offering immunogenicity. Studies with analogous strategies, such as NDV-ICOSL and CD40L-expressing adenoviruses, have demonstrated improved infiltration of activated T cells when combined with immune checkpoint inhibitors (Garofalo et al., 2021a). This approach ensured the induction of an immune cascade leading to the recruitment of antigen-presenting cells and the development of cellular and humoral immune responses (against the vector and the presented antigens). Moreover, our preliminary data (Baran et al., 2023) and the resulting hypothesis led to reliable and optimized model for immunogenic factors evaluation by analyzing the activation of different immune cell subsets before and after stimulation.

The main goal of my studies was the development of adequate screening and confirmatory assays to measure immune responses against the platform factors as the basis of the evaluation of immunogenicity. Thus, the evaluation immunogenicity was based on particular non-clinical (*in vitro*) analyses of immunological efficacy and biosafety data (*in vivo*) of the modulating factors, such as the adjuvant - adenovirus (AdV1 or AdV2 without ICOSL and CD40L) and the antigen (recombinant Receptor Binding Domain (rRBD) protein or recombinant spike-S1 and/or nucleocapsid). I accomplished the main goal by:

I.   I established the *in vitro* model to study human immune response stimulated by the immunogenic vectors. I optimized the isolation of peripheral blood mononuclear cells (PBMCs) from healthy donors and used them in combination with lung epithelial cells Calu-3 to establish the 2D and 3D models.

II.   I identified and quantified apoptotic hallmarks and plasma membrane integrity of human cells stimulated with the platform. I assessed whether the immunogenic factors affected cell viability and induced apoptosis.

III.   I tested several mechanisms by which adenoviruses (AdV1 and AdV2 without ICOSL and CD40L) act as adjuvants. I focused on innate and adaptive immune cells which could be helpful in revealing cell-mediated responses. In detail, I used the flow cytometry-based assays to assess the percentage of $CD4^+$, $CD8^+$, and $CD19^+$ subpopulations. ICOSL is a member of the CD28/B7 family of co-stimulatory molecules and play a crucial role in T cell activation. When $T_{NAÏVE}$ encounter antigens presented by APCs, the interaction between TCR and the antigen-MHC complex is often not sufficient for full T cell activation. Co-stimulatory signals from ICOS/ICOSL are required for optimal T cell responses. ICOS/ICOSL pathway is also particularly involved in $CD4^+$ T cells differentiation. ICOS stimulation promotes the generation of Th2 cells and T_{fh} cells.

IV.   I explored whether the stimulation of PBMCs with the vaccine platform affects T cells and could have lasting effects on the antiviral capacity of the $CD4^+$ and $CD8^+$T cells. Thus, I characterized the central memory T_{CM}, effector memory T_{EM}, and effector memory cells re-expressing CD45RA T_{EMRA} which were targeted by adjuvant.

V.   I tested whether the vaccine platform stimulates B cell development and differentiation. I searched for the antigen-specific B cells after immunization. I compared the *in vitro* distribution of memory, naïve and transitional B cells in PBMCs stimulated with the vaccine platform.

VI.   I studied the production of a series of cytokines which influence the effector cytotoxic T cells or B cells.

VII.   I examined the effects of the immunogenic factors on the CD40 expression in the VERO E6 cells. VERO E6 cells express CD40L receptors. CD40/CD40L interaction is a critical signaling pathway in the immune system, and it can modulate immune responses. VERO E6 cells are also highly permissive to a wide range of viruses,

including SARS-CoV-2, which make it suitable to study the viral replication effect on the cell line.

VIII.   I performed RNA-seq gene expression data analysis of the Calu 3 and PBMC treated with the vaccine platform. The up and down-regulations were registered in each condition with highest number of differentially expressed genes. I identified the signaling pathways that control immunological mechanisms by which the platform induces protective immunity.

IX.   Finally, I conducted a 30-day biosafety analysis using BALB/c mice to determine the potential *in vivo* risk of the platform.

3. Materials and methods

The research has a comprehensive character (Figure 13). It began with preliminary studies involving the development of a methodology for dealing with PBMC (isolation, culture, cryopreservation), followed by the assessment of immunogenic factors' cytotoxicity and immunogenicity. Subsequently, a model of the alveolus was established on a 3D insert, and *in vivo* tests were performed in the last phase of the study.

Preliminary studies

In vitro cytotoxicity and programmed cell death assessment
- MTS assay to study VERO E6 and PBMC cell proliferation and viability
- Apoptosis assay by using Annexin V staining method

Microscopic imaging
- Analysis of pseudo-SARS-CoV-2 internalisation by CSLM,
- SEM imaging of the hCoV-OC43 virus and pseudo-SARS-CoV-2

Virus titer determination
- Spearman-Karber method for estimating viral infectious titer

Ex vivo studies 2D model

Immunogenicity assessment
- Analysis of subpopulations of CD4+T cells, CD8+T cells, and CD19+ cells

Genome sequencing

CD40 gene expression analysis
- RT-qPCR studies using VERO E6 cells

Ex vivo studies 3D model

Immunogenicity assessment
- Analysis of subpopulations of CD4+T cells, CD8+T cells, and CD19+ cells
- Analysis of cytokines

In vivo studies

Figure 13 The plan of dissertation studies.

3.1. List of laboratory equipment

- Scanning Electron Microscope (Hitachi SU8230)
- Eppendorf Research Plus pipettes with Eppendorf tips
- Spark plate reader (Tecan, Switzerland)
- Flow cytometer (BD FACSLyricTM)
- Laminar chambers CleanAir (Baker, BioVanguard) and Alpina (BIO130 CYTO, Alpina), both BSLII level
- Incubator (PHCBI)
- Centrifuge 5910 R (Eppendorf)
- Chambers for working with nucleic acids (ISOCIDE ESCO)
- Thermocycler PCR T100 (BioRad USA)
- BioRad CFX96 Touch Real Time PCR (BioRad USA)
- Laboratory freezer (-86˚C; PHCBI)
- Laboratory freezer (-150˚C; PHCBI)
- Refrigerators (4˚C; SANYO)
- Inverted microscope (Leica DMIL)
- Confocal Laser Scanning Microscopy (Zeiss Axio Observer 7 with LSM 900 and Airyscan 2 detector)

3.2. Preparation of materials for research - cell lines, rRBD, viruses and adenoviral vectors

3.2.1. Adherent cell culture

Depending on the experiment, different cell lines were used (**Table 5**). VERO E6 cell line was used for the Spearman-Kärber method and CD40 gene relative expression analysis (Sections 3.4. and 3.13.) H226 and MSTO-211H cell lines were used for the Spearman-Kärber method (Section 3.2.6.). Calu-3 cell line was used for the 3D model of alveoli (Section 3.2.5.). The cells were cultured in the appropriate cell growth medium supplemented with 10% inactivated fetal bovine serum (FBS; Gibco) (Table 5) and incubated at 37°C with 5% CO_2 upon reaching semi-confluence (80-90%). The culture was carried out in 25 cm^2, 75 cm^2 and 175 cm^2 culture bottles, as well as 96-well and 24-well plates were used. Cells were split upon reaching semi-confluence using 0.25% trypsin (Biomed Lublin S.A.) and versene (0.02% buffered with PBS; pH 7.6). Cells were seeded at a defined concentration:

- 96 well plates: 10^4 cells/100 µL,
- 24 well plates: 10^5 cells/mL.

Cell line	Cell growth medium	Reference
VERO E6	Minimum Essential Medium (1x) + GlutaMAX TM (Gibco) with addition of 10% FBS (Gibco), 5 mM pyruvate (Gibco), penicillin at final concentration of 100 U/mL (Gibco), streptomycin at final concentration of 100 U/mL (Gibco)	*Cercopithecus aethiops* monkey kidney epithelial cells (ATCC) (VERO C1008 [VERO 76, clone E6, VERO E6]) The base cell line in virology research
H226	RPMI Medium 1640 (1X) (Gibco) with addition of 10% FBS (Gibco), penicillin at final concentration of 100 U/mL (Gibco), streptomycin at final concentration of 100 U/mL (Gibco)	Human lung tumor (mesothelioma) epithelial cells (ATCC) (NCI-H226 [H226])
MSTO-211H	RPMI Medium 1640 (1X) (Gibco) with addition of 10% FBS (Gibco), penicillin at final concentration of 100 U/mL (Gibco), streptomycin at final concentration of 100 U/mL (Gibco)	Human lung tumor (biphasic mesothelioma) fibroblasts (MSTO-211H)

Calu-3	Eagle's Minimum Essential Medium (1X) (ATCC) with addition of 10% FBS (Gibco), 5 mM pyruvate (Gibco), penicillin at final concentration of 100 U/mL (Gibco), streptomycin at final concentration of 100 U/mL (Gibco)	Human lung tumor (adenocarcinoma) epithelial cells (ATCC) (Calu-3)

Table 5 Cell lines used in the research.

3.2.2. PBMC isolation

Peripheral blood mononuclear cells (PBMCs) are a heterogeneous population of immune cells that play a critical role in the body's defence against pathogens and foreign substances. These cells are composed of lymphocytes, monocytes, and dendritic cells, and are widely used as an *ex vivo* model of the immune response in many research studies (Baran et al., 2022). PBMCs can be isolated from buffy coats, and their isolation is performed using various techniques, including density gradient centrifugation and automated cell separation systems. In this study, PBMCs were isolated from buffy coats collected from healthy donors in Regional Centre for Blood Donation and Haemotherapy (Warsaw). The use of PBMCs as an *ex vivo* model of the immune response provides a valuable tool for investigating immune function and may have important implications for the development of new immunotherapeutic approaches. For the isolation, Ficoll®-Paque Premium reagent was applied. Ficoll is a widely used density gradient medium for the isolation of PBMC from whole blood samples or buffy coats. This method of isolation is important in many immunology studies, as PBMCs play a crucial role in the immune response to infections and diseases. Ficoll®-Paque Premium is a sterile, isotonic solution containing a colloidal suspension of micron-sized particles made of polysaccharide molecules (cytvia). When mixed with a blood sample, Ficoll®-Paque Premium separates the blood into layers according to density. PBMCs, which have a lower density than other blood cells, such as red blood cells and granulocytes, float to the top of the ficoll layer. Meanwhile, the more dense cells, such as neutrophils and erythrocytes, they are separated to the bottom of the tube. This separation method is based on the principle of centrifugation and is performed at a specific gravity of 1.077 g/mL. The isolated PBMCs are washed, counted, and used for various downstream applications, such as flow cytometry, ELISA, and cell culture. Prior to isolation, buffy coats were stored at room temperature.

Ficoll®-Paque Premium isolation:

1. Bags with buffy coats were gently mixed and placed under the laminar. Then, the suspension was transferred to 50 mL falcon tubes up to the 50% of the tube's volume. Tubes with cell suspension were then filled with growth medium (no additives).

2. 20 mL of Ficoll®-Paque Premium was transferred to empty and sterile 50 mL falcon tubes, taking particular care not to spread the solution over the walls of the tube.

3. 25 mL of the cell suspension from step 1 was transferred to ficoll tubes without mixing the two components with each other.

4. Tubes were centrifuged at 760×g for 20 min with the brakes OFF (Centrifuge 5910 R, Eppendorf).

5. The PBMC layer was then transferred using pipettes to sterile centrifuge tubes. PBMCs were washed three times with culture medium (no additives) using centrifugation at 350×g for 8 min with brakes ON.

3.2.3. PBMCs cryopreservation and thawing

Cryopreservation is crucial in preserving biological samples for long-term storage and analysis. It is particularly important in research involving human blood cells, as fresh samples can be difficult to obtain and can exhibit significant variability due to factors such as donor variability, handling, and storage conditions. The use of cryopreserved PBMCs provides a convenient and reliable source of cells for analysis, allowing for more extensive and comprehensive studies of the immune response. All of the samples used in the research were cryopreserved before the tests. After the last washing of the "*PBMC isolation*" procedure, the cell pellet was suspended in the freezing medium containing 20% of FBS and 10% of DMSO. The cryovials with suspension were placed into CellCamper® and stored overnight at -80°C. The cryovials were transferred to a low-temperature freezer (-150°C) for the long-term storage. Before the tests, PBMCs were thawed immediately, and the cell growth medium (warmed up at room temperature prior to use) was added dropwise till the duplicated volume was achieved. The cells were then centrifuged at 150×g for 5 min to remove DMSO from the suspension (Centrifuge 5910 R, Eppendorf).

3.2.4. PBMC culture

In the study, the cryopreserved PBMCs were used. Cells were seeded in a defined concentration:

- 96 well plates: 10^5 cells/100 µL of the cell growth medium,
- 24 well plates and Corning® Transwell® Inserts: $2.5 - 3 \times 10^6$ cells/mL of the cell growth medium.

PBMCs were cultured in Opti-MEM (Gibco) medium with 10% inactivated fetal bovine serum (FBS; Gibco) and incubated at 37°C with 5% CO_2. Depending on the experiment, the overnight rest was assessed. The time of the culture depended on the experiment length. Passages were not applied when PBMCs were mature and did not proliferate.

3.2.5. 3D co-culture model of human alveoli

One of the models used in the study is a 3D alveoli-like co-culture consisting of Calu-3 cells and PBMCs onto Corning® Transwell® Inserts. Transwell inserts are widely used *in vitro* systems that allow the co-culture of two different cell types separated by a porous membrane. In the case of studying the alveoli immune response, the Transwell insert with epithelial lung cells and PBMCs provides several benefits. The model brings insight into the alveolar cell interactions during an immune response.

For the experiment, 10^5 cells/mL of the Calu-3 cell line were seeded onto Corning® Transwell® Inserts (700 µL of cell growth medium under the insert, 300 µL of cell suspension onto the insert) and incubated for 72 h at 37°C with 5% CO_2. Then the culture medium above the Calu-3 monolayer was discarded to create air-liquid culture allowing the Calu-3 cells to form microvilli, which is related to the differentiation of the cells. Microvilli creation was monitored by SEM. This provides a more physiologically relevant model, as it mimics the *in vivo* architecture of the airway epithelium (Ji et al., 2022; Kreft et al., 2015). The cells were cultured for 14 days with the medium exchange every 72 h to stimulate the cell growth. After 14 days, the culture cell medium was switched to Opti-MEM, and PBMCs in the total volume of 700 µL ($2.5 - 3 \times 10^6$ cells/mL) were added to the liquid site of the culture. The model prepared in this way was immediately used for further experiments. A schematic representation of the model is shown in **Figure 14**.
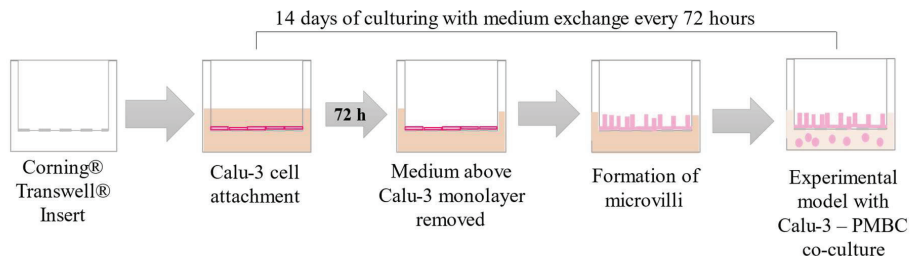
Figure 14 Schematic of human alveolar model containing Calu-3 and PBMCs.

3.2.6. Spearman-Kärber method of determining virus titer

The Spearman-Kärber method is a widely used statistical method for determining the titer of a virus, which represents the number of infectious particles in a given sample. This method was first introduced by Spearman in 1908 and later modified by Kärber in 1931, and has since become a standard technique in virology (Lei et al., 2021). The Spearman-Kärber method is based on the principle of endpoint dilution assay, which involves diluting a virus sample in a series of wells or tubes and determining the dilution at which 50% of the cells or animals inoculated with the virus become infected. This dilution is referred as the endpoint dilution, and the reciprocal of this dilution represents the virus titer. To calculate the virus titer using the Spearman-Kärber method, the data obtained from the endpoint dilution assay is analyzed using a statistical formula that takes into account the dilutions, the number of replicates, and the number of infected and uninfected cells or animals. This formula is based on the assumption that virus infectivity follows a binomial distribution and allows for the calculation of the titer with a high degree of accuracy and precision. Overall, the Spearman-Kärber method is a valuable tool for determining the virus titer and is widely used in the development and testing of vaccines, antiviral drugs, and other therapeutics (Añez et al., 2016).

Human betacoronavirus hCoV-OC43 was gathered from National Institute of Public Health-National Institute of Hygiene (NIPH-NIH). Cultures of hCoV-OC43 were handled in BSL-2 laboratory in CEZAMAT. The content of the ampoule containing virus suspension (approximately 0.4 mL) was transferred to a 75 cm^2 flask of VERO E6 or H226 cells. When 75 to 100% of cells showed cytopathic effect (CPE), the flask was transfered to < 0°C. The content of the flask was frozen and thawed (repeated two additional times), the semi-thawed content was shaken to ensure that all cells were disrupted. Then the cell debris

was centrifuged (Centrifuge 5910 R, Eppendorf). The supernatant was used for determination of the virus titer or frozen and stored at -80°C until use (WHO).

In order to determine the infectious titer of viruses according to Spearman-Kärber method (WHO), a viral suspension was applied to the cell monolayer and after 10 days the CPE was assessed. In this purpose, the virus-designed cells in concentration of 10^4 cells/100µL were seeded onto a 96-well plate (*Adherent cell culture*) and incubated for 18 h at 37°C with 5% CO_2. The cell monolayer was examined for quality (i.e. an entire monolayer of healthy cells), and absence of contamination as determined by inverted microscopic inspection. Then the series of virus dilutions was added onto the cell monolayer (typically starting from 10^{-1} to 10^{-6}, 20 wells per each concentration (**Figure 15**).
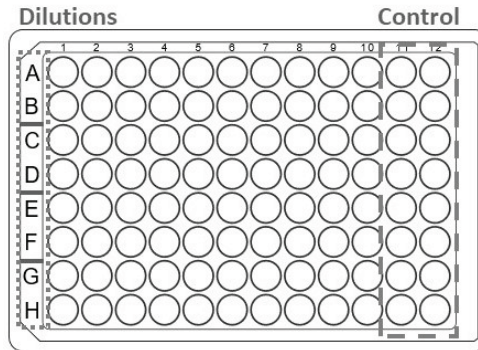
Figure 15 Plate scheme for Spearman-Karber method. Legend: Control means untreated monolayer of cells; Dilutions stands for virus suspension 10-fold diluted.

After ten days of incubation at 34.5°C with 5% CO_2, CPE was observed – compared to untreated control wells. Moreover, the inoculated culture was examined daily, using an inverted microscope, for the appearance of CPE. All of the wells with cytopathic effect were marked as "+", others as "-". The effect was documented photographically. The virus titer was calculated according to the Kärber formula (**Formula 1**):

$$log\ _{TCID50} = L - d \times (S - 0.5)$$

Formula 1

where:

L – log of lowest dilution used in the test

d – difference between successive dilutions in log

S – sum of proportion of "positive" wells (cytopathic effect observed) to all wells used for one dilution

3.2.7. Adenoviral vectors

Ad5/3-D24-ICOS-CD40L (AdV1; stock concentration of 3.2×10^3 TCID$_{50}$/mL) was obtained from the virus collection of the National Science Centre (NCN), MINIATURA project (2018/02/X/NZ7/00727) (Garofalo et al., 2021a). AdV1 is equipped with two powerful co-stimulatory molecules, namely inducible co-stimulator ligand (ICOSL) and CD40 ligand (CD40L, CD154), which can activate the immune system (**Figure 16**).
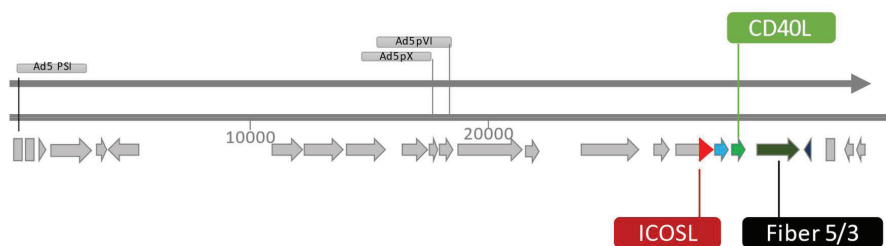
Figure 16 Schematic representation of genetic sequence of Ad5/3-D24-ICOS-CD40L. Abbreviations: ICOSL (Inducible T cell CO-Stimulator Ligand); CD40L (CD40 receptor Ligand); Fiber 5/3 (Fiberknob region of AdV1 and AdV2). Modified on the basis of (Garofalo et al., 2021a).

Inducible co-stimulator (ICOS) is a molecule similar to CD28 that is expressed on activated T cells and can interact with ICOSL found on dendritic cells (DCs), B lymphocytes, and some cancer cells. Moreover, the interaction of CD40, which is expressed on B cells, macrophages, and DCs, with CD40L can activate the immune system, leading to the development of CD8$^+$ cytotoxic T lymphocytes (CTLs) (Mohib et al., 2020). The reference for AdV1 was **AdV5/3-d24-E3** (AdV2; stock concentration of 7.7×10^{12} VP/mL) – an adenovirus with the same 5/3 serotype but without CD40L and ICOSL (Garofalo et al., 2021b). In the studies, both AdVs were used as immune response inducers (adjuvants) – alone and in combination with the proteins described below. The dissertation studies including genetically modified adenoviruses were performed at the Department of Genetic Engineering of National Institute of Public Health – National Institute of Hygiene established according to the decision of Ministry of the Environment, no. 196/2017 on December 12, 2017.

3.2.8. Recombinant Receptor Binding Domain protein

The recombinant protein (stock concentration of 0.1 mg/mL) was prepared by the team of Anna Mazurkiewicz-Pisarek PhD (Warsaw University of Technology) and delivered for the use in experiments of this research (Baran et al., 2023 accepted for publication). To create the recombinant Receptor Binding Domain (rRBD) gene, genetic engineering methods were utilized. The amino acid sequence was used to design the gene sequence for protein expression, and the specific region of the SARS-CoV-2 virus coding protein with the highest probability of inducing an immune response (amino acid 331-524 of SARS-CoV-2 S protein) was selected. The T4 folded protein (F4) was added to increase the probability of correct assembly of the protein tertiary structure. To facilitate purification, a tag was added at the N-terminus, allowing the use of a simple affinity chromatography method. The gene sequence was optimized for bacterial codon usage and ordered in the pUC57 vector. The vector was transformed into the *E. coli* DH5α competent cells and isolated. The vector was then digested with NdeI/XbaI restriction enzymes, and the resulting DNA fragment of 696 bp was isolated. The pDM vector was digested with the same enzymes and used for ligation with the DNA fragment. The resulting ligation mixture was transformed into *E. coli* NEB Turbo competent cells, and plasmid DNA was isolated from the bacterial colonies. The correctness of the DNA sequences was confirmed by sequence analysis, and the pDM/RBD expression vector was transformed by electroporation into *E. coli* competent cells. Growing conditions were set to 37°C for 1 h in LB medium supplemented with tetracycline (100 µg/mL). Recombinant RBD protein was obtained in inclusion bodies form, and the method for isolating inclusion bodies and purifying recombinant protein using Ni-NTA affinity chromatography was developed. In the studies, rRBD protein was used as an immune response inducer (antigen) – alone and in combination with adenoviral vectors.

3.2.9. Commercial spike and nucleocapsid proteins

Spike-S1-His is a recombinant protein created by InvivoGen (cat. code his-sars2-s1). It contains the S1 subunit of the spike protein from SARS-CoV-2, which is responsible for binding to the ACE2 receptor of host cells. The protein is modified with a histidine (His) tag at its C-terminus (InvivoGen). **Nucleocapsid-**His is another recombinant protein generated by InvivoGen (cat. code his-sars2-n). It contains the nucleocapsid protein from SARS-CoV-2, which is an internal protein that plays an essential role in viral replication and packaging. The protein is modified with a histidine (His) tag at its C-terminus (InvivoGen). In the studies, both proteins were used as an immune response inducers (antigens) – alone and in combination

with adenoviral vectors. However, although His-tags do not usually interfere with folding of the protein and guarantee that the protein is well purified, it has been reported that his-tagged antigens can alter humoral and cellular immune responses (Randolph, 2012). Spike-S1-His and Nucleocapsid-His were generated by recombinant DNA technology, produced in HEK293 cells, and purified by Ni^{2+} affinity chromatography (InvivoGen).

3.2.10. SARS-CoV-2 pseudovirus

Lentifect™ SARS-CoV-2 Spike is a type of pseudotyped lentivirus that uses the VS.V vector as a backbone (GeneCopoeia, USA). VS.V is a virus that carries a negatively charged RNA strand and enters cells with the help of the envelope glycoprotein G (Chen and Zhang, 2021). The VS.V-G envelope glycoprotein of VS.V was replaced with the S protein of the SARS-CoV-2 virus to create the pseudovirus. As a result, the pseudovirus can infect cells with the ACE2 receptor, including the VERO E6 cell line. Additionally, the SARS-CoV-2 pseudovirus encodes the luciferase gene from the *Photinus pyralis* firefly and Green Fluorescent Protein gene (eGFP), which allow to detect its entry into the cell. The successful neutralization of the pseudovirus by antibodies or antiviral compounds results in reductions in both the number of eGFP-expressing cells (indicating pseudovirus entry) and the level of luminescence (indicating successful inhibition of viral replication). Pseudovirus enters the ACE-2 expressing cell by membrane fusion and then integrates luciferase and eGFP genes with the cell genome. To measure the luciferase activity there is a need to provide a substrate for that enzyme. eGFP analyzis do not require additional reagents – just laser excitation (https://www.genecopoeia.com/). SARS-CoV-2 pseudovirus was used as the inducer of immune response and for the studies concerning inhibition of the virus internalization (expression of eGFP studied using CLSM). Cultures of pseudo-SARS-CoV-2 were handled in BSL-2 laboratory in CEZAMAT.

3.2.11. SARS-CoV-2 spike antibody

'SARS-CoV-2 Spike Antibody' (Ab; stock concentration of 1 mg/mL; Genecopoeia) an antibody directed for the SARS-CoV-2 spike protein. Ab was used in the virus internalization studies.

3.3. Scanning Electron Microscope (SEM) imaging of hCoV-OC43, AdV1 and Calu-3 microvilli

3.3.1. Imaging of virus on cell monolayer

SEM is a powerful imaging technique that is well-suited for visualizing the morphology and structure of viruses. In this study, SEM was used as a visualization method of individual virus particles. For the experiment, a 12-well plate containing a cell culture membrane and a 24-well plate containing glass slides were used. VERO E6 and H226 suspensions were added to 12-well plates at a density of 10^4 cells/mL of cell growth medium. A suspension of VERO E6 cells at a density of 10^5 cells/mL of cell growth medium was added to a 24-well plates containing glass slides. After 15 days of incubation at 37°C with 5% CO_2, the cell growth medium was discarded. Two types of samples were analyzed:

- the infectious titer of the OC43 virus in 500 μL of culture medium (5% FBS) onto the VERO E6 cell monolayer (2.84×10^8 VP/mL),
- 100 VP/mL of AdV1 in 500 μL of culture medium (5% FBS) onto the H226 cell monolayer.

After 48 h of incubation at 34.5°C with 5% CO_2, the following sequence of washes (1 mL per insert of each reagent) and incubation conditions were performed:

1. 5% glutaraldehyde in 0.1 M phosphate buffer, pH 7.2 for 24 h at 4°C,
2. 0.1 M phosphate buffer for 10 min at room temperature (RT) x 3 times,
3. 1% osmium tetroxide in 0.1 M phosphate buffer for 1-2 h at RT,
4. Distilled water for 10 min at RT x 2 times,
5. 35% ethanol for 15 min at RT,
6. 50% ethanol 15 min at RT,
7. 75% ethanol 15 min at RT,
8. 95% ethanol 15 min at RT.

After fixation, membranes were cut out from the 12-well plate, and coverslips were removed from the 24-well plate. Membranes and coverslips were then coated with a mixture of gold and palladium and visualized using SEM (Hitachi SU8230).

3.3.2. Imaging of the Calu-3 cell culture on Corning® Transwell® Inserts

The study focused on the SEM imaging of the Calu-3 cell line grown as an air-liquid 3D culture onto Corning® Transwell® Insert showing the formation of cilia-like structures on its

surface. For the experiment, the untreated Calu-3 samples onto Corning® Transwell® Insert prepared according to the "*Immune response models*" were used. The following washes (1 mL of each reagent per insert) were performed:

1. 5% glutaraldehyde in 0.1 M phosphate buffer, pH 7.2 for 24 h at 4°C,

2. 0.1 M phosphate buffer for 10 min at room temperature (RT) x 3 times,

3. 1% osmium tetroxide in 0.1 M phosphate buffer for 1-2 h at RT,

4. Distilled water for 10 min at RT x 2 times,

5. 35% ethanol for 15 min at RT,

6. 50% ethanol 15 min at RT,

7. 75% ethanol 15 min at RT,

8. 95% ethanol 15 min at RT.

After fixation, membranes were cut out from the Corning® Transwell® Inserts. Membranes were then coated with a mixture of gold and palladium and visualized using SEM (Hitachi SU8230).

3.4. Virus Particles quantification

One way to quantify the number of virus particles (VP) presented in a sample is the method based on the estimation of the amount of viral RNA presented in the sample. This method is based on the assumption that there is a fixed ratio of viral RNA to VP, and therefore, the amount of viral RNA can be used as a proxy for the number of VP. To quantify the amount of viral RNA, the sample was first lysed, which released the RNA into solution. Then, the measurement of the absorbance at 260 nm was performed. The dilutions of the viral suspension were prepared in Virus Lysis Buffer (VLB: 9.75 mM Tris-EDTA pH 7.5 + 0.5% SDS) according to **Table 6**.

Dilution factor	Volume of viral suspension	VLB buffer volume
1:3	33 μl	67 μl
1:5	20 μl	80 μl
1:10	10 μl	90 μl
1:50	2 μl	98 μl
1:100	1 μl	99 μl

Table 6 Scheme for preparing dilutions of viral suspension in VLB buffer (9.75 mM Tris-EDTA at pH 7.5 + 0.5% SDS) for determining the amount of VP.

The blank sample was prepared using 100 μl of the VLB buffer. VP dilutions and blank were incubated at 95°C for 15 min. Spectrophotometric analysis of the tested samples was performed after a short centrifugation at 1,500 rpm for 10 s (Centrifuge 5910 R, Eppendorf). Spectrophotometric analysis was performed using the Spark automatic plate reader (Tecan, Switzerland), for wavelengths of 260 nm and 280 nm. Blank values were subtracted from the test results. The VP number was averaged for dilutions for which the A260/A280 values were similar to the range of 1.2 – 1.4, VP was determined according to the **Formula 2**:

$$VP = A_{260} \times dilution\ factor \times 1.1 \times 10^{12} \left[\frac{VP}{mL}\right]$$

Formula 2

Where:

A_{260} – absorbance at 260 nm

1.1×10^{12} – extinction coefficient

3.5. Virus internalization study using Confocal Laser Scanning Microscopy imaging

The experiment using Confocal Laser Scanning Microscopy (CLSM) was carried out to determine whether the "SARS-CoV-2 Spike Antibody" and components of the vaccine platform: a mixture of rRBD protein with AdV1 at tested concentrations reduce the penetration of the SARS-CoV-2 pseudovirus into the VERO E6 cells. In this experiment, the tested concentration of "SARS-CoV-2 Spike Antibody" and rRBD protein was twice of the IC50 value (GeneCopoeia). The VERO E6 cells were used as a negative control, and a positive control was examined by adding the SARS-CoV-2 pseudovirus to the VERO E6 cells at the tested concentrations. The decreased internalization of the SARS-CoV-2 pseudovirus into the cells was indicated by the decrease in the intensity of eGFP-induced fluorescence produced by the VERO E6 cells after the incubation with the virus, compared to the positive control containing the VERO E6 cells and SARS-CoV-2 pseudovirus. Hoechst 33342 dye was used to stain live and dead cells, and propidium iodide was used to show dead cells.

3.6. Cell metabolic activity assay

Assessing the metabolic activity and viability of cells is a critical aspect of many experimental studies, as it provides important information on cellular responses to different stimuli, including immunogenic factors. One commonly used approach for evaluating cellular viability is the 3-(4,5-dimethylthiazol-2-yl)-5-(3-carboxymethoxyphenyl)-2-(4-sulfophenyl)-

2H-tetrazolium (MTS) assay. It is based on the conversion of MTS into a colored formazan product by active mitochondria in living cells. The amount of the produced formazan is proportional to the number of metabolically active cells present in the sample. In this study, the MTS assay was used to evaluate the metabolic activity of cells in response to the immunogenic factors. The results of this assay can be used to draw conclusions about the efficacy of immunogenic factors in promoting or inhibiting cellular activity and to estimate their cytotoxicity. The cells in concentration of $10^4/100$ μL (adherent cells) or $10^5/100$ μL (PBMCs) of culture medium were seeded in triplicates in the 96-well plate (*"Cell culture"*) and left overnight at 37°C with 5% CO_2. Then, the cells were treated with the immunogenic factors for 18 h at 34.5°C with 5% CO_2. Untreated cells were used as controls. Then the metabolic activity of the cells was evaluated using the MTS assay kit, according to the manufacturer's instruction (Promega G3582, CellTiter 96® AQueous One Solution Cell Proliferation Assay). Briefly, after the incubation of cells with the immunogenic factors, 20 μl of MTS solution was added to each well and incubated at 37°C with 5% CO_2 for 2 h. The absorbance was measured at a wavelength of 490 nm using a microplate reader.

The following experiments were conducted:

1. Series of dilutions of AdV1 and rRBD alone and in combination (subsequent dilutions 1-8 together) were added to the VERO E6 cell monolayer (three technical replicates in three biological replicates). The concentrations are presented in **Table 7**. The experiment determined the appropriate concentrations for further testing.

Nr	AdV1 [VP/mL]		rRBD [μg/mL]
1	5.20×10^9		5.24
2	5.20×10^8		5.24×10^{-1}
3	5.20×10^7		5.24×10^{-2}
4	5.20×10^6	AdV1 and rRBD alone or in combination	5.24×10^{-3}
5	5.20×10^5		5.24×10^{-4}
6	5.20×10^4		5.24×10^{-5}
7	5.20×10^3		5.24×10^{-6}
8	5.20×10^2		5.24×10^{-7}

Table 7 Concentrations of AdV1 and rRBD applied to study the VERO E6 cell metabolic activity. Every number is a treatment for one well in three technical replicates. Legend: AdV1 stands for serotype 5/3 equipped with ICOSL and CD40L (Garofalo et al., 2021a). rRBD stands for recombinant receptor binding domain protein (Baran et al., 2023 accepted for publication).

2. Different concentrations of pseudo-SARS-CoV-2 were used to treat the VERO E6 cell monolayer (three technical replicates in three biological replicates). The concentrations are presented in **Table 8**.

3. The experiment was performed to determine the appropriate concentrations for further testing.

Pseudo-SARS-CoV-2 [RFU/mL]
>0.000001
>1000
>100
>10

Table 8 Concentrations of pseudo-SARS-CoV-2 to study the VERO E6 cell metabolic activity. Legend: Pseudo-SARS-CoV-2 stands for pseudotyped lentivirus (Genecopeia, USA). RFU stands for relative fluorescence units.

4. A complete set of the treatments used for further experiments with the PBMCs (three technical replicates in three biological replicates) are presented in **Table 9**.

Immunogenic factor	Concentration
LPS	0.25 µg/mL
AdV1	
AdV2	100 VP/mL
Pseudo-SARS-CoV-2	
hCoV-OC43	
rRBD	2.62 µg/mL
Spike-S1-His	0.25 µg/mL
Nucleocapsid-His	0.25 µg/mL
AdV1+rRBD	100 VP/mL+2.62 µg/mL
AdV2+rRBD	100 VP/mL+2.62 µg/mL
rRBD+Ab	2.62 µg/mL+2.62 µg/mL
Pseudo-SARS-CoV-2+Ab (IC100)	100 VP/mL+5.62 µg/mL

Table 9 Concentrations of different immunogenic factors used to study PBMC metabolic activity. Legend: LPS stands for bacterial lipopolysaccharide. AdV1 stands for 5/3 serotype equipped with ICOSL and CD40L (Garofalo et al., 2021a). hCoV-OC43 means human betacoronavirus. rRBD stands for recombinant receptor binding domain protein (Baran et al., 2023 accepted for publication). ADV2 stands for serotype 5/3 without ICOSL and CD40L (Garofalo et al., 2021a). Pseudo-SARS-CoV-2 stands for pseudotyped lentivirus (Genecopeia, USA). Spike-S1-His and Nucleocapsid-His mean recombinant protein (InvivoGen, USA).

3.7. PBMC exposed to the immunogenic factors (24-h experiments using 2D model)

PBMCs were seeded onto 24-well plates (Section 3.2.4.) for the overnight rest incubation at 37°C with 5% CO_2. Then, the cell growth medium was replaced by 1 mL/well of the OptiMEM medium with reduced FBS concentration (5% v/v) and the immunogenic factors were added in concentrations showed in Table 10. All treatments were performed in triplicates. Plates were incubated for 24 h at 34.5°C with 5% CO_2 and then cells were collected for the immunophenotyping (Section 3.10.). The cell growth medium was collected and stored at -80°C (cryopreservation for the cytokine profiling; Section 3.12.).

Immunogenic factor	Concentration
LPS	0.25 µg/mL
AdV1	
AdV2	100 VP/mL
Pseudo-SARS-CoV-2	
hCoV-OC43	
rRBD	2.62 µg/mL
AdV1+Spike-S1-His	100 VP/mL+0.25 µg/mL
AdV1+Nucleocapsid-His	100 VP/mL+0.25 µg/mL
AdV1+Spike-S1-His+Nucleocapsid-His	100 VP/mL+0.25 µg/mL+0.25 µg/mL
AdV1+rRBD	100 VP/mL+2.62 µg/mL
AdV2+rRBD	100 VP/mL+2.62 µg/mL
rRBD+Ab	2.62 µg/mL+2.62 µg/mL
Pseudo-SARS-CoV-2+Ab	100 VP/mL+5.62 µg/mL

Table 10 Concentrations of different immunogenic factors and viruses used in the immune response preliminary studies (24-h experiment). Legend: LPS stands for bacterial lipopolysaccharide. AdV1 stands for serotype 5/3 equipped with ICOSL and CD40L (Garofalo et al., 2021a). hCoV-OC43 means human betacoronavirus. rRBD stands for recombinant receptor binding domain protein (Baran et al., 2023 accepted for publication). ADV2 stands for serotype 5/3 without ICOSL and CD40L (Garofalo et al., 2021a). Pseudo-SARS-CoV-2 stands for pseudotyped lentivirus (Genecopeia, USA). Spike-S1-His and Nucleocapsid-His mean recombinant protein (InvivoGen, USA).

3.8. 7-day exposition of PBMCs to the immunogenic factors with increased AdV1 concentrations (7-day experiment using 2D model)

To stimulate higher immune response, the increased concentration of adjuvant in the form of AdV1 was assessed. PBMCs were seeded into the 24-well plates (Section 3.2.4.) in triplicates to study all of the immunogenic factors and left for the overnight rest incubation at 37°C with 5% CO_2. Then, the cell growth medium was replaced by 1 mL/well of the OptiMEM medium with reduced FBS concentration (5% v/v) and the immunogenic factors were added in the concentrations showed in **Table 11.** Plates were incubated for 7 days at 34.5°C with 5% CO_2 and then the cells were collected for the immunophenotyping and apoptosis assay. The cell growth medium was collected and stored at -80°C (cryopreservation for the cytokine profiling).

Immunogenic factor	Concentration
Untreated control	
AdV1	100 VP/cell
Spike-S1-His	0.25 µg/mL
Nucleocapsid-His	0.25 µg/mL
AdV1+Spike-S1-His+Nucleocapsid-His	100 VP/cell+0.25 µg/mL+0.25 µg/mL

Table 11 Concentrations of different immunogenic factors and viruses used in the immune response preliminary studies (7-day experiment). Legend: AdV1 stands for serotype 5/3 equipped with ICOSL and CD40L (Garofalo et al., 2021a). Spike-S1-His and Nucleocapsid-His mean recombinant protein (InvivoGen USA).

3.9. Immune response of PBMCs using 3D co-culture model of human alveoli

The development of effective immune response models is crucial to prevent the spread of infectious diseases and protect public health. The process of vaccine development involves testing the immunogenicity of various factors to ensure a robust immune response. In this study, the immunogenic factors were added to cell growth medium including PBMCs located under the insert with the human lung epithelial cell line (Calu-3), and plates were incubated to assess their effect on the immune response. The schematic representation of the experiment is shown in **Figure 17**.
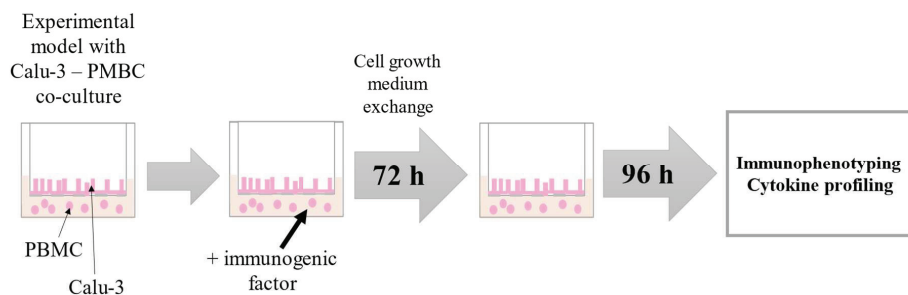
Figure 17 Schematic presentation of the PBMCs' response to the immunogenic factors in 3D co-culture model of the human alveoli experiment.

Immunogenic factors representing the vaccination process were added to the cell growth medium (OptiMEM with 5% of FBS) including PBMCs located under the insert. The incubation was performed for 72 h at 34.5°C with 5% CO_2 (**Table 12**). After 72 h incubation, PBMCs were rinsed and returned to the wells in the fresh culture medium without the immunogenic factors for the next 4 days of incubation at 34.5°C with 5% CO_2, and PBMCs were collected to perfrom the immunophenotyping and apoptosis assay. The cell growth medium was used to assess the cytokine profiling, the untreated Calu-3 inserts standing as the control were used in the SEM analysis. Every individual treatment was repeated at least three times, the appropriate controls were included without the immunological factors (named vaccination), and untreated (control). The concentrations used in the experiments are shown in **Table 12**. Different models applied are represented in **Table 13**.

Immunogen	Concentration / infectivity
AdV1	100 VP/cell
Spike-S1-His	0.25 µg/mL
Nucleocapsid-His	0.25 µg/mL

Table 12 Concentrations of immunogens used in the 3D model experiment. Legend: AdV1 stands for serotype 5/3 equipped with ICOSL and CD40L (Garofalo et al., 2021a). Spike-S1-His and Nucleocapsid-His mean recombinant protein (InvivoGen, USA).

Nr	Immunogenic factor ("vaccination")	Comment
1	-	Untreated control
2	AdV1+Spike-S1-His	Vaccination without infection - control
3	AdV1+Nucleocapsid-His	
4	AdV1+Spike-S1-His+Nucleocapsid-His	
5	AdV5 wild type	Wild type adenovirus - control

Table 13 Different experimental approaches to assess the immune response using the 3D co-culture model of human alveoli. Legend: AdV1 stands for 5/3 serotype equipped with ICOSL and CD40L (Garofalo et al., 2021a). Spike-S1-His and Nucleocapsid-His mean recombinant protein (InvivoGen USA). AdV5 stands for wild type adenovirus serotype 5.

3.10. Immunophenotyping

Immunophenotyping is a technique that is commonly used to identify and characterize different types of cells in a biological sample, based on the expression of cell surface markers. This method involves labeling cells with specific antibodies that bind to unique cell surface molecules, and analyzing the resulting fluorescence using flow cytometry. In this study, the development and use of three antibody panels for immunophenotyping of PBMCs were assessed. The composition of each panel is optimized for the full picture of cellular and humoral response. The resulting data provide valuable insights into the immune cell populations present in the samples treated with different immunogenic factors, allowing the analysis of the immune response.Cell staining was performed according to the manufacturer's protocol (BD Biosciences, USA). Briefly, the 50 µL of the antibodies mixture was added to 50 µL of the PBMC suspension containing 10^6 cells. Three panels of antibodies were developed, they were described in **Tables 14**, **15**, and **16**. The suspension was then mixed, incubated for 30 min and protected from light at room temperature. After the incubation, the cells were washed twice. Two milliliters of BD® Cell WASH were added do each tube, and the cells were centrifuged at 150×g for 5 min (Centrifuge 5910 R, Eppendorf). The each cell pellet was suspended in 250 µL of BD® Cell WASH and flow cytometry analysis was performed.

	PANEL 1							
Detector	**BB515**	**PE**	**PerCP**	**PE-Cy7**	**APC**	**APC-H7**	**Brilliant™ Stain Buffer**	**Stain Buffer (FBS)**
Cell receptor	CD197	CD95	CD8	CD4	CD45RA	CD3	-	-
Catalogue number (BD Biosciences)	566764	555674	345774	557852	550855	560176	566349	554656
Volume per 1 sample tube [µL]	2,50	10,00	10,00	2,50	10,00	2,50	10,00	2,50

Table 14 Phenotyping mixture ingredients (Panel 1).

PANEL 2

Detector	BB515	PE	BB700	PE-Cy7	APC	APC-H7	Brilliant ™ Stain Buffer	Stain Buffer (FBS)
Cluster of differentiation	CD24	CD38	CD19	IgD	CD27	CD20	-	-
Catalogue number (BD Biosciences)	564521	555460	566396	561314	558664	335829	566349	554656
Volume per 1 sample tube [µL]	2,50	10,00	2,50	2,50	10,00	2,50	10,00	10,00

Table 16 Phenotyping mixture ingredients (Panel 2).

PANEL 3

Detector	BB515	PE	BB700	PE-Cy7	APC	APC-H7	Brilliant™ Stain Buffer	Stain Buffer (FBS)
Cluster of differentiation	IgM	CD38	CD19	IgD	CD27	IgG	-	-
Catalogue number (BD Biosciences)	564422	555460	566396	561314	558664	561297	566349	554656
Volume per 1 sample tube [µL]	2,50	10,00	2,50	2,50	10,00	2,50	10,00	10,00

Table 17 Phenotyping mixture ingredients (Panel 3).

Analyzes were performed using a BD FACSLyric ™ Flow Cytometry System. Before each series of analyzes, the Performance QC protocol was conducted as recommended by the supplier. Gating strategies and hierarchy are shown in **Figures 18-21**.
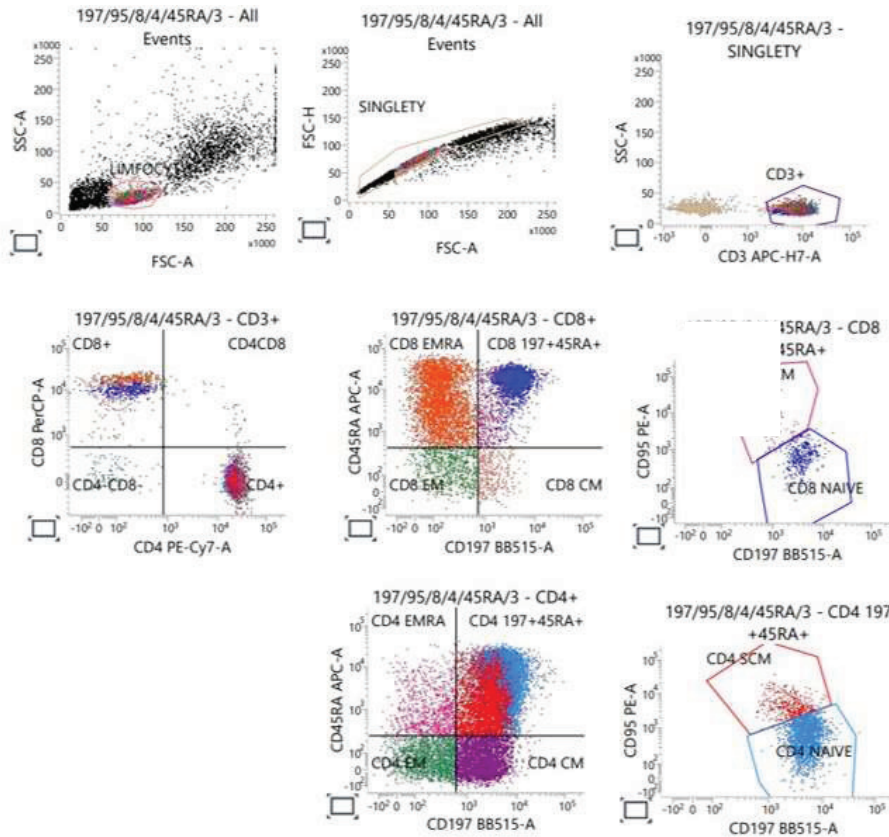
Figure 18 Gating strategy for "Panel 1" of immunophenotyping.
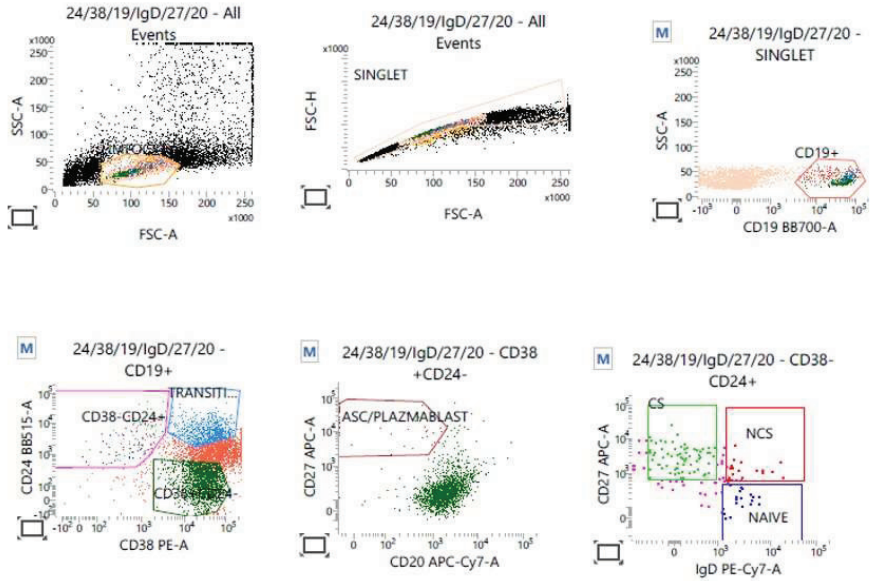
Figure 19 Gating strategy for "Panel 2" of immunophenotyping.
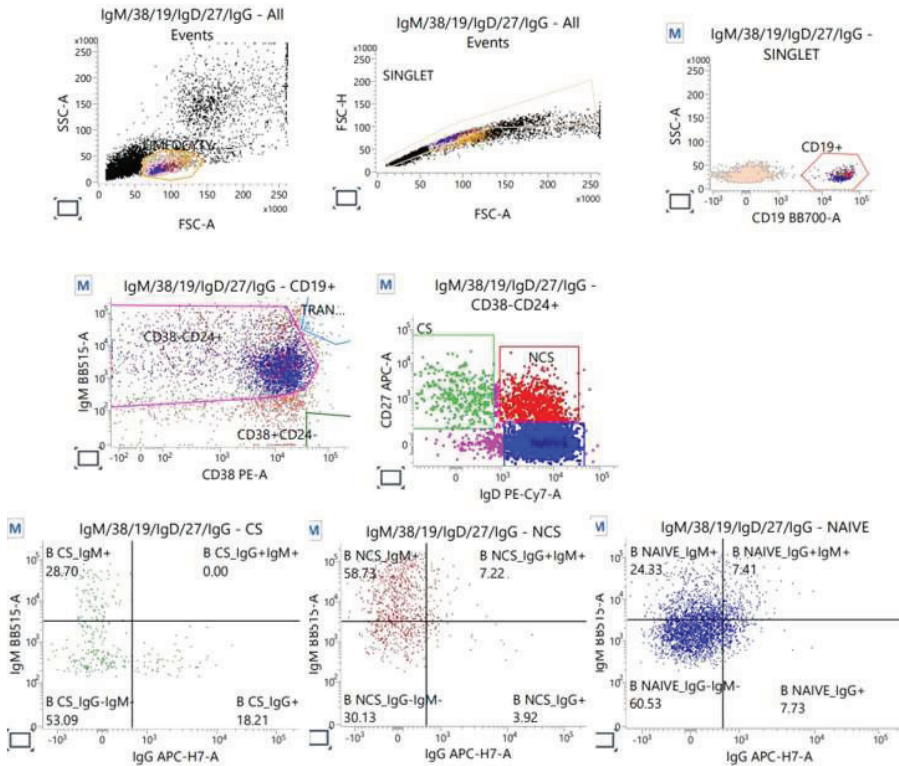
Figure 20 Gating strategy for "Panel 3" of immunophenotyping.

3.11. Apoptosis assay

In the context of studying immunogenic factors, the apoptosis assay is an important tool to assess the effect of these factors on cell death. The assay can determine whether the immunogenic factors trigger programmed cell death, and if so, through which pathway. This assay provides important information on the effect of immunogenic factors on cell viability and apoptosis, which is crucial for understanding the immune response.

In the apoptosis assay, the following solutions were used (BD Biosciences, USA):

- 10X Binding Buffer (cat. no. 556454): 0.1 M HEPES, pH 7.4; 1.4 M NaCl; 25 mM CaCl$_2$,
- BD® Cell WASH (cat. no. 349524),
- Propidium Iodide (PI, cat. no. 556463),
- Annexin V-FITC (cat. no. 556420, 556419).

The cell staining was performed according to the manufacturer's protocol. PBMCs were collected, washed with cold BD® Cell WASH and suspended in 1X Binding Buffer (BD Biosciences, USA) at a concentration of 1x 10^6 cells/mL. Then, 100 µL of the cell suspension (about 10^5 cells/100 µL) was transferred to a 5 mL tube. PI (0.5 µL) and Annexin V-FITC (2.5 µL) were added to a suspension and incubated for 15 min (protected from light). Then, 400 µL of 1X Binding Buffer was added. Analyzes were performed using a BD FACSLyric™ Flow Cytometry System (BD Biosciences, USA). Before each series of analyzes, the Quality Control protocol was performed as recommended by the supplier (BD Biosciences, USA). Gating strategy is shown in **Figure 21**.
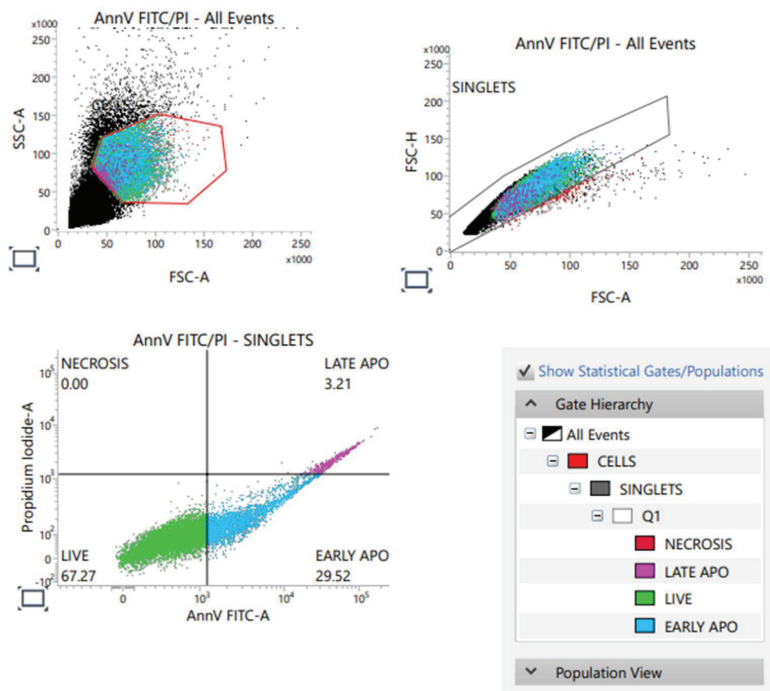
Figure 21 Gating strategy for Apoptosis assay.

3.12. Cytokine profiling

The levels of cytokines produced by immune cells indicate the activation status of the immune system. Therefore, cytokine profiling has become an important tool in the study of immunogenic factors and their effect on the immune cell function. This approach enables the simultaneous quantification of multiple cytokines in a single sample, providing a comprehensive view of the cytokine profile in response to the immunogenic factors.

The culture medium of the immunostimulated PBMC cell suspensions in 3D models were examined for the profile of cytokines. The cell supernatant after first centrifugation before the cell wash was cryopreserved and stored at -80°C until analysis (Centrifuge 5910 R, Eppendorf). Freshly thawed culture medium was diluted 100 times in the Assay buffer (BD Biosciences, USA), followed by the procedure according to the manual instruction of BD Cytometric Bead Array (CBA) Human Soluble Protein Master Buffer Kit:

1. Preparing Human Flex Set Standards

- Lyophylized standards were pooled into 15 mL centrifuge tube labeled as Top Standard (Centrifuge 5910 R, Eppendorf).

- 4 mL of the Assay Diluent were added to the tube. After 15 min incubation at room temperature the suspension was mixed by gently pipetting 4-5 times.

500 µL of the Assay diluent were pipetted to twelve cytometric tubes labelled as in **Figure 22** and Top standard was serially diluted. The standards' concentrations in each Standard tube were presented in **Table 18**.
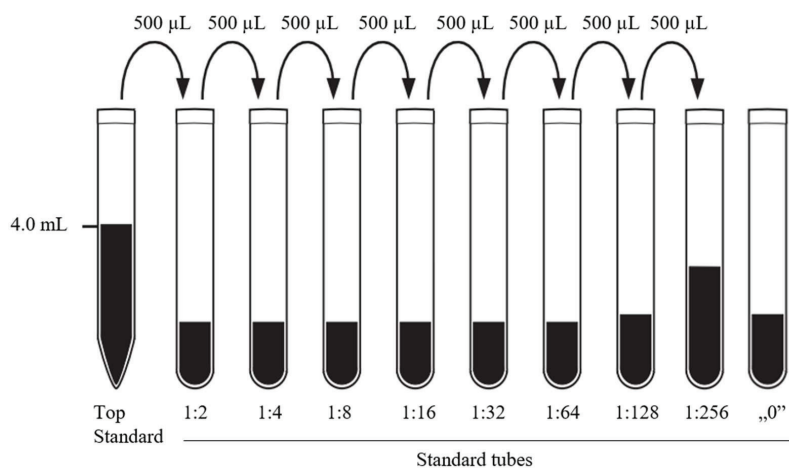
Figure 22 Preparation of Standard tubes. "0" stands for negative control. As negative control Assay buffer was used. Modified on the basis of: [BD CBA Human Soluble Protein Master Buffer Kit Instruction manual].

Dilution	Standard tubes									
	Top standard	1:2	1:4	1:8	1:16	1:32	1:64	1:128	1:256	0
Protein concentration [pg/mL]	2,500	1,250	625	312.5	156	80	40	20	10	0

Table 18 Protein concentration in Standard tubes.

2. Mixing Human Soluble Protein Flex Set Capture Beads

- Vials with capture beads were vortexed for 15 s to achieve uniform suspension.
- Volumes of the reagents were calculated as follows:

$$V_{Mixed\ Capture\ Beads} = n \times 50\ \mu L$$

Where:

$V_{Mixed\ Capture\ Beads}$ stands for the final volume of capture beads suspension

n stands for number of the assay tubes, including standards.

Individual Capture Beads are added following the rule 1.0 µL per test.

$$V_{Capture\ Beads\ Diluent} = V_{Mixed\ Capture\ Beads} - n \times 1\ \mu L$$

The appropriate volumes of each capture beads (**Table 18**) were pipetted into a tube labeled Mixed Capture Beads.

Cytokine name	Catalogue number (BD Biosciences)
Human TNF	558273
Human IFN-γ	558269
Human IL-1α	560153
Human IL-1β	558279
Human IL-2	558270
Human IL-4	558270
Human IL-6	558276
Human IL-8	558277
Human IL-10	558274
Human IL-12p70	558283
Human 17A	560383
Human IL-17F	562151

Table 19 List of cytokines used in flow cytometry assay.

3. Preparing Human Soluble Protein Flex Set PE Detection Reagents

- Using the calculations from the point 2, Human Detection Reagents were prepared:

$$V_{Mixed\ Capture\ Beads} = V_{Human\ Detection\ Reagents};$$

$$V_{Capture\ Beads\ Diluent} = V_{Detection\ Reagent\ Diluent}.$$

- The appropriate volumes were pipetted into a tube labeled Mixed PE Detection Reagents and stored at 4°C, protected from light until use.

4. Assay procedure

- 50 µL of Flex Set Standard dilutions (**Table 17**) were added to the labeled tubes (1-10) according to increasing concentration.

- 50 µL of each unknown samples were added to the separate test labeled tubes (11-X).

- Mixed Capture Beads were vortexed for 5 s.

- 50 µL of the Mixed Capture Beads were added to the assay tubes (test and standard tubes). The samples were then gently mixed.

- Assay tubes were incubated for 1 h at room temperature, protected from the light.

- 50 µL of the Mixed PE Detection Reagents were added to all assay tubes. The tubes were then gently mixed.

- Assay tubes were incubated for 2 h at room temperature (RT), protected from the light.

- 1 mL of the Wash Buffer was added to assay tubes. Tubes were centrifuged at 200 *g* for 5 min (Centrifuge 5910 R, Eppendorf).

- The supernatants were discarded from assay tubes.

- 300 µL of the Wash Buffer was added to each assay tube. Tubes were vortexed before the analysis.

5. Acquisition of the samples using the flow cytometer. Analyzes were performed using a BD FACSLyric ™ Flow Cytometry System. Data was analyzed using FCAP Array v 3 software (BD Biosciences, USA).

3.13. CD40 gene expression using RT-qPCR

CD40 is a key protein in the immune response, playing a critical role in the activation and differentiation of B cells, as well as the maturation of dendritic cells. To study CD40 gene expression in the context of immune response, RT-qPCR was performed.

The VERO E6 cells were seeded onto 24 well plates in triplicates as described in Section 3.2.1. Then, the cell growth medium was replaced with solutions of different immunogenic factors in the cell culture medium with reduced FBS and without antibiotics (MEM with 5% FBS v/v). Concentrations of the tested factors were shown in **Table 20**.

RNA was extracted from the cell pellets using Total RNA Mini Kit (A&A Biotechnology, Gdansk, Poland) and reverse-transcribed using High-Capacity cDNA Reverse Transcription Kit with RNase Inhibitor (ThermoFisher Scientific, Waltham, USA). RNA and cDNA were measured with two complementary methods – NanoQuant plate, Spark plate reader (Tecan, Switzerland) and Qubit Fluorometric Quantification (Thermo Fisher Scientific Inc., USA) (described in Paragraph 3.14).

cDNA was diluted to obtain similar levels of the GAPDH reference gene, then 1 µL was added to 20 µL of the PCR reactions containing random primers, MultiScribe™ Reverse, Transcriptase, and buffer (ThermoFisher Scientific, Waltham, USA, Cat. 4374966). RT-qPCR was performed using a CFX96 (Bio-Rad, USA) for 5 min at 95°C followed by 45 cycles of 95°C for 30 s, 61°C for 1 min, 72°C for 1 min, and melting at 50–95°C. The sequences of the primers is shown in **Table 20**. The GAPDH reference gene was run together with each target to normalize target gene levels relative to mRNA levels.

Gene name	Primer	
GAPDH *Housekeeping gene*	Forward	5'TGGACTCCACGACGTACTCA3'
	Reverse	5'ATGCTGCATTCGCCCTCTT3'
CD40 *Gene of interest*	Forward	5'GAGGCTGCAAATGGAAGTGC3'
	Reverse	5'GCTGCTGGAGTCCCCATATC3'

Table 20 Primer sequences for RT-PCR. Legend: GAPDH stands for glyceraldehyde 3-phosphate dehydrogenase. CD40 means cluster of differentiation 40, a type I transmembrane protein found on antigen-presenting cells.

Immunogenic factor	Concentration
Untreated control	
AdV1	50 VP/mL
	100 VP/mL
AdV2	50 VP/mL
	100 VP/mL
rRBD	2.62 µg/mL
	5.24 µg/mL
AdV1 + rRBD	50 VP/mL + 2.62 µg/mL
	100 VP/mL + 5.24 µg/mL
AdV2 + rRBD	50 VP/mL + 2.62 µg/mL
	100 VP/mL + 5.24 µg/mL
pseudo-SARS-CoV-2	50 VP/mL
	100 VP/mL
AdV1 + pseudo-SARS-CoV-2	50 VP/mL + 50 VP/mL
	100 VP/mL + 100 VP/mL
AdV2 + pseudo-SARS-CoV-2	50 VP/mL + 50 VP/mL
	100 VP/mL + 100 VP/mL
pseudo-SARS-CoV-2 + Ab	50 VP/mL + 2.62 µg/mL
	100 VP/mL + 5.24 µg/mL
rRBD + Ab	2.62 µg/mL + 2.62 µg/mL
	5.24 µg/mL + 5.24 µg/mL
hCoV-OC43	50 VP/mL
	100 VP/mL

Table 21 Concentrations of immunogenic factors used for the CD40 gene relative expression analysis. Legend: AdV1 stands for 5/3 serotype equipped with ICOSL and CD40L (Garofalo et al., 2021a). hCoV-OC43 means human betacoronavirus. rRBD stands for recombinant receptor binding domain protein (Baran et al., 2023 accepted for publication). ADV2 stands for serotype 5/3 without ICOSL and CD40L (Garofalo et al., 2021a). Pseudo-SARS-CoV-2 stands for pseudotyped lentivirus (Genecopeia, USA). Spike-S1-His and Nucleocapsid-His mean recombinant protein (InvivoGen, USA).

A minimum of 3 technical repetitions were used for each sample. The results were analyzed and the relative fold gene expression was calculated as follows **(Formula 3 – 5):**

1. Calculating ΔCT for each sample:

$$\Delta CT = (CT_{CD40}) - (CT_{GAPDH})$$

(3)

CT_{CD40} and CT_{GAPDH} – Average Ct values for any technical replicates

2. Selecting calibrator sample and calculating $-\Delta\Delta CT$:

$$-\Delta\Delta CT = -\left((\Delta CT_{CD40}) - (\Delta CT_{VERO\ E6})\right)$$

(4)

3. Calculate the fold gene expression values:

$$Fold\ gene\ expression = 2^{-\Delta\Delta CT}$$

(5)

3.14. RNA-seq sample preparation

RNA was extracted from cell pellets using Total RNA Mini Kit (A&A Biotechnology, Gdansk, Poland) and measured with two complementary methods – on NanoQuant plate, Spark plate reader (Tecan, Switzerland) and Qubit Fluorometric Quantification (Thermo Fisher Scientific Inc., USA). RNA samples were stored at -80°C and shipped in dry ice within 24 h to CeGaT GmbH (Tübingen, Germany).

RNA quantification using Spark plate reader capabilities

RNA was measured using NanoQuant plate and Nucleic Acid Quantitation application. Firstly, based on the number of samples, wells on the plate were selected and procedure appropriate for RNA was chosen. Individual blanking with molecular grade water was performed for all of the chosen wells (2 µL/well). Then, the quartz wells were wiped with a piece of lint-free paper to remove any remaining blanking buffer from the sample positions, and 2 µL of the samples were applied. The plate was then inserted into the plate carrier with the sample-side facing up, and the measurement was started by selecting Start. Incoming values were retrieved from the information header of the Measurement Progress window. The measurements were recorded and analyzed accordingly. Total RNA quality was documented as an absorbance ratio A260/280 = 2.0.

Qubit fluorometric quantification

The Qubit Fluorometric Quantification of RNA was carried out with two assay kits (Qubit RNA Assay Kit and Qubit RNA HS Assay Kit, where HS stands for High Sensitive. The Qubit RNA Assay Kit (or Qubit RNA HS Assay Kit) and RNA samples were warmed to room temperature before use. The Qubit 2.0 Fluorometer was set up according to the manufacturer's instructions. The working solution of the Qubit RNA Assay Kit (or Qubit RNA HS Assay Kit) was prepared by adding 200 µL of Qubit RNA reagent to 20 mL of Qubit RNA Buffer (Qubit RNA HS Buffer) and mixed well. The Qubit 2.0 Fluorometer was turned on and RNA was selected as the assay type. The instrument was allowed to warm up for a few min. Then, 190 µL of the Qubit RNA working solution (or Qubit RNA HS working solution) was added to each microcentrifuge tube. Ten µL of the RNA sample was added to the respective microcentrifuge tube containing the working solution and mixed well. The samples were then incubated for 2 min at room temperature. The microcentrifuge tubes were inserted into the Qubit 2.0 Fluorometer, and "Read Sample" was selected. The RNA concentration for each sample was recorded as displayed on the Qubit 2.0 Fluorometer.

3.15. RNA sequencing

RNA sequencing, also known as RNA-seq, is a powerful tool used to analyze gene expression levels and identify novel transcripts. In the context of immunology, RNA-seq is used to investigate the immune response of PBMCs to various immunogenic factors. In this study, RNA-seq was performed by CeGaT GmbH (Tübingen, Germany) (**Table 22**). RNA-seq studies can provide valuable insights into the complex mechanisms involved in the immune response.

The sequencing reads were demultiplexed using Illumina bcl2fastq (2.20). Skewer (version 0.2.2) (Jiang et al., 2014) was used to trim adapters. Quality trimming of the reads was not performed. For samples prepared with the Takara kit, the first three nucleotides of the second sequencing read were derived from the Pico v2 SMART adapter. Skewer (version 0.2.2) (Jiang et al., 2014) was used to trim those three nucleotides. In paired-end sequencing, read 2 corresponds to the sense strand. The quality of the FASTQ files was analyzed using FastQC (version 0.11.5-cegat) (Andrews). Plots were created in R (version 4.0.4) (R Core Team 2015) using ggplot2 (Wickham, 2009).

Sample number	Sample description		Sent material
1	PBMC control 1	PBMCs cultured for 72 h in cell growth medium.	
2	PBMC control 2		
3	PBMC control 3		
4	PBMC AdV1+rRBD 1	PBMCs treated with AdV1 (100 VP/mL) and rRBD (2.62 µg/mL), incubated for 72 h 34.5°C with 5% CO_2.	
5	PBMC AdV1+rRBD 2		
6	PBMC AdV1+rRBD 3		
7	PBMC AdV1+S+N 1	PBMCs treated with AdV1 (100 VP/mL), S-His and N-His (0.25 µg/mL), incubated for 72 h at 34.5°C with 5% CO_2.	RNA
8	PBMC AdV1+S+N 2		
9	PBMC AdV1+S+N 3		
10	Calu-3 control 1	Calu-3 cells cultured for 72 h in cell growth medium.	
11	Calu-3 control 2		
12	Calu-3 control 3		
13	Calu-3 AdV1+S+N 1	Calu-3 cells treated with AdV1 (100 VP/mL), S-His and N-His (0.25 µg/mL), incubated for 72 h at 34.5°C with 5% CO_2.	
14	Calu-3 AdV1+S+N 2		
15	Calu-3 AdV1+S+N 3		

Table 22 Sample types used in the study of the RNA transcripts. Legend: PBMC stands for peripheral blood mononuclear cells, AdV1 stands for serotype 5/3 equipped with ICOSL and CD40L (Garofalo et al., 2021a). rRBD stands for recombinant receptor binding domain protein (Baran et al., 2023 accepted for publication). Spike-S1-His and Nucleocapsid-His mean recombinant protein (InvivoGen, USA). Calu-3 means human lung tumor epithelial cells (ATCC).

To prepare the sequencing libraries, rRNA depletion was conducted. The sequencing process was carried out on an Illumina NovaSeq 6000 machine, which produced 2 x 100 bp reads. The company trimmed the reads from adapters and excluded nucleotides with a Phred score below a certain threshold. Only reads that were longer than 35 nucleotides were kept. The reads were aligned to the human GRCH.38 genome with GENCODE version 43 primary annotation, using RSEM-1.3.3 coupled with STAR-2.7.10b pipeline. Estimated read counts per gene were used for differential expression analysis using the DESeq2-1.34.0 R package. However, sample nr 8 from PBMC AdV1+S+N condition was identified as an outlier due to its clustering outside of all PBMC cell samples and almost double the read count compared to other samples. The samples were clustered using the complete linkage hierarchical clustering method. The transformed read counts were measured by R dist (Distance Matrix Computation) function with default parameters using the Euclidean distance between samples. All conditions were included in the DE-seq2 model, and three comparisons were made. Differentially expressed genes were analyzed separately for gene ontology enrichment with GPrifiler or the DAVID tool. The threshold of Benjamini-Hochberg adjusted FDR was used to extract differentially expressed genes from each comparison. Genomic data were provided by PhD Teresa Szczepińska (CEZAMAT, WUT).

3.16. *In vivo* analysis of adenovirus-based platform

The *in vivo* experiment was focused on the safety assessment of an adenovirus-based vaccine platform. The study employed a mouse model BALB/c to evaluate the potential adverse effects and safety profile of the therapeutic intervention. Three mice were included in each experimental group, and the animals' health and well-being were monitored daily. The therapeutics were administered via subcutaneous injections, with a standardized dose of 500 µl. The administration of therapeutics begins on the Day 0 of the experiment. These injections were provided in a series of up to three doses, with intervals of 3-4 days between each injection.

Precise administration dates were documented to monitor the timing of interventions. The experiment encompasses three cycles of therapeutic administration to assess the safety profile over an extended period. The weight of the mice was evaluated before each injection to track any changes that may indicate safety concerns. In **Table 23** the details of experiment are shown. The *in vivo* experiments including breeding, platform administration, euthanasia were performed by specialist Marta Prygiel PhD (superior of Animal Laboratory) at the National Institute of Public Health – National Institute of Hygiene – National Research Institute. The

whole procedure was performed according to the Ethical Statement no WAW2/150/2022 of December 7, 2022 of the Local Ethical Commission for Animal Experiments in Warsaw.

Experiment Name of eppendorf	N=mouse	Treatment	Place of injection	Volume	Repetition
1	3	PBS	Subcutaneously	500 µL	3 injections
2	3	AdVwt (1×10^{10} VP/mL)			
3	3	AdV1 (1×10^{10} VP/mL)			
4	3	S-His (10 µg/mL) + N-His (10 µg/mL)			
5	3	AdVwt (1×10^{10} VP/mL) + S-His (10 µg/mL) + N-His (10 µg/mL)			
6	3	AdV1 (1×10^{10} VP/mL) + S-His (10 µg/mL) + N-His (10 µg/mL)			

Table 23 *In vivo* analysis of adenovirus-based platform. The table contains the conversion of the concentration of the viruses and proteins (S-His and N-His) into 500 µL dose volumes.

3.17. Statistical analyses

The quantitative and qualitative data obtained in this study were subjected to statistical analysis. The mean ± SD was used to express continuous data, unless stated otherwise. Various tests were employed to evaluate multiple variables, such as multiple unpaired t-tests, Wilcoxon signed rank test, paired t-test, RM one-way ANOVA, and correlation (Pearson r). These tests were used to identify any significant changes in variables between the different groups. A P-value of ≤0.05 was considered statistically significant for all tests performed. GraphPad Prism 9.5.1.733 (San Diego, USA) was used to analyze the data.

4. Results

4.1. Optimization and validation of an *ex vivo* Peripheral Blood Mononuclear Cell (PBMC): cell viability and programmed cell death

As it was reviewed (Baran et al., 2022), PBMCs are very sensitive to many physical and chemical factors. Low temperature and cryopreservation can influence the population contents, it can reduce the number of $T_{NAÏVE}$ and T_{CM} cells, and increase $CD8^+$ population. The isolated cells are mature and do not have an ability to effectively proliferate, so the changes in their response are not very strong. However, the observed tendencies in a well-established research model are good for studying immune response and bridging the gap between animal tests and clinical trials (Tapia-Calle et al., 2019). As a result of the literature review (Baran et al., 2022) and preliminary studies (Baran et al., 2024), it was found that it is beneficial to isolate PBMCs from buffy coats at room temperature. This prevents the formation of agglomerates and facilitates the cell separation. Subsequently, it is preferable to use PBS with culture medium (RPMI or OptiMEM) for washing the cells. According to the literature review (Baran et al., 2022), the cells were frozen in a gradient temperature using a CellCamper, in which the temperature drops by an average of 1°C/min successively in -80°C, and after 24 h cryotubes were moved to -150°C. The composition of the OptiMEM cryopreservation medium was as follows: 20% of FBS and 10% of cryopreservant - DMSO. Then, cryopreserved PBMCs were thawed at room temperature prior to the scheduled experiment, washed with fresh culture medium, and plated in OptiMEM (10% FBS, 1% penicillin-streptomycin). The cells were leaved for overnight incubation, during which it was possible to remove apoptotic cells (so-called rest day).

The MTS viability test and cytometric analysis to detect cell apoptosis were performed. Firstly, it was studied how the PBMCs viability was changing over time of culture. Measurements after 24 h, 48 h and 7 days were performed. As shown in **Figure 23**, there are no statistically significant differences between the 24-h culture and 48-h culture, however after 7 days the decrease in cell viability was significant. Due to the planned long-term experiments, the conditions of the 7-day culture were optimized.
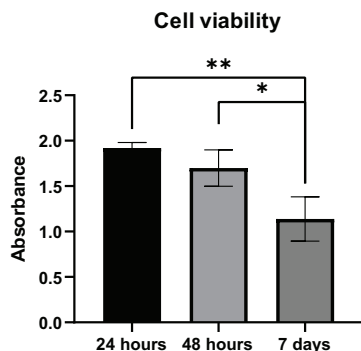
Cell viability

Figure 23 PBMCs viability over the time of culture (before optimization). *P ≤ 0.05, **P ≤ 0.01.

The cell apoptosis in seventh day of culture before and after optimization is shown in **Figure 24**. The approximately 40% increase in the number of viable cells was achieved in the 7-day culture after optimizing the PBMCs handling conditions. PBMCs isolated from the buffy coats of healthy donors were used as the *ex vivo* model to study the immune response.

Before optimization   **After optimization**
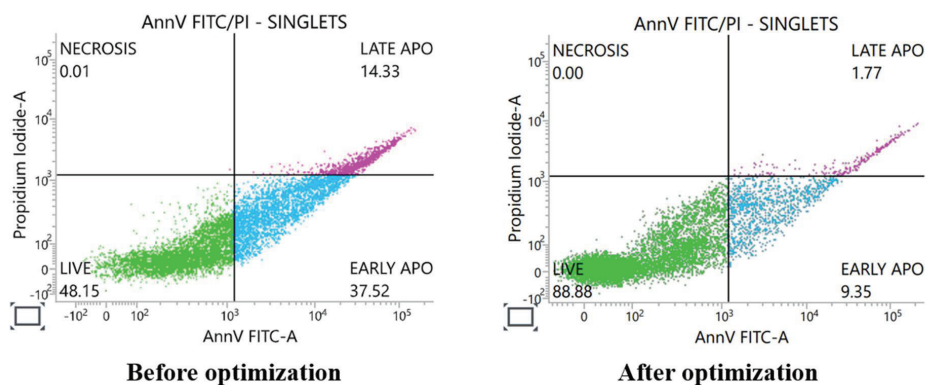
Figure 24 Apoptosis assay results of PBMCs after 7-day culture, before and after optimization of cell isolation and culture conditions. Legend: AnnV FITC-A stands for annexin V, $35 - 36$ kD Ca^{2+}-dependent phospholipid-binding protein conjugated to the FITC fluorochrome. PI means propidum iodide. Singlets mean single cells separated from aggregates using forward side channel-Aria (FSC-A) vs. forward side channel – Height (FSC-H). EARLY APO stands for early apoptosis. LATE APO means late apoptosis.

4.2. Cytopathic effect (CPE) generated by viruses: examples

The viruses were propagated using the appropriate cell line and banked in collaboration with the National Institute of Public Health - National Institute of Hygiene (NIPH-NIH). CPE was photographically documented (**Figures 25, 26**). Coronavirus titer was determined using the VERO E6 (ATCC CRL-1586) cell line derived from green monkey kidney

(**Figure 25**). The cells were selected due to their very high susceptibility to the SARS-CoV-2 infection compared with the human lines such as Caco-2 or Huh-7 (Zupin et al., 2021). Determination of adenovirus 5 (wt) titer was performed in H226 cells (human lung tumor epithelial cells, NCI-H226 ATCC) (**Figure 26**). Spearman-Kärber infection titers were determined for the following viruses:

- Human coronavirus OC43 (hCoV-OC43) is a respiratory virus that causes mild cold symptoms (D. X. Liu et al., 2021). Titer was determined using the VERO E6 cell line: 1.5×10^7 TCID50/mL. Both, hCoV-OC43 and SARS-CoV-2 belong to the coronavirus family and share certain structural and genomic features, including the presence of spike proteins on their surface. Studying hCoV-OC43 can provide insights into general coronavirus biology, replication strategy, and immune responses, at the same time being a easy to handle option in a laboratory setting. hCoV-OC43 is a BSL2 coronavirus, which makes it a safer option than highly pathogenic SARS-CoV-2.

VERO E6 cell monolayer
Control

Lysis of the VERO E6 cells
by hCoV-OC43
Cythopathic effect
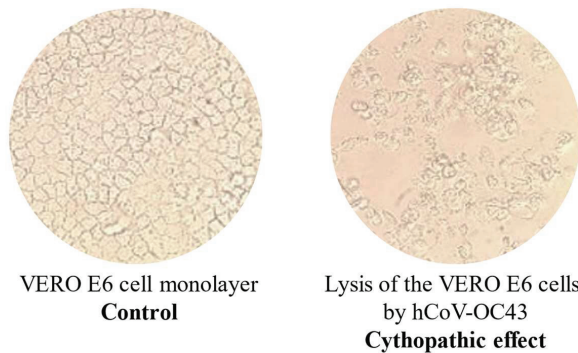
Figure 25 Representative visualisation of human betacoronavirus OC43 (hCoV-OC43) cythopathic effect using the VERO E6 cell line.

- Adenovirus 5 wt (AdV5) titer was assessed in the H226 cell line: 1×10^4 TCID50/mL. In the studies, AdV5 served as a control to modified adenovirus expressing co-stimulatory molecules. It is important to include proper controls in the set of experiments aiming at assessing immune response and to verify which virus backbone or genetic component of used adjuvant has more potent boosting properties on different subpopulations of lymphocytes.

H226 cell monolayer
Control

Lysis of the H226 cells
by AdV5
Cythopathic effect
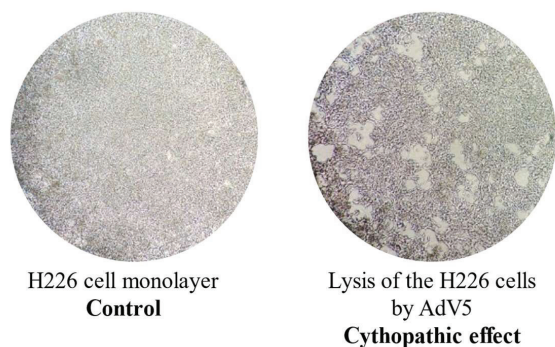
Figure 26 Representative visualisation of Adenovirus 5 wt (AdV5) cythopathic effect using the H226 cell line.

4.3. Cytotoxicity study of the immunogenic factors

Immunogenic factors were tested in various concentrations and combinations to establish their influence on viability and metabolic activity of the VERO E6 and PBMC cells. The VERO E6 cells were exposed to different dilutions of rRBD. As presented in

Figure 27, the VERO E6 cells treated with rRBD in the concentration of 5.24 µg/mL for 24 h showed significant decrease in the viability (13.3±0.7%) compared to the untreated control (100.0±12.0%). The VERO E6 cells were exposed to different dilutions of AdV1 (**Figure 28**). The VERO E6 cells treated with AdV1 in the concentration of 5.2×10^4 VP/mL for 24 h showed slight increase in the viability (127.0±3.0%) compared to the untreated control (100.0±16.0%) (**Figure 28**). The remaining results did not show any statistically significant deviations compared to the untreated control.

As presented in **Figure 29**, the VERO E6 cells treated with the mixture of AdV1 and rRBD in concentrations of 5.2×10^9 VP/mL and 5.24 µg/mL for 24 h showed significant decrease in the cells' viability (7.5±1.0%) compared to the untreated control (100.00±13.00%). The remaining results did not show any statistically significant deviations compared to the untreated control. The VERO E6 cell line exposed to different concentrations of pseudo-SARS-CoV-2 (**Figure 30**), did not show any significant changes in the viability. After selecting the immunogenic factors' concentrations to be tested in further experiments, the PBMC metabolic activity was assessed using the MTS assay (**Figure 31**). No significant changes compared to the control were noted (**Figure 31**).
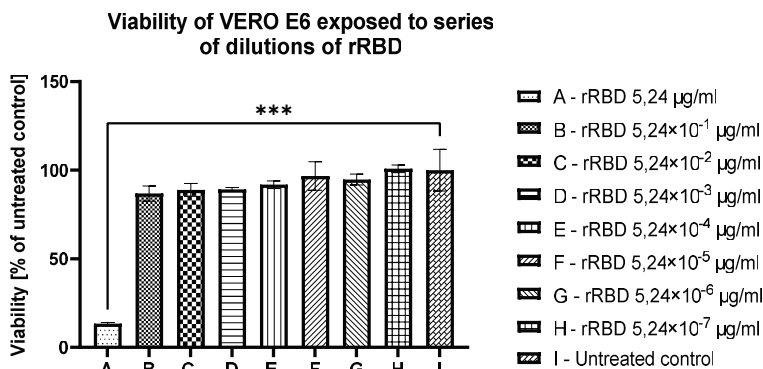
Figure 27 Viability of the VERO E6 cell line exposed to series of dilutions of rRBD (recombinant Receptor Binding Domain protein) for 24 h.
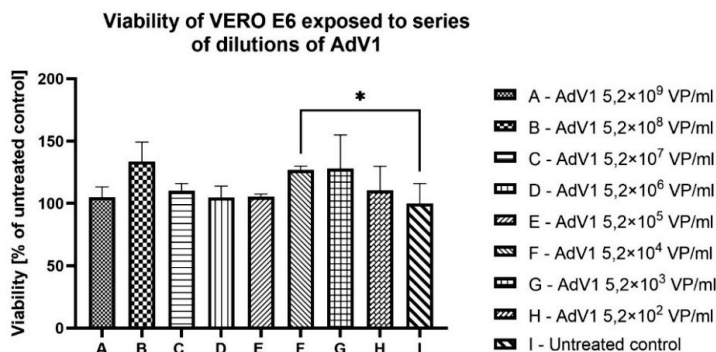
Figure 28 Viability of the VERO E6 cell line exposed to series of dilutions of AdV1 for 24 h. Legend: AdV1 stands for adenovirus serotype 5/3 with ICOSL and CD40L.
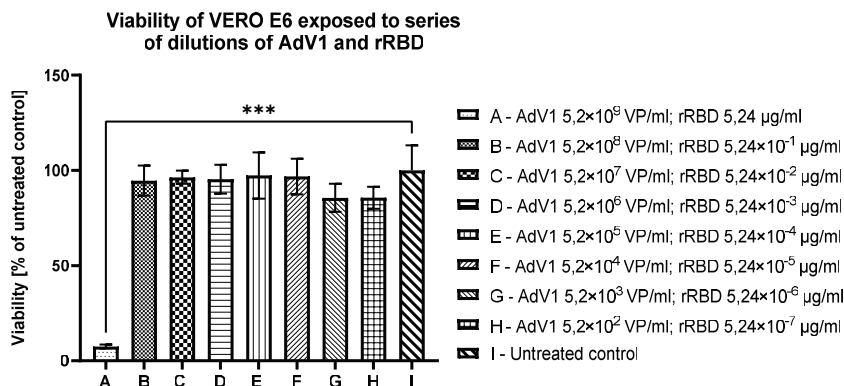
Figure 29 Viability of the VERO E6 cell line exposed to series of dilutions of AdV1 and rRBD combinations for 24 h. Legend: rRBD (recombinant Receptor Binding Domain protein, Baran et al., accepted for publication). AdV1 means adenovirus serotype 5/3 with ICOSL and CD40L (Garofalo et al., 2021a).
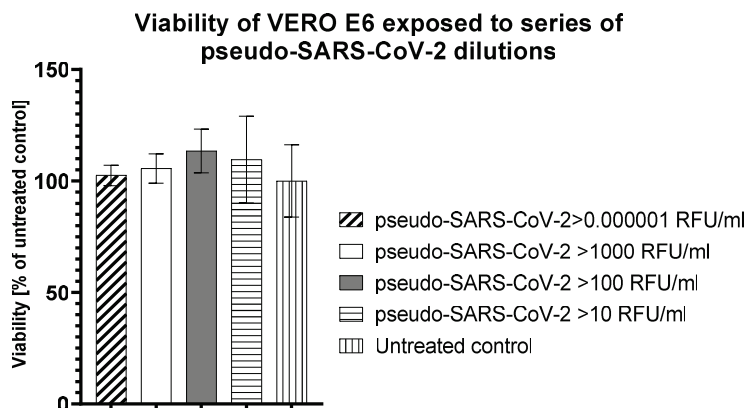
Figure 30 Viability of the VERO E6 cell line exposed to series of dilutions of pseudo-SARS-CoV-2 (pseudotyped lentivirus, GeneCopoeia, USA) for 24 h.
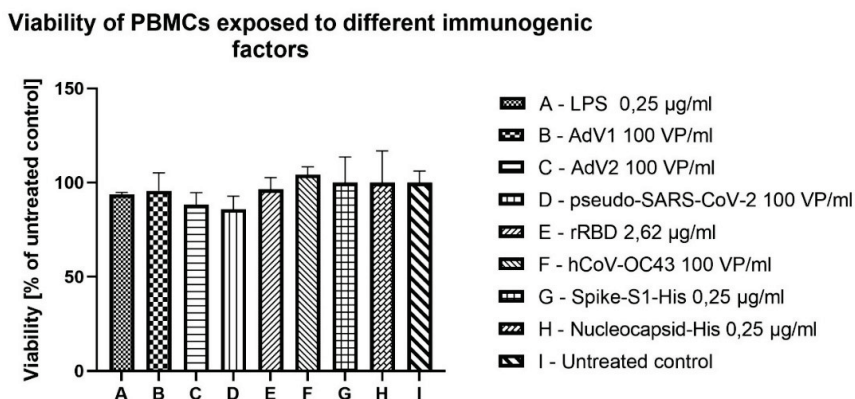
Figure 31 Viability of PBMC exposured to different immunogenic factors for 24 h. Legend: LPS means bacterial lipopolysaccharide. AdV1 stands for 5/3 serotype equipped with ICOSL and CD40L (Garofalo et al., 2021a). hCoV-OC43 means human betacoronavirus. rRBD stands for recombinant receptor binding domain protein (Baran et al., 2023 accepted for publication). ADV2 stands for serotype 5/3 without ICOSL and CD40L (Garofalo et al., 2021a). Pseudo-SARS-CoV-2 stands for pseudotyped lentivirus (Genecopeia, USA). Spike-S1-His and Nucleocapsid-His mean recombinant protein (InvivoGen, USA).

4.4. Scanning electron microscopy (SEM) analyses of viruses

SEM analyses of human coronavirus hCoV-OC43 allowed to identify individual virus particles of the size about 120 – 150 nm, depending on the unimpaired viral capsid or destroyed one (**Figure 32**). The size of pseudo-SARS-CoV-2 capsids ranged from 80 to 100 nm (**Figure 33**). Adenovirus (AdV1) showed a chain of capsids (marked by yellow arrow in **Figure 34**), which is unique for adenoviruses.
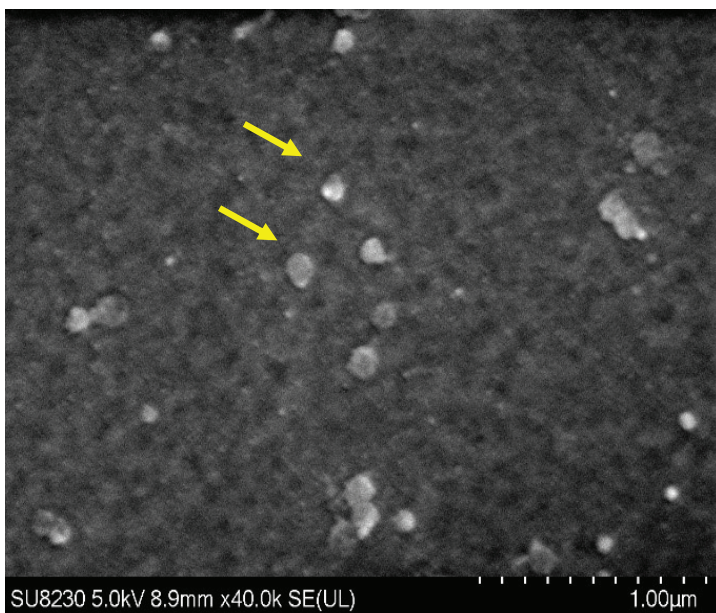
Figure 32 SEM (Hitachi SU8230): human betacoronavirus OC43 hCoV-OC43 titer exposed onto the VERO E6 monolayer (yellow arrows – capsid of the virus).
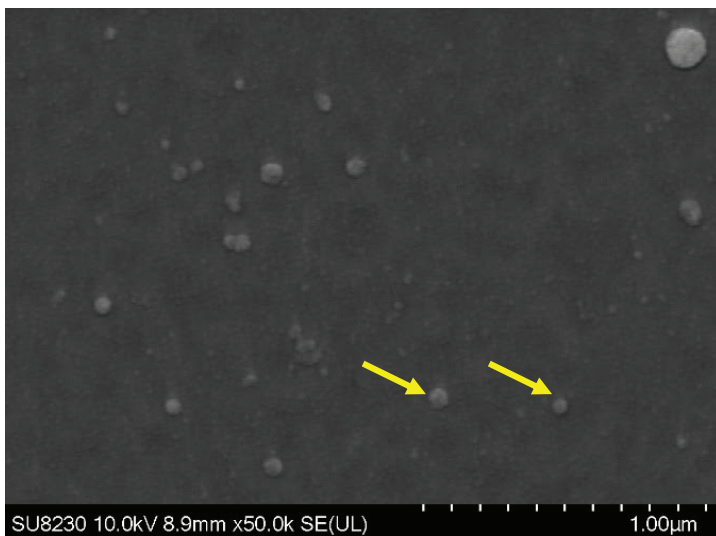
Figure 33 SEM (Hitachi SU8230): pseudo-SARS-CoV-2 titer determined onto the VERO E6 monolayer (yellow arrows – capsid of the virus). Legend: pseudo-SARS-CoV-2 stands for pseudotyped lentivirus (Genecopeia, USA).
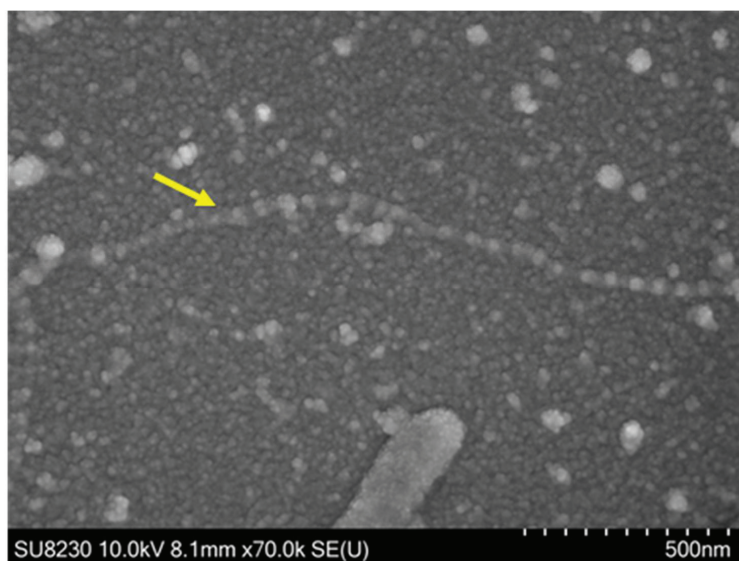
Figure 34 SEM (Hitachi SU8230): AdV1 titer determined onto the VERO E6 monolayer (yellow arrow – chain of capsids characteristic of adenoviruses). Legend: AdV1 means adenovirus serotype 5/3 with ICOSL and CD40L.

4.5. Confocal Laser Scanning Microscopy analyses

Pseudo-SARS-CoV-2 internalization was studied using Confocal Laser Scanning Microscopy (CLSM, Zeiss, Germany). Three different approaches were tested as follows: (1) pseudo-SARS-CoV-2 preincubated with the tested formulation including rRBD+AdV1 (100 VP/mL+100 VP/mL+2.62 µg/mL); (2) pseudo-SARS-CoV-2 preincubated with anti-spike antibody (100 VP/mL+2.62 µg/mL); (3) pseudo-SARS-CoV-2 (100 VP/mL) standing for positive control. The sample containing pseudo-SARS-CoV-2+AdV1+rRBD showed decreased expression of green fluorescence protein GFP (**Figure 35** C1, G1, PI1) compared to the pseudo-SARS-CoV-2 control (**Figure 35** C3, G3, PI3). A few necrotic nuclei were observed (**Figure 35** PI1). Pseudo-SARS-CoV-2 was effectively internalized by the VERO E6 cells (**Figure 35** C3, G3, PI3). GFP was expressed inside the cells (**Figure 35** G3). Small number of necrotic nuclei occurred (marked red with propidium iodide in **Figure 35** PI3). Pseudo-SARS-CoV-2 displayed internalization blocked by the anti-spike antibody (preincubated for 24 h before applying onto the cell monolayer) in **Figure 35** (C2, G2, PI2). GFP signal significantly decreased in the VERO E6 cells (**Figure 35** C2, G2, PI2) compared to the control - pseudo-SARS-CoV-2 (**Figure 35** C3, G3, PI3). There were also no necrotic nuclei visible in the approach (**Figure 35** C2, G2, PI2).
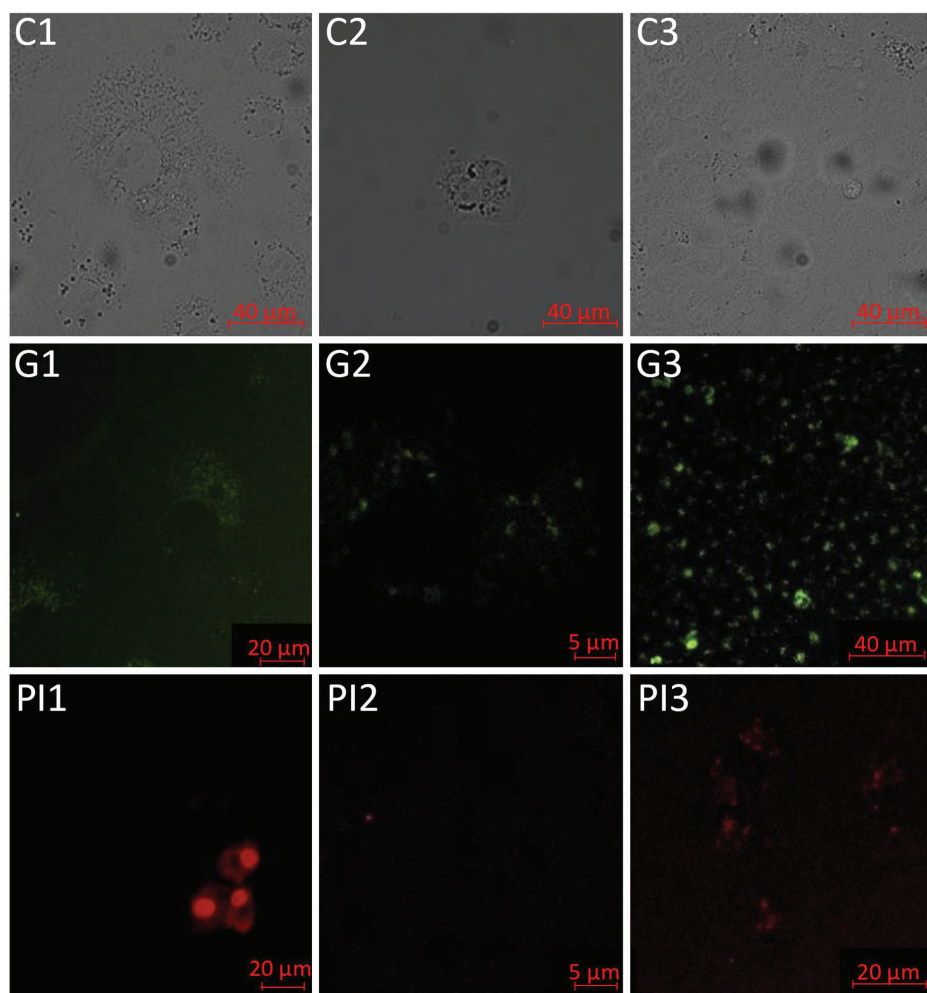
Figure 35 Confocal Laser Scanning Microscopy (CLSM) analysis of pseudo-SARS-CoV-2 internalization. Legend: 1 - Pseudo-SARS-CoV-2+AdV1+rRBD (100 VP/mL+100 VP/mL+2.62 µg/mL), 2 – Pseudo-SARS-CoV-2+Ab (100 VP/mL+2.62 µg/mL), 3 – Pseudo-SARS-CoV-2 (100 VP/mL). *C – phase-contrast, G – GFP, PI – propidium iodide.* AdV1 stands for 5/3 serotype equipped with ICOSL and CD40L (Garofalo et al., 2021a). rRBD stands for recombinant receptor binding domain protein (Baran et al., 2023). Pseudo-SARS-CoV-2 stands for pseudotyped lentivirus (Genecopeia, USA).

4.6. The CD40 gene expression

To study the effect of activation of the VERO E6 function under the immunogenic factors' treatment, real-time RT-qPCR was used to assess the expression of CD40. The cells were incubated for 24 h with or without the immunogenic factors at 34.5°C with 5% CO_2. As shown in **Figure 36**, CD40 gene was significantly upregulated when cells were stimulated with the following factors compared to the untreated control:

1. AdV1 50 or 100 VP/mL;
2. rRBD 2.62 or 5.24 µg/mL;
3. AdV1 50 VP/mL+rRBD 2.62 µg/mL;
4. AdV2 50 VP/mL+ rRBD 2.62 µg/mL;
5. AdV2 100 VP/mL+ rRBD 5.24 µg/mL;
6. AdV1 50 VP/mL+ pseudo-SARS-CoV-2 50 VP/mL;
7. AdV1 100 VP/mL+ pseudo-SARS-CoV-2 100 VP/mL;
8. AdV2 50 VP/mL+ pseudo-SARS-CoV-2 50 VP/mL;
9. AdV2 100 VP/mL+ pseudo-SARS-CoV-2 100 VP/mL;
10. pseudo-SARS-CoV-2 50 VP/mL+Ab 2.62 µg/mL;
11. pseudo-SARS-CoV-2 100 VP/mL+Ab 5.24 µg/mL;
12. rRBD 2.62+Ab 2.62 µg/mL;
13. rRBD 5.24 µg/mL+ Ab 5.24 µg/mL. A strong upregulation of the CD40 gene was shown when VEROE6 was treated with hCoV-OC43 (50 or 100 VP/mL).
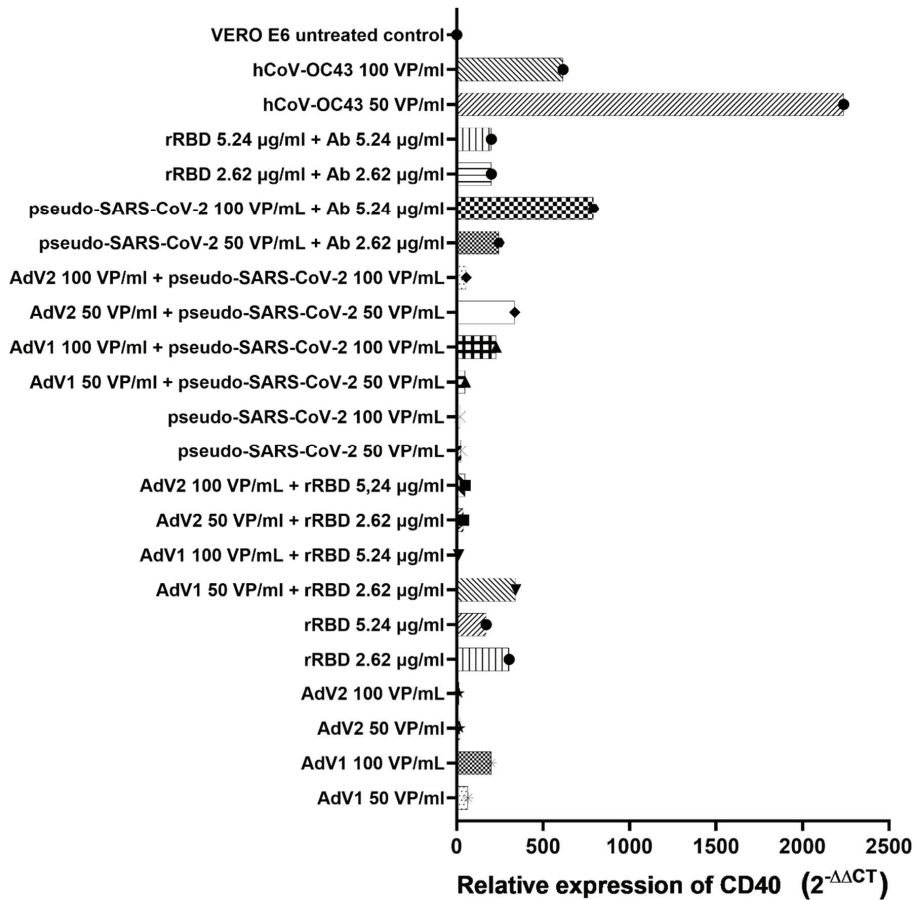
Figure 36 Relative expression of the CD40 gene of VERO E6. Legend: Values are given as the cycle threshold (Ct, mean of triplicate samples). Normalization factors were calculated as the geometric mean of the expression levels of the most stable reference gene GAPDH. As a calibrator, untreated VERO E6 sample was used (=1). Fold gene expression $2^{-\Delta\Delta Ct}$ was calculated according to the formula: $\Delta\Delta Ct = \Delta Ct$ (Sample) – ΔCt (Control average) and $\Delta Ct = Ct$ (gene of interest) – Ct (housekeeping gene). AdV1 stands for 5/3 serotype equipped with ICOSL and CD40L (Garofalo et al., 2021a). hCoV-OC43 stands for human betacoronavirus. rRBD stands for recombinant receptor binding domain protein (Baran et al., 2023). ADV2 stands for serotype 5/3 without ICOSL and CD40L (Garofalo et al., 2021a). Pseudo-SARS-CoV-2 stands for pseudotyped lentivirus (Genecopeia, USA).

4.7. Human PBMC for the immunogenicity assessment of the vaccine factors. T lymphocyte subsets in response to the immune-stimulatory molecules after 24 h

The aim of the experiment was to study how isolated and cryopreserved PBMCs react to the immunogenic agents in a short time (24 h). The optimization of the PBMC culturing, the process of cell immunophenotyping, and selection of the immunogenic factors' concentrations were presented in the previous stages. To accomplish the current topic, PBMCs were seeded into 24-well plate and incubated for 24 h with the following factors: LPS (0.125 µg/mL), rRBD (2.62 µg/mL), rRBD+Ab (2.62 µg/mL+2.62 µg/mL preincubated for 24 h at 34.5°C with 5% CO_2;), AdV1 (100 VP/mL), AdV2 (100 VP/mL), AdV1+rRBD (100 VP/mL+2.62 µg/mL), AdV2+rRBD (100 VP/mL+2.62 µg/mL), pseudo-SARS-CoV-2 (100 VP/mL), pseudo-SARS-CoV-2+Ab (100 VP/mL+5.24 µg/mL), hCoV-OC43 (100 VP/mL), MIX1 (AdV1+rRBD+pseudo-SARS-CoV-2: 100 VP/mL+2.62 µg/mL+ 100 VP/mL) and MIX2 (AdV2+rRBD+pseudo-SARS-CoV-2: 100 VP/mL+2.62 µg/mL+ 100 VP/mL at 34.5°C with 5% CO_2). After the incubation, the cells were stained as described in the "*Immunophenotyping*". CD4+ T cells, CD8+ T cells, and their subpopulations: central memory (CM), effector memory (EM), effector memory terminally differentiated (EMRA) were analyzed. The results were compared with the untreated control and with the LPS treated control (MOCK). Statistically significant differences in different populations of T and B lymphocytes compared to the untreated control were observed. Decrease in the amount of CD4+ T cells was observed in the samples treated with rRBD+Ab (57.50±2.30%), AdV1+rRBD (55.40±0.00%), AdV2+rRBD (54.87±0.00%) compared to the untreated control (72.60±2.84%) (**Figure 37**). Increase in the amount of CD8+ T cells was observed in the samples treated with AdV1+rRBD (37.17±0.00%) and AdV2+rRBD (37.27±1.03%) compared to the untreated control (23.13±2.10%). The amount of CD4+CD8+ increased in the sample treated with AdV2+rRBD (2.15±0.13%) compared to the untreated control (1.44±0.38%). CD4+CD8+ subpopulation when treated with rRBD decreased (1.30±0.05%) compared to MOCK (1.53±0.06%). By comparing samples to MOCK, it is possible to check whether the changes observed after the rRBD treatment are due to rRBD itself, or to bacterial contamination with LPS, as it is a recombinant protein produced in *E. coli*. Moreover, CD4+CD8+ increased when treated with the combination of adenoviruses and rRBD (AdV1+rRBD: 2.05±0.04, AdV2+rRBD: 2.15±0.13%) compared to the untreated control. Population of CD4-CD8- T cells increased significantly when treated with AdV1+rRBD

(5.38±0.18%) and AdV2+rRBD (5.70±0.44%) compared to the untreated control (2.79±0.42%).
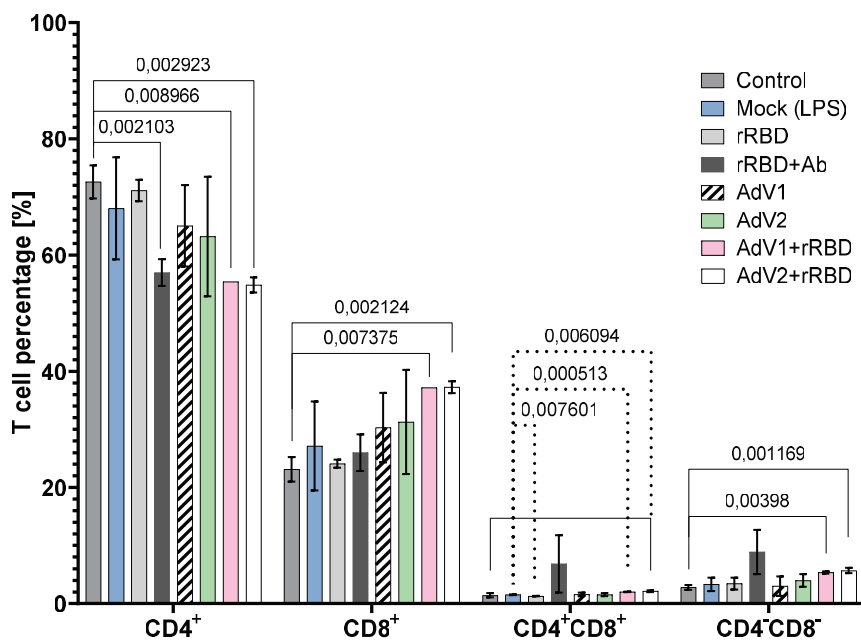
Figure 37 Percentage of T cells (CD4$^+$, CD8$^+$, CD4$^+$CD8$^+$, CD4$^-$CD8$^-$) incubated for 24 h with the immunogenic factors: MOCK (LPS), rRBD, rRBD+Ab, AdV1, AdV2, AdV1+rRBD, AdV2+rRBD. Legend: MOCK means peripheral blood mononuclear cells (PBMCs) treated with lypopolysacharide (LPS) in conc. of 0.125 μg/mL, AdV1 stands for 5/3 serotype equipped with ICOSL and CD40L (Garofalo et al., 2021a), AdV1 in conc. of 100 VP/mL. rRBD stands for recombinant receptor binding domain protein in conc. of 2.62 μg/mL (Baran et al., 2023). ADV2 stands for serotype 5/3 without ICOSL and CD40L (Garofalo et al., 2021a). AdV2 in conc. of 100 VP/mL. Ab means antibody against rRBD, both in conc. of 2.62 μg/mL.

Analysis of the samples treated with hCoV-OC43 showed as follows: decrease in CD4$^+$ T cells (58.00±1.85%) compared to the untreated control (72.60±2.84%), increase in CD8$^+$ T cells (35.00±1.2% vs. 23.13±2.10%) and CD4$^-$CD8$^-$ T cells (4.45±0.68% vs. 2.79±0.42%) (**Figure 38**). Similar trends were observed in the samples treated with MIX2 (AdV2+rRBD+pseudo-SARS-CoV-2): decrease in CD4$^+$ T cells (54.87±1.31%) vs. the untreated control (72.60±2.84%), increase in CD8$^+$ T cells (37.27±1.03%) vs. (23.13±2.10%), and increase in CD4$^-$CD8$^-$ T cells (5.70±0.44%) vs. (2.79±0.42%).
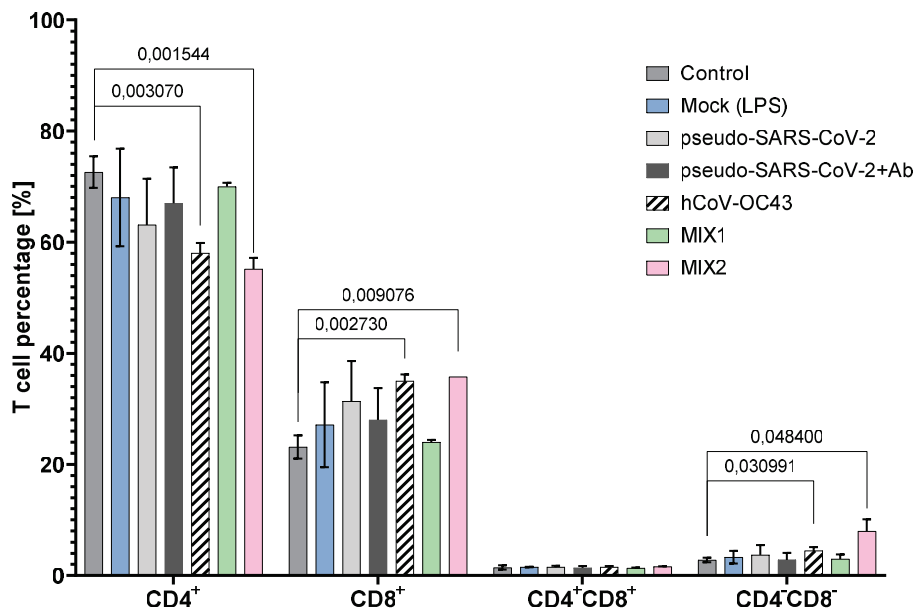
Figure 38 Percentage of T cells (CD4+, CD8+, CD4+CD8+, CD4-CD8-) incubated for 24 h with immunogenic factors: MOCK (LPS), pseudo-SARS-CoV-2, pseudo-SARS-CoV-2+Ab, hCoV-OC43, MIX1, MIX2. Legend: MOCK means peripheral blood mononuclear cells (PBMCs) treated with lypopolysacharide (LPS) in conc. of 0.125 µg/mL. Pseudo-SARS-CoV-2 (100 VP/mL) stands for pseudotyped lentivirus (Genecopoeia, USA). Ab (5.24 µg/mL) means antibody against spike protein. MIX1 (AdV1+rRBD+pseudo-SARS-CoV-2: 100 VP/mL+2.62 µg/mL+100 VP/mL) and MIX2 (AdV2+rRBD+pseudo-SARS-CoV-2: 100 VP/mL+2.62 µg/mL+100 VP/mL), where AdV1 stands for 5/3 serotype equipped with ICOSL and CD40L (Garofalo et al., 2021a), ADV2 stands for serotype 5/3 without ICOSL and CD40L (Garofalo et al., 2021a), rRBD stands for recombinant receptor binding domain protein in conc. of 2.62 µg/mL (Baran et al., 2023). hCoV-OC43 (100 VP/mL) stands for human betacoronavirus OC43.

It was analyzed how the population of cells was changed: NAÏVE and stem-cell like memory T cells (SCM) with a high potential for differentiation into the effector cells. The decrease in the number of SCM CD4$^+$ and CD8$^+$ T cells was observed in all of the treated samples compared to the untreated control (**Figure 38, Figure 40**).
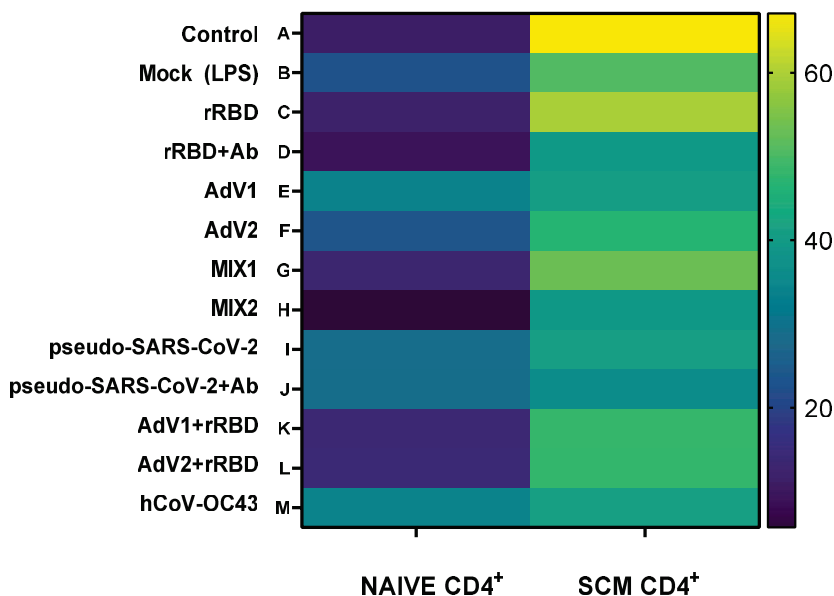
Figure 39 The heat map analysis of markers expressed by the subpopulations of CD4$^+$CD45RA$^+$CD197$^+$ of PBMCs treated with LPS, rRBD, rRBD+Ab, AdV1, AdV2, AdV1+rRBD, AdV2+rRBD, MIX1, MIX2, pseudo-SARS-CoV-2, pseudo-SARS-CoV-2+Ab and hCoV-OC43. Legend: Control means untreated peripheral blood mononuclear cells (PBMCs). MOCK means PBMCs treated with lypopolysacharide (LPS) in conc. of 0.125 µg/mL. rRBD stands for recombinant receptor binding domain protein in conc. of 2.62 µg/mL (Baran et al., 2023). Ab (5.24 µg/mL) means antibody against spike protein. AdV1 (100 VP/mL) stands for 5/3 serotype equipped with ICOSL and CD40L (Garofalo et al., 2021a). ADV2 (100 VP/mL) stands for serotype 5/3 without ICOSL and CD40L (Garofalo et al., 2021a). Pseudo-SARS-CoV-2 (100 VP/mL) stands for pseudotyped lentivirus (Genecopoeia, USA). MIX1 (AdV1+rRBD+pseudo-SARS-CoV-2: 100 VP/mL+2.62 µg/mL+ 100 VP/mL) and MIX2 (AdV2+rRBD+pseudo-SARS-CoV-2: 100 VP/mL+2.62 µg/mL+100 VP/mL). hCoV-OC43 (100 VP/mL) stands for human betacoronavirus OC43.

Figure 40 The heat map analysis of markers expressed by the subpopulations of CD8^{+}CD45RA^{+}CD197^{+} of PBMCs treated with LPS, rRBD, rRBD+Ab, AdV1, AdV2, AdV1+rRBD, AdV2+rRBD, MIX1, MIX2, pseudo-SARS-CoV-2, pseudo-SARS-CoV-2+Ab and hCoV-OC43. Legend: Control means untreated peripheral blood mononuclear cells (PBMCs). MOCK means PBMCs treated with lypopolysacharide (LPS) in conc. of 0.125 µg/mL. rRBD stands for recombinant receptor binding domain protein in conc. of 2.62 µg/mL (Baran et al., 2023). Ab (5.24 µg/mL) means antibody against spike protein. AdV1 (100 VP/mL) stands for 5/3 serotype equipped with ICOSL and CD40L (Garofalo et al., 2021a). ADV2 (100 VP/mL) stands for serotype 5/3 without ICOSL and CD40L (Garofalo et al., 2021a). Pseudo-SARS-CoV-2 (100 VP/mL) stands for pseudotyped lentivirus (Genecopoeia, USA). MIX1 (AdV1+rRBD+pseudo-SARS-CoV-2: 100 VP/mL+2.62 µg/mL+ 100 VP/mL) and MIX2 (AdV2+rRBD+pseudo-SARS-CoV-2: 100 VP/mL+2.62 µg/mL+100 VP/mL). hCoV-OC43 (100 VP/mL) stands for human betacoronavirus OC43.

Detailed analysis of CD4^{+} T cell subpopulations is shown in **Figure 41** and **Table1A** (Annex). It was studied whether PBMCs undergo the process of differentiation into effector and memory cells when exposed to the immunogenic factors. Both proposed vaccine platforms caused statistically significant changes in T cell subpopulations compared to the untreated control. The AdV1+rRBD treatment caused increase in the number of CM CD4^{+} T cells (21.50±0.00% vs. 14.50±1.47%), EM CD4^{+} T cells (9.67±0.00% vs. 4.77±0.99%), and EMRA CD4^{+} T cells (6.87±0.00 vs. 2.13±0.84). Decrease in the number of CD197^{+}CD45RA^{+} (61.93±0.00%) was noted compared to the untreated control (78.63±0.87%). Treatment the cells with AdV2+rRBD caused increase in the number of CM

CD4^{+} T cells (21.83±0.65% vs. 14.50±1.47%), EM CD4^{+} T cells (9.50±1.06% vs. 4.77±0.99%), and EMRA CD4^{+} T cells (6.57±0.49% vs. 2.13±0.84%). Decrease in the number of CD197^{+}CD45RA^{+} was observed (62.10±1.28%) compared to the untreated control (78.63±0.87%). Treatment the cells with rRBD caused a significant increase in the amount of EM CD4^{+} T when compared to the untreated control (7.20±3.11% vs. 4.77±0.99%). The slight increase in EMRA CD4^{+} T cells (2.25±0.49%) compared to the untreated control (2.13±0.84%) was observed. Decrease in the number of CD197^{+}CD45RA^{+} occurred when compared to the untreated control (71.45±9.12% vs. 78.63±0.87%) and MOCK (71.45±9.12% vs. 74.23±10.28%).
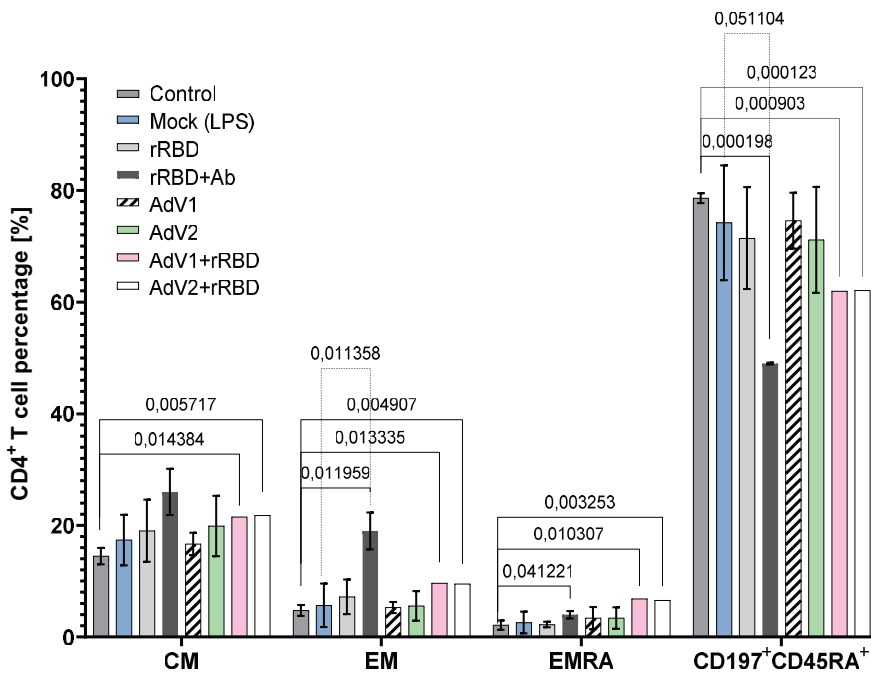
Figure 41 Percentage of central memory (CM), effector memory (EM), effector memory terminally differentiated (EMRA), and CD197+CD45RA+ among CD4+ after 24 h incubation with LPS, rRBD, rRBD+Ab, AdV1, AdV2, AdV1+rRBD and AdV2+rRBD. Legend: Control means untreated peripheral blood mononuclear cells (PBMCs). MOCK means PBMCs treated with lypopolysacharide (LPS) in conc. 0.125 µg/mL, AdV1 stands for 5/3 serotype equipped with ICOSL and CD40L (Garofalo et al., 2021a), AdV1 in conc. of 100 VP/mL. rRBD stands for recombinant receptor binding domain protein in conc. of 2.62 µg/mL (Baran et al., 2023). ADV2 stands for serotype 5/3 without ICOSL and CD40L (Garofalo et al., 2021a). AdV2 in conc. of 100 VP/mL. Ab means antibody against rRBD, both in conc. of 2.62 µg/mL.

As shown in **Figure 42**, significant changes were observed in all of the subpopulations treated with MIX2 (AdV2+rRBD+pseudo-SARS-CoV-2: 100 VP/mL+2.62 µg/mL+

100 VP/mL). There were changes as follows: CM CD4$^+$ T cells (19.07±0.00% vs. untreated control of 14.50±1.47%), EM CD4$^+$ T cells (26.70±9.00% vs. 4.77±0.99%), EMRA CD4$^+$ T cells (9.63±0.00% vs. 2.13±0.84%) and CD197$^+$CD45RA$^+$ CD4$^+$ T cells (44.60±9.00% vs. 78.63±0.87%). Increase in the number of EM CD4$^+$ T cells (26.70±9.00%) proved to be statistically significant also when compared to MOCK (5.70±3.89%). The sample treated with hCoV-OC43 showed increase in the EMRA CD4$^+$ T cells vs. the untreated control (4.00±0.65% vs. 2.13±0.84%).
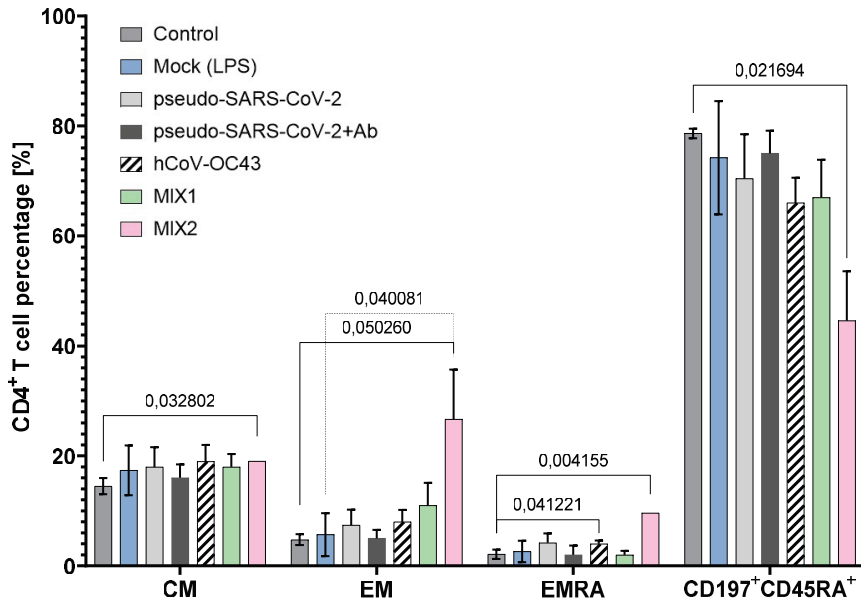
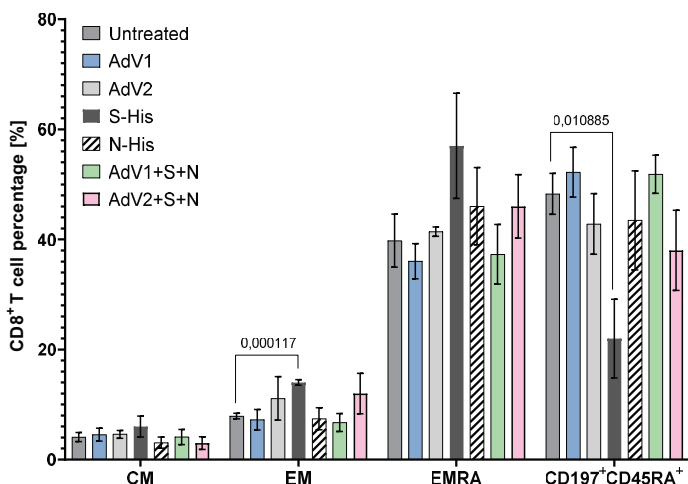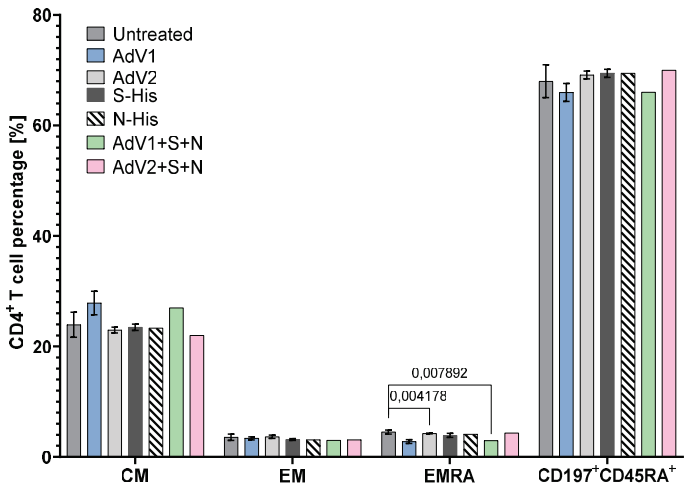**Figure 42** Percentage of central memory (CM), effector memory (EM), effector memory terminally differentiated (EMRA), and CD197$^+$CD45RA$^+$ among CD4$^+$ after 24 h incubation with LPS, pseudo-SARS-CoV-2, pseudo-SARS-CoV-2+Ab, hCoV-OC43, MIX1 and MIX2. Legend: Control means untreated peripheral blood mononuclear cells (PBMCs). MOCK means PBMCs treated with lypopolysacharide (LPS) in conc. Of 0.125 µg/mL. Pseudo-SARS-CoV-2 (100 VP/mL) stands for pseudotyped lentivirus (Genecopoeia, USA). Ab (5.24 µg/mL) means antibody against spike protein. hCoV-OC43 (100 VP/mL) stands for human betacoronavirus OC43. MIX1 (AdV1+rRBD+pseudo-SARS-CoV-2: 100 VP/mL+2.62 µg/mL+100 VP/mL) and MIX2 (AdV2+rRBD+pseudo-SARS-CoV-2: 100 VP/mL+2.62 µg/mL+100 VP/mL), where AdV1 (100 VP/mL) stands for 5/3 serotype equipped with ICOSL and CD40L (Garofalo et al., 2021a), ADV2 (100 VP/mL) stands for serotype 5/3 without ICOSL and CD40L (Garofalo et al., 2021a), rRBD stands for recombinant receptor binding domain protein in conc. Of 2.62 µg/mL (Baran et al., 2023).

CD8$^+$ cells play a critical role in the body's immune response to viral infections. It was checked how CD8$^+$ cytotoxic lymphocytes change their phenotype when exposed to the immunogenic factors. **Figure 43** shows changes in the levels of CM, EM, EMRA,

and CD197+CD45RA+ among CD8+ after 24 h incubation with LPS, rRBD, rRBD+Ab, AdV1, AdV2, AdV1+rRBD and AdV2+rRBD. The PBMCs treated with rRBD displayed several changes in CD8+ T cells, as follows: increase in the number of EM CD8+ T cells vs. the untreated control (7.23±1.86% vs. 7.90±0.50%) or MOCK (7.23±1.86% vs. 7.23±1.86%), increase in the number of EMRA CD8+ T cells vs. MOCK (41.40±0.85% vs. 36.03±3.20%), decrease in the number of CD197+CD45RA+ CD8+ T cells vs. the untreated control (42.80±5.52% vs. 48.27±3.73%) or MOCK (42.80±5.52% vs. 52.20±4.54%). Samples treated with the combination of AdV1 and rRBD showed elevated amount of EM CD8+ T cells vs. the untreated control (6.33±0.40% vs. 7.90±0.50%). EMRA CD8+ T cells increased in both, AdV1+rRBD (50.17±1.34% vs. 36.03±3.20%) and AdV2+rRBD vs. MOCK (49.40±1.04% vs. 36.03±3.20%).
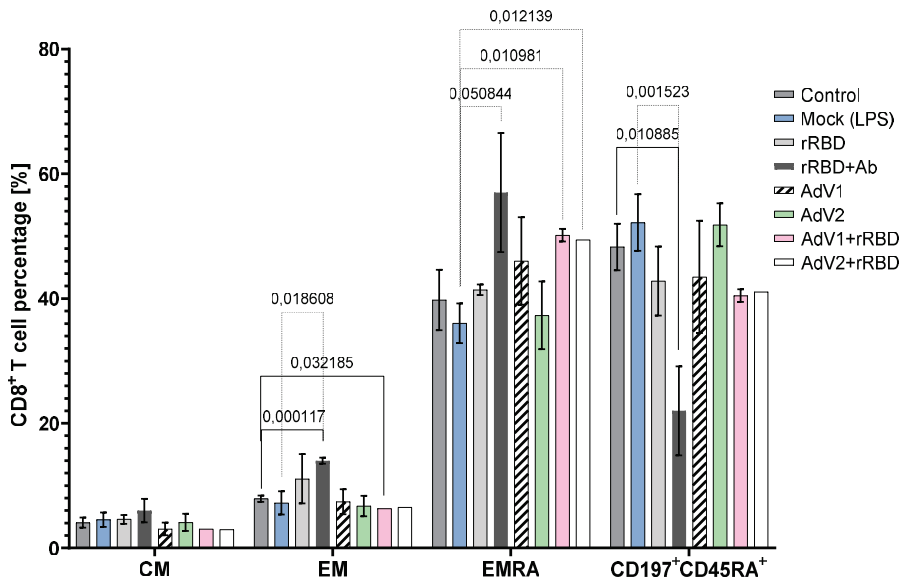
Figure 43 Percentage of central memory (CM), effector memory (EM), effector memory terminally differentiated (EMRA), and CD197+CD45RA+ among CD8+ after 24 h incubation with LPS, rRBD, rRBD+Ab, AdV1, AdV2, AdV1+rRBD and AdV2+rRBD. Legend: Control means untreated peripheral blood mononuclear cells (PBMCs). MOCK means PBMCs treated with lypopolysacharide (LPS) in conc. 0.125 µg/mL, AdV1 stands for 5/3 serotype equipped with ICOSL and CD40L (Garofalo et al., 2021a), AdV1 in conc. of 100 VP/mL. rRBD stands for recombinant receptor binding domain protein in conc. of 2.62 µg/mL (Baran et al., 2023). ADV2 stands for serotype 5/3 without ICOSL and CD40L (Garofalo et al., 2021a). AdV2 in conc. of 100 VP/mL. Ab means antibody against rRBD, both in conc. of 2.62 µg/mL.

In **Figure 44,** the samples exposed to MIX2 showed changes in a few populations. CM
CD8^{+} T cells increased vs. the untreated control (1.33±0.05% vs. 4.07±0.82%) or MOCK
(1.33±0.05% vs. 4.53±1.16%). In the samples treated with MIX2, EMRA CD8^{+} T cell level
increased vs. the untreated control (57.57±3.16% vs. 39.77±4.83%) or MOCK (57.57±3.16%
vs. 36.03±3.20%). The subpopulation of CD197^{+}CD45RA^{+} CD8^{+} T cells decreased vs. the
untreated control (23.53±3.21% vs. 48.27±3.73%) or MOCK (23.53±3.21% vs. 52.20±4.54%).
Samples treated with hCoV-OC43 showed significant changes in CM subpopulation of CD8^{+}
T cells, 2.55±0.55% compared with the untreated control (4.07±0.82%) or MOCK
(4.53±1.16%).
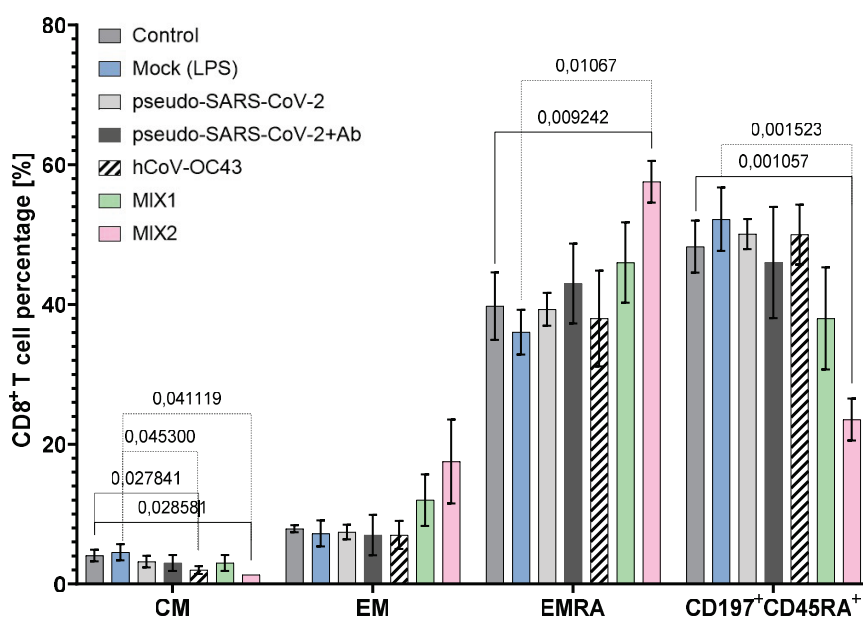
Figure 44 Percentage of central memory (CM), effector memory (EM), effector memory terminally
differentiated (EMRA), and CD197^{+}CD45RA^{+} among CD8^{+} after 24 h incubation with LPS, pseudo-
SARS-CoV-2, pseudo-SARS-CoV-2+Ab, hCoV-OC43, MIX1 and MIX2. Legend: Control means
untreated peripheral blood mononuclear cells (PBMCs). MOCK means PBMCs treated with
lypopolysacharide (LPS) in conc. of 0.125 µg/mL. Pseudo-SARS-CoV-2 (100 VP/mL) stands for
pseudotyped lentivirus (Genecopoeia, USA). Ab (5.24 µg/mL) means antibody against spike protein.
hCoV-OC43 (100 VP/mL) stands for human betacoronavirus OC43. MIX1 (AdV1+rRBD+pseudo-
SARS-CoV-2: 100 VP/mL+2.62 µg/mL+100 VP/mL) and MIX2 (AdV2+rRBD+pseudo-SARS-CoV-
2: 100 VP/mL+2.62 µg/mL+100 VP/mL), where AdV1 (100 VP/mL) stands for 5/3 serotype equipped
with ICOSL and CD40L (Garofalo et al., 2021a), ADV2 (100 VP/mL) stands for serotype 5/3 without
ICOSL and CD40L (Garofalo et al., 2021a), rRBD stands for recombinant receptor binding domain
protein in conc. of 2.62 µg/mL (Baran et al., 2023).

4.8. CD19^{+} B cell subsets after the 24-h stimulation with the immunogenic factors

CD19^{+} B cells play a critical role in the adaptive immune response, particularly in humoral immunity, by recognizing and binding to foreign antigens, leading to the production of antibodies. Due to its specific expression on B cells, CD19 is commonly used as a marker for identifying and isolating B cells in research studies. In this study, a specific panel was used to investigate the influence of immunogenic factors on CD19^{+} B cells (**Figure 45**). Statistically significant changes were observed in PBMCs treated with rRBD (11.93±0.31%), MIX1 (12.10±0.10%), rRBD+Ab (7.15±1.06%), AdV1+rRBD (12.60±0.00%), and AdV2+rRBD (12.33±0.29%) compared with the untreated control (9.70±0.50%) or MOCK (9.67±0.42%).
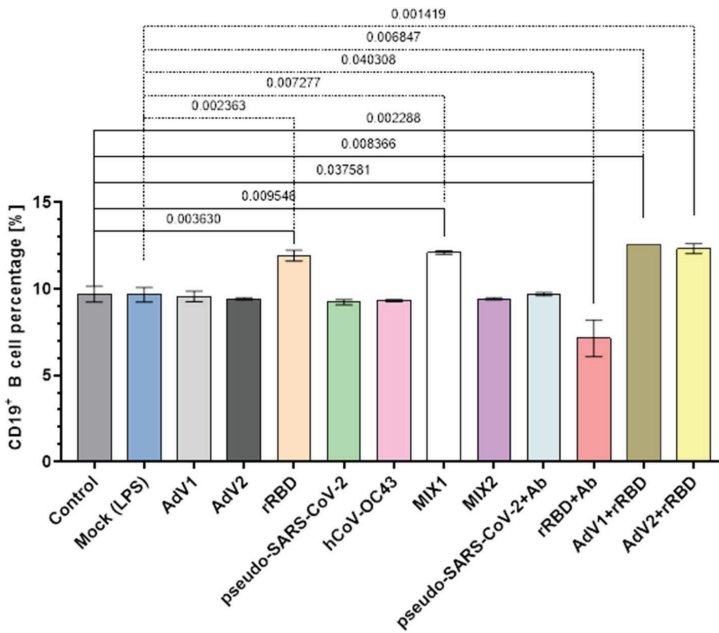
Figure 45 Percentage of CD19+ B cells after 24-h incubation with LPS, rRBD, rRBD+Ab, AdV1, AdV2, AdV1+rRBD, AdV2+rRBD, pseudo-SARS-CoV-2, pseudo-SARS-CoV-2+Ab, hCoV-OC43, MIX1 and MIX2. Legend: Control means untreated peripheral blood mononuclear cells (PBMCs). MOCK means PBMCs treated with lypopolysacharide (LPS) in conc. of 0.125 µg/mL. AdV1 (100 VP/mL) stands for 5/3 serotype equipped with ICOSL and CD40L (Garofalo et al., 2021a). ADV2 (100 VP/mL) stands for serotype 5/3 without ICOSL and CD40L (Garofalo et al., 2021a). rRBD stands for recombinant receptor binding domain protein in conc. of 2.62 µg/mL (Baran et al., 2023). Pseudo-SARS-CoV-2 (100 VP/mL) stands for pseudotyped lentivirus (Genecopoeia, USA). hCoV-OC43 (100 VP/mL) stands for human betacoronavirus OC43. Ab (5.24 µg/mL) means antibody against spike protein. MIX1 (AdV1+rRBD+pseudo-SARS-CoV-2: 100 VP/mL+2.62 µg/mL+ 100 VP/mL) and MIX2 (AdV2+rRBD+pseudo-SARS-CoV-2: 100 VP/mL+2.62 µg/mL+100 VP/mL).

The subsets of memory B cells were sorted based on their CD27 and IgD status, as shown in **Figure 46**. The CD27$^+$ B cells were further categorized into two groups: the class-switched memory B cells (IgD$^-$) and non-switched memory B cells (IgD$^+$). The NAÏVE B cells were identified as CD27$^-$IgD$^+$, while the double negative population (CD27$^-$IgD$^-$) was not well-defined and reported to have memory B cell-like properties. Numerous statistically significant changes in the content of individual subpopulations were observed in the samples treated with LPS, rRBD, rRBD+Ab, AdV1, AdV2, AdV1+rRBD, AdV2+rRBD when compared to the untreated control (**Figure 46**, **Table2A** (Annex)). The changes in CD19$^+$ CS population were noted when PBMCs were treated with AdV1 (6.07±0.35% vs. 9.67±0.21%), rRBD (13.80±0.87% vs. 9.67±0.21%), and rRBD+Ab (19.05±1.34% vs. 9.67±0.21%), compared with MOCK. Class-switched CD19$^+$ B cells are a subset of B cells that have undergone a process called class-switch recombination (CSR). They play an important role in the adaptive immune response by producing antibodies with different effector functions. The significant decrease comparing to MOCK was observed in NAÏVE B cells in the samples treated with rRBD (49.10±1.85% vs. 54.83±0.55%) and rRBD+Ab (38.20±0.85% vs. 54.83±0.55%). Similarly, changes in the content of individual subpopulations were observed in the samples treated with pseudo-SARS-CoV-2, pseudo-SARS-CoV-2+Ab, hCoV-OC43, MIX1 and MIX2 when compared to the untreated control (**Figure 47**, **Table2A** (Annex)). The statistically significant changes in CS CD19$^+$ subpopulation occurred when compared to Mock. These changes were noted for PBMCs treated with pseudo-SARS-CoV-2 (5.97±0.06% vs. 9.67±0.21%), MIX1 (17.73±2.61% vs. 9.67±0.21%) and MIX2 (5.77±0.06% vs. 9.67±0.21%). The statistically significant changes in NAÏVE B cells were observed when PBMCs were treated with MIX1 (45.17±2.25 vs. 54.83±0.55%).
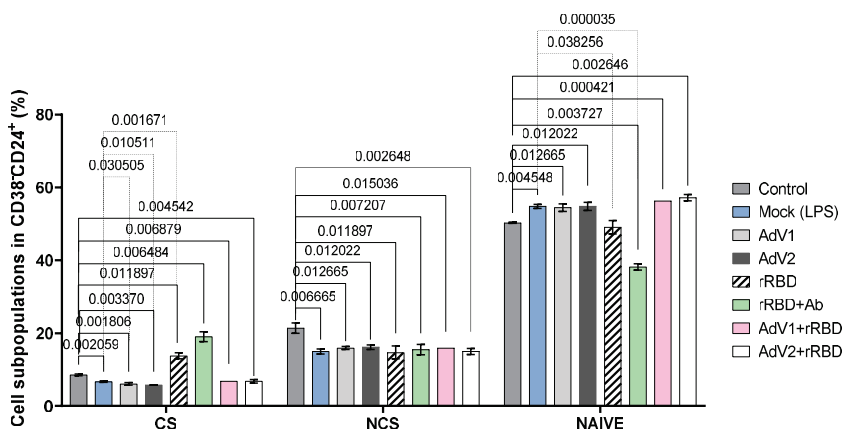
Figure 46 The subsets of the memory B cells (CD19+CD24+CD38-) CS, NCS, and NAÏVE incubated for 24 h with immunogenic factors: LPS, rRBD, rRBD+Ab, AdV1, AdV2, AdV1+rRBD, AdV2+rRBD. Legend: Control means untreated peripheral blood mononuclear cells (PBMCs). MOCK means PBMCs treated with lypopolysacharide (LPS) in conc. 0.125 µg/mL, AdV1 stands for 5/3 serotype equipped with ICOSL and CD40L (Garofalo et al., 2021a), AdV1 in conc. of 100 VP/mL. rRBD stands for recombinant receptor binding domain protein in conc. of 2.62 µg/mL (Baran et al., 2023). ADV2 stands for serotype 5/3 without ICOSL and CD40L (Garofalo et al., 2021a). AdV2 in conc. of 100 VP/mL. Ab means antibody against rRBD, both in conc. of 2.62 µg/mL.
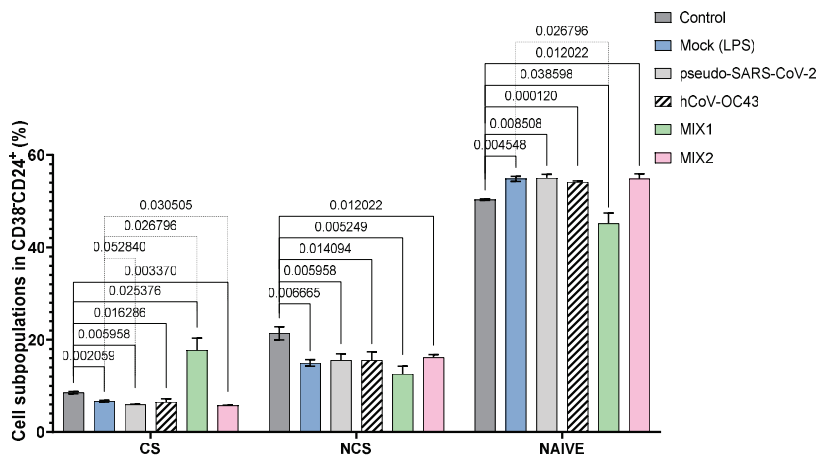
Figure 47 The subsets of the memory B cells (CD19+CD24+CD38-) CS, NCS, and NAÏVE incubated for 24 h with immunogenic factors: LPS, pseudo-SARS-CoV-2, pseudo-SARS-CoV-2+Ab, hCoV-OC43, MIX1 and MIX2. Legend: Control means untreated peripheral blood mononuclear cells (PBMCs). MOCK means PBMCs treated with lypopolysacharide (LPS) in conc. of 0.125 µg/mL. Pseudo-SARS-CoV-2 (100 VP/mL) stands for pseudotyped lentivirus (Genecopoeia, USA). hCoV-OC43 (100 VP/mL) stands for human betacoronavirus OC43. MIX1 (AdV1+rRBD+pseudo-SARS-CoV-2: 100 VP/mL+2.62 µg/mL+100 VP/mL) and MIX2 (AdV2+rRBD+pseudo-SARS-CoV-2: 100 VP/mL+2.62 µg/mL+100 VP/mL), where AdV1 (100 VP/mL) stands for 5/3 serotype equipped with ICOSL and CD40L (Garofalo et al., 2021a), ADV2 (100 VP/mL) stands for serotype 5/3 without ICOSL and CD40L (Garofalo et al., 2021a), rRBD stands for recombinant receptor binding domain protein in conc. of 2.62 µg/mL (Baran et al., 2023).

4.9. T lymphocyte subsets in response to the immunogenic factors after 7 days

The next stage of optimization was to prolong the exposure of PBMCs to the immunogenic factors in order to examine T cell subpopulations. Cells were seeded in 24-well plates and incubated with the immunogenic factors for 7 days. Briefly, after 3 days of culture, the medium was replaced with fresh one containing another equal dose of the immunogenic factors. In the experiment, LPS (0.125 µg/mL), rRBD (2.62 µg/mL), rRBD+Ab (2.62 µg/mL+2.62 µg/mL preincubated for 24 h at 34.5°C with 5% CO_2), AdV1 (100 VP/mL), AdV2 (100 VP/mL), AdV1+rRBD (100 VP/mL+2.62 µg/mL), AdV2+rRBD (100 VP/mL+ 2.62 µg/mL) were applied. After 7 days of culture, the "*Immunophenotyping*" (Panel 3) was carried out. CD19^{+} subpopulation are shown in **Figure 48**. It was observed that CD19^{+} cells were significantly activated when treated with rRBD alone or in the combination with adenoviruses or antibody.
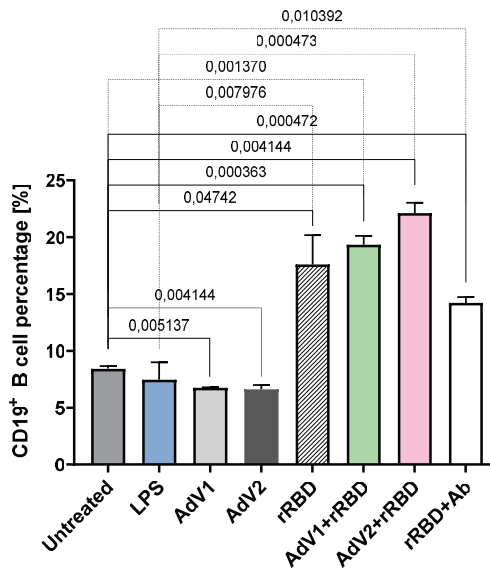
Figure 48 The percentage of CD19^{+} B cells after 7 day incubation of PBMCs with LPS, rRBD, rRBD+Ab, AdV1, AdV2, AdV1+rRBD, AdV2+rRBD. Legend: Control means untreated peripheral blood mononuclear cells (PBMCs). LPS means PBMCs treated with lypopolysacharide (LPS) in conc. 0.125 µg/mL. AdV1 stands for 5/3 serotype equipped with ICOSL and CD40L (Garofalo et al., 2021a), AdV1 in conc. of 100 VP/mL. rRBD stands for recombinant receptor binding domain protein in conc. of 2.62 µg/mL (Baran et al., 2023). ADV2 stands for serotype 5/3 without ICOSL and CD40L (Garofalo et al., 2021a). AdV2 in conc. of 100 VP/mL. Ab means antibody against rRBD, both in conc. of 2.62 µg/mL.

The rRBD used in this study is a product of genetic recombination of *E. coli*. The significant toxicity of rRBD against PBMCs (assessed in the MTS assays, **Figure 27**) and the strong activation of lymphocytes (**Figure 37**) raised doubts about its purity. The product was expressed in the bacterial system and there was the possible contamination with highly immunogenic bacterial LPS. Thus it was decided to discontinue rRBD from further analyses. In subsequent studies, commercially available spike and nucleocapsid proteins of SARS-CoV-2 were used. Commercially available proteins were produced using highly controlled and standardized processes, resulting in consistent and highly pure proteins. For example, in the studies we used InvivoGen proteins that were subjected to two-step quality control by the producer: 1) The protein has been validated by ELISA upon incubation with a coated Anti-SARS-CoV-Spike-RBD antibodies, 2) The absence of bacterial LPS (and different substances, e.g. endotoxins) has been confirmed using HEK-Blue™ TLR2 and HEK-Blue™ TLR4 cellular assays (his-sars2-n, his-sars2-s1 (InvivoGen, 2023).

Analysis of the commercial proteins (**Figures 49–52**) showed that only statistically significant changes occurred between T cells of $CD4^+$ subpopulation. Increase in the amount of CM $CD4^+$ T cells, EM $CD4^+$ T cells, EMRA $CD4^+$ T cells and decrease in the amount of $CD197^+CD45RA^+$ $CD4^+$ T cells compared with the untreated control were noted (**Figure 50**).
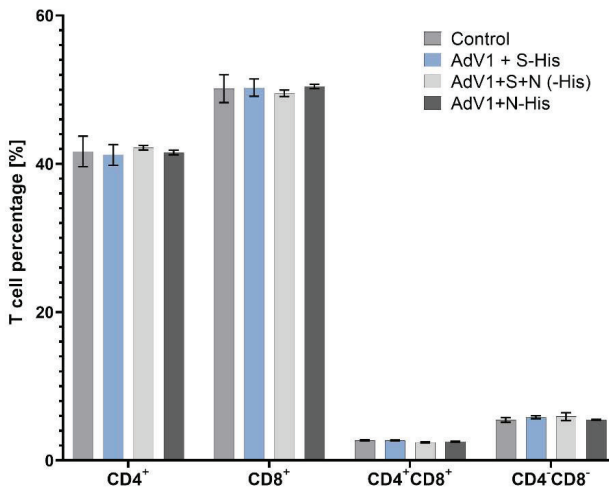
Figure 49 T cell percentage (CD4+, CD8+, CD4+CD8+, CD4-CD8-) after 24-h incubation of PBMCs with immunogenic factors: AdV1+S-His, AdV1+S-His+N-His, AdV1+N-His. Legend: Control means peripheral blood mononuclear cells. AdV1 stands for serotype 5/3 equipped with ICOSL and CD40L (Garofalo et al., 2021a), AdV1 in conc. of 100 VP/cell. Spike-S1-His (0.25 µg/mL) and Nucleocapsid-His (0.25 µg/mL) mean recombinant protein (InvivoGen USA).
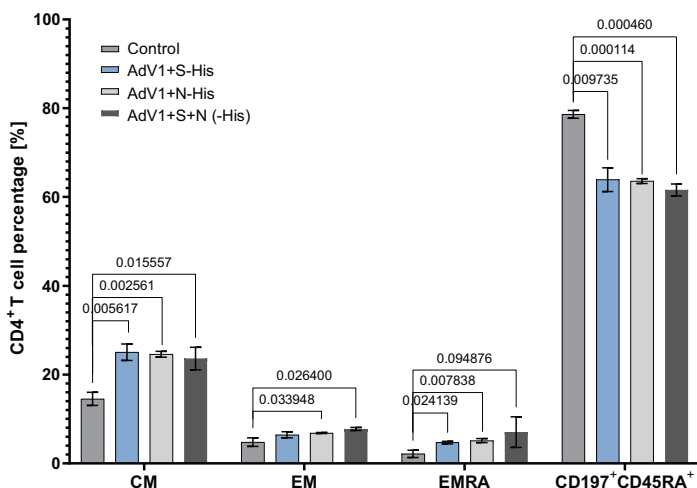
Figure 50 The percentage of central memory (CM) CD4^{+}, effector memory (EM) CD4^{+}, effector memory terminally differentiated (EMRA) CD4^{+}, and CD197^{+}CD45RA^{+} CD4^{+} after 24-h incubation with AdV1+S-His, AdV1+S-His+N-His, AdV1+N-His. Legend: Control means peripheral blood mononuclear cells. AdV1 stands for serotype 5/3 equipped with ICOSL and CD40L (Garofalo et al., 2021a), AdV1 in conc. of 100 VP/cell. Spike-S1-His (0.25 µg/mL) and Nucleocapsid-His (0.25 µg/mL) mean recombinant protein (InvivoGen USA).
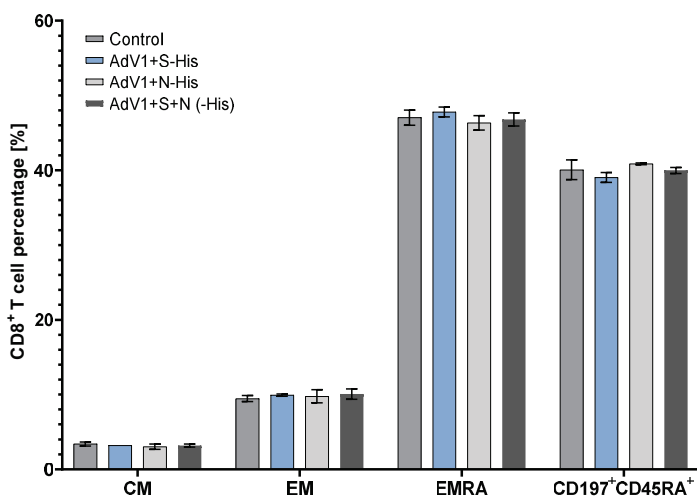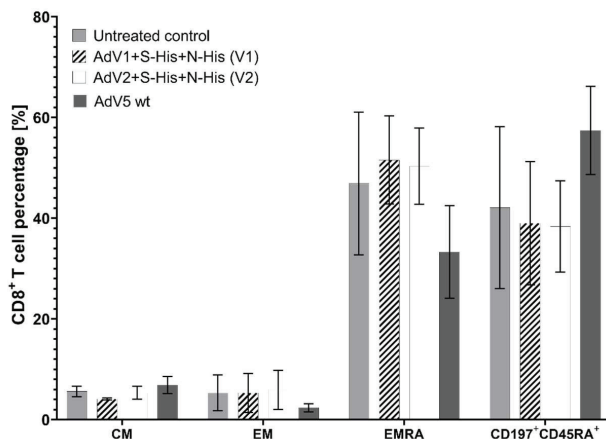

Figure 51 The percentage of central memory (CM) CD8+, effector memory (EM) CD8+, effector memory terminally differentiated (EMRA) CD8+, and CD197+CD45RA+ CD8+ after 24-h incubation of PBMCs with AdV1+S-His, AdV1+S-His+N-His, AdV1+N-His. Legend: Control means peripheral blood mononuclear cells. AdV1 stands for serotype 5/3 equipped with ICOSL and CD40L (Garofalo et al., 2021a), AdV1 in conc. of 100 VP/cell. Spike-S1-His (0.25 µg/mL) and Nucleocapsid-His (0.25 µg/mL) mean recombinant protein (InvivoGen USA).
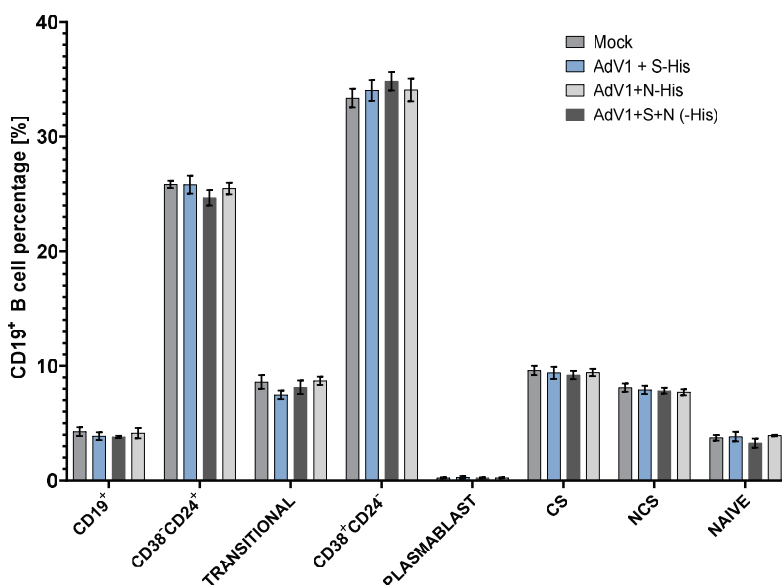
Figure 52 The percentage of CD19$^+$ B cells after 24-h incubation of PBMCs with AdV1+S-His, AdV1+S-His+N-His, AdV1+N-His. Legend: Control means peripheral blood mononuclear cells. AdV1 stands for serotype 5/3 equipped with ICOSL and CD40L (Garofalo et al., 2021a), AdV1 in conc. of 100 VP/cell. Spike-S1-His (0.25 µg/mL) and Nucleocapsid-His (0.25 µg/mL) mean recombinant protein (InvivoGen USA).

In order to optimized the model, it was studied how the AdV1 and AdV2 concentrations influence the immune resposne of PBMC and whether it directs the cells to apoptosis. Cells were seeded and incubated with the immunogenic factors for 7 days. In the experiment, the cells were treated with AdV1 (1000 VP/PBMC), AdV2 (1000 VP/PBMC), S-His (0.25 µg/mL), N-His (0.25 µg/mL), AdV1+S-His+N-His (1000 VP/PBMC+0.25 µg/mL+0.25 µg/mL), AdV2+S-His+N-His (1000 VP/PBMC+0.25 µg/mL+0.25 µg/mL). After 7 days of culture, the immunophenotyping and apoptosis assay were carried out.

The results of the apoptosis assay are shown in **Figure 53**. It was confirmed, that the proposed *ex vivo* model works effectively. Significant increase in the amount of the cells in early apoptosis was observed when PBMCs were treated with AdV1 (42.34±1.07% vs. 11.48±3.13%), AdV1+S-His+N-His (48.55±0.69% vs. 11.48±3.13%) and a slighter but significant increase was observed in the samples treated with AdV2+S-His+N-His (19.84±0.78% vs. 11.48±3.13%). Importantly, no amount of cells in necrosis occurred, cells in late apoptosis were also not numerous.
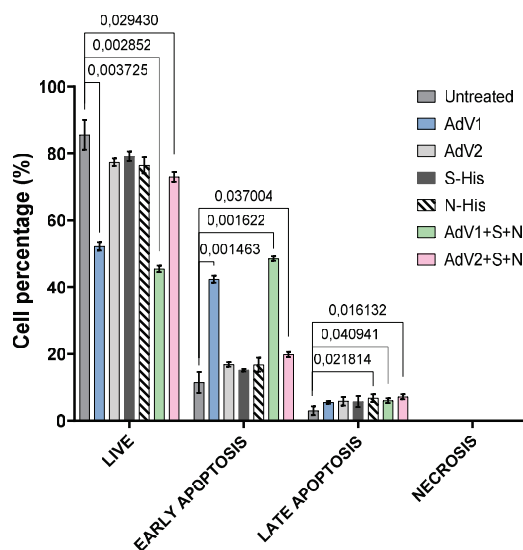
Figure 53 Apoptotic PBMC after 7-day incubation with AdV1, AdV2, S-His, N-His, AdV1+S-His+N-His, AdV2+S-His+N-His. Legend: Untreated means peripheral blood mononuclear cells. AdV1 stands for serotype 5/3 equipped with ICOSL and CD40L (Garofalo et al., 2021a), AdV1 in conc. of 1000 VP/cell. AdV2 stands for serotype 5/3 without ICOSL and CD40L (Garofalo et al., 2021a), AdV2 in conc. of 1000 VP/cell. Spike-S1-His (0.25 µg/mL) and Nucleocapsid-His (0.25 µg/mL) mean recombinant protein (InvivoGen USA).

The induction of an immune response was assessed. Significant increase in the number of CD4$^+$ cells was observed when PBMCs were treated with AdV1 (56.00±0.26% vs. 48.17±1.10%) and AdV1+S-His+N-His (46.70±1.61% vs. 48.17±1.10%) (**Figure 54**). In contrast, there was an observed decrease in CD8$^+$ cells treated with AdV1 (37.93±0.35%) vs. untreated (44.63±1.07%) and CD8+ cells treated with AdV1+S-His+N-His (38.47±0.38%) vs. untreated 44.63±1.07%. N-His caused the slight increase in the number of CD4$^+$CD8$^+$ cells (5.27±0.15%) compared to the untreated control (4.81±0.04%). Decrease in the amount of CD4$^-$CD8$^-$ was observed for the samples treated with AdV1+S-His+N-His (1.83±0.14% vs. 2.38±0.19%). Subsequently, it was analyzed how CD4$^+$ and CD8$^+$ cells differentiate under the influence of antigens and adjuvants (**Figures 55, 56**). No changes were observed in the number of EM CD8$^+$ when PBMCs were treated with S-His compared with the untreated PBMCs (6.23±0.40% vs. 6.27±1.03%). Decrease in the number of CD197$^+$CD45RA$^+$ (50.17±2.20% vs. 51.73±2.81%) was observed (**Figure 55**). No changes in the number of the EMRA CD4$^+$ subpopulations were noted when PBMCs were treated with AdV2 compared with untreated one (4.27±0.06% vs. 4.50±0.35%). Decrease in number of EMRA was observed when PBMCs were treated with the AdV1+S-His+N-His (2.97±0.23% vs. 4.50±0.35%) in **Figure 56**.

Moreover, it was noted that PBMCs treated with AdV1 alone or in combination with S-His and N-His showed elevated number of NAÏVE $CD4^+/CD8^+$ and SCM $CD4^+/CD8^+$ (**Figures 57, 58**).
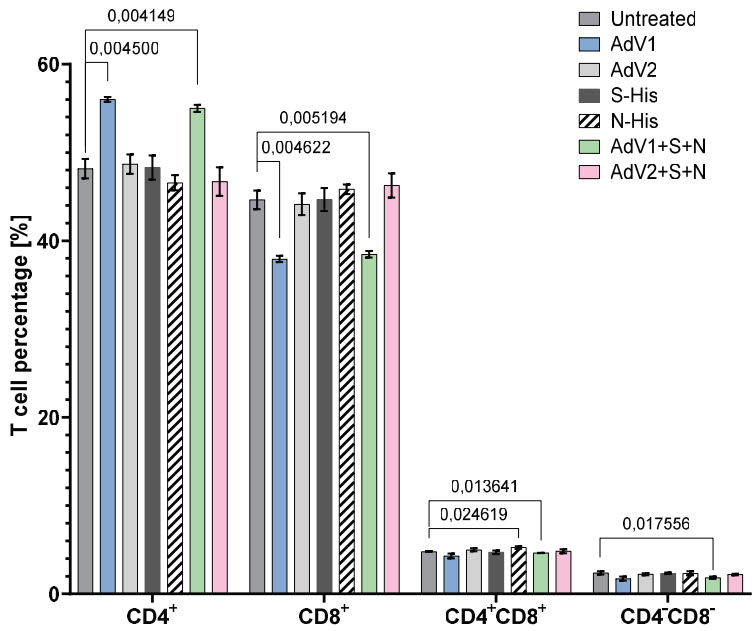
Figure 54 T cell percentage ($CD4^+$, $CD8^+$, $CD4^+CD8^+$, $CD4^-CD8^-$) after 7-day incubation of PBMCs with AdV1, AdV2, S-His, N-His, AdV1+S-His+N-His, AdV2+S-His+N-His. Legend: Untreated means peripheral blood mononuclear cells. AdV1 stands for serotype 5/3 equipped with ICOSL and CD40L (Garofalo et al., 2021a), AdV1 in conc. of 1000 VP/cell. AdV2 stands for serotype 5/3 without ICOSL and CD40L (Garofalo et al., 2021a), AdV2 in conc. of 1000 VP/cell. Spike-S1-His (0.25 μg/mL) and Nucleocapsid-His (0.25 μg/mL) mean recombinant protein (InvivoGen USA).

**Figure 55** T cell percentage (central memory (CM) CD8^{+}, effector memory (EM) CD8^{+}, effector memory terminally differentiated (EMRA) CD8^{+}, and CD197^{+}CD45RA^{+} CD8^{+}) after 7-day incubation with AdV1, AdV2, S-His, N-His, AdV1+S-His+N-His, AdV2+S-His+N-His. Legend: Untreated means peripheral blood mononuclear cells. AdV1 stands for serotype 5/3 equipped with ICOSL and CD40L (Garofalo et al., 2021a), AdV1 in conc. of 1000 VP/cell. AdV2 stands for serotype 5/3 without ICOSL and CD40L (Garofalo et al., 2021a), AdV2 in conc. of 1000 VP/cell. Spike-S1-His (0.25 µg/mL) and Nucleocapsid-His (0.25 µg/mL) mean recombinant protein (InvivoGen USA).

Figure 56 T cell percentage (central memory (CM), effector memory (EM), effector memory terminally differentiated (EMRA), and CD197^{+}CD45RA^{+} among CD4^{+}) after 24 h incubation with AdV1, AdV2, S-His, N-His, AdV1+S-His+N-His, AdV2+S-His+N-His. Legend: Untreated means peripheral blood mononuclear cells. AdV1 stands for serotype 5/3 equipped with ICOSL and CD40L (Garofalo et al., 2021a), AdV1 in conc. of 1000 VP/cell. AdV2 stands for serotype 5/3 without ICOSL and CD40L (Garofalo et al., 2021a), AdV2 in conc. of 1000 VP/cell. Spike-S1-His (0.25 µg/mL) and Nucleocapsid-His (0.25 µg/mL) mean recombinant protein (InvivoGen USA).
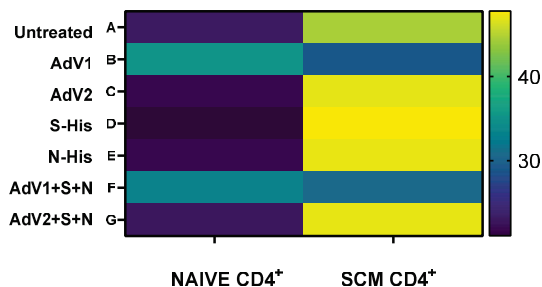
Figure 57 The heat map analysis of NAÏVE and SCM cells from the subpopulations of CD4+CD45RA+CD197+ after 7-day treatment of PBMCs with AdV1, AdV2, S-His, N-His, AdV1+S-His+N-His, AdV2+S-His+N-His. Legend: Untreated means peripheral blood mononuclear cells. AdV1 stands for serotype 5/3 equipped with ICOSL and CD40L (Garofalo et al., 2021a), AdV1 in conc. of 1000 VP/cell. AdV2 stands for serotype 5/3 without ICOSL and CD40L (Garofalo et al., 2021a), AdV2 in conc. of 1000 VP/cell. Spike-S1-His (0.25 µg/mL) and Nucleocapsid-His (0.25 µg/mL) mean recombinant protein (InvivoGen USA).
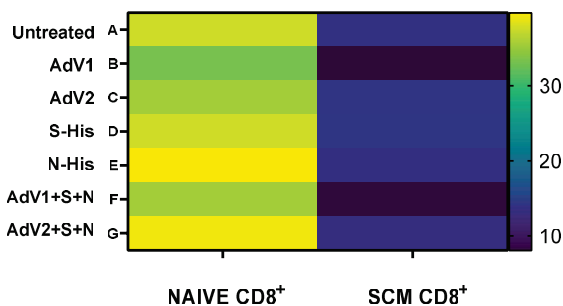
Figure 58 The heat map analysis of NAÏVE and SCM cells from the subpopulations of CD8+CD45RA+CD197+ by PBMCs treated with AdV1, AdV2, S-His, N-His, AdV1+S-His+N-His, AdV2+S-His+N-His. Legend: Untreated means peripheral blood mononuclear cells. AdV1 stands for serotype 5/3 equipped with ICOSL and CD40L (Garofalo et al., 2021a), AdV1 in conc. of 1000 VP/cell. AdV2 stands for serotype 5/3 without ICOSL and CD40L (Garofalo et al., 2021a), AdV2 in conc. of 1000 VP/cell. Spike-S1-His (0.25 µg/mL) and Nucleocapsid-His (0.25 µg/mL) mean recombinant protein (InvivoGen USA).

Analysis of the humoral response induced by AdV1, AdV2, S-His, N-His, AdV1+S-His+N-His, AdV2+S-His+N-His showed that AdV1 alone (4.17±0.25% vs. 3.17±0.06%) and in combination with S-His and N-His (3.87±0.25% vs. 3.17±0.06%) slightly increased the number of CD19+ cells (**Figure 59**). Decrease in the number of CD19+ cells was also observed in PBMCs treated with S-His (3.03±0.06% vs. 3.17±0.06%). The use of both platforms resulted in changes in the number of NCS cells. NCS decreased in PBMCs treated with AdV1+S-His+N-His (66.93±1.40% vs. 82.07±0.50%). NCS increased in PBMCs treated with AdV2+S-His+N-His (84.23±0.55% vs. 82.07±0.50%) (**Figure 60**).
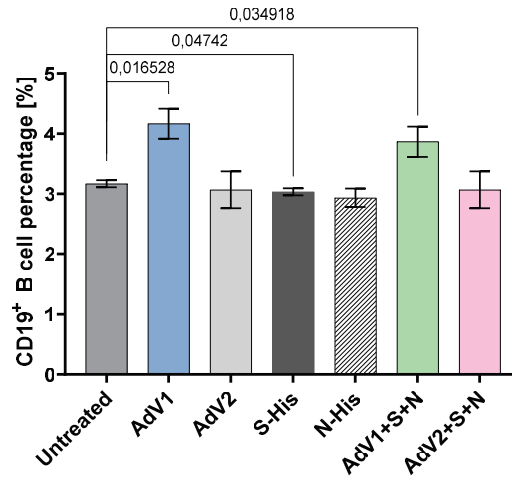
Figure 59 The percentage of CD19$^+$ B cells after 7-day incubation of PBMCs with AdV1, AdV2, S-His, N-His, AdV1+S-His+N-His, AdV2+S-His+N-His. Legend: Untreated means peripheral blood mononuclear cells. AdV1 stands for serotype 5/3 equipped with ICOSL and CD40L (Garofalo et al., 2021a), AdV1 in conc. of 1000 VP/cell. AdV2 stands for serotype 5/3 without ICOSL and CD40L (Garofalo et al., 2021a), AdV2 in conc. of 1000 VP/cell. Spike-S1-His (0.25 µg/mL) and Nucleocapsid-His (0.25 µg/mL) mean recombinant protein (InvivoGen USA).
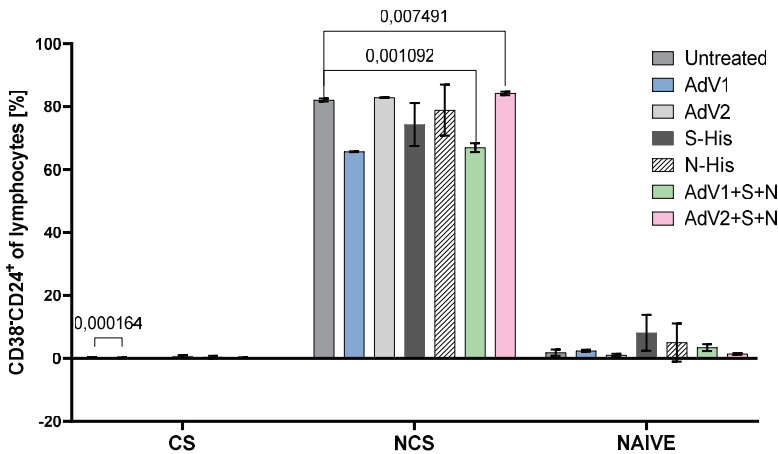
Figure 60 The subsets of the memory B cell (CD19$^+$CD24$^+$CD38$^-$) CS, NCS, and NAÏVE noted after 24-h incubation of PBMCs with immunogenic factors: AdV1, AdV2, S-His, N-His, AdV1+S-His+N-His, AdV2+S-His+N-His. Legend: Untreated means peripheral blood mononuclear cells. AdV1 stands for serotype 5/3 equipped with ICOSL and CD40L (Garofalo et al., 2021a), AdV1 in conc. of 1000 VP/cell. AdV2 stands for serotype 5/3 without ICOSL and CD40L (Garofalo et al., 2021a), AdV2 in conc. of 1000 VP/cell. Spike-S1-His (0.25 µg/mL) and Nucleocapsid-His (0.25 µg/mL) mean recombinant protein (InvivoGen USA).

4.10. Calu-3 micovilli imaging using SEM

Calu-3 cells cultured on Corning® Transwell® Inserts developed microvilli on their surface of a maximum length 1 μm (**Figure 61**).
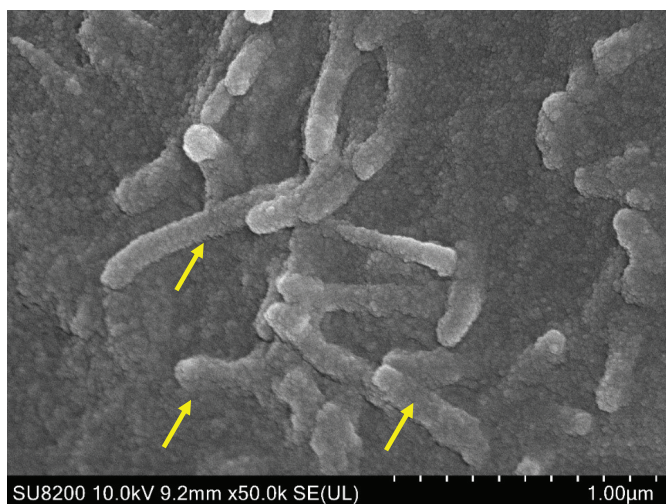
Figure 61 SEM nr 1 (Hitachi SU8230): Microvilli (yellow arrows) on the surface of Calu-3 cell line growing on Corning® Transwell® Inserts. Bar=1 μm.

4.11. PBMC and Calu-3 transcriptome analysis

In recent years, genome sequencing has become a powerful tool for investigating theintricate complexity of genetic information and providing new insights into the molecular basis of the immune studies. In these studies, the focus was put on the comprehensive genome sequencing of two distinct cellular system: PBMC and Calu-3. Through genome sequencing of PBMCs, we aim to shed a light on key genetic variants, gene expression profiles, and potential biomarkers associated with the immune system function during the vaccination process. Similarly, the Calu-3 cell line derived from human lung adenocarcinoma is the model system for studying respiratory diseases, drug discovery, and host-pathogen interactions. PBMCs were treated with AdV1+rRBD (100 VP/mL+2.62 µg/mL) and AdV1+S+N (100 VP/mL+ 0.25 µg/mL+0.25 µg/mL) and incubated for 72 h at 34.5°C with 5% CO_2 (three technical replicates). Calu-3 cells were treated with AdV1+S+N (100 VP/mL+0.25 µg/mL+0.25 µg/mL) and incubated for 72 h at 34.5°C with 5% CO_2 (three technical replicates). After the incubation, RNA was extracted from the cell pellets using Total RNA Mini Kit (A&A Biotechnology, Gdansk, Poland). RNA was measured with two complementary methods – NanoQuant plate, Spark plate reader (Tecan, Switzerland) and Qubit Fluorometric Quantification (Thermo Fisher Scientific Inc., USA). Table **23** presents the summary of the up- and downregulated genes.

Sample comparison	PBMC AdV1+rRBD vs. Control	PBMC AdV1+S+N vs. Control	Calu-3 Ad1+S+N vs. Control
Genes **Up**regulated / **Down**regulated	4036 genes (11%) **Up**	53 gens (0.15%) **Up**	3 gens (0.0083%) **Up**
	5376 genes (15%) **Down**	127 genes (0.35%) **Down**	1 genes (0.0028%) **Down**

Table 24 Summary of gene numbers up- and downregulated in the sequenced samples.

4.11.1. PBMCs treated with AdV1+rRBD vs. Control

RNA seq of PBMCs treated with AdV1+rRBD showed changes in the expression of many genes (**Figure 62**). It is possible, that rRBD was contaminated with LPS, as it was extracted from the *E. coli* expression system. LPS binds to multiple sites on the SARS-CoV-2 spike protein, resulting in amplified proinflammatory responses. The S protein acts as an intermediary in the transfer of LPS to the host receptors, suggesting that the S protein contributes to hyperinflammation (Samsudin et al., 2022).
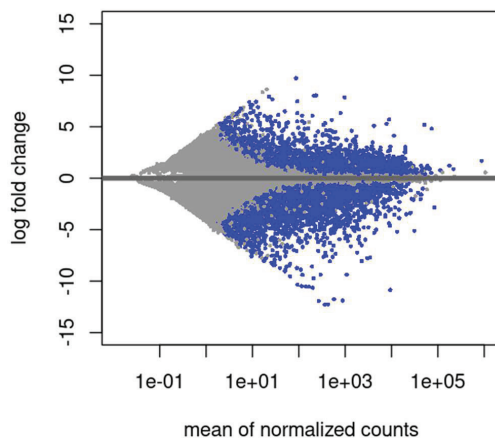
Figure 62 Gene expression changes in PBMC treated with AdV1+rRBD vs. PBMC control. Significantly up and downregulated genes marked in blue (adj p-value < 0.05). Legend: PBMC control means peripheral blood mononuclear cells. AdV1 stands for serotype 5/3 equipped with ICOSL and CD40L (Garofalo et al., 2021a), AdV1 in conc. of 100 VP/cell. rRBD stands for recombinant receptor binding domain protein (Baran et al., 2023 accepted for publication), rRBD in conc. of 2.62 µg/mL.

4.11.2. PBMCs treated with AdV1+S+N vs. Control

RNA-seq of PBMCs treated with AdV1+S+N (vs. control) showed 53 upregulated genes and 127 downregulated genes (padj < 0.05) (**Figure 63**). Among them special attention should be put on genes related to the Rap1 signalling pathway (p_{adj}=3.447×10^{-2}, **24**): ENSG00000154380, ENSG00000076864, ENSG00000101333, ENSG00000164742, ENSG00000160867, ENSG00000138193, ENSG00000114353, ENSG00000183454. The Rap1 signaling plays a key role in the immune response to the antigens. RAP1 is:

- involved in the development and differentiation of the T-cells,

- a component of the TCR signaling pathway,

- required for optimal T-cell activation and proliferation,

- involved in the regulation of Treg cells,

- playing a role in B-cell development (Katagiri et al., 2002; Kinashi and Katagiri, 2005).
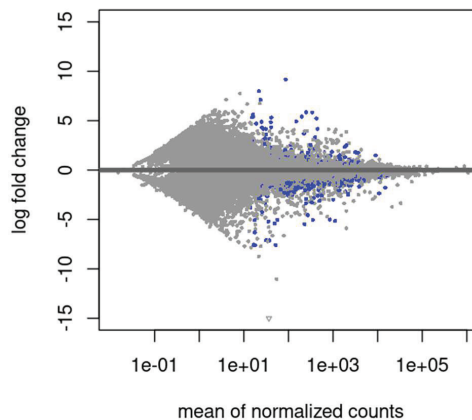
Figure 63 PBMC AdV1+S+N vs. PBMC control gene expression changes. In blue are significantly up and downregulated genes (adj p-value < 0.05). Legend: PBMC control means peripheral blood mononuclear cells. AdV1 stands for serotype 5/3 equipped with ICOSL and CD40L (Garofalo et al., 2021a), AdV1 in conc. of 100 VP/cell. Spike-S1-His (0.25 µg/mL) and Nucleocapsid-His (0.25 µg/mL) are recombinant proteins (InvivoGen USA).

Ensembl Gene ID	Comments
ENSG00000 154380	*ENAH* Gene The *ENAH* gene encodes a protein involved in actin-based motility, regulating actin filament assembly and cell adhesion/motility. Certain splice variants of this gene are associated with tumor invasiveness, potentially serving as prognostic markers. ENAH is part of the Ena/VASP protein family, contributing to cytoskeleton remodeling and cell polarity, including filopodia formation.
ENSG000000 76864	RAP1 GTPase Activating Protein (RAP1GAP) The RAP1GAP gene encodes a GTPase-activating protein (GAP) that regulates the activity of the RAP1 protein. RAP1 acts as a molecular switch, cycling between an inactive GDP-bound form and an active GTP-bound form. RAP1GAP promotes the hydrolysis of GTP, returning RAP1 to its inactive state. RAP1 is involved in various cellular processes such as cell proliferation, adhesion, differentiation, and embryogenesis. Mutations in RAP1GAP have been associated with Tuberous Sclerosis.
ENSG00000 101333	*PLCB4* gene The *PLCB4* gene encodes a protein that catalyzes the conversion of phosphatidylinositol 4,5-bisphosphate into inositol 1,4,5-trisphosphate and diacylglycerol. This reaction, which requires calcium, plays a crucial role in intracellular signal transduction in the retina.
ENSG00000 164742	*ADCY1* gene The *ADCY1* gene encodes a member of the adenylate cyclase gene family that is primarily expressed in the brain. ADCY1 is involved in catalyzing the formation of cyclic AMP (cAMP) in response to G-protein signaling and may play roles in regulatory processes, memory, learning, and circadian rhythm regulation in the retina.

Table 25 Genes related to Rap1 pathway expressed in PBMCs treated with AdV1+S+N (GeneCards.org; Accessed on: 01.06.2023 r.)

ENSG00000 160867	*FGFR4* gene The *FGFR4* gene encodes a tyrosine kinase and cell surface receptor for fibroblast growth factors (FGFs). This protein is involved in the regulation of various pathways, including cell proliferation, differentiation, migration, lipid metabolism, bile acid biosynthesis, vitamin D metabolism, glucose uptake, and phosphate homeostasis.
ENSG00000 138193	*PLCE1* gene The *PLCE1* gene encodes a phospholipase enzyme that plays a crucial role in cellular signaling. It catalyzes the breakdown of phosphatidylinositol-4,5-bisphosphate to generate two important second messengers, inositol 1,4,5-triphosphate (IP3) and diacylglycerol (DAG). These second messengers regulate various cellular processes such as cell growth, differentiation, and gene expression. The enzyme is regulated by small GTPases of the Ras and Rho families as well as heterotrimeric G proteins. Mutations in the *PLCE1* gene are associated with early-onset nephrotic syndrome, characterized by proteinuria, edema, and kidney abnormalities. PLCE1 has a bifunctional nature, also serving as a Ras guanine-exchange factor (RasGEF) that regulates small GTPases of the Ras superfamily. **It plays roles in cell survival, cell growth, actin organization, and T-cell activation.**
ENSG00000 114353	*GNAI2* gene The *GNAI2* gene encodes an alpha subunit of guanine nucleotide binding proteins (G proteins). These proteins are involved in various signaling pathways as modulators or transducers.
ENSG00000 183454	*GRIN2A* gene The *GRIN2A* is a gene that encodes a subunit of NMDA receptors, which are involved in memory and learning. The GRIN2A protein contributes to excitatory postsynaptic current, synaptic potentiation, and learning.

Table 25 (continued) Genes related to Rap1 pathway expressed in PBMCs treated with AdV1+S+N (GeneCards.org; Accessed on: 01.06.2023 r.)

4.11.3. Calu-3 treated with AdV1+S+N vs. Control

Analysis of Calu-3 sample treated with AdV1+S+N showed statistically significant expression of genes engaged in interleukin-10 production, regulation of interleukin-10 production, IL10-IL10RA complex, Delta1 homodimer complex, and Toxoplasmosis (**Figure 64**).

Gene name		"baseMean"	"log2Fold Change"	"pvalue"	"padj"
ENSG0000010 2245.9	CD40LG	300.93	7.40	7.90E-10	2.87 E-05
ENSG0000011 0324.12	IL10RA	4,261.17	-4.37	1.20E-07	2.18 E-03
ENSG0000019 8719.9	DLL1	262.31	3.09	1.90E-07	2.30 E-03
ENSG0000013 7642.13	SORL1	5.281.54	1.61	3.07E-06	2.78 E-02
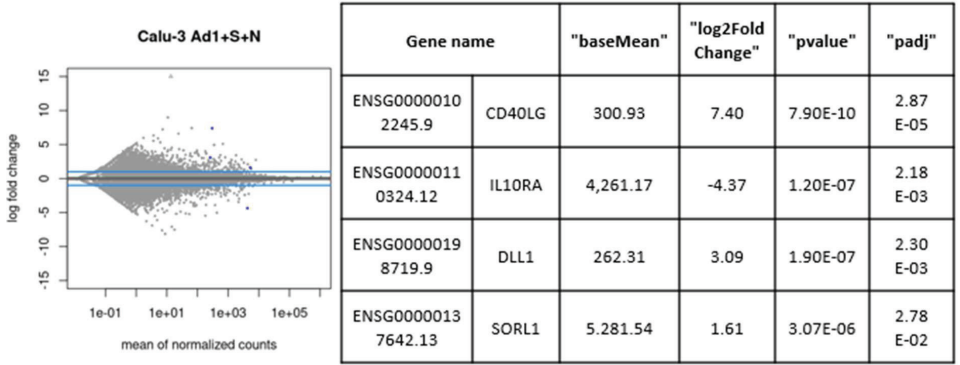
Figure 64 Calu-3 Ad1+S+N vs. Calu-3 control gene expression changes. Blue dots mark significantly up and downregulated genes (adj p-value < 0.05), blue lines show two fold change. Legend: PBMC control means peripheral blood mononuclear cells. AdV1 stands for serotype 5/3 equipped with ICOSL and CD40L (Garofalo et al., 2021a), AdV1 in conc. of 100 VP/cell. Spike-S1-His (0.25 µg/mL) and Nucleocapsid-His (0.25 µg/mL) are recombinant proteins (InvivoGen USA).

4.12. 3D model implementation in T cells' response studies

The establishment of 3D model was followed by the immune studies (**Figures 65 –67**). No statistically significant differences between the treatments and the untreated control were noted. V2 (AdV2+S-His+N-His) resulted in CD4$^+$ slightly increased (61.07±9.15%) compared to the untreated control (59.13±8.84%). For V1 (AdV1+S-His+N-His) vs. untreated control, the statistically insignificant changes were noted in CD8$^+$EMRA subpopulation (51.57±8.74% vs. 46.93±46.18%). Similar response was observed in V2 (AdV2-S-His+N-His) treated samples – 50.33±7.55% of CD8$^+$EMRA subpopulation compared to 46.93±46.18% in the untreated control . It is known that EMRA T cells show strong lymphocyte activation (Tian et al., 2017). The proposed model works and can be used as a non-clinical method fortesting immunogenic factors.
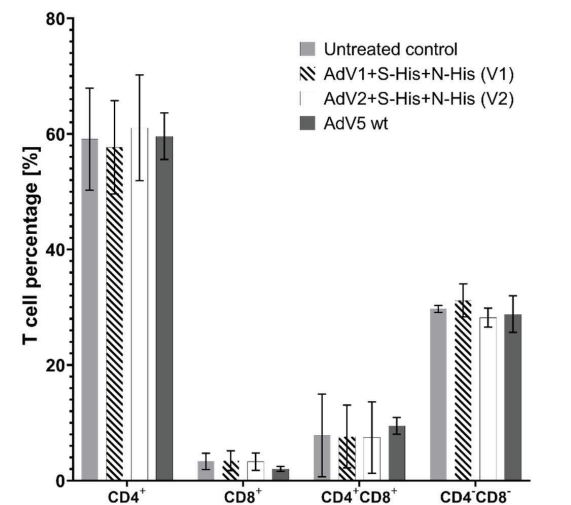
Figure 65 Percentage of T cells (CD4$^+$, CD8$^+$, CD4$^+$CD8$^+$, CD4$^-$CD8$^-$) incubated according to the following manner. AdV1+S-His+N-His (V1) and AdV2+S-His+N-His (V2) were added to the PBMC site of culture and left for 72 h incubation. The cells were rinsed and followed by 96 h immunogen-free incubation. Untreated control is peripheral blood mononuclear cells (PBMCs). AdV1 stands for serotype 5/3 equipped with ICOSL and CD40L (Garofalo et al., 2021a), AdV1 in conc. of 100 VP/cell. AdV2 meansadenovirus serotype 5/3 without ICOSL and CD40L. Spike-S1-His (0.25 µg/mL) and Nucleocapsid-His (0.25 µg/mL) are recombinant proteins (InvivoGen USA).

Figure 66 The percentage of central memory (CM) CD8$^+$, effector memory (EM) CD8$^+$, effector memory terminally differentiated (EMRA) CD8$^+$, and CD197$^+$CD45RA$^+$ CD8$^+$ incubated according to the following manner. AdV1+S-His+N-His (V1) and AdV2+S-His+N-His (V2) were added to the PBMC site of culture and left for 72 h incubation. The cells were rinsed and followed by 96 h immunogen-free incubation. Untreated control means peripheral blood mononuclear cells (PBMC). AdV1 stands for serotype 5/3 equipped with ICOSL and CD40L (Garofalo et al., 2021a), AdV1 in conc. of 100 VP/cell. AdV2 stands foradenovirus serotype 5/3 without ICOSL and CD40L. Spike-S1-His (0.25 µg/mL) and Nucleocapsid-His (0.25 µg/mL) are recombinant proteins (InvivoGen USA).
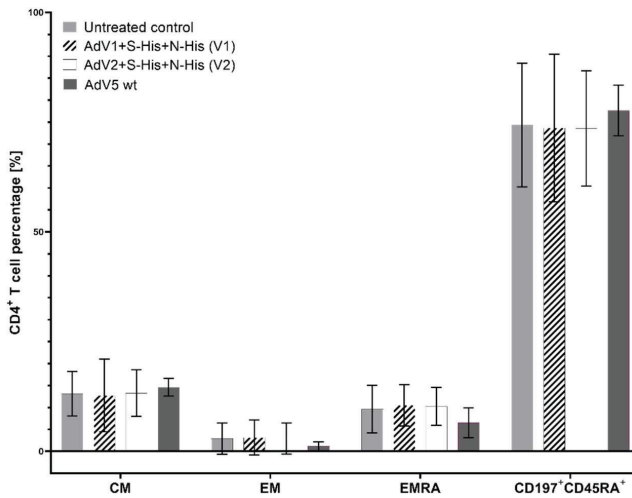
Figure 67 The percentage of central memory (CM) CD8^{+}, effector memory (EM) CD8^{+}, effector memory terminally differentiated (EMRA) CD8^{+}, and CD197^{+}CD45RA^{+} CD8^{+} incubated according to the following manner. AdV1+S-His+N-His (V1), AdV2+S-His+N-His (V2) and AdV5 were added to the PBMC site of culture and left for 72 h incubation. The cells were rinsed and followed by 96 h immunogen-free incubation. Untreated control means peripheral blood mononuclear cells (PBMC). AdV1 stands for serotype 5/3 equipped with ICOSL and CD40L (Garofalo et al., 2021a), AdV1 in conc. of 100 VP/cell. AdV2 means adenovirus serotype 5/3 without ICOSL and CD40L. Spike-S1-His (0.25 µg/mL) and Nucleocapsid-His (0.25 µg/mL) mean recombinant protein (InvivoGen USA). AdV5 wt stands for adenovirus serotype 5.

4.13. Detection of soluble cytokines

The cytometric bead array was performed to measure the secretion of 12 cytokines (IL-1 alpha, IL-1 beta, IL-2, IL-4, IL-6, IL-8, IL-10, IL-12p70, IL-17A, IL-17F, TNF alpha, INF gamma). Immunogenic factors representing the vaccination process were added to cell growth medium including PBMCs located under the insert. After 72 h incubation, PBMCs were rinsed and returned to the wells in the fresh culture medium without the immunogenic factors for the next 4 days of incubation. In the sample with proposed vaccine platform several cytokines were elevated compared to the control. AdV1+S-His+N-His caused increase in IL-10, IL-12p70, and IL-8 compared to the untreated control (**Figure 68**). Interestingly, the samples treated with AdV1+S-His, AdV1+N-His and AdV1+S-His+N-His showed elevated level of INF-γ. Treatment of the cells with the composition of AdV1+N-His, without spike protein, caused increase in IL-6 and IL-17F levels, and decrease in IL-17A and IL-2 levels, when compared to the untreated control. No changes in the level of IL-1α were observed.
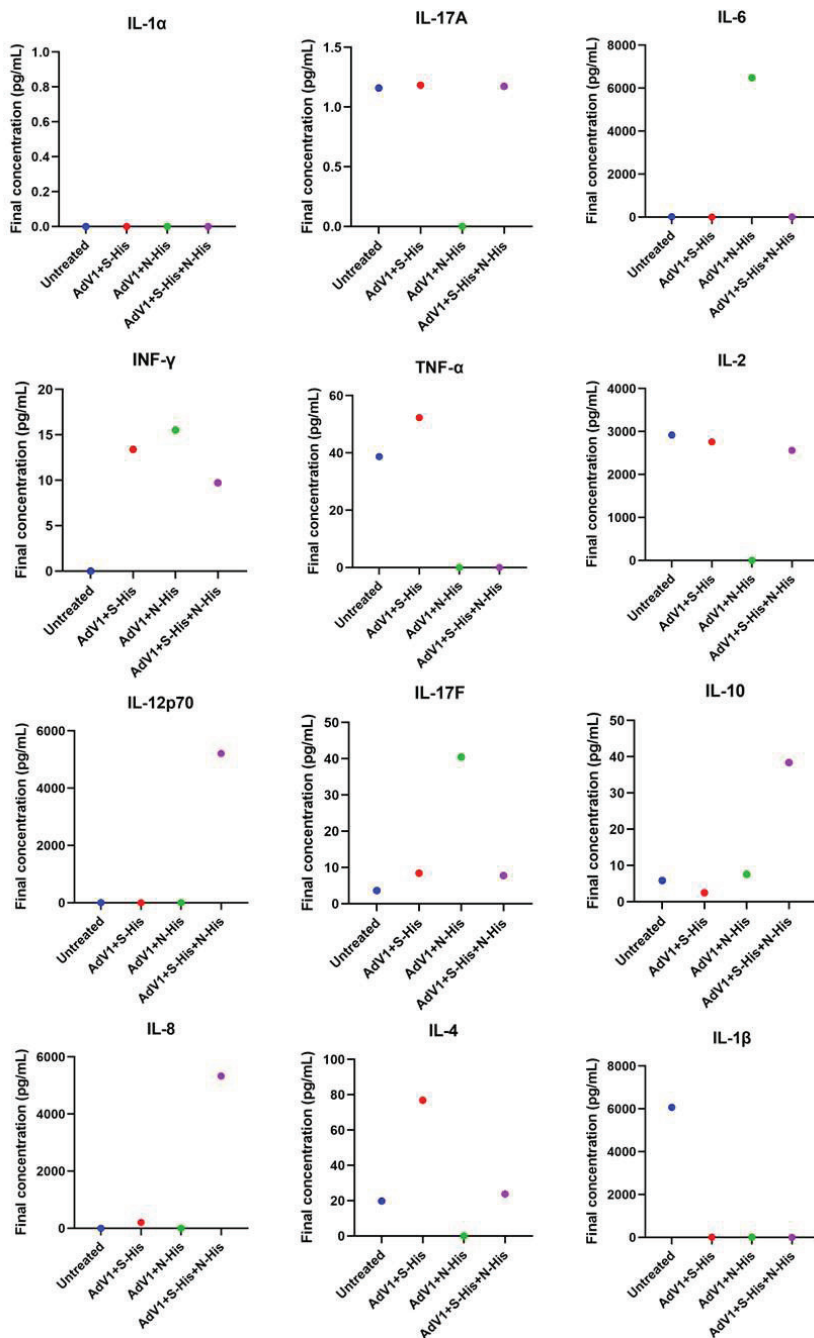
Figure 68 Cytokine profiling from 3D model samples. Legend: Untreated control means PBMCs. AdV1 stands for serotype 5/3 equipped with ICOSL and CD40L (Garofalo et al., 2021a), AdV1 in conc. of 100 VP/cell. Spike-S1-His (0.25 µg/mL) and Nucleocapsid-His (0.25 µg/mL) mean recombinant protein (InvivoGen USA).

4.14. *In vivo* analysis of adenovirus-based platform

In order to check the effect of the components of the vaccine platform on the survival of mice, an *in vivo* experiment was performed. For all treatments used, 100% survival was recorded on the 28th day of the experiment (**Figure 70**). Over the course of 7 days, increasing weight of mice was observed in all study groups (**Figure 69**). The exception is one of the mice treated with AdV1+S-His+N-His, which showed a statistically insignificant weight loss on day 7 (**Figure 71**). After the experiment was completed, organs were prepared from the mice. No significant differences were observed in the size of the lungs, peritoneal sac, liver, heart, spleen and kidneys between the tested samples and the control (PBS) (**Table 26**).
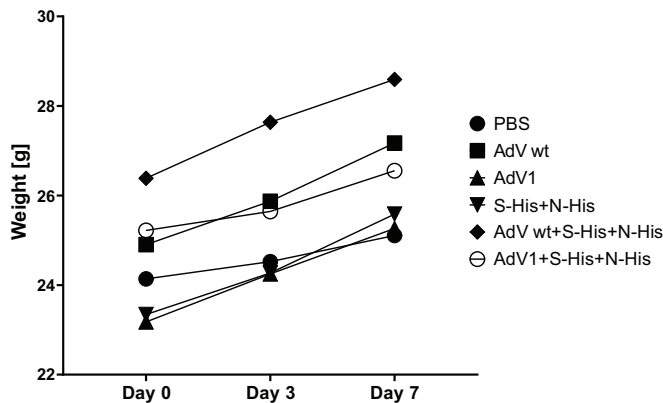
Figure 69 Mouse weight gain curves – the means. AdV1 stands for serotype 5/3 equipped with ICOSL and CD40L (Garofalo et al., 2021a), AdV wt stands for serotype 5/3 without costimulatory ligands. AdV's were used in conc. of 1×10^{10} VP/mL. Spike-S1-His (10 µg/mL) and Nucleocapsid-His (10 µg/mL) mean recombinant protein (InvivoGen USA).
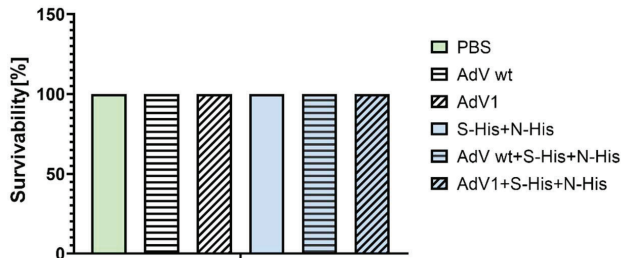
Figure 70 Mouse survivability in 28th day of the experiment – the means. AdV1 stands for serotype 5/3 equipped with ICOSL and CD40L (Garofalo et al., 2021a), AdV wt stands for serotype 5/3 without costimulatory ligands. AdV's were used in conc. of 1×10^{10} VP/mL. Spike-S1-His (10 µg/mL) and Nucleocapsid-His (10 µg/mL) mean recombinant protein (InvivoGen USA).
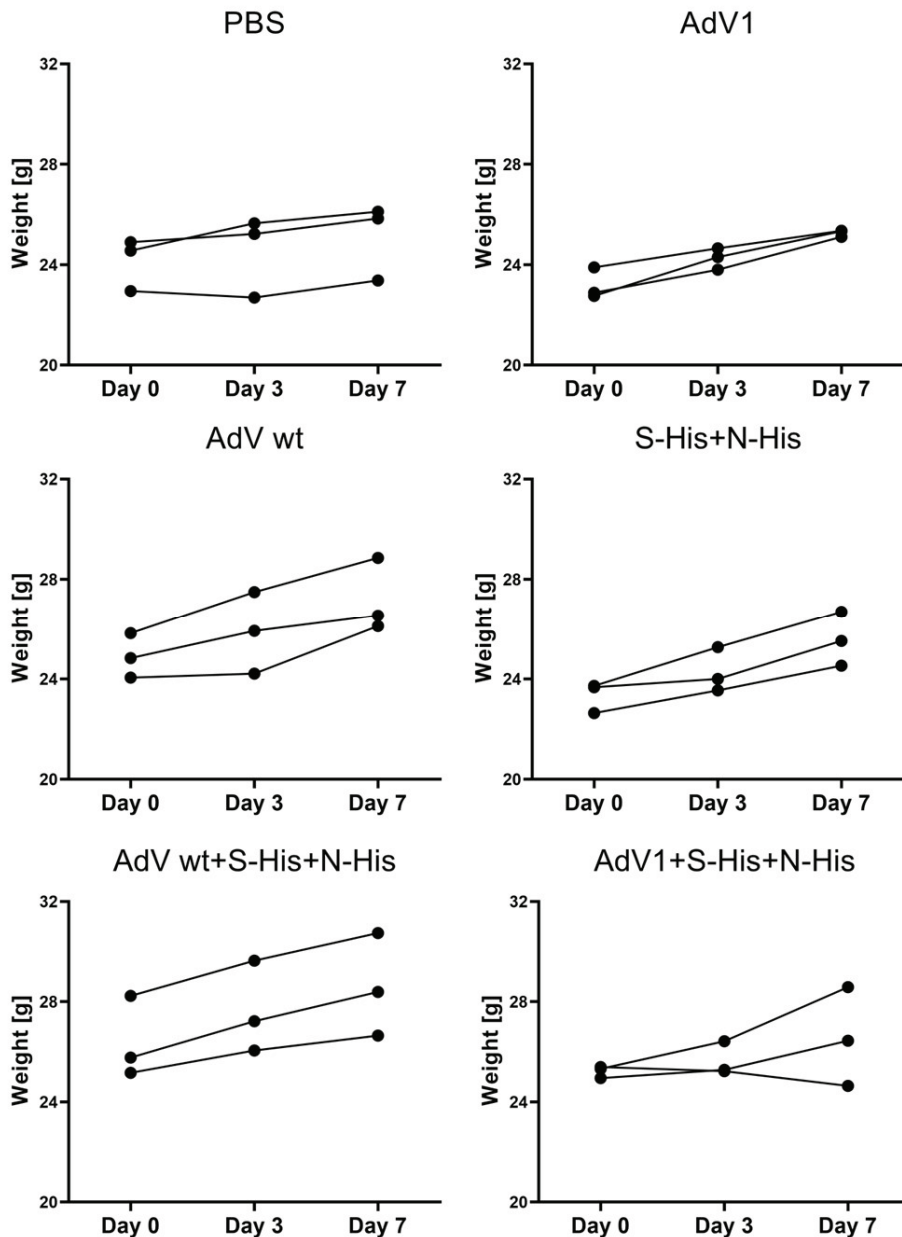
Figure 71 Mouse individual weight gain curves. AdV1 stands for serotype 5/3 equipped with ICOSL and CD40L (Garofalo et al., 2021a), AdV wt stands for serotype 5/3 without costimulatory ligands. AdV's were used in conc. of 1×10^{10} VP/mL. Spike-S1-His (10 µg/mL) and Nucleocapsid-His (10 µg/mL) mean recombinant protein (InvivoGen USA).

Treatment	Lungs	Peritoneal sac	Liver	Heart	Spleen	Kidneys
PBS						
AdV wt						
AdV1						
S-His+N-His						
AdV wt+ S-His+N-His						
AdV1+ S-His+N-His						

Table 26 Pictures of mouse organs prepared after day 7 of in vivo analysis of adenovirus-based platform. AdV1 stands for serotype 5/3 equipped with ICOSL and CD40L (Garofalo et al., 2021a), AdV wt stands for serotype 5/3 without costimulatory ligands. AdV's were used in conc. of 1×10^{10} VP/mL. Spike-S1-His (10 µg/mL) and Nucleocapsid-His (10 µg/mL) mean recombinant protein (InvivoGen USA).

Discussion

Understandring the immune response is essential for developing effective immunotherapy. In recent years, the use of PBMCs as an *in vitro* model has gained significant attention for studying immune response. The aim of my study was to establish reliable and optimized model engaging PBMCs along with the Calu-3 cell line for immunogenic factors development. Moreover, I presented the first *in vitro* investigation utilizing the adenoviral platform for delivering T cell immunogens ICOS and CD40 ligands in combination with antigens: rRBD or S-His or/and N-His.

Since the Calu-3 cells demonstrate a respiratory bronchial epithelial cell-like phenotype, these cells are used to study the pathology of the respiratory infections (Bol et al., 2014; Harcourt et al., 2011; Lee et al., 2021; Lodes et al., 2020). The Calu-3 cells are capable of secreting mucus, which makes them a good reflection of the conditions in the human body. My results indicated that the Calu-3 cell line cultured onto Transwell inserts in air-liquid conditions managed towards mucociliary phenotype, which is expressed as a cilia structure on its surface in contact with air (**Figure 61**). Harcourt et al., (2011) showed that the polarized Calu-3 cells are susceptible to respiratory syncytial virus (RSV) infection and predominantly release infectious virus from their apical surface, that proved the Calu-3 as a valuable *in vitro* model for investigating host responses to RSV infection. Since there was the emerging need of the respiratory infection model in COVID-19 pandemic, the Calu-3 cells' susceptibility to SARS-CoV-2 was studied. In the study (Dighe et al., 2022), several cell lines such as Caco-3, Calu-3 and VERO E6 were tested simultaneously to establish their susceptibility to SARS-CoV-2 entry and response mechanism to infections. SARS-CoV-2 Omicron (BA.1.1) replicates in Calu-3 more efficiently than in Caco-2. SARS-CoV and SARS-CoV-2 enter host cells via ACE2, and the kinetics of the STAT transcription factor's phosphorylation after virus infection can vary depending on the cell type (Dighe et al., 2022). In Calu-3 cells infected with SARS-CoV-2, STAT1 and STAT3 are activated, the inhibitors targeting STAT3 effectively suppress the SARS-CoV-2 production. The same transcription factors are activated in the VERO E6 cell line; however the mechanism of the virus entry and replication differs between these cell lines. In VERO E6, the phosphorylation of STAT1 and STAT3 decreases over time. Contrariwise, in Calu-3, phosphorylation persists leading to lower virus production (Dighe et al., 2022). It is therefore crucial to consider that the cellular responses to the SARS-CoV-2 infection vary depending on the host cell type, emphasizing the importance of using appropriate cell lines to study the pathophysiology and evaluate therapeutics for SARS-CoV-2 (Dighe et al., 2022).

In vitro studies of the immune response require not only careful cell line selection, but also experimental conditions. Cell lines are grown in culture media with the addition of FBS providing essential nutrients and growth factors necessary for cell growth. However, FBS also contains bioactive molecules that may influence the immune response of PBMCs *in vitro* (Liu et al., 2023). These include cytokines, growth factors, hormones, lipids and proteins. In my study, in order to minimize the influence of exogenous factors on the immune response, the Opti-MEM medium was used, which allowed to reduce the amount of FBS to 5%. Moreover, it is an optimal medium for co-culture of cell lines in the 3D models used in my study. Total resignation from FBS decreases cell viability and destabilizes cellular protein expression (Rashid and Coombs, 2019).

PBMCs are heterogenous population of blood cells that includes monocytes, lymphocytes, and macrophages. The composition of PBMCs' may vary based on factors like the donor's age. They are easily accessible from peripheral blood samples, such as buffy coats, and serve a valuable source for studying immune cell function and interactions. In my study, the incorporation of Opti-MEM into cell culture systems provided comparable outcomes in terms of viability and programmed cell death (**Figures 23–24**). It is important to consider the specific requirements of each study and the impact of the isolation and cryopreservation processes on the parameters being measured (Baran, 2022). Jeurink et al., (2008) showed that the kinetics of non-viable cells is changing during the passing time of the culture. Furthermore, Głaczynska et al., (2021) showed that low temperature and wrong culture media negatively affect the viability of PBMCs.

Before the optimization of PBMCs isolation and culture conditions, the results showed a significant decrease in the cell viability after 48 h ($P \leq 0.05$) and after 7 days of culture growth (**$P \leq 0.01$) (**Figure 23**). The introduction of optimal factors such as: conditioning of the skins bags before isolation at room temperature, dilution (1:1) of buffy coats with a mixture of culture medium and PBS, temperature gradient cryopreservation using the Cell Camper, and rapid thawing and washing away of cell-toxic DMSO, resulted in an increase in the number of viable cells from 48.15% to 88.88% on day 7 of culture (**Figure 24**). Thus, the optimization of storage temperature, freezing method, and culture media, allows to improve the cell viability significantly.

To evaluate the working concentrations of the immunogenic factors, the cell viability assays were applied. The cell viability is a critical aspect to assess the safety and efficacy of any immunization strategy (Pollard and Bijker, 2021). It provides valuable insights into the potential cytotoxic effects and overall health of cells upon exposure to immunogens

(Falahi and Kenarkoohi, 2022; Pollard and Bijker, 2021). I aimed to evaluate the impact of adenoviruses with and without co-stimulatory ligands CD40L and ICOSL in combination with antigens (rRBD or S-His, and/or N-His). To my knowledge, it is the first *in vitro* study with the adenoviral platform delivering the T cell immunogenes ICOS and CD40 ligands in formulation with SARS-CoV-2 antigens (Baran et al., 2024). Additionally, pseudo-SARS-CoV-2 and the anti-spike antibody were used. The comprehensive analysis of the cell viability using the MTS assay and flow cytometry were assessed. I obtained the comprehensive understanding of the cellular response to immunogenic stimulation (**Figures 32–35**).

The effects of immunogenic factors on the viability and cell metabolic activity of VERO E6 and PBMC cells in various combinations were examined (**Figures 27–31**). VERO E6 is valuable model of studying cytotoxicity and viral internalization (J. Wang et al., 2021). It is highly permissive to SARS-CoV-2 and related viruses (Essaidi-Laziosi et al., 2021). VERO E6 expresses the ACE2 receptor, which is a primary receptor used by SARS-CoV-2 to enter host cells (Mossel et al., 2005). This cell line provides a suitable environment for the propagation of SARS-CoVs, making it easier to study various aspects of viral biology (Keyaerts et al., 2005; Ogando et al., 2020). While VEROE6 cells may not fully represent the complexity and diversity of human respiratory cells, the findings should be studied with caution and complemented with relevant cell lines and models, e.g. PBMCs, Calu-3 cells, and 3D alveoli models. Additionally, the VERO E6 monolayer was used to visualize adenoviruses using SEM. The fibers of one adenoviral capsid can attach to the penton base of another capsid, forming a chain (Cao et al., 2012). In **Figure 34,** the effect of linking the multiple adenoviral capsids by the fibers was observed. These structures located on the surface of the capsid mediate the virus's attachment to host cells (Cao et al., 2012).

In the dissertation**,** the cytotoxicity assessment started from evaluating the impact of rRBD at different dillutions on theVEROE6 cells. **Figure 27** demonstrates that VEROE6 cells treated with rRBD in the concentration of 5.24 µg/mL exhibited a significant decrease in viability (13.3±0.7%) compared to the untreated control (100.0±12.0%). When working with the *E. coli*-derived proteins, the endotoxin contamination can occur (Schwarz et al., 2014). LPS endotoxin can trigger immune responses and cause unwanted effects in experimental systems (Sampath, 2018). The purifying process to remove the endotoxin contamination can be challenging due to technological standpoints such as, the heat-stable nature of endotoxin and their persistence after protein purification steps (Mamat et al., 2015; Petsch, 2000). The presence of endotoxins can lead to immune activation, inflammation, and inaccurate experimental results (Hannon and Prina-Mello, 2021; Virzì et al., 2022). The latter is in line

with our studies, rRBD induced excessive immune response of PBMCs (**Figure 37 - 48**). This led to the hypothesis that rRBD can be contaminated with the LPS endotoxin. Therefore, to ensure the quality of the further studies, the commercial proteins with proved standard quality were tested (Gao et al., 2022; Matsunaga and Tsumoto, 2022; McGuire et al., 2022; Merkuleva et al., 2022). **Figure 29** illustrates that the VERO E6 cells treated with the mixture of AdV1 and rRBD at concentrations of 5.2×10^9 VP/mL and 5.24 µg/mL, respectively, exhibited a significant decrease in viability (7.5±1.0%) compared to the untreated control (100.0±13.0%). Thus, the viability of the VERO E6 cells exposed to different dilutions of AdV1 was evaluated. As shown in **Figure 28**, the VERO E6 cells treated with AdV1 in the concentration of 5.2×10^4 VP/mL showed slightly increased metabolic activity (127.0±3.0%) compared to the untreated control (100.0±16.0%). AdV1 is armed with two costimulatory ligands, CD40L and ICOSL, which can contribute to that increase. As it was shown in **Figure 36**, AdV1 induces the CD40 gene relative expression in the VERO E6 cells. Next, the viability of the VERO E6 cells exposed to different concentrations of pseudo-SARS-CoV-2 was investigated (**Figure 30**). No significant decrease in the cell viability was observed. These findings highlight the differential effects of the tested immunogenic factors on the cell viability. Based on these results, specific concentrations were selected for the further experiments. My analysis revealed no significant changes in the PBMC viability compared to the control group (**Figure 30**), suggesting that the selected concentrations are accurate to study immune response.

The results from the study using CLSM demonstrated the effects of the immunogenic factors on pseudo-SARS-CoV-2 internalization in the VERO E6 cell line. The negative control (pseudo-SARS-CoV-2) showed effective internalization into the VERO E6 cells (**Figure 35**). Additionally, there are a few cells with necrotic nuclei stained with propidium iodide. The positive control sample displayed the limited internalization achieved by preincubating pseudo-SARS-CoV-2 with the anti-spike antibody. Compared to the control with pseudo-SARS-CoV-2, the presence of GFP in VERO E6 significantly decreased. Importantly, no necrotic nuclei were found in this approach. When VERO E6 was treated with the mixture of pseudo-SARS-CoV-2, AdV1, and rRBD, the GFP expression decreased (few necrotic nuclei occurred) compared to the control (pseudo-SARS-CoV-2). These results suggested that the tested formulation (AdV1+rRBD) can decrease the internalization of pseudo-SARS-CoV-2 into the VERO E6 cells. The presence of small number of necrotic nuclei indicates a potential cytotoxic effect associated with this formulation. My results are in line with the previous studies (Barh et al., 2021; Alexandre et al., 2022; Tamming et al., 2021). Briefly, Barh et al., (2021) discussed the interactions between the Spike receptor-binding domain (RBD) of

the SARS-CoV-2 virus and various extracellular domains of CD40, CD45, CD80, CD86, CD95, and CTLA4/CD152. The Authors (Barh et al., 2021) performed the protein–protein docking using ZDOCK and HDOCK servers, showing that the Spike-RBD interacts with a several hydrogen bonds in two complexes with the extracellular domain of CD40 (Barh et al., 2021). Alexandre et al., (2022) showed that the αCD40.RBD vaccine significantly reduces the infection of target cells in the trachea by 99.6% compared to the naïve group. This indicated a strong protective effect of the vaccine in preventing the internalization of the virus into these cells. In line with these studies, research based on Syrian hamsters showed, that a vaccine with CD40L has a beneficial effect on lung pathology, significantly reducing the damage, when compared to a non-adjuvanted with CD40L vaccine (Tamming et al., 2021). CD40 receptor is not directly used in the internalization process (Chatterjee et al., 2012). However, CD40 signaling can modulate intrnalization indirectly by influencing the expression of cytoskeletal regulatory proteins. For example, NF-κB activation downstream of CD40 signaling can regulate the expression of cytoskeletal regulators like Rho GTPases, which play a central role in controlling actin dynamics and cytoskeletal organization (Tong and Tergaonkar, 2014). The previous studies (Norris and Ovádi, 2021; Owczarek et al., 2018; Wen et al., 2021) suggested that cytoskeletal rearrangements play a crucial role in SARS-CoV-2. CoVs utilize various interactions with the host cell's cytoskeleton to facilitate their entry and replication (Norris and Ovádi, 2021; Wen et al., 2021). CoVs navigate along filopodia on the host membrane to reach entry sites, utilize specific intermediate filament proteins as co-receptors for cellular entry, hijack microtubules for transport to replication and assembly sites, and promote actin filament polymerization to facilitate viral egress (Norris and Ovádi, 2021; Wen et al., 2021). During CoV infection, disturbances in the host cell's cytoskeleton homeostasis and modification state are tightly linked to pathological processes such as defective cytokinesis, demyelination, cilia loss, and neuron necrosis. In my RNA-seq analysis, several connections to the described mechanisms occurred. For example, in the PBMCs treated with AdV1+S+N, genes connected to filopodium were significantly (p_{adj} =3.451×10^{-2}) up- and downregulated (Annex: g:Profiler GO analysis). In analysis of the Calu-3 cell line treated with immunogenic platform, CD40L gene (ENSG00000102245, p_{adj}=2.87×10^{-5}) was highly upregulated with the fold change equal to 7.40. It is worth emphasizing that release of CD40LG is directly regulated by actin polymerization (Furman et al., 2004). Following the conclusions on the importance of CD40 receptor in the SARS-CoV-2 pathogenesis, studies on the CD40 gene expression were conducted. To study the effect of the immunogenic factors on the VERO E6 cell activation, RT-qPCR was employed to assess the expression of CD40. The cells were incubated for 24 h

with or without stimulation at 34.5°C and 5% CO_2. The results, as shown in **Figure 36**, revealed that the CD40 gene expression was upregulated when cells were stimulated with AdV1 at 100 VP/mL, rRBD in 2.62 µg/mL, AdV1 in 50 VP/mL + rRBD at 2.62 µg/mL, and pseudo-SARS-CoV-2 in 100 VP/mL + Ab (antibody) in 5.24 µg/mL, compared to the untreated control (VERO E6 cells). Notably, a strong upregulation of the CD40 gene was observed in the sample treated with hCoV-OC43. These findings suggest that activation of the CD40 pathway may play a role in the immunogenic response to SARS-CoV-2 and may be a potential target for therapeutic interventions. Salvi et al., (2021) analyzed the expression of CD40 (mean fluorescence intensity) induced with the SARS-CoV-2–associated molecular patterns (SAMPs). SAMPs can include viral proteins, nucleic acids (RNA or DNA), or other molecules that are either produced by the viruses or are host molecules modified by the viral infection. These molecular patterns can be detected by the immune system and play a role in the immune response to the virus. The Authors (Salvi et al., 2021) found that SAMPs (SCV2-RNA1 and SCV2-RNA) induced the expression of CD40 in wild type mouses. However, the mechanisms underlying CD40 receptor involvement and its implications in the context of SARS-CoV-2 infection require further studies. Our previous studies (Baran et al. 2023) determined the signaling pathways that control immunological mechanisms by which the AdV1+rRBD platform induces protective immunity with the following: MAPK cascade, adipocytokine, cAMP, TNF, and Toll-like receptor (TLR).

Taken together the results from CD40 relative expression, RNA-Seq and the internalization studies, it was hypothesized, that cytoskeletal rearrangements can limit the viral internalization and lung damage, and can be a possible therapeutical target for coronavirus diseases. Further studies into the intricate relationship between coronaviruses and the host cell cytoskeleton hold promise for the development of targeted therapeutics in the future. While my study provides valuable insights into the dynamics of virus infection, it is important to acknowledge its limitations. Firstly, the study included VERO E6 and Calu-3 cell lines as models, and although they have proven to be reliable for studying viral infections, the findings may not directly translate to human organism *in vivo*. Therefore, caution should be exercised in extrapolating the results to human immunological responses.

PBMC provide a valuable model for investigating the impact of viruses on the immune system (Baran, 2022). By exposing PBMCs to viral antigens, we create the model of immune studies for preclinical step. For example, PBMCs were used to investigate immune responses to various viruses, including SARS-CoV-2, HIV, Dengue virus, or Influenza (Ducos et al., 1996; Kierstead et al., 2007; Still, n.d.; Tapia-Calle et al., 2019). Transcriptomic analysis of the PBMC data from COVID-19 patients identified abnormal mRNA and lncRNA

(long non-coding RNA) expression patterns, which can serve as potential biomarkers for disease severity (Shaath and Alajez, 2021). Additionally, the increased expression of genes such as TNF, IFN-γ, antiviral, HLA-DQA1, and HLA-F was observed in severe COVID-19 patients (Sadanandam et al., 2020). Sałkowska et al., (2020) investigated the impact of SARS-CoV-2 proteins, such as the spike (S) and nucleocapsid (N) proteins on the differentiation of CD4$^+$ lymphocytes. The study (Sałkowska et al., 2020) revealed the induction of IFNG (Interferon Gamma) in CD4$^+$ cells, suggesting the involvement of these lymphocytes in the response to SARS-CoV-2.

In the first step of the immune response studies, the 24-h exposition was applied (**Figures 37 – 47**). The PBMC-based system was established to evaluate the immunogenicity of the vaccine platform components. The samples were prepared by treating PBMCs for 24 h, and statistically significant changes were observed in the tested samples. The objective of the experiment was to assess the reaction of isolated and cryopreserved PBMCs to immunogenic factors within a short period of time, optimize the process of immunophenotyping, and evaluate the concentrations selected in previous stage. The results were compared with the untreated control and the LPS-treated control (MOCK). It was observed that the addition of rRBD to the samples tested in each of the cases caused a very strong immune response, which was manifested by decrease in CD4$^+$ T cells, an increase in CD8$^+$ T cells and CD19$^+$ B cells. In **Figures 46 – 47**, the increase in the class switching of B cells was observed (CD38$^-$CD24$^+$). Second step, was the elongation of the incubation time to 7 days of culture (**Figure 48**). A continued increase in the number of CD19$^+$ cells was observed in the rRBD-containing samples. As mentioned before, rRBD used in this study was 95% pure. Bacterial LPS activates the TLR4 receptor, which induces an early innate immune response. In addition, depending on the environment, CD4$^+$ cells differentiate into different subsets, such as Th1, Th2 and Th17 (Vella and McAleer, 2008). It is worthy to emphasize, that SARS-CoV-2 spike protein interacts with bacterial LPS in a critical way. It leads to aggravated inflammation both *in vitro* and *in vivo* by enhancing NF-κB activation and cytokine responses (Samsudin et al., 2022). The increased immune response can contribute to excessive inflammation seen in COVID-19 patients and can be linked to the severity of the disease. The activation of TLR4 by LPS and the potential involvement of spike protein in TLR4 signaling indicate a possible connection between SARS-CoV-2 infection and sepsis development (Zhao et al., 2021). Mechanistically, the spike protein of SARS-CoV-2 possesses multiple hydrophobic pockets, which are regions within the protein structure that have a strong affinity for hydrophobic molecules. These hydrophobic pockets exist in both the S1 and S2 subunits of the spike protein. LPS can

bind to these pockets with different affinity, which can have implications for viral entry, pathogenesis, and immune response (Petruk et al., 2020). The latter is in line with my results, as the samples treated with LPS and other immunogens, such as AdV1 and AdV2, generally did not generate significant changes compared to the control and MOCK.

Subsequent experiments were conducted without the additional LPS and with the use of the commercial spike and nucleocapsid proteins. Thieme et al., (2020) proved that it is crucial to evaluate the spike and nucleocapsid proteins individually for their ability to induce T-cell responses. Both proteins should be considered as prophylactic targets (Thieme et al., 2020). I provided the nucleocapsid to further studies to follow the most recent trends in the vaccine designs. The use of the proposed AdV1+S-His, AdV1+S+N (-His) and AdV1+N-His platforms after 24 h resulted in a significant increase in the number of $CD4^+$ T_{CM}, $CD4^+$ T_{EMRA} and in the samples treated with nucleocapsid, alone or in combination with spike, $CD4^+$ T_{EM} (**Figure 50**). My results correspond to the finding of Thieme et al., (2020), in which stronger response of $CD4^+$ T cells compared to $CD8^+$ T cells was observed. Subpopulations of $CD4^+$ T cells play a synergistic role in orchestrating the immune response (Pulendran and Ahmed, 2011). $CD4^+$ T cells have the ability to differentiate into various subsets of helper T cells with effector functions that provide protection against different pathogens (Pulendran and Ahmed, 2011).

I tested whether AdV1-treated samples showed a significant increase in the number of cells in early apoptosis compared to control and AdV2-treated samples (**Figure 24**) AdV1 is armed with co-stimulatory ligands CD40L and ICOSL (Garofalo et al. 2021a). The ability of the CD40 ligand to induce apoptosis is widely used in therapies using oncolytic viruses. While the precise mechanisms are not fully understood, CD40L-mediated apoptosis involves the modulation of apoptotic regulators and upregulation of pro-apoptotic molecules such as Fas ligand (FasL) and TNF-related apoptosis-inducing ligand (TRAIL) (Tong et al., 2000). CD40L drives the activation of a T_h1 response by engaging with CD40 on APCs. This response involves the secretion of IFN-γ and other cytokines, which enhance the immune response. The 7-day exposition of PBMCs to the treatments including AdV1 caused a strong induction of $CD4^+$ T cells. The strong implications in $CD4^+$ $T_{NAÏVE}$ and T_{SCM} were observed (**Figure 57**). T_{SCM} cells have antiviral potential and downregulate the expression of programmed cell death protein 1 (PD1), according to the findings of Cencioni et al. (2021). I noted significant decrease in T_{SCM} cells (**Figure 57**). This suggested that the experimental treatments used in the study resulted in the cytotoxic effects, leading to the death of these specific cell populations, which correlates with the apoptosis studies (**Figure 53**). The use of AdV1 in the tested samples also contributed to an increase in the number of $CD19^+$ cells (**Figure 65**). In the study by Schulz et

al., (2021) it was proven, that there is a strong correlation between the number of CD19$^+$IgD$^+$CD27$^-$ naïve B cells and the antibody level, it can be the predictor of the humoral response. The 7-day experiment proved that by extending the time we can obtain stronger immune responses in the proposed model (**Figure 48**), which are coherent with the *in vivo* studies in the matter of tendencies (Bardelli et al., 2013).

The next step was the evaluation of the more complex model with the co-culture of highly differentiated lung epithelial cells, and the PBMCs, as a model for vaccination and pathogenesis studies. It was checked how the use of the AdV1+S+N vaccine platform affects the genome level on the cells used in co-culture in the 3D model. PBMCs showed increased expression of eight genes associated with the RAP1 pathway, which are crucial for the immune response, affecting the differentiation of T and B lymphocytes (**Figure 63**,). Moreover, Rap1 acts as a key regulator of T cell and APC interactions by modulating the adhesive interactions between T cells and antigen-loaded APCs (Katagiri et al., 2002). The activation state of Rap1 plays a crucial role in determining the outcome of T cell responses to antigen stimulation (Katagiri et al., 2002), ranging from productive activation to activation-induced cell death or unresponsiveness. It is worth emphasizing that in my studies one of the Rap1 genes, FGFR4 is underregulated (p_{adj}=7.83×10^{-5}) in the PBMC genome. In the study by Easter et al., (2020) including mice, it was proven that FGFR4 plays a key role in the process of airway inflammation. The absence of FGFR4 in the lungs is associated with increased levels of inflammatory mediators, such as IL-6 (Easter et al., 2020). On the contrary, downregulation of the FGFR4 gene in our study do not correlate with the increased IL-6 expression.

The variations in cytokine levels were additionally checked using flow cytometry cytokine profiling. Increase in IL-10, IL-12p70, and IL-8 in sample treated with AdV1+S-His+N-His was observed (**Figure 68**). The increase in IL-10 level suggests that the formulation caused anti-inflammatory response. It may indicate that immune cells try to regulate vaccine induced inflammation to manage tissue damage. At the same time, IL-12p70 indicated a robust immune activation. This cytokine is associated with immune response involving T-cells and NK cells, which are the effective defence against infections. Elevated concentrations of IL-8 and IL-12P70 were found to induce antibody levels (Loughran et al., 2018). Notably, IL-12P70, recognized as a pivotal cytokine in fostering a Th1-dominated cellular immune response, exhibited the capacity to activate B lymphocytes, consequently promoting the synthesis of antibodies (Fu et al., 2021). In all of the proposed vaccine formulations containing AdV1 elevated INF-γ level was observed (**Figure 68**). It suggests a specific immune response involving cellular immunity. INF-γ plays crucial role in activating

immune cells, such as macrophages and T cells to targeted infected cells. In the context of assessing cellular immunity following COVID-19 vaccination, the dynamics of interferon (IFN-γ) changes have emerged as a significant indicator of immune responses. IFNs have been implicated in the body's defence against SARS-CoV-2, the virus causing COVID-19 (Feng et al., 2021; Hadjadj et al., 2020; Liu et al., 2022). A well-modulated IFN response can help control viral replication and promote the development of immune memory (Wakui et al., 2022). Looking at the vaccine without the spike protein, increase in IL-6 and IL-17F were observed (**Figure 68**). IL-6 increase is a typical in the patients vaccinated with inactivated

SARS-CoV-2 vaccines (Fu et al., 2021). At the same time, decrease in IL-17A and IL-2 levels could indicate about the controlled immune response, as the elevated level of IL-17A is associated to COVID-19 severity and progression (Lv et al., 2022; Maione et al., 2021).

The completion of the research was an *in vivo* experiment in which it was proven that the proposed vaccine platform system based on non-replicating adenoviruses AdV1 and AdV2 does not negatively affect the survival of mice (100% survival in a 28-day experiment; **Figure 71**) and does not cause changes in the development of organs such as lungs, heart, kidneys, spleen and perinate sac (**Table 26**).

5. Limitations of the study and future prospects

The research carried out in this thesis provided many new conclusions but contains some limitations. The proposed model of vaccine platform contains commercially available proteins with His-tags. Some studies suggest that His-tag increases the overall immunogenicity and alters the fine specificity of immune responses (Randolph, 2012). In the recent studies on non C-terminal tagged SARS-CoV-2 RBD it was proven, that the addition of a His-tag may significantly impair protein immunogenicity against SARS-CoV-2 (Khan et al., 2012; Lin et al., 2022). However, other studies indicate that its presence has no apparent effect on the immune response (Mason et al., 2002). Ambiguous conclusions from literature studies indicate that it would be beneficial to test the vaccine platform also using proteins that do not contain a His-tag, but this poses numerous challenges in terms of antigen purification at the production stage. As presented in the dissertation, RBD without His-tag, after using a different purification method, carries the risk of contamination with endotoxins, which undoubtedly interfere with the results of immune response tests (Schwarz et al. (2014)). Endotoxins, specifically lipopolysaccharide (LPS), have the capacity to trigger immune responses and introduce undesired effects in experimental systems, as reported by Sampath (2018). The challenge lies in the purification process, where removing endotoxin contamination can be intricate due to technological constraints, including the heat-stable nature of endotoxins and their persistence even after protein purification steps, as noted by Mamat et al. (2015) and Petsch (2000). The presence of endotoxins introduces the risk of immune activation, inflammation, and the generation of inaccurate experimental results (Hannon and Prina-Mello (2021) and Virzì et al. (2022). In alignment with these concerns, the study observed that rRBD induced an excessive immune response in peripheral blood mononuclear cells (PBMCs). This observation led to the hypothesis that rRBD used in the initial study set-up may be contaminated with LPS endotoxin.

Another limitation of the study is the length of the immune response experiments. It is a well-known fact, that in human organism antibody production after vaccination generally occurs within 2 – 4 weeks, with some detectable as early as 2 days, but peak titers are reached between 1 – 8 weeks (Jamshidi et al., 2022). Most of the corresponding 3D models are not possible to be cultured for such long periods of time, especially with keeping a reliable amount of each immune cells subpopulations, which are already isolated in their mature forms (Tapia-Calle et al., 2019). This leads to the use of the animal models, which have their own limitations themselves.

The choice of the cell lines have a great impact on utility of the model too. VERO E6 and Calu-3 have proven to be reliable for studying viral infections (Park et al., 2021). However, the findings may not directly translate to human organism *in vivo*. Therefore, caution should be exercised in extrapolating the results to human immunological responses.

Analysis of the genome background of the immune responses is a key for full understanding of these processes. RNA-Seq is valuable for comprehensive transcriptome analysis, while RT-qPCR excels in targeted, high-precision quantification of specific genes. Both of these methods are complementary, although to show a full picture and obtaining more statistically relevant answers, much more samples (RNA-Seq) and genes (RT-qPCR) should be analysed.

Therefore, an important reinforcement for the conducted research would be the use of different antigens with different or without tags to find out what effect they have on the immune response. It is also crucial for future research to extend the duration of experiments, which would enable the vaccines to come closer to the time of action in the human body. It could also be beneficial to explore more cell lines and create more complex 3D models that would further reflect *in vivo* interactions. Widening of the genome analysis to different genes from immune response pathways is crucial for expanding research with new conclusions. What is more, native viruses should also be tested on the model in the next step.

6. Conclusions

This PhD dissertation aimed to unravel the intricacies of immune responses and their interplay with diverse immunogenic using a carefully refined *in vitro* model. The study made significant progress in understanding immune responses and their interactions with various immunogenic factors, such as novel adenovirus-based vaccine platforms using an optimized *in vitro* model. The study revealed the complexities of virus-host dynamics, shedding a light on potential therapeutic avenues to combat viral infections. The chosen approach proved effective in addressing research questions.

- Establishment of a 3D *in vitro* model using PBMCs and the Calu-3 cell line allowed comprehensive exploration leading to insightful findings into immune response to viruses. Longer culture times proved critical in capturing the nuances of the immune response, revealing the dynamics of these interactions.

- It was proven that adenovirus-based platforms act as adjuvants impacting $CD4^+$, $CD8^+$, and $CD19^+$ subpopulations. The crucial role of ICOS/ICOSL pathway well known and reported *in vivo* occurred also in *in vitro* model, due to T cell activation and differentiation. The stimulation of PBMCs with the vaccine platform has lasting effects on $CD4^+$ and $CD8^+$ T cells, affecting central memory, effector memory, and T_{EMRA} cells. The platform shows also potential in stimulating B cells development and differentiation, with the focus on antigen-specific B cells.

- The variations in cytokine levels suggest distinct immune reactions, including inflammation, immune cell activation, regulatory responses, and potential shifts in the balance of specific immune cell populations. Adenovirus-based platform influence the production of cytokines influencing effector cytotoxic T cells or B cells.

- The research showed new facts of immune regulation and influence of CD40 pathway on immune cell populations. Novel insight highlighted the potential for therapeutic approaches targeting this pathway. For further research, deeper evaluation of the CD40 pathway's mechanistic role would be beneficial. Exploring its impact on the different viral infections could reveal broader therapeutic applications. Moreover, extending the framework of this study to investigate immune responses in more complex *ex vivo* settings could provide a comprehensive understanding of the translational changes.

- The findings presented in the dissertation show how *in vitro* and *ex vivo* testing is important, proving that these are promising directions for further research and practical applications for immunotherapy.

- It has been shown that equipping adenoviruses with CD40L and ICOSL co-stimulating ligands has a high immunostimulatory potential with initially confirmed safety and biodistribution in *in vivo* studies.

List of figures

List of tables

Reference list

1. Abbasifard, M., Khorramdelazad, H., 2020. The bio-mission of interleukin-6 in the pathogenesis of COVID-19: A brief look at potential therapeutic tactics. Life Sciences 257, 118097. https://doi.org/10.1016/j.lfs.2020.118097

2. Agrawal, P., Nawadkar, R., Ojha, H., Kumar, J., Sahu, A., 2017. Complement Evasion Strategies of Viruses: An Overview. Front. Microbiol. 8, 1117. https://doi.org/10.3389/fmicb.2017.01117

3. Aitken, C., 2010. Clinical Virology, 3rd Edition Clinical Virology, 3rd Edition Edited by D. D. Richman , R. J. Whitley , and F. G. Hayden Washington, DC: ASM Press, 2009. 1408 pp, Illustrated. $259.59 (hardcover). CLIN INFECT DIS 50, 1692–1692. https://doi.org/10.1086/652862

4. Alam, I., Radovanovic, A., Incitti, R., Kamau, A.A., Alarawi, M., Azhar, E.I., Gojobori, T., 2021. CovMT: an interactive SARS-CoV-2 mutation tracker, with a focus on critical variants. The Lancet Infectious Diseases 21, 602.

5. Albornoz, E.A., Amarilla, A.A., Modhiran, N., Parker, S., Li, X.X., Wijesundara, D.K., Aguado, J., Zamora, A.P., McMillan, C.L.D., Liang, B., Peng, N.Y.G., Sng, J.D.J., Saima, F.T., Fung, J.N., Lee, J.D., Paramitha, D., Parry, R., Avumegah, M.S., Isaacs, A., Lo, M.W., Miranda-Chacon, Z., Bradshaw, D., Salinas-Rebolledo, C., Rajapakse, N.W., Wolvetang, E.J., Munro, T.P., Rojas-Fernandez, A., Young, P.R., Stacey, K.J., Khromykh, A.A., Chappell, K.J., Watterson, D., Woodruff, T.M., 2022. SARS-CoV-2 drives NLRP3 inflammasome activation in human microglia through spike protein. Molecular Psychiatry. https://doi.org/10.1038/s41380-022-01831-0

6. Andrews, S., n.d. A quality control tool for high throuput sequence data.

7. Añez, G., Volkova, E., Fares, R.C.G., Jiang, Z., Rios, M., 2016. EXPERT COMMITTEE ON BIOLOGICAL STANDARDIZATION Geneva, 17-21 October 2016.

8. Bacchetta, R., 2016. Immunodysregulation, Polyendocrinopathy, and Enteropathy, X-Linked (IPEX) Syndrome, in: Encyclopedia of Immunobiology. Elsevier, pp. 444–450. https://doi.org/10.1016/B978-0-12-374279-7.18008-7

9. Baran, J., 2022. Practical applications of peripheral blood mononuclear cells (PBMCs) in immunotherapy preclinical research. Journal of Current Science and Technology 12, 592604. https://doi.org/10.14456/JCST.2022.45

10. Bardelli, M., Alleri, L., Angiolini, F., Buricchi, F., Tavarini, S., Sammicheli, C., Nuti, S., Degl'Innocenti, E., Isnardi, I., Fragapane, E., Del Giudice, G., Castellino, F., Galli, G., 2013. Ex Vivo Analysis of Human Memory B Lymphocytes Specific for A and B Influenza Hemagglutinin by Polychromatic Flow-Cytometry. PLoS ONE 8, e70620. https://doi.org/10.1371/journal.pone.0070620

11. Batty, C.J., Heise, M.T., Bachelder, E.M., Ainslie, K.M., 2021. Vaccine formulations in clinical development for the prevention of severe acute respiratory syndrome coronavirus 2 infection. Advanced Drug Delivery Reviews 169, 168–189. https://doi.org/10.1016/j.addr.2020.12.006

12. Baum, A., Fulton, B.O., Wloga, E., Copin, R., Pascal, K.E., Russo, V., Giordano, S., Lanza, K., Negron, N., Ni, M., 2020. Antibody cocktail to SARS-CoV-2 spike protein prevents rapid mutational escape seen with individual antibodies. Science 369, 1014–1018.

13. Bednarek, A., Balcer, N., Samborski, W., Jabłecka, A., n.d. Leki biologiczne stosowane w reumatologii – część 1 Biological treatment in rheumatic diseases – part 9.

14. Bol, L., Galas, J.-C., Hillaireau, H., Le Potier, I., Nicolas, V., Haghiri-Gosnet, A.-M., Fattal, E., Taverna, M., 2014. A microdevice for parallelized pulmonary permeability studies. Biomed Microdevices 16, 277–285. https://doi.org/10.1007/s10544-013-9831-3

15. Burrell, C.J., Howard, C.R., Murphy, F.A., 2017. Chapter 6 - Adaptive Immune Responses to Infection, in: Burrell, C.J., Howard, C.R., Murphy, F.A. (Eds.), Fenner and White's Medical Virology (Fifth Edition). Academic Press, London, pp. 65–76. https://doi.org/10.1016/B978-0-12-375156-0.00006-0

16. Calu-3, n.d.

17. Campbell, G.R., To, R.K., Hanna, J., Spector, S.A., 2021. SARS-CoV-2, SARS-CoV-1, and HIV-1 derived ssRNA sequences activate the NLRP3 inflammasome in human macrophages through a non-classical pathway. iScience 24, 102295. https://doi.org/10.1016/j.isci.2021.102295

18. Cao, C., Dong, X., Wu, X., Wen, B., Ji, G., Cheng, L., Liu, H., 2012. Conserved fiber-penton base interaction revealed by nearly atomic resolution cryo-electron microscopy of the structure of adenovirus provides insight into receptor interaction. J Virol 86, 12322–12329. https://doi.org/10.1128/JVI.01608-12

19. Catalán, D., Mansilla, M.A., Ferrier, A., Soto, L., Oleinika, K., Aguillón, J.C., Aravena, O., 2021. Immunosuppressive Mechanisms of Regulatory B Cells. Front. Immunol. 12, 611795. https://doi.org/10.3389/fimmu.2021.611795

20. Cencioni, M.T., Ali, R., Nicholas, R., Muraro, P.A., 2021. Defective CD19+CD24hiCD38hi transitional B-cell function in patients with relapsing-remitting MS. Mult Scler 27, 1187–1197. https://doi.org/10.1177/1352458520951536

21. Chatterjee, B., Smed-Sörensen, A., Cohn, L., Chalouni, C., Vandlen, R., Lee, B.-C., Widger, J., Keler, T., Delamarre, L., Mellman, I., 2012. Internalization and endosomal degradation of receptor-bound antigens regulate the efficiency of cross presentation by human dendritic cells. Blood 120, 2011–2020. https://doi.org/10.1182/blood-2012-01-402370

22. Chavda, V.P., Bezbaruah, R., Valu, D., Patel, B., Kumar, A., Prasad, S., Kakoti, B.B., Kaushik, A., Jesawadawala, M., 2023. Adenoviral Vector-Based Vaccine Platform for COVID-19: Current Status. Vaccines 11, 432. https://doi.org/10.3390/vaccines11020432

23. Chen, A.T., Altschuler, K., Zhan, S.H., Chan, Y.A., Deverman, B.E., 2021. COVID-19 CG enables SARS-CoV-2 mutation and lineage tracking by locations and dates of interest. eLife 10, e63409. https://doi.org/10.7554/eLife.63409

24. Chen, M., Zhang, X.-E., 2021. Construction and applications of SARS-CoV-2 pseudoviruses: a mini review. Int. J. Biol. Sci. 17, 1574–1580. https://doi.org/10.7150/ijbs.59184

25. Cid, R., Bolívar, J., 2021. Platforms for Production of Protein-Based Vaccines: From Classical to Next-Generation Strategies. Biomolecules 11, 1072. https://doi.org/10.3390/biom11081072

26. cytvia, n.d. Methodology and applications - Isolation of mononuclear cells.

27. Dai, L., Gao, G.F., 2021. Viral targets for vaccines against COVID-19. Nature Reviews Immunology 21, 73–82. https://doi.org/10.1038/s41577-020-00480-0

28. Dighe, H., Sarkale, P., Patil, D.Y., Mohandas, S., Shete, A.M., Sahay, R.R., Lakra, R., Patil, S., Majumdar, T., Gawande, P., Yemul, J., Vedpathak, P., Yadav, P.D., 2022. Differential Cell Line Susceptibility to the SARS-CoV-2 Omicron BA.1.1 Variant of Concern. Vaccines 10, 1962. https://doi.org/10.3390/vaccines10111962

29. Ducos, J., Bianchi-Mondain, A.-M., Pageaux, G., Conge, A.M., Poncet, R., Vendrell, J.P., Segondy, M., Serre, A., 1996. Hepatitis B virus (HBV)-specific in vitro antibody production by peripheral blood mononuclear cells (PBMC) after vaccination by recombinant hepatitis B surface antigen (rHBsAg). Clin Exp Immunol 103, 15–18. https://doi.org/10.1046/j.1365-2249.1996.928621.x

30. Duffy, S., 2018. Why are RNA virus mutation rates so damn high? PLoS Biol 16, e3000003. https://doi.org/10.1371/journal.pbio.3000003

31. Easter, M., Garth, J., Harris, E.S., Shei, R.-J., Helton, E.S., Wei, Y., Denson, R., Zaharias, R., Rowe, S.M., Geraghty, P., Faul, C., Barnes, J.W., Krick, S., 2020. Fibroblast Growth Factor Receptor 4 Deficiency Mediates Airway Inflammation in the Adult Healthy Lung? Front. Med. 7, 317. https://doi.org/10.3389/fmed.2020.00317

32. Essaidi-Laziosi, M., Perez Rodriguez, F.J., Hulo, N., Jacquerioz, F., Kaiser, L., Eckerle, I., 2021. Estimating clinical SARS-CoV-2 infectiousness in Vero E6 and primary airway epithelial cells. The Lancet Microbe 2, e571. https://doi.org/10.1016/S2666-5247(21)00216-0

33. European Medicines Agency, n.d. Treatments and vaccines for COVID-19 [WWW Document]. Treatments and vaccines for COVID-19. URL https://www.ema.europa.eu/en/human-regulatory/overview/public-health-threats/coronavirus-disease-covid-19/treatments-vaccines-covid-19 (accessed 9.22.22).

34. European Medicines Agency (EMA), n.d. COVID-19 treatments: authorised. URL https://www.ema.europa.eu/en/human-regulatory/overview/public-health-threats/coronavirus-disease-covid-19/treatments-vaccines/treatments-covid-19/covid-19-treatments-authorised

35. Falahi, S., Kenarkoohi, A., 2022. Host factors and vaccine efficacy: Implications for COVID-19 vaccines. Journal of Medical Virology 94, 1330–1335. https://doi.org/10.1002/jmv.27485

36. Feng, H., Zhang, Y.-B., Gui, J.-F., Lemon, S.M., Yamane, D., 2021. Interferon regulatory factor 1 (IRF1) and anti-pathogen innate immune responses. PLoS Pathog 17, e1009220. https://doi.org/10.1371/journal.ppat.1009220

37. Fiedler, K., Lazzaro, S., Lutz, J., Rauch, S., Heidenreich, R., 2016. mRNA Cancer Vaccines, in: Walther, W. (Ed.), Current Strategies in Cancer Gene Therapy, Recent Results in Cancer Research. Springer International Publishing, Cham, pp. 61–85. https://doi.org/10.1007/978-3-319-42934-2_5

38. Flanagan, K.L., Best, E., Crawford, N.W., Giles, M., Koirala, A., Macartney, K., Russell, F., Teh, B.W., Wen, S.C., 2020. Progress and Pitfalls in the Quest for Effective SARS-CoV-2 (COVID-19) Vaccines. Front. Immunol. 11, 579250. https://doi.org/10.3389/fimmu.2020.579250

39. Fu, Y., Chen, F., Cui, L., Zhao, Y., Zhang, H., Fu, S., Zhang, J., 2021. Immunological Analysis of People in Northeast China after SARS-CoV-2 Inactivated Vaccine Injection. Vaccines 9, 1028. https://doi.org/10.3390/vaccines9091028

40. Furman, M.I., Krueger, L.A., Linden, M.D., Barnard, M.R., Frelinger, A.L., Michelson, A.D., 2004. Release of soluble CD40L from platelets is regulated by glycoprotein IIb/IIIa and actin polymerization. Journal of the American College of Cardiology 43, 2319–2325. https://doi.org/10.1016/j.jacc.2003.12.055

41. Gadotti, A.C., de Castro Deus, M., Telles, J.P., Wind, R., Goes, M., Garcia Charello Ossoski, R., de Padua, A.M., de Noronha, L., Moreno-Amaral, A., Baena, C.P., Tuon, F.F., 2020. IFN-γ is an independent risk factor associated with mortality in patients with moderate and severe COVID-19 infection. Virus Research 289, 198171. https://doi.org/10.1016/j.virusres.2020.198171

42. Gao, X., Peng, S., Mei, S., Liang, K., Khan, M.S.I., Vong, E.G., Zhan, J., 2022. Expression and functional identification of recombinant SARS-CoV-2 receptor binding domain (RBD) from *E. coli* system. Preparative Biochemistry & Biotechnology 52, 318–324. https://doi.org/10.1080/10826068.2021.1941106

43. Garofalo, M., Bertinato, L., Staniszewska, M., Wieczorek, M., Salmaso, S., Schrom, S., Rinner, B., Pancer, K.W., Kuryk, L., 2021a. Combination Therapy of Novel Oncolytic Adenovirus with Anti-PD1 Resulted in Enhanced Anti-Cancer Effect in Syngeneic Immunocompetent Melanoma Mouse Model. Pharmaceutics 13, 547. https://doi.org/10.3390/pharmaceutics13040547

44. Garofalo, M., Bertinato, L., Staniszewska, M., Wieczorek, M., Salmaso, S., Schrom, S., Rinner, B., Pancer, K.W., Kuryk, L., 2021b. Combination Therapy of Novel Oncolytic Adenovirus with Anti-PD1 Resulted in Enhanced Anti-Cancer Effect in Syngeneic Immunocompetent Melanoma Mouse Model 1–22.

45. Garofalo, M., Staniszewska, M., Salmaso, S., Caliceti, P., Pancer, K.W., Wieczorek, M., Kuryk, L., 2020. Prospects of Replication-Deficient Adenovirus Based Vaccine Development against SARS-CoV-2. Vaccines 8, 293. https://doi.org/10.3390/vaccines8020293

46. Gattinger, P., Ohradanova-Repic, A., Valenta, R., 2023. Importance, Applications and Features of Assays Measuring SARS-CoV-2 Neutralizing Antibodies. IJMS 24, 5352. https://doi.org/10.3390/ijms24065352

47. Gazzano-Santoro, H., Ralph, P., Ryskamp, T.C., Chen, A.B., Mukku, V.R., 1997. A non-radioactive complement-dependent cytotoxicity assay for anti-CD20 monoclonal antibody. J Immunol Methods 202, 163–171. https://doi.org/10.1016/s0022-1759(97)00002-1

48. GeneCopoeia, n.d. COVID-19 Neutralizing Antibody Screening Services.

49. Głaczynska, M., Machcinska, M., Donskow-Lysoniewska, K., 2021. Effects of Different Media on Human T Regulatory Cells Phenotype. In Vivo 35, 283–289. https://doi.org/10.21873/invivo.12257

50. Glanz, A., Chakravarty, S., Varghese, M., Kottapalli, A., Fan, S., Chakravarti, R., Chattopadhyay, S., 2021. Transcriptional and Non-Transcriptional Activation, Posttranslational Modifications, and Antiviral Functions of Interferon Regulatory Factor 3 and Viral Antagonism by the SARS-Coronavirus. Viruses 13, 575. https://doi.org/10.3390/v13040575

51. Golubovskaya, V., Wu, L., 2016. Different Subsets of T Cells, Memory, Effector Functions, and CAR-T Immunotherapy. Cancers 8, 36. https://doi.org/10.3390/cancers8030036

52. Gordon, D.E., Jang, G.M., Bouhaddou, M., Xu, J., Obernier, K., O'Meara, M.J., Guo, J.Z., Swaney, D.L., Tummino, T.A., Huettenhain, R., Kaake, R.M., Richards, A.L., Tutuncuoglu, B., Foussard, H., Batra, J., Haas, K., Modak, M., Kim, M., Haas, P., Polacco, B.J., Braberg, H., Fabius, J.M., Eckhardt, M., Soucheray, M., Bennett, M.J., Cakir, M., McGregor, M.J., Li, Q., Naing, Z.Z.C., Zhou, Y., Peng, S., Kirby, I.T., Melnyk, J.E., Chorba, J.S., Lou, K., Dai, S.A., Shen, W., Shi, Y., Zhang, Z., Barrio-Hernandez, I., Memon, D., Hernandez-Armenta, C., Mathy, C.J.P., Perica, T., Pilla, K.B., Ganesan, S.J., Saltzberg, D.J., Ramachandran, R., Liu, X., Rosenthal, S.B., Calviello, L., Venkataramanan, S., Liboy-Lugo, J., Lin, Y., Wankowicz, S.A., Bohn, M., Sharp, P.P., Trenker, R., Young, J.M., Cavero, D.A., Hiatt, J., Roth, T.L., Rathore, U., Subramanian, A., Noack, J., Hubert, M., Roesch, F., Vallet, T., Meyer, B., White, K.M., Miorin, L., Rosenberg, O.S., Verba, K.A., Agard, D., Ott, M., Emerman, M., Ruggero, D., García-Sastre, A., Jura, N., von Zastrow, M., Taunton, J., Ashworth, A., Schwartz, O., Vignuzzi, M., d'Enfert, C., Mukherjee, S., Jacobson, M., Malik, H.S., Fujimori, D.G., Ideker, T., Craik, C.S., Floor, S., Fraser, J.S., Gross, J., Sali, A., Kortemme, T., Beltrao, P., Shokat, K., Shoichet, B.K., Krogan, N.J., 2020. A SARS-CoV-2-Human Protein-Protein Interaction Map Reveals Drug Targets and Potential Drug-Repurposing. bioRxiv 2020.03.22.002386. https://doi.org/10.1101/2020.03.22.002386

53. Gu, J., Gong, E., Zhang, B., Zheng, J., Gao, Z., Zhong, Y., Zou, W., Zhan, J., Wang, S., Xie, Z., Zhuang, H., Wu, B., Zhong, H., Shao, H., Fang, W., Gao, D., Pei, F., Li, X., He, Z., Xu, D., Shi, X., Anderson, V.M., Leong, A.S.-Y., 2005. Multiple organ infection and the pathogenesis of SARS. Journal of Experimental Medicine 202, 415–424. https://doi.org/10.1084/jem.20050828

54. Guideline on clinical evaluation of vaccines, n.d.

55. Guo, Y., Hu, K., Li, Y., Lu, C., Ling, K., Cai, C., Wang, W., Ye, D., 2022. Targeting TNF-α for COVID-19: Recent Advanced and Controversies. Front. Public Health 10, 833967. https://doi.org/10.3389/fpubh.2022.833967

56. Hadjadj, J., Yatim, N., Barnabei, L., Corneau, A., Boussier, J., Smith, N., Péré, H., Charbit, B., Bondet, V., Chenevier-Gobeaux, C., Breillat, P., Carlier, N., Gauzit, R., Morbieu, C., Pène, F., Marin, N., Roche, N., Szwebel, T.-A., Merkling, S.H., Treluyer, J.-M., Veyer, D., Mouthon, L., Blanc, C., Tharaux, P.-L., Rozenberg, F., Fischer, A., Duffy, D., Rieux-Laucat, F., Kernéis, S., Terrier, B., 2020. Impaired type I interferon activity and inflammatory responses in severe COVID-19 patients. Science 369, 718–724. https://doi.org/10.1126/science.abc6027

57. Hagmann, M., 2000. Computers Aid Vaccine Design. Science 290, 80–82. https://doi.org/10.1126/science.290.5489.80

58. Hamming, I., Timens, W., Bulthuis, M., Lely, A., Navis, G., van Goor, H., 2004. Tissue distribution of ACE2 protein, the functional receptor for SARS coronavirus. A first step in understanding SARS pathogenesis. J. Pathol. 203, 631–637. https://doi.org/10.1002/path.1570

59. Hannon, G., Prina-Mello, A., 2021. Endotoxin contamination of engineered nanomaterials: Overcoming the hurdles associated with endotoxin testing. WIREs Nanomed Nanobiotechnol 13, e1738. https://doi.org/10.1002/wnan.1738

60. Haque, S.M., Ashwaq, O., Sarief, A., Azad John Mohamed, A.K., 2020. A comprehensive review about SARS-CoV-2. Future Virology 15, 625–648. https://doi.org/10.2217/fvl-2020-0124

61. Harcourt, J.L., Caidi, H., Anderson, L.J., Haynes, L.M., 2011. Evaluation of the Calu-3 cell line as a model of in vitro respiratory syncytial virus infection. Journal of Virological Methods 174, 144–149. https://doi.org/10.1016/j.jviromet.2011.03.027

62. Hashimoto, G., Wright, P.F., Karzon, D.T., 1983. Antibody-dependent cell-mediated cytotoxicity against influenza virus-infected cells. J Infect Dis 148, 785–794. https://doi.org/10.1093/infdis/148.5.785

63. Hashimoto, M., Im, S.J., Araki, K., Ahmed, R., 2019. Cytokine-Mediated Regulation of CD8 T-Cell Responses During Acute and Chronic Viral Infection. Cold Spring Harb Perspect Biol 11, a028464. https://doi.org/10.1101/cshperspect.a028464

64. Hoffmann, M., Kleine-Weber, H., Pöhlmann, S., 2020a. A Multibasic Cleavage Site in the Spike Protein of SARS-CoV-2 Is Essential for Infection of Human Lung Cells. Molecular Cell 78, 779-784.e5. https://doi.org/10.1016/j.molcel.2020.04.022

65. Hoffmann, M., Kleine-Weber, H., Schroeder, S., Krüger, N., Herrler, T., Erichsen, S., Schiergens, T.S., Herrler, G., Wu, N.-H., Nitsche, A., Müller, M.A., Drosten, C., Pöhlmann, S., 2020b. SARS-CoV-2 Cell Entry Depends on ACE2 and TMPRSS2 and Is Blocked by a Clinically Proven Protease Inhibitor. Cell 181, 271-280.e8. https://doi.org/10.1016/j.cell.2020.02.052

66. Holm, M.R., Poland, G.A., 2021. Critical aspects of packaging, storage, preparation, and administration of mRNA and adenovirus-vectored COVID-19 vaccines for optimal efficacy. Vaccine 39, 457–459. https://doi.org/10.1016/j.vaccine.2020.12.017

67. https://www.genecopoeia.com/, n.d. Lentifect™ SARS-CoV-2 Spike-Pseudotyped Lentivirus.

68. InvivoGen, n.d. SARS-CoV-2 Spike S1-His fusion protein.

69. InvivoGen, n.d. SARS-CoV-2 Nucleocapsid-His fusion protein.

70. Islam, H., Chamberlain, T.C., Mui, A.L., Little, J.P., 2021. Elevated Interleukin-10 Levels in COVID-19: Potentiation of Pro-Inflammatory Responses or Impaired Anti-Inflammatory Action? Front. Immunol. 12, 677008. https://doi.org/10.3389/fimmu.2021.677008

71. Jamilloux, Y., Henry, T., Belot, A., Viel, S., Fauter, M., El Jammal, T., Walzer, T., François, B., Sève, P., 2020. Should we stimulate or suppress immune responses in COVID-19? Cytokine and anti-cytokine interventions. Autoimmunity Reviews 19, 102567. https://doi.org/10.1016/j.autrev.2020.102567

72. Jamshidi, E., Asgary, A., Shafiekhani, P., Khajeamiri, Y., Mohamed, K., Esmaily, H., Jamal Rahi, S., Mansouri, N., 2022. Longevity of immunity following COVID-19 vaccination: a comprehensive review of the currently approved vaccines. Human Vaccines & Immunotherapeutics 18, 2037384. https://doi.org/10.1080/21645515.2022.2037384

73. Jeurink, P.V., Vissers, Y.M., Rappard, B., Savelkoul, H.F.J., 2008. T cell responses in fresh and cryopreserved peripheral blood mononuclear cells: Kinetics of cell viability, cellular subsets, proliferation, and cytokine production. Cryobiology 57, 91–103. https://doi.org/10.1016/j.cryobiol.2008.06.002

74. Ji, X., Sheng, Y., Guan, Y., Li, Y., Xu, Y., Tang, L., 2022. Evaluation of Calu-3 cell lines as an *in vitro* model to study the inhalation toxicity of flavoring extracts. Toxicology Mechanisms and Methods 32, 171–179. https://doi.org/10.1080/15376516.2021.1977880

75. Jiang, H., Lei, R., Ding, S.-W., Zhu, S., 2014. Skewer: a fast and accurate adapter trimmer for next-generation sequencing paired-end reads. BMC Bioinformatics 15, 182. https://doi.org/10.1186/1471-2105-15-182

76. Katagiri, K., Hattori, M., Minato, N., Kinashi, T., 2002. Rap1 Functions as a Key Regulator of T-Cell and Antigen-Presenting Cell Interactions and Modulates T-Cell Responses. Molecular and Cellular Biology 22, 1001–1015. https://doi.org/10.1128/MCB.22.4.1001-1015.2002

77. Kawabe, T., Matsushima, M., Hashimoto, N., Imaizumi, K., Hasegawa, Y., 2011. CD40/CD40 ligand interactions in immune responses and pulmonary immunity. Nagoya J Med Sci 73, 69–78.

78. Kempuraj, D., Selvakumar, G.P., Ahmed, M.E., Raikwar, S.P., Thangavel, R., Khan, A., Zaheer, S.A., Iyer, S.S., Burton, C., James, D., Zaheer, A., 2020. COVID-19, Mast Cells, Cytokine Storm, Psychological Stress, and Neuroinflammation. Neuroscientist 26, 402–414. https://doi.org/10.1177/1073858420941476

79. Kervevan, J., Chakrabarti, L.A., 2021. Role of CD4+ T Cells in the Control of Viral Infections: Recent Advances and Open Questions. IJMS 22, 523. https://doi.org/10.3390/ijms22020523

80. Kesheh, M.M., Hosseini, P., Soltani, S., Zandi, M., 2022. An overview on the seven pathogenic human coronaviruses. Reviews in Medical Virology 32. https://doi.org/10.1002/rmv.2282

81. Keyaerts, E., Vijgen, L., Maes, P., Neyts, J., Ranst, M.V., 2005. Growth kinetics of SARS-coronavirus in Vero E6 cells. Biochemical and Biophysical Research Communications 329, 1147–1151. https://doi.org/10.1016/j.bbrc.2005.02.085

82. Khan, F., Legler, P.M., Mease, R.M., Duncan, E.H., Bergmann-Leitner, E.S., Angov, E., 2012. Histidine affinity tags affect MSP1 $_{42}$ structural stability and immunodominance in mice. Biotechnology Journal 7, 133–147. https://doi.org/10.1002/biot.201100331

83. Khani, E., Shahrabi, M., Rezaei, H., Pourkarim, F., Afsharirad, H., Solduzian, M., 2022. Current evidence on the use of anakinra in COVID-19. International Immunopharmacology 111, 109075. https://doi.org/10.1016/j.intimp.2022.109075

84. Kierstead, L.S., Dubey, S., Meyer, B., Tobery, T.W., Mogg, R., Fernandez, V.R., Long, R., Guan, L., Gaunt, C., Collins, K., Sykes, K.J., Mehrotra, D.V., Chirmule, N., Shiver, J.W., Casimiro, D.R., 2007. Enhanced Rates and Magnitude of Immune Responses Detected against an HIV Vaccine: Effect of Using an Optimized Process for Isolating PBMC. AIDS Research and Human Retroviruses 23, 86–92. https://doi.org/10.1089/aid.2006.0129

85. Kinashi, T., Katagiri, K., 2005. Regulation of immune cell adhesion and migration by regulator of adhesion and cell polarization enriched in lymphoid tissues. Immunology 116, 164–171. https://doi.org/10.1111/j.1365-2567.2005.02214.x

86. Kozlov, E.M., Ivanova, E., Grechko, A.V., Wu, W.-K., Starodubova, A.V., Orekhov, A.N., 2021. Involvement of Oxidative Stress and the Innate Immune System in SARS-CoV-2 Infection. Diseases 9, 17. https://doi.org/10.3390/diseases9010017

87. Kreft, M.E., Jerman, U.D., Lasič, E., Hevir-Kene, N., Rižner, T.L., Peternel, L., Kristan, K., 2015. The characterization of the human cell line Calu-3 under different culture conditions and its use as an optimized in vitro model to investigate bronchial epithelial function. European Journal of Pharmaceutical Sciences 69, 1–9. https://doi.org/10.1016/j.ejps.2014.12.017

88. Kuzmicki, M., Telejko, B., Wawrusiewicz-Kurylonek, N., Lipinska, D., Pliszka, J., Wilk, J., Zielinska, A., Skibicka, J., Szamatowicz, J., Kretowski, A., Gorska, M., 2013. The expression of genes involved in NF-κB activation in peripheral blood mononuclear cells of patients with gestational diabetes. European Journal of Endocrinology 168, 419–427. https://doi.org/10.1530/EJE-12-0654

89. Kyriazopoulou, E., Huet, T., Cavalli, G., Gori, A., Kyprianou, M., Pickkers, P., Eugen-Olsen, J., Clerici, M., Veas, F., Chatellier, G., Kaplanski, G., Netea, M.G., Pontali, E., Gattorno, M., Cauchois, R., Kooistra, E., Kox, M., Bandera, A., Beaussier, H., Mangioni, D., Dagna, L., van der Meer, J.W.M., Giamarellos-Bourboulis, E.J., Hayem, G., Kyriazopoulou, E., Huet, T., Cavalli, G., Gori, A., Kyprianou, M., Pickkers, P., Eugen-Olsen, J., Clerici, M., Veas, F., Chatellier, G., Kaplanski, G., Netea, M.G.,

Pontali, E., Gattorno, M., Cauchois, R., Kooistra, E., Kox, M., Bandera, A., Beaussier, H., Mangioni, D., Dagna, L., van der Meer, J.W.M., Giamarellos-Bourboulis, E.J., Hayem, G., Volpi, S., Sormani, M.P., Signori, A., Bozzi, G., Minoia, F., Aliberti, S., Grasselli, G., Alagna, L., Lombardi, A., Ungaro, R., Agostoni, C., Blasi, F., Costantino, G., Fracanzani, A.L., Montano, N., Peyvandi, F., Sottocorno, M., Muscatello, A., Filocamo, G., Papadopoulos, A., Mouktaroudi, M., Karakike, E., Saridaki, M., Gkavogianni, T., Katrini, K., Vechlidis, N., Avgoustou, C., Chalvatzis, S., Marantos, T., Damoulari, C., Damoraki, G., Ktena, S., Tsilika, M., Koufargyris, P., Karageorgos, A., Droggiti, D.-I., Koliakou, A., Poulakou, G., Tsiakos, K., Myrodia, D.-M., Gravvani, A., Trontzas, I.P., Syrigos, K., Kalomenidis, I., Kranidioti, E., Panagopoulos, P., Petrakis, V., Metallidis, S., Loli, G., Tsachouridou, O., Dalekos, G.N., Gatselis, N., Stefos, A., Georgiadou, S., Lygoura, V., Milionis, H., Kosmidou, M., Papanikolaou, I.C., Akinosoglou, K., Giannitsioti, E., Chrysos, G., Mavroudis, P., Sidiropoulou, C., Adamis, G., Fragkou, A., Rapti, A., Alexiou, Z., Symbardi, S., Masgala, A., Kostaki, K., Kostis, E., Samarkos, M., Bakakos, P., Tzavara, V., Dimakou, K., Tzatzagou, G., Chini, M., Kotsis, V., Tsoukalas, G., Bliziotis, I., Doumas, M., Argyraki, A., Kainis, I., Fantoni, M., Cingolani, A., Angheben, A., Cardellino, C.S., Castelli, F., Serino, F.S., Nicastri, E., Ippolito, G., Bassetti, M., Selmi, C., 2021. Effect of anakinra on mortality in patients with COVID-19: a systematic review and patient-level meta-analysis. The Lancet Rheumatology 3, e690–e697. https://doi.org/10.1016/S2665-9913(21)00216-2

90. Le Bon, A., Tough, D.F., 2002. Links between innate and adaptive immunity via type I interferon. Current Opinion in Immunology 14, 432–436. https://doi.org/10.1016/S0952-7915(02)00354-0

91. Lee, D.F., Lethem, M.I., Lansley, A.B., 2021. A comparison of three mucus-secreting airway cell lines (Calu-3, SPOC1 and UNCN3T) for use as biopharmaceutical models of the nose and lung. European Journal of Pharmaceutics and Biopharmaceutics 167, 159–174. https://doi.org/10.1016/j.ejpb.2021.07.016

92. Lei, C., Yang, J., Hu, J., Sun, X., 2021. On the Calculation of TCID50 for Quantitation of Virus Infectivity. Virol. Sin. 36, 141–144. https://doi.org/10.1007/s12250-020-00230-5

93. Lin, T.-W., Huang, P.-H., Liao, B.-H., Chao, T.-L., Tsai, Y.-M., Chang, S.-C., Chang, S.-Y., Chen, H.-W., 2022. Tag-Free SARS-CoV-2 Receptor Binding Domain (RBD),

but Not C-Terminal Tagged SARS-CoV-2 RBD, Induces a Rapid and Potent Neutralizing Antibody Response. Vaccines 10, 1839. https://doi.org/10.3390/vaccines10111839

94. Linterman, M.A., Vinuesa, C.G., 2010. T Follicular Helper Cells During Immunity and Tolerance, in: Liston, A. (Ed.), Progress in Molecular Biology and Translational Science. Academic Press, pp. 207–248. https://doi.org/10.1016/S1877-1173(10)92009-7

95. Liu, D.X., Liang, J.Q., Fung, T.S., 2021. Human Coronavirus-229E, -OC43, -NL63, and -HKU1 (Coronaviridae), in: Encyclopedia of Virology. Elsevier, pp. 428–440. https://doi.org/10.1016/B978-0-12-809633-8.21501-X

96. Liu, Q., Chi, S., Dmytruk, K., Dmytruk, O., Tan, S., 2022. Coronaviral Infection and Interferon Response: The Virus-Host Arms Race and COVID-19. Viruses 14, 1349. https://doi.org/10.3390/v14071349

97. Liu, S., Yang, W., Li, Y., Sun, C., 2023. Fetal bovine serum, an important factor affecting the reproducibility of cell experiments. Scientific Reports 13, 1942. https://doi.org/10.1038/s41598-023-29060-7

98. Liu, Z., VanBlargan, L.A., Bloyet, L.-M., Rothlauf, P.W., Chen, R.E., Stumpf, S., Zhao, H., Errico, J.M., Theel, E.S., Liebeskind, M.J., 2021. Identification of SARS-CoV-2 spike mutations that attenuate monoclonal and serum antibody neutralization. Cell host & microbe 29, 477–488.

99. Lodes, N., Seidensticker, K., Perniss, A., Nietzer, S., Oberwinkler, H., May, T., Walles, T., Hebestreit, H., Hackenberg, S., Steinke, M., 2020. Investigation on Ciliary Functionality of Different Airway Epithelial Cell Lines in Three-Dimensional Cell Culture. Tissue Engineering Part A 26, 432–440. https://doi.org/10.1089/ten.tea.2019.0188

100. Loganathan, S., Kuppusamy, M., Wankhar, W., Gurugubelli, K.R., Mahadevappa, V.H., Lepcha, L., Choudhary, A. kumar, 2021. Angiotensin-converting enzyme 2 (ACE2): COVID 19 gate way to multiple organ failure syndromes. Respiratory Physiology & Neurobiology 283, 103548. https://doi.org/10.1016/j.resp.2020.103548

101. Loughran, S.T., Power, P.A., Maguire, P.T., McQuaid, S.L., Buchanan, P.J., Jonsdottir, I., Newman, R.W., Harvey, R., Johnson, P.A., 2018. Influenza infection directly alters

innate IL-23 and IL-12p70 and subsequent IL-17A and IFN-γ responses to pneumococcus in vitro in human monocytes. PLoS ONE 13, e0203521. https://doi.org/10.1371/journal.pone.0203521

102. Lukashev, A.N., Zamyatnin, A.A., 2016. Viral Vectors for Gene Therapy: Current State and Clinical Perspectives. Biochemistry (Mosc) 81, 700–708. https://doi.org/10.1134/S0006297916070063

103. Lv, Z., Li, Q., Feng, Z., Zheng, X., NaYin, Yang, H., Gu, Q., Ying, S., Qi, Y., Li, X., Wu, R., Wu, Z., Yu, X., Zou, N., Qin, D., Wan, C., 2022. Inactivated SARS-CoV-2 vaccines elicit immunogenicity and T-cell responses in people living with HIV. International Immunopharmacology 102, 108383. https://doi.org/10.1016/j.intimp.2021.108383

104. Maecker, H.T., McCoy, J.P., Nussenblatt, R., 2012. Standardizing immunophenotyping for the Human Immunology Project. Nat Rev Immunol 12, 191–200. https://doi.org/10.1038/nri3158

105. Mahase, E., 2021. Covid-19: Pfizer's paxlovid is 89% effective in patients at risk of serious illness, company reports. BMJ 375. https://doi.org/10.1136/bmj.n2713

106. Maione, F., Casillo, G.M., Raucci, F., Salvatore, C., Ambrosini, G., Costa, L., Scarpa, R., Caso, F., Bucci, M., 2021. Interleukin-17A (IL-17A): A silent amplifier of COVID-19. Biomedicine & Pharmacotherapy 142, 111980. https://doi.org/10.1016/j.biopha.2021.111980

107. Makaremi, S., Asgarzadeh, A., Kianfar, H., Mohammadnia, A., Asghariazar, V., Safarzadeh, E., 2022. The role of IL-1 family of cytokines and receptors in pathogenesis of COVID-19. Inflamm. Res. 71, 923–947. https://doi.org/10.1007/s00011-022-01596-w

108. Mamat, U., Wilke, K., Bramhill, D., Schromm, A.B., Lindner, B., Kohl, T.A., Corchero, J.L., Villaverde, A., Schaffer, L., Head, S.R., Souvignier, C., Meredith, T.C., Woodard, R.W., 2015. Detoxifying Escherichia coli for endotoxin-free production of recombinant proteins. Microbial Cell Factories 14, 57. https://doi.org/10.1186/s12934-015-0241-5

109. Martinelli, D.D., 2022. In silico vaccine design: A tutorial in immunoinformatics. Healthcare Analytics 2, 100044. https://doi.org/10.1016/j.health.2022.100044

110. Mason, A.B., He, Q.-Y., Halbrooks, P.J., Everse, S.J., Gumerov, D.R., Kaltashov, I.A., Smith, V.C., Hewitt, J., MacGillivray, R.T.A., 2002. Differential Effect of a His Tag at the N- and C-Termini: Functional Studies with Recombinant Human Serum Transferrin. Biochemistry 41, 9448–9454. https://doi.org/10.1021/bi025927l

111. Masre, S.F., Jufri, N.F., Ibrahim, F.W., Abdul Raub, S.H., 2021. Classical and alternative receptors for SARS-CoV-2 therapeutic strategy. Rev Med Virol 31, 1–9. https://doi.org/10.1002/rmv.2207

112. Matsunaga, R., Tsumoto, K., 2022. Addition of arginine hydrochloride and proline to the culture medium enhances recombinant protein expression in Brevibacillus choshinensis: The case of RBD of SARS-CoV-2 spike protein and its antibody. Protein Expression and Purification 194, 106075. https://doi.org/10.1016/j.pep.2022.106075

113. McGuire, B.E., Mela, J.E., Thompson, V.C., Cucksey, L.R., Stevens, C.E., McWhinnie, R.L., Winkler, D.F.H., Pelech, S., Nano, F.E., 2022. Escherichia coli recombinant expression of SARS-CoV-2 protein fragments. Microb Cell Fact 21, 21. https://doi.org/10.1186/s12934-022-01753-0

114. Mellors, J., Tipton, T., Longet, S., Carroll, M., 2020. Viral Evasion of the Complement System and Its Importance for Vaccines and Therapeutics. Front. Immunol. 11, 1450. https://doi.org/10.3389/fimmu.2020.01450

115. Mendonça, S.A., Lorincz, R., Boucher, P., Curiel, D.T., 2021. Adenoviral vector vaccine platforms in the SARS-CoV-2 pandemic. npj Vaccines 6, 97. https://doi.org/10.1038/s41541-021-00356-x

116. Merkuleva, I.A., Shcherbakov, D.N., Borgoyakova, M.B., Shanshin, D.V., Rudometov, A.P., Karpenko, L.I., Belenkaya, S.V., Isaeva, A.A., Nesmeyanova, V.S., Kazachinskaia, E.I., Volosnikova, E.A., Esina, T.I., Zaykovskaya, A.V., Pyankov, O.V., Borisevich, S.S., Shelemba, A.A., Chikaev, A.N., Ilyichev, A.A., 2022. Comparative Immunogenicity of the Recombinant Receptor-Binding Domain of Protein S SARS-CoV-2 Obtained in Prokaryotic and Mammalian Expression Systems. Vaccines 10, 96. https://doi.org/10.3390/vaccines10010096

117. Mohib, K., Cherukuri, A., Zhou, Y., Ding, Q., Watkins, S.C., Rothstein, D.M., 2020. Antigen-dependent interactions between regulatory B cells and T cells at the T:B border

inhibit subsequent T cell interactions with DCs. American Journal of Transplantation 20, 52–63. https://doi.org/10.1111/ajt.15546

118. Montazersaheb, S., Hosseiniyan Khatibi, S.M., Hejazi, M.S., Tarhriz, V., Farjami, A., Ghasemian Sorbeni, F., Farahzadi, R., Ghasemnejad, T., 2022. COVID-19 infection: an overview on cytokine storm and related interventions. Virology Journal 19, 92. https://doi.org/10.1186/s12985-022-01814-1

119. Mossel, E.C., Huang, C., Narayanan, K., Makino, S., Tesh, R.B., Peters, C.J., 2005. Exogenous ACE2 Expression Allows Refractory Cell Lines To Support Severe Acute Respiratory Syndrome Coronavirus Replication. J Virol 79, 3846–3850. https://doi.org/10.1128/JVI.79.6.3846-3850.2005

120. MSTO-211H, n.d.

121. Mungmunpuntipantip, R., Wiwanitkit, V., 2022. Letter Regarding "Delayed-onset Anaphylaxis After COVID-19 Vaccination." Pediatric Infectious Disease Journal 41, e342–e342. https://doi.org/10.1097/INF.0000000000003566

122. NCI-H226 [H226], n.d.

123. Norris, V., Ovádi, J., 2021. Role of Multifunctional Cytoskeletal Filaments in Coronaviridae Infections: Therapeutic Opportunities for COVID-19 in a Nutshell. Cells 10, 1818. https://doi.org/10.3390/cells10071818

124. Ogando, N.S., Dalebout, T.J., Zevenhoven-Dobbe, J.C., Limpens, R.W.A.L., van der Meer, Y., Caly, L., Druce, J., de Vries, J.J.C., Kikkert, M., Bárcena, M., Sidorov, I., Snijder, E.J., 2020. SARS-coronavirus-2 replication in Vero E6 cells: replication kinetics, rapid adaptation and cytopathology. Journal of General Virology 101, 925–940. https://doi.org/10.1099/jgv.0.001453

125. Ortiz Bezara, M.E., Thurman, A., Pezzulo, A.A., Leidinger, M.R., Klesney-Tait, J.A., Karp, P.H., Tan, P., Wohlford-Lenane, C., McCray, P.B., Meyerholz, D.K., 2020. Heterogeneous expression of the SARS-Coronavirus-2 receptor ACE2 in the human respiratory tract. bioRxiv 2020.04.22.056127. https://doi.org/10.1101/2020.04.22.056127

126. Owczarek, K., Szczepanski, A., Milewska, A., Baster, Z., Rajfur, Z., Sarna, M., Pyrc, K., 2018. Early events during human coronavirus OC43 entry to the cell. Sci Rep 8, 7124. https://doi.org/10.1038/s41598-018-25640-0

127. Pan, P., Shen, M., Yu, Z., Ge, W., Chen, K., Tian, M., Xiao, F., Wang, Z., Wang, J., Jia, Y., Wang, W., Wan, P., Zhang, J., Chen, W., Lei, Z., Chen, X., Luo, Z., Zhang, Q., Xu, M., Li, G., Li, Y., Wu, J., 2021. SARS-CoV-2 N protein promotes NLRP3 inflammasome activation to induce hyperinflammation. Nature Communications 12, 4664. https://doi.org/10.1038/s41467-021-25015-6

128. Park, B.K., Kim, D., Park, S., Maharjan, S., Kim, J., Choi, J.-K., Akauliya, M., Lee, Y., Kwon, H.-J., 2021. Differential Signaling and Virus Production in Calu-3 Cells and Vero Cells upon SARS-CoV-2 Infection. Biomol Ther (Seoul) 29, 273–281. https://doi.org/10.4062/biomolther.2020.226

129. Petruk, G., Puthia, M., Petrlova, J., Samsudin, F., Strömdahl, A.-C., Cerps, S., Uller, L., Kjellström, S., Bond, P.J., Schmidtchen, and A., 2020. SARS-CoV-2 spike protein binds to bacterial lipopolysaccharide and boosts proinflammatory activity. Journal of Molecular Cell Biology 12, 916–932. https://doi.org/10.1093/jmcb/mjaa067

130. Petsch, D., 2000. Endotoxin removal from protein solutions. Journal of Biotechnology 76, 97–119. https://doi.org/10.1016/S0168-1656(99)00185-6

131. Pilote, S., Simard, C., Drolet, B., 2021. REMDESIVIR (VEKLURY) FOR TREATING COVID-19 PATIENTS: WHAT TO EXPECT FROM A CARDIAC ELECTROPHYSIOLOGICAL PERSPECTIVE. Canadian Journal of Cardiology 37, S44. https://doi.org/10.1016/j.cjca.2021.07.093

132. Pollard, A.J., Bijker, E.M., 2021. A guide to vaccinology: from basic principles to new developments. Nature Reviews Immunology 21, 83–100. https://doi.org/10.1038/s41577-020-00479-7

133. Pulendran, B., Ahmed, R., 2011. Immunological mechanisms of vaccination. Nature Immunology 12, 509–517. https://doi.org/10.1038/ni.2039

134. Raeber, M.E., Zurbuchen, Y., Impellizzieri, D., Boyman, O., 2018. The role of cytokines in T-cell memory in health and disease. Immunological reviews 283, 176–193.

135. Raj, R., 2021. Analysis of non-structural proteins, NSPs of SARS-CoV-2 as targets for computational drug designing. Biochemistry and Biophysics Reports 25, 100847. https://doi.org/10.1016/j.bbrep.2020.100847

136. Randolph, T.W., 2012. The two faces of His-tag: Immune response versus ease of protein purification. Biotechnology Journal 7, 18–19. https://doi.org/10.1002/biot.201100459

137. Rashid, M., Coombs, K.M., 2019. Serum-reduced media impacts on cell viability and protein expression in human lung epithelial cells. Journal Cellular Physiology 234, 7718–7724. https://doi.org/10.1002/jcp.27890

138. Sadanandam, A., Bopp, T., Dixit, S., Knapp, D.J.H.F., Emperumal, C.P., Vergidis, P., Rajalingam, K., Melcher, A., Kannan, N., 2020. A blood transcriptome-based analysis of disease progression, immune regulation, and symptoms in coronavirus-infected patients. Cell Death Discov. 6, 141. https://doi.org/10.1038/s41420-020-00376-x

139. Saito, T., Gale, M., 2007. Principles of intracellular viral recognition. Current Opinion in Immunology 19, 17–23. https://doi.org/10.1016/j.coi.2006.11.003

140. Sampath, V., 2018. Bacterial endotoxin-lipopolysaccharide; structure, function and its role in immunity in vertebrates and invertebrates. Agriculture and Natural Resources 52, 115–120. https://doi.org/10.1016/j.anres.2018.08.002

141. Samsudin, F., Raghuvamsi, P., Petruk, G., Puthia, M., Petrlova, J., MacAry, P., Anand, G.S., Bond, P.J., Schmidtchen, A., 2022. SARS-CoV-2 spike protein as a bacterial lipopolysaccharide delivery system in an overzealous inflammatory cascade. Journal of Molecular Cell Biology 14, mjac058. https://doi.org/10.1093/jmcb/mjac058

142. Sant, A.J., McMichael, A., 2012. Revealing the role of CD4+ T cells in viral immunity. Journal of Experimental Medicine 209, 1391–1395. https://doi.org/10.1084/jem.20121517

143. Schulz, E., Hodl, I., Forstner, P., Hatzl, S., Sareban, N., Moritz, M., Fessler, J., Dreo, B., Uhl, B., Url, C., Grisold, A.J., Khalil, M., Kleinhappl, B., Enzinger, C., Stradner, M.H., Greinix, H.T., Schlenke, P., Steinmetz, I., 2021. CD19+IgD+CD27- Naïve B Cells as Predictors of Humoral Response to COVID 19 mRNA Vaccination in Immunocompromised Patients. Front. Immunol. 12, 803742. https://doi.org/10.3389/fimmu.2021.803742

144. Schwarz, H., Schmittner, M., Duschl, A., Horejs-Hoeck, J., 2014. Residual endotoxin contaminations in recombinant proteins are sufficient to activate human CD1c+ dendritic cells. PLoS One 9, e113840. https://doi.org/10.1371/journal.pone.0113840

145. Sen, G.C., 2001. Viruses and Interferons. Annu. Rev. Microbiol. 55, 255–281. https://doi.org/10.1146/annurev.micro.55.1.255

146. Shaath, H., Alajez, N.M., 2021. Identification of PBMC-based molecular signature associational with COVID-19 disease severity. Heliyon 7, e06866. https://doi.org/10.1016/j.heliyon.2021.e06866

147. Shang, J., Wan, Y., Luo, C., Ye, G., Geng, Q., Auerbach, A., Li, F., 2020. Cell entry mechanisms of SARS-CoV-2. Proc. Natl. Acad. Sci. U.S.A. 117, 11727–11734. https://doi.org/10.1073/pnas.2003138117

148. Sidebottom, D.B., Gill, D., 2021. Ronapreve for prophylaxis and treatment of covid-19. BMJ 374. https://doi.org/10.1136/bmj.n2136

149. Śliwa-Dominiak, J., Tokarz-Deptuła, B., Deptuła, W., 2014. The role of immune system cells and their receptors in viral infections – selected data. Postepy Hig Med Dosw 68, 404–409. https://doi.org/10.5604/17322693.1098150

150. Snijder, E.J., Decroly, E., Ziebuhr, J., 2016. The Nonstructural Proteins Directing Coronavirus RNA Synthesis and Processing, in: Advances in Virus Research. Elsevier, pp. 59–126. https://doi.org/10.1016/bs.aivir.2016.08.008

151. Still, F.M., n.d. DENGUE VIRUS INFECTION OF B LYMPHOCYTES IN VITRO 48.

152. Syed, Y.Y., 2021. Regdanvimab: First Approval. Drugs 81, 2133–2137. https://doi.org/10.1007/s40265-021-01626-7

153. Tamming, L.A., Duque, D., Tran, A., Zhang, W., Pfeifle, A., Laryea, E., Wu, J., Raman, S.N.T., Gravel, C., Russell, M.S., Hashem, A.M., Alsulaiman, R.M., Alhabbab, R.Y., Gao, J., Safronetz, D., Cao, J., Wang, L., Chen, W., Johnston, M.J.W., Sauve, S., Rosu-Myles, M., Li, X., 2021. DNA Based Vaccine Expressing SARS-CoV-2 Spike-CD40L Fusion Protein Confers Protection Against Challenge in a Syrian Hamster Model. Front Immunol 12, 785349. https://doi.org/10.3389/fimmu.2021.785349

154. Tapia-Calle, G., Born, P.A., Koutsoumpli, G., Gonzalez-Rodriguez, M.I., Hinrichs, W.L.J., Huckriede, A.L.W., 2019. A PBMC-Based System to Assess Human T Cell Responses to Influenza Vaccine Candidates In Vitro. Vaccines 7, 181. https://doi.org/10.3390/vaccines7040181

155. Tapia-Calle, G., Stoel, M., Jacqueline De Vries-Idema, Huckriede, A., 2017. Distinctive Responses in an In Vitro Human Dendritic Cell-Based System upon Stimulation with Different Influenza Vaccine Formulations. Vaccines 5, 21. https://doi.org/10.3390/vaccines5030021

156. Thieme, C.J., Anft, M., Paniskaki, K., Blazquez-Navarro, A., Doevelaar, A., Seibert, F.S., Hoelzer, B., Konik, M.J., Brenner, T., Tempfer, C., Watzl, C., Dolff, S., Dittmer, U., Westhoff, T.H., Witzke, O., Stervbo, U., Roch, T., Babel, N., 2020. The SARS-CoV-2 T-cell immunity is directed against the spike, membrane, and nucleocapsid protein and associated with COVID 19 severity (preprint). Infectious Diseases (except HIV/AIDS). https://doi.org/10.1101/2020.05.13.20100636

157. Thompson, M.R., Kaminski, J.J., Kurt-Jones, E.A., Fitzgerald, K.A., 2011. Pattern Recognition Receptors and the Innate Immune Response to Viral Infection. Viruses 3, 920–940. https://doi.org/10.3390/v3060920

158. Thomson, E.C., Rosen, L.E., Shepherd, J.G., Spreafico, R., da Silva Filipe, A., Wojcechowskyj, J.A., Davis, C., Piccoli, L., Pascall, D.J., Dillen, J., 2021. Circulating SARS-CoV-2 spike N439K variants maintain fitness while evading antibody-mediated immunity. Cell 184, 1171–1187.

159. Tian, Y., Babor, M., Lane, J., Schulten, V., Patil, V.S., Seumois, G., Rosales, S.L., Fu, Z., Picarda, G., Burel, J., Zapardiel-Gonzalo, J., Tennekoon, R.N., De Silva, A.D., Premawansa, S., Premawansa, G., Wijewickrama, A., Greenbaum, J.A., Vijayanand, P., Weiskopf, D., Sette, A., Peters, B., 2017. Unique phenotypes and clonal expansions of human CD4 effector memory T cells re-expressing CD45RA. Nature Communications 8, 1473. https://doi.org/10.1038/s41467-017-01728-5

160. Todorović-Raković, N., Whitfield, J.R., 2021. Between immunomodulation and immunotolerance: The role of IFNγ in SARS-CoV-2 disease. Cytokine 146, 155637. https://doi.org/10.1016/j.cyto.2021.155637

161. Tong, A.W., Seamour, B., Chen, J., Su, D., Ordonez, G., Frase, L., Netto, G., Stone, M.J., 2000. CD40 Ligand-Induced Apoptosis is Fas-Independent in Human Multiple Myeloma Cells. Leukemia & Lymphoma 36, 543–558. https://doi.org/10.3109/10428190009148403

162. Tong, L., Tergaonkar, V., 2014. Rho protein GTPases and their interactions with NFκB: crossroads of inflammation and matrix biology. Bioscience Reports 34, e00115. https://doi.org/10.1042/BSR20140021

163. Tse, L.V., Hamilton, A.M., Friling, T., Whittaker, G.R., 2014. A novel activation mechanism of avian influenza virus H9N2 by furin. J Virol 88, 1673–1683. https://doi.org/10.1128/JVI.02648-13

164. Vabret, N., Britton, G.J., Gruber, C., Hegde, S., Kim, J., Kuksin, M., Levantovsky, R., Malle, L., Moreira, A., Park, M.D., Pia, L., Risson, E., Saffern, M., Salomé, B., Esai Selvan, M., Spindler, M.P., Tan, J., van der Heide, V., Gregory, J.K., Alexandropoulos, K., Bhardwaj, N., Brown, B.D., Greenbaum, B., Gümüş, Z.H., Homann, D., Horowitz, A., Kamphorst, A.O., Curotto de Lafaille, M.A., Mehandru, S., Merad, M., Samstein, R.M., Agrawal, M., Aleynick, M., Belabed, M., Brown, M., Casanova-Acebes, M., Catalan, J., Centa, M., Charap, A., Chan, A., Chen, S.T., Chung, J., Bozkus, C.C., Cody, E., Cossarini, F., Dalla, E., Fernandez, N., Grout, J., Ruan, D.F., Hamon, P., Humblin, E., Jha, D., Kodysh, J., Leader, A., Lin, M., Lindblad, K., Lozano-Ojalvo, D., Lubitz, G., Magen, A., Mahmood, Z., Martinez-Delgado, G., Mateus-Tique, J., Meritt, E., Moon, C., Noel, J., O'Donnell, T., Ota, M., Plitt, T., Pothula, V., Redes, J., Reyes Torres, I., Roberto, M., Sanchez-Paulete, A.R., Shang, J., Schanoski, A.S., Suprun, M., Tran, M., Vaninov, N., Wilk, C.M., Aguirre-Ghiso, J., Bogunovic, D., Cho, J., Faith, J., Grasset, E., Heeger, P., Kenigsberg, E., Krammer, F., Laserson, U., 2020. Immunology of COVID-19: Current State of the Science. Immunity 52, 910–941. https://doi.org/10.1016/j.immuni.2020.05.002

165. Varghese, P.M., Tsolaki, A.G., Yasmin, H., Shastri, A., Ferluga, J., Vatish, M., Madan, T., Kishore, U., 2020. Host-pathogen interaction in COVID-19: Pathogenesis, potential therapeutics and vaccination strategies. Immunobiology 225, 152008. https://doi.org/10.1016/j.imbio.2020.152008

166. Vella, A.T., McAleer, J.P., 2008. Understanding How Lipopolysaccharide Impacts CD4 T-Cell Immunity. Crit Rev Immunol 28, 281–299. https://doi.org/10.1615/CritRevImmunol.v28.i4.20

167. VERO C1008 [Vero 76, clone E6, Vero E6], n.d.

168. Virzì, G.M., Mattiotti, M., de Cal, M., Ronco, C., Zanella, M., De Rosa, S., 2022. Endotoxin in Sepsis: Methods for LPS Detection and the Use of Omics Techniques. Diagnostics (Basel) 13, 79. https://doi.org/10.3390/diagnostics13010079

169. Wakui, M., Uwamino, Y., Yatabe, Y., Nakagawa, T., Sakai, A., Kurafuji, T., Shibata, A., Tomita, Y., Noguchi, M., Tanabe, A., Arai, T., Ohno, A., Yokota, H., Uno, S., Yamasawa, W., Sato, Y., Ikeda, M., Yoshimura, A., Hasegawa, N., Saya, H., Murata, M., 2022. Assessing anti-SARS-CoV-2 cellular immunity in 571 vaccines by using an IFN-γ release assay. Eur J Immunol 52, 1961–1971. https://doi.org/10.1002/eji.202249794

170. Wang, J., Yang, G., Wang, Xinxin, Wen, Z., Shuai, L., Luo, J., Wang, C., Sun, Z., Liu, R., Ge, J., He, X., Hua, R., Wang, Xijun, Yang, X., Chen, W., Zhong, G., Bu, Z., 2021. SARS-CoV-2 uses metabotropic glutamate receptor subtype 2 as an internalization factor to infect cells. Cell Discov 7, 119. https://doi.org/10.1038/s41421-021-00357-z

171. Wang, Y., Qiu, F., Xu, Y., Hou, X., Zhang, Z., Huang, L., Wang, H., Xing, H., Wu, S., 2021. Stem cell-like memory T cells: the generation and application. Journal of Leukocyte Biology 110, 1209–1223.

172. Watkins, D.I., Burton, D.R., Kallas, E.G., Moore, J.P., Koff, W.C., 2008. Nonhuman primate models and the failure of the Merck HIV-1 vaccine in humans. Nat Med 14, 617–621. https://doi.org/10.1038/nm.f.1759

173. Wen, W., Chen, C., Tang, J., Wang, C., Zhou, M., Cheng, Y., Zhou, X., Wu, Q., Zhang, X., Feng, Z., Wang, M., Mao, Q., 2022. Efficacy and safety of three new oral antiviral treatment (molnupiravir, fluvoxamine and Paxlovid) for COVID-19：a meta-analysis. Annals of Medicine 54, 516–523. https://doi.org/10.1080/07853890.2022.2034936

174. Wen, Y., Jing, Y., Yang, L., Kang, D., Jiang, P., Li, N., Cheng, J., Li, J., Li, X., Peng, Z., Sun, X., Miller, H., Sui, Z., Gong, Q., Ren, B., Yin, W., Liu, C., 2019. The regulators

of BCR signaling during B cell activation. Blood Science 1, 119–129. https://doi.org/10.1097/BS9.0000000000000026

175. Wen, Z., Zhang, Y., Lin, Z., Shi, K., Jiu, Y., 2021. Cytoskeleton—a crucial key in host cell for coronavirus infection. Journal of Molecular Cell Biology 12, 968–979. https://doi.org/10.1093/jmcb/mjaa042

176. Wickham, H., 2009. ggplot2: Elegant Graphics for Data Analysis. Springer New York, New York, NY. https://doi.org/10.1007/978-0-387-98141-3

177. Wise, J., 2022. Covid-19: UK approves Novavax's protein based vaccine. BMJ o309. https://doi.org/10.1136/bmj.o309

178. Wu, M.Y., Carr, E.J., Harvey, R., Mears, H.V., Kjaer, S., Townsley, H., Hobbs, A., Ragno, M., Herman, L.S., Adams, L., Gamblin, S., Howell, M., Beale, R., Brown, M., Williams, B., Gandhi, S., Swanton, C., Wall, E.C., Bauer, D.L.V., 2022. WHO's Therapeutics and COVID-19 Living Guideline on mAbs needs to be reassessed. The Lancet S0140673622019389. https://doi.org/10.1016/S0140-6736(22)01938-9

179. Xu, S., Yang, K., Li, R., Zhang, L., 2020. mRNA Vaccine Era-Mechanisms, Drug Platform and Clinical Prospection. Int J Mol Sci 21, E6582. https://doi.org/10.3390/ijms21186582

180. Yang, K., Zhang, X.J., Cao, L.J., Liu, X.H., Liu, Z.H., Wang, X.Q., Chen, Q.J., Lu, L., Shen, W.F., Liu, Y., 2014. Toll-like receptor 4 mediates inflammatory cytokine secretion in smooth muscle cells induced by oxidized low-density lipoprotein. PLoS One 9, e95935. https://doi.org/10.1371/journal.pone.0095935

181. Yang, Y., Du, L., 2022. Neutralizing antibodies and their cocktails against SARS-CoV-2 Omicron and other circulating variants. Cellular & Molecular Immunology 19, 962–964. https://doi.org/10.1038/s41423-022-00890-1

182. Yang, Y., Shen, C., Li, J., Yuan, J., Wei, J., Huang, F., Wang, F., Li, G., Li, Y., Xing, L., Peng, L., Yang, M., Cao, M., Zheng, H., Wu, W., Zou, R., Li, D., Xu, Z., Wang, H., Zhang, M., Zhang, Z., Gao, G.F., Jiang, C., Liu, L., Liu, Y., 2020. Plasma IP-10 and MCP-3 levels are highly associated with disease severity and predict the progression of COVID-19. Journal of Allergy and Clinical Immunology 146, 119-127.e4. https://doi.org/10.1016/j.jaci.2020.04.027

183. Yao, H., Song, Y., Chen, Y., Wu, N., Xu, J., Sun, C., Zhang, J., Weng, T., Zhang, Z., Wu, Z., Cheng, L., Shi, D., Lu, X., Lei, J., Crispin, M., Shi, Y., Li, L., Li, S., 2020. Molecular Architecture of the SARS-CoV-2 Virus. Cell 183, 730-738.e13. https://doi.org/10.1016/j.cell.2020.09.018

184. Yi, C., Sun, X., Lin, Y., Gu, C., Ding, L., Lu, X., Yang, Z., Zhang, Y., Ma, L., Gu, W., Qu, A., Zhou, X., Li, X., Xu, J., Ling, Z., Xie, Y., Lu, H., Sun, B., 2021. Comprehensive mapping of binding hot spots of SARS-CoV-2 RBD-specific neutralizing antibodies for tracking immune escape variants. Genome Medicine 13, 164. https://doi.org/10.1186/s13073-021-00985-w

185. Zhang, H., Penninger, J.M., Li, Y., Zhong, N., Slutsky, A.S., 2020. Angiotensin-converting enzyme 2 (ACE2) as a SARS-CoV-2 receptor: molecular mechanisms and potential therapeutic target. Intensive Care Med 46, 586–590. https://doi.org/10.1007/s00134-020-05985-9

186. Zhang, L., Zhang, Y., Wang, R., Liu, X., Zhao, J., Tsuda, M., Li, Y., 2023. SARS-CoV-2 infection of intestinal epithelia cells sensed by RIG-I and DHX-15 evokes innate immune response and immune cross-talk. Front. Cell. Infect. Microbiol. 12, 1035711. https://doi.org/10.3389/fcimb.2022.1035711

187. Zhang, Q., Bastard, P., Liu, Z., Le Pen, J., Moncada-Velez, M., Chen, J., Ogishi, M., Sabli, I.K.D., Hodeib, S., Korol, C., Rosain, J., Bilguvar, K., Ye, J., Bolze, A., Bigio, B., Yang, R., Arias, A.A., Zhou, Q., Zhang, Y., Onodi, F., Korniotis, S., Karpf, L., Philippot, Q., Chbihi, M., Bonnet-Madin, L., Dorgham, K., Smith, N., Schneider, W.M., Razooky, B.S., Hoffmann, H.-H., Michailidis, E., Moens, L., Han, J.E., Lorenzo, L., Bizien, L., Meade, P., Neehus, A.-L., Ugurbil, A.C., Corneau, A., Kerner, G., Zhang, P., Rapaport, F., Seeleuthner, Y., Manry, J., Masson, Cecile, Schmitt, Yohann, Schlüter, A., Le Voyer, T., Khan, T., Li, J., Fellay, J., Roussel, L., Shahrooei, Mohammad, Alosaimi, M.F., Mansouri, Davood, Al-Saud, H., Al-Mulla, F., Almourfi, F., Al-Muhsen, S.Z., Alsohime, F., Al Turki, S., Hasanato, R., van de Beek, D., Biondi, A., Bettini, L.R., D'Angio', M., Bonfanti, P., Imberti, L., Sottini, A., Paghera, S., Quiros-Roldan, E., Rossi, C., Oler, A.J., Tompkins, M.F., Alba, C., Vandernoot, I., Goffard, J.-C., Smits, G., Migeotte, I., Haerynck, F., Soler-Palacin, P., Martin-Nalda, A., Colobran, R., Morange, P.-E., Keles, S., Çölkesen, F., Ozcelik, T., Yasar, K.K., Senoglu, S., Karabela, Ş.N., Rodríguez-Gallego, C., Novelli, G., Hraiech, S., Tandjaoui-Lambiotte,

Y., Duval, X., Laouénan, C., COVID-STORM Clinicians, COVID Clinicians, Imagine COVID Group, French COVID Cohort Study Group, CoV-Contact Cohort, Amsterdam UMC Covid-19 Biobank, COVID Human Genetic Effort, NIAID-USUHS/TAGC COVID Immunity Group, Snow, A.L., Dalgard, C.L., Milner, J.D., Vinh, D.C., Mogensen, T.H., Marr, N., Spaan, A.N., Boisson, B., Boisson-Dupuis, S., Bustamante, J., Puel, A., Ciancanelli, M.J., Meyts, I., Maniatis, T., Soumelis, V., Amara, A., Nussenzweig, M., García-Sastre, A., Krammer, F., Pujol, A., Duffy, D., Lifton, R.P., Zhang, S.-Y., Gorochov, G., Béziat, V., Jouanguy, E., Sancho-Shimizu, V., Rice, C.M., Abel, L., Notarangelo, L.D., Cobat, A., Su, H.C., Casanova, J.-L., Foti, G., Bellani, G., Citerio, G., Contro, E., Pesci, A., Valsecchi, M.G., Cazzaniga, M., Abad, J., Aguilera-Albesa, S., Akcan, O.M., Darazam, I.A., Aldave, J.C., Ramos, M.A., Nadji, S.A., Alkan, G., Allardet-Servent, J., Allende, L.M., Alsina, L., Alyanakian, M.-A., Amador-Borrero, B., Amoura, Z., Antolí, A., Arslan, S., Assant, S., Auguet, T., Azot, A., Bajolle, F., Baldolli, A., Ballester, M., Feldman, H.B., Barrou, B., Beurton, A., Bilbao, A., Blanchard-Rohner, G., Blanco, I., Blandinières, A., Blazquez-Gamero, D., Bloomfield, M., Bolivar-Prados, M., Borie, R., Bosteels, C., Bousfiha, A.A., Bouvattier, C., Boyarchuk, O., Bueno, M.R.P., Bustamante, J., Cáceres Agra, J.J., Calimli, S., Capra, R., Carrabba, M., Casasnovas, C., Caseris, M., Castelle, M., Castelli, F., de Vera, M.C., Castro, M.V., Catherinot, E., Chalumeau, M., Charbit, B., Cheng, M.P., Clavé, P., Clotet, B., Codina, A., Colkesen, F., Çölkesen, F., Colobran, R., Comarmond, C., Dalmau, D., Darley, D.R., Dauby, N., Dauger, S., de Pontual, L., Dehban, A., Delplancq, G., Demoule, A., Diehl, J.-L., Dobbelaere, S., Durand, S., Eldars, W., Elgamal, M., Elnagdy, M.H., Emiroglu, M., Erdeniz, E.H., Aytekin, S.E., Euvrard, R., Evcen, R., Fabio, G., Faivre, L., Falck, A., Fartoukh, M., Faure, M., Arquero, M.F., Flores, C., Francois, B., Fumadó, V., Fusco, F., Solis, B.G., Gaussem, P., Gil-Herrera, J., Gilardin, L., Alarcon, M.G., Girona-Alarcón, M., Goffard, J.-C., Gok, F., González-Montelongo, R., Guerder, A., Gul, Y., Guner, S.N., Gut, M., Hadjadj, J., Haerynck, F., Halwani, R., Hammarström, L., Hatipoglu, N., Hernandez-Brito, E., Heijmans, C., Holanda-Peña, M.S., Horcajada, J.P., Hoste, L., Hoste, E., Hraiech, S., Humbert, L., Iglesias, A.D., Íñigo-Campos, A., Jamme, M., Arranz, M.J., Jordan, I., Jorens, P., Kanat, F., Kapakli, H., Kara, I., Karbuz, A., Yasar, K.K., Keles, S., Demirkol, Y.K., Klocperk, A., Król, Z.J., Kuentz, P., Kwan, Y.W.M., Lagier, J.-C., Lambrecht, B.N., Lau, Y.-L., Le Bourgeois, F., Leo, Y.-S., Lopez, R.L., Leung, D., Levin, M., Levy, M., Lévy, R., Li, Z., Linglart, A., Loeys, B., Lorenzo-Salazar, J.M., Louapre, C., Lubetzki, C., Luyt,

C.-E., Lye, D.C., Mansouri, Davood, Marjani, M., Pereira, J.M., Martin, A., Pueyo, D.M., Martinez-Picado, J., Marzana, I., Mathian, A., Matos, L.R.B., Matthews, G.V., Mayaux, J., Mège, J.-L., Melki, I., Meritet, J.-F., Metin, O., Meyts, I., Mezidi, M., Migeotte, I., Millereux, M., Mirault, T., Mircher, C., Mirsaeidi, M., Melián, A.M., Martinez, A.M., Morange, P., Mordacq, C., Morelle, G., Mouly, S., Muñoz-Barrera, A., Naesens, L., Nafati, C., Neves, J.F., Ng, L.F.P., Medina, Y.N., Cuadros, E.N., Ocejo-Vinyals, J.G., Orbak, Z., Oualha, M., Özçelik, T., Pan-Hammarström, Q., Parizot, C., Pascreau, T., Paz-Artal, E., Pellegrini, S., de Diego, Rebeca Pérez, Philippe, A., Philippot, Q., Planas-Serra, L., Ploin, D., Poissy, J., Poncelet, G., Pouletty, M., Quentric, P., Raoult, D., Rebillat, A.-S., Reisli, I., Ricart, P., Richard, J.-C., Rivet, N., Rivière, J.G., Blanch, G.R., Rodrigo, C., Rodriguez-Gallego, C., Rodríguez-Palmero, A., Romero, C.S., Rothenbuhler, A., Rozenberg, F., Ruiz del Prado, M.Y., Riera, J.S., Sanchez, O., Sánchez-Ramón, S., Schluter, A., Schmidt, M., Schweitzer, C.E., Scolari, F., Sediva, A., Seijo, L.M., Sene, D., Senoglu, S., Seppänen, M.R.J., Ilovich, A.S., Shahrooei, Mohammad, Slabbynck, H., Smadja, D.M., Sobh, A., Moreno, X.S., Solé-Violán, J., Soler, C., Soler-Palacín, P., Stepanovskiy, Y., Stoclin, A., Taccone, F., Tandjaoui-Lambiotte, Y., Taupin, J.-L., Tavernier, S.J., Terrier, B., Thumerelle, C., Tomasoni, G., Toubiana, J., Alvarez, J.T., Trouillet-Assant, S., Troya, J., Tucci, A., Ursini, M.V., Uzunhan, Y., Vabres, P., Valencia-Ramos, J., Van Braeckel, E., Van de Velde, S., Van Den Rym, A.M., Van Praet, J., Vandernoot, I., Vatansev, H., Vélez-Santamaria, V., Viel, S., Vilain, C., Vilaire, M.E., Vincent, A., Voiriot, G., Vuotto, F., Yosunkaya, A., Young, B.E., Yucel, F., Zannad, F., Zatz, M., Belot, A., Bole-Feysot, C., Lyonnet, S., Masson, Cécile, Nitschke, P., Pouliet, A., Schmitt, Yoann, Tores, F., Zarhrate, M., Abel, L., Andrejak, C., Angoulvant, F., Bachelet, D., Basmaci, R., Behillil, S., Beluze, M., Benkerrou, D., Bhavsar, K., Bompart, F., Bouadma, L., Bouscambert, M., Caralp, M., Cervantes-Gonzalez, M., Chair, A., Coelho, A., Couffignal, C., Couffin-Cadiergues, S., D'Ortenzio, E., Da Silveira, C., Debray, M.-P., Deplanque, D., Descamps, D., Desvallées, M., Diallo, A., Diouf, A., Dorival, C., Dubos, F., Duval, X., Eloy, P., Enouf, V.V., Esperou, H., Esposito-Farese, M., Etienne, M., Ettalhaoui, N., Gault, N., Gaymard, A., Ghosn, J., Gigante, T., Gorenne, I., Guedj, J., Hoctin, A., Hoffmann, I., Jaafoura, S., Kafif, O., Kaguelidou, F., Kali, S., Khalil, A., Khan, C., Laouénan, C., Laribi, S., Le, M., Le Hingrat, Q., Le Mestre, S., Le Nagard, H., Lescure, F.-X., Lévy, Y., Levy-Marchal, C., Lina, B., Lingas, G., Lucet, J.C., Malvy, D., Mambert, M., Mentré, F., Mercier, N., Meziane, A., Mouquet, H., Mullaert, J.,

Neant, N., Noret, M., Pages, J., Papadopoulos, A., Paul, C., Peiffer-Smadja, N., Petrov-Sanchez, V., Peytavin, G., Picone, O., Puéchal, O., Rosa-Calatrava, M., Rossignol, B., Rossignol, P., Roy, C., Schneider, M., Semaille, C., Mohammed, N.S., Tagherset, L., Tardivon, C., Tellier, M.-C., Téoulé, F., Terrier, O., Timsit, J.-F., Trioux, T., Tual, C., Tubiana, S., van der Werf, S., Vanel, N., Veislinger, A., Visseaux, B., Wiedemann, A., Yazdanpanah, Y., Alavoine, L., Amat, K.K.A., Behillil, S., Bielicki, J., Bruijning, P., Burdet, C., Caumes, E., Charpentier, C., Coignard, B., Costa, Y., Couffin-Cadiergues, S., Damond, F., Dechanet, A., Delmas, C., Descamps, D., Duval, X., Ecobichon, J.-L., Enouf, V., Espérou, H., Frezouls, W., Houhou, N., Ilic-Habensus, E., Kafif, O., Kikoine, J., Le Hingrat, Q., Lebeaux, D., Leclercq, A., Lehacaut, J., Letrou, S., Lina, B., Lucet, J.-C., Malvy, D., Manchon, P., Mandic, M., Meghadecha, M., Motiejunaite, J., Nouroudine, M., Piquard, V., Postolache, A., Quintin, C., Rexach, J., Roufai, L., Terzian, Z., Thy, M., Tubiana, S., van der Werf, S., Vignali, V., Visseaux, B., Yazdanpanah, Y., van Agtmael, M., Algera, A.G., van Baarle, F., Bax, D., Beudel, M., Bogaard, H.J., Bomers, M., Bos, L., Botta, M., de Brabander, J., de Bree, G., Brouwer, M.C., de Bruin, S., Bugiani, M., Bulle, E., Chouchane, O., Cloherty, A., Elbers, P., Fleuren, L., Geerlings, S., Geerts, B., Geijtenbeek, T., Girbes, A., Goorhuis, B., Grobusch, M.P., Hafkamp, F., Hagens, L., Hamann, J., Harris, V., Hemke, R., Hermans, S.M., Heunks, L., Hollmann, M.W., Horn, J., Hovius, J.W., de Jong, M.D., Koning, R., van Mourik, N., Nellen, J., Paulus, F., Peters, E., van der Poll, T., Preckel, B., Prins, J.M., Raasveld, J., Reijnders, T., Schinkel, M., Schultz, M.J., Schuurman, A., Sigaloff, K., Smit, M., Stijnis, C.S., Stilma, W., Teunissen, C., Thoral, P., Tsonas, A., van der Valk, M., Veelo, D., Vlaar, A.P.J., de Vries, H., van Vugt, M., Wiersinga, W.J., Wouters, D., Zwinderman, A.H. (Koos), van de Beek, D., Abel, L., Aiuti, A., Al Muhsen, S., Al-Mulla, F., Anderson, M.S., Arias, A.A., Feldman, H.B., Bogunovic, D., Bolze, A., Bondarenko, A., Bousfiha, A.A., Brodin, P., Bryceson, Y., Bustamante, C.D., Butte, M., Casari, G., Chakravorty, S., Christodoulou, J., Cirulli, E., Condino-Neto, A., Cooper, M.A., Dalgard, C.L., David, A., DeRisi, J.L., Desai, M., Drolet, B.A., Espinosa, S., Fellay, J., Flores, C., Franco, J.L., Gregersen, P.K., Haerynck, F., Hagin, D., Halwani, R., Heath, J., Henrickson, S.E., Hsieh, E., Imai, K., Itan, Y., Karamitros, T., Kisand, K., Ku, C.-L., Lau, Y.-L., Ling, Y., Lucas, C.L., Maniatis, T., Mansouri, Davoud, Marodi, L., Meyts, I., Milner, J., Mironska, K., Mogensen, T., Morio, T., Ng, L.F.P., Notarangelo, L.D., Novelli, A., Novelli, G., O'Farrelly, C., Okada, S., Ozcelik, T., de Diego, Rebeca Perez, Planas, A.M., Prando, C., Pujol, A., Quintana-Murci, L.,

Renia, L., Renieri, A., Rodríguez-Gallego, C., Sancho-Shimizu, V., Sankaran, V., Barrett, K.S., Shahrooei, Mohammed, Snow, A., Soler-Palacín, P., Spaan, A.N., Tangye, S., Turvey, S., Uddin, F., Uddin, M.J., van de Beek, D., Vazquez, S.E., Vinh, D.C., von Bernuth, H., Washington, N., Zawadzki, P., Su, H.C., Casanova, J.-L., Jing, H., Tung, W., Luthers, C.R., Bauman, B.M., Shafer, S., Zheng, L., Zhang, Z., Kubo, S., Chauvin, S.D., Meguro, K., Shaw, E., Lenardo, M., Lack, J., Karlins, E., Hupalo, D.M., Rosenberger, J., Sukumar, G., Wilkerson, M.D., Zhang, X., 2020. Inborn errors of type I IFN immunity in patients with life-threatening COVID-19. Science 370, eabd4570. https://doi.org/10.1126/science.abd4570

188. Zhao, Y., Kuang, M., Li, J., Zhu, L., Jia, Z., Guo, X., Hu, Y., Kong, J., Yin, H., Wang, X., You, F., 2021. SARS-CoV-2 spike protein interacts with and activates TLR41. Cell Research 31, 818–820. https://doi.org/10.1038/s41422-021-00495-9

Annex

Gating hierarchy for panels 1-3

g:Profiler GO analysis

PBMC AdV1+S+N vs. PBMC control

GO:MF	stats			»»
Term name	Term ID		p_{adj}	$-\log_{10}(p_{adj})$
protein binding	GO:0005515		1.864×10^{-2}	
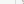
GO:BP	stats			»»
Term name	Term ID		p_{adj}	$-\log_{10}(p_{adj})$
cellular component disassembly	GO:0022411		2.108×10^{-2}	
response to lithium ion	GO:0010226		4.632×10^{-2}	

GO:CC	stats			»»
Term name	Term ID		p_{adj}	$-\log_{10}(p_{adj})$
cytoplasm	GO:0005737		3.256×10^{-3}	
lamellipodium	GO:0030027		2.945×10^{-2}	
filopodium	GO:0030175		3.451×10^{-2}	

Calu-3 Ad1+S+N vs. Control

GO:MF

Term name	Term ID		stats p_{adj}	$-\log_{10}(p_{adj})$			
interleukin-10 binding	GO:0019969		4.977×10^{-2}				

1 to 1 of 1 ⏮ ‹ Page 1 of 1 › ⏭

GO:BP

Term name	Term ID		stats p_{adj}	$-\log_{10}(p_{adj})$			
interleukin-10 production	GO:0032613		3.253×10^{-2}				
regulation of interleukin-10 production	GO:0032653		3.253×10^{-2}				

1 to 2 of 2 ⏮ ‹ Page 1 of 1 › ⏭

KEGG

Term name	Term ID		stats p_{adj}	$-\log_{10}(p_{adj})$			
Toxoplasmosis	KEGG:05145		2.503×10^{-2}				

1 to 1 of 1 ⏮ ‹ Page 1 of 1 › ⏭

CORUM

Term name	Term ID		stats p_{adj}	$-\log_{10}(p_{adj})$			
Delta1 homodimer complex	CORUM:3270		4.993×10^{-2}				
IL10-IL10RA complex	CORUM:7310		4.993×10^{-2}				

SUBPOPULATION OF LYMPHOCYTES	IMMUNOGENIC FACTORS												
	Untreated control	MOCK	rRBD	AdV1	AdV2	Pseudo-virus	MIX1	MIX2	hCoV-OC43	AdV1 +rRBD	AdV2 +rRBD	Pseudo +Ab	rRBD +Ab
CD8^{+}	23.13 ±2.10	27.13 ±7.65	24.10 ±0.71	30.30 ±6.79	31.27 ±8.89	31.33 ±7.26	24.87 ±0.42	35.77 ±0.94	35.60 ±1.20	37.17 ±0.71	37.27 ±1.03	28.03 ±5.73	26.85 ±3.15
CD197^{+} CD45RA^{+}	48.27 ±3.73	52.20 ±4.54	42.80 ±5.52	43.47 ±9.05	51.83 ±3.45	50.07 ±2.15	38.07 ±7.29	23.53 ±3.21	50.80 ±4.30	40.47 ±1.30	41.07 ±1.38	46.07 ±7.95	22.45 ±7.15
NAÏVE	41.00 ±5.74	32.47 ±6.35	33.10 ±5.80	24.27 ±11.55	32.97 ±9.74	29.9 ±5.30	29.57 ±7.42	21.27 ±7.73	33.05 ±7.05	30.97 ±0.87	30.97 ±0.93	25.1 ±10.74	16.8 ±2.55
SCM	6.00 ±1.77	10.63 ±5.03	7.65 ±2.90	14.03 ±6.01	10.93 ±11.18	14.33 ±8.06	6.83 ±0.99	2.27 ±1.98	16.2 ±11.45	8.57 ±0.76	9.23 ±0.42	14.93 ±7.13	5.15 ±2.70
CM	4.07 ±0.82	4.53 ±1.16	4.60 ±0.71	3.07 ±1.03	4.10 ±1.37	3.20 ±0.83	3.07 ±1.14	1.33 ±0.05	2.55 ±0.55	3.03 ±0.26	2.97 ±0.19	3.23 ±1.14	6.00 ±1.90
EM	7.90 ±0.50	7.23 ±1.86	11.10 ±3.96	7.43 ±2.41	6.73 ±1.63	7.43 ±1.06	12.87 ±3.68	17.53 ±6.27	7.70 ±2.00	6.33 ±0.40	6.53 ±0.45	7.67 ±2.89	14.50 ±0.50
EMRA	39.77 ±4.83	36.03 ±3.20	41.40 ±0.85	46.03 ±7.90	37.30 ±5.43	39.30 ±2.34	46.00 ±5.76	57.57 ±3.16	38.95 ±0.85	50.17 ±1.34	49.40 ±1.04	43.07 ±5.72	57.05 ±9.55

Table 1A Percentage of CD8^{+} lymphocyte subpopulations after 24-h treatment with various immunogenic factors.

Note. MOCK - LPS-treated cells (1.25 μg/mL), rRBD – recombinant protein, receptor binding domain (2.62 μg/mL), AdV1 - AdV5 / 3-d24-ICOSL-CD40L (100 VP/mL), AdV2 - AdV5 / 3-d24-WT (100 VP/mL), Pseudovirus - GeneCopoeia's Lentifect ™ SARS- CoV-2 Spike-pseudotyped lentivirus (100 VP/mL), MIX1 - AdV1 + rRBD + pseudovirus (100 VP/mL+2.62 μg/mL+100 VP/mL), MIX2 - AdV2 + rRBD + pseudovirus (100 VP/mL+2.62 μg/mL+100 VP/mL), hCoV-OC43 - human coronavirus OC43 (100 VP/mL), Pseudo+Ab - pseudovirus + SARS-CoV-2 Spike Antibody (GeneCopoeia; 100 VP/mL+2.62 μg/mL), rRBD+Ab (2.62 μg/mL +2.62 μg/mL).

CeGaT sample sheet form

Nr	primary sample source	sample name	Soncentration measured by NanoQuant plate. Tekan (indyvidual blanking)	Concentration measured by Qubit RNA HSA Assay kit (Original calculated sample concentration;Qubit tube concentration) [ng/µL]	Concentration measured by Qubit RNA Broad Range Assay kit (Original calculated sample concentration;Qubit tube concentration) [ng/µL]	Sample volume (in water) [µL]	Used methology for measurement
1	PBMCs	PBMC control 1	249.68 ng/µL A260/280=1.82	180 ng/mL;7.20 ng/µL	21.9 ng/mL;0.547 ng/µL	13	Tekan NanoQuant Spectrometer/Qubit Fluorometric Quantification High sensitive (HS) i Broad Range (BR)
2		PBMC control 2	318.32 ng/µL A260/280=1.97	231 ng/mL;9.24 ng/µL	21 ng/mL;0.524 ng/µL	13	Tekan NanoQuant Spectrometer/Qubit Fluorometric Quantification High sensitive (HS) i Broad Range (BR)
3		PBMC control 3	119.28 ng/µL A260/280=2.26	300 ng/mL;12 ng/µL	20.4 ng/mL;0.509 ng/µL	13	Tekan NanoQuant Spectrometer/Qubit Fluorometric Quantification High sensitive (HS) i Broad Range (BR)
4		PBMC AdV1 +rRBD 1	157.92 ng/µL A260/280=1.89	152 ng/mL;6.08 ng/µL	18 ng/mL;0.451 ng/µL	13	Tekan NanoQuant Spectrometer/Qubit Fluorometric Quantification High sensitive (HS) i Broad Range (BR)
5		PBMC AdV1 +rRBD 2	137.76 ng/µL A260/280=1.96	177 ng/mL;7.08 ng/µL	17.7 ng/mL;0.443 ng/µL	13	Tekan NanoQuant Spectrometer/Qubit Fluorometric Quantification High sensitive (HS) i Broad Range (BR)
6		PBMC AdV1 +rRBD 3	137.04 ng/µL A260/280=1.94	222 ng/mL;8.88 ng/µL	22.8 ng/mL;0.570 ng/µL	13	Tekan NanoQuant Spectrometer/Qubit Fluorometric Quantification High sensitive (HS) i Broad Range (BR)

No.	Cell line	Sample	Concentration	ng/mL;ng/µL	ng/mL;ng/µL	13	Method
7		PBMC AdV1 +S+N 1	102.8 ng/µL A260/280=1.91	152 ng/mL;6.08 ng/µL	15.4 ng/mL;0.386 ng/µL	13	Tekan NanoQuant Spectrometer/Qubit Fluorometric Quantification High sensitive (HS) i Broad Range (BR)
8		PBMC AdV1 +S+N 2	136.48 ng/µL A260/280=1.9	193 ng/mL;7.72 ng/µL	13.6 ng/mL;0.339 ng/µL	13	Tekan NanoQuant Spectrometer/Qubit Fluorometric Quantification High sensitive (HS) i Broad Range (BR)
9		PBMC AdV1 +S+N 3	192.32 ng/µL A260/280=2.11	170 ng/mL;6.8 ng/µL	18.7 ng/mL;0.468 ng/µL	13	Tekan NanoQuant Spectrometer/Qubit Fluorometric Quantification High sensitive (HS) i Broad Range (BR)
10		Calu-3 control 1	45.36 ng/µL A260/280=1.96	315 ng/mL;12.6 ng/µL	15.0 ng/mL;0.374 ng/µL	13	Tekan NanoQuant Spectrometer/Qubit Fluorometric Quantification High sensitive (HS) i Broad Range (BR)
11		Calu-3 control 2	73.68 ng/µL A260/280=2.05	260 ng/mL;52.0 ng/µL	51.2 ng/mL;1.28 ng/µL	13	Tekan NanoQuant Spectrometer/Qubit Fluorometric Quantification High sensitive (HS) i Broad Range (BR)
12	Calu-3 cell line	Calu-3 control 3	36.96 ng/µL A260/280=1.92	486 ng/mL;19.4 ng/µL	17.4 ng/mL;0.435 ng/µL	13	Tekan NanoQuant Spectrometer/Qubit Fluorometric Quantification High sensitive (HS) i Broad Range (BR)
13		Calu-3 AdV1 +S+N 1	85.84 ng/µL A260/280=2.08	307 ng/mL;61.4 ng/µL	60.8 ng/mL;1.52 ng/µL	13	Tekan NanoQuant Spectrometer/Qubit Fluorometric Quantification High sensitive (HS) i Broad Range (BR)
14		Calu-3 AdV1 +S+N 2	35.84 ng/µL A260/280=1.91	80.9 ng/mL;16.2 ng/µL	15 ng/mL;0.376 ng/µL	13	Tekan NanoQuant Spectrometer/Qubit Fluorometric Quantification High sensitive (HS) i Broad Range (BR)
15		Calu-3 AdV1 +S+N 3	40.16 ng/µL A260/280=2.06	610 ng/mL;24.4 ng/µL	26.4 ng/mL;0.659 ng/µL	13	Tekan NanoQuant Spectrometer/Qubit Fluorometric Quantification High sensitive (HS) i Broad Range (BR)

SUBPOPULATION OF LYMPHOCYTES	IMMUNOGENIC FACTORS												
	Untreated control	MOCK	rRBD	AdV1	AdV2	Pseudo-virus	MIX1	MIX2	hCoV-OC43	AdV1 +rRBD	AdV2 +rRBD	Pseudo +Ab	rRBD +Ab
CD4+	72.60 ±2.84	68.03 ±8.78	71.10 ±1.84	65.03 ±7.75	63.20 ±10.31	63.10 ±8.30	70.87 ±0.68	55.17 ±2.45	58.45 ±1.85	55.40 ±0.71	54.87 ±1.31	67.77 ±6.45	57.40 ±2.30
CD197+ CD45RA+	78.63 ±0.87	74.23 ±10.28	71.45 ±9.12	74.60 ±5.65	71.13 ±9.50	70.40 ±8.08	67.30 ±6.85	44.60 ±9.62	66.55 ±4.55	61.93 ±0.62	62.10 ±1.28	75.93 ±4.16	49.05 ±0.15
NAÏVE	67.10 ±4.66	50.30 ±6.35	59.40 ±5.80	40.13 ±11.55	46.57 ±9.74	40.47 ±5.30	53.67 ±7.42	38.73 ±7.73	36.35 ±7.05	48.13 ±0.87	47.93 ±0.93	41.20 ±10.74	39.65 ±2.55
SCM	11.23 ±3.80	23.03 ±5.03	11.75 ±2.90	33.73 ±6.01	23.60 ±11.18	28.67 ±8.06	13.20 ±0.99	5.70 ±1.98	29.55 ±11.45	13.53 ±0.76	14.03 ±0.42	34.03 ±7.13	9.20 ±2.70
CM	14.50 ±1.47	17.40 ±4.52	19.05 ±5.59	16.67 ±2.74	19.90 ±5.40	17.97 ±3.63	18.73 ±2.33	19.07 ±0.47	19.70 ±3.00	21.50 ±0.79	21.83 ±0.65	16.33 ±2.46	26.75 ±4.15
EM	4.77 ±0.99	5.70 ±3.89	7.20 ±3.11	5.30 ±1.63	5.60 ±2.65	7.40 ±2.83	11.10 ±4.10	26.70 ±9.19	8.90 ±2.20	9.67 ±0.83	9.50 ±1.06	5.00 ±1.56	19.50 ±3.30
EMRA	2.13 ±0.84	2.63 ±1.96	2.25 ±0.49	3.40 ±2.21	3.40 ±1.93	4.23 ±1.67	2.83 ±0.74	9.63 ±0.90	4.85 ±0.65	6.87 ±0.56	6.57 ±0.49	2.70 ±1.70	4.65 ±0.65

Table 2A Percentage of CD4+ lymphocyte subpopulations after 24-h treatment with various immunogenic factors.

*Note. **MOCK** - LPS-treated cells (1.25 µg/mL), **rRBD** – recombinant protein, receptor binding domain (2.62 µg/mL), **AdV1** - AdV5 / 3-d24-ICOSL-CD40L (100 VP/mL), **AdV2** - AdV5 / 3-d24-WT (100 VP/mL), **Pseudovirus** - GeneCopoeia's Lentifect ™ SARS- CoV-2 Spike-pseudotyped lentivirus (100 VP/mL), **MIX1** - AdV1 + rRBD + pseudovirus (100 VP/mL+2.62 µg/mL+100 VP/mL), **MIX2** - AdV2 + rRBD + pseudovirus (100 VP/mL+2.62 µg/mL+100 VP/mL), **hCoV-OC43** - human coronavirus OC43 (100 VP/mL), **Pseudo+Ab** - pseudovirus + SARS-CoV-2 Spike Antibody '(GeneCopoeia; 100 VP/mL+2.62 µg/mL +2.62 µg/mL), **rRBD+Ab** (2.62 µg/mL +2.62 µg/mL).*

SUBPOPULATION OF LYMPHOCYTES	IMMUNOGENIC FACTORS												
	Untreated control	MOCK	rRBD	AdV1	AdV2	Pseudo-virus	MIX1	MIX2	hCoV-OC43	AdV1 +rRBD	AdV2 +rRBD	Pseudo +Ab	rRBD +Ab
CD19$^+$	9.70 ±0.46	9.67 ±0.42	9.57 ±0.31	9.43 ±0.06	11.93 ±0.31	9.23 ±0.15	9.33 ±0.06	12.10 ±0.10	9.43 ±0.06	9.70 ±0.10	7.15 ±1.06	12.60 ±0.22	12.33 ±0.29
CD38$^-$ CD24$^+$	84.93 ±1.10	82.33 ±0.45	81.87 ±1.45	82.30 ±0.96	94.60 ±0.30	82.47 ±0.93	82.43 ±0.50	95.03 ±0.38	82.30 ±0.96	82.00 ±0.44	94.60 ±0.14	84.13 ±0.82	83.80 ±0.08
TRANSITIONAL	0.27 ±0.06	0.93 ±0.06	1.27 ±0.15	1.00 ±0.35	0.03 ±0.06	1.10 ±0.10	1.20 ±0.10	0.03 ±0.06	1.00 ±0.35	1.33 ±0.06	0.05 ±0.07	0.17 ±0.05	0.20 ±0.08
CD38$^+$ CD24$^-$	0.03 ±0.06	0.17 ±0.06	0.17 ±0.06	0.17 ±0.06	0.00 ±0.00	0.20 ±0.00	0.13 ±0.06	0.00 ±0.00	0.17 ±0.06	0.17 ±0.06	0.00 ±0.00	0.00 ±0.00	0.07 ±0.05
CS	8.57 ±0.25	6.70 ±0.20	6.07 ±0.35	5.77 ±0.06	13.80 ±0.87	5.97 ±0.06	6.53 ±0.68	17.73 ±2.61	5.77 ±0.06	7.73 ±0.74	19.05 ±1.34	6.83 ±0.21	6.80 ±0.51
NCS	21.40 ±1.44	14.97 ±0.72	15.93 ±0.40	16.17 ±0.64	14.70 ±1.77	15.53 ±1.42	15.53 ±1.85	12.57 ±1.70	16.17 ±0.64	11.13 ±0.15	15.50 ±1.41	15.93 ±0.21	14.97 ±0.87
NAÏVE	50.33 ±0.15	54.83 ±0.55	54.50 ±1.05	54.83 ±1.10	49.10 ±1.85	55.00 ±0.82	54.13 ±0.23	45.17 ±2.25	54.83 ±1.10	54.97 ±1.16	38.20 ±0.85	56.33 ±0.54	57.20 ±0.86

Table 3A CD19$^+$ B cells subpopulation after treatment with immunogenic factors for 24 h.

*Note. **MOCK** - LPS-treated cells (1.25 µg/mL), **rRBD** – recombinant protein, receptor binding domain (2.62 µg/mL), **AdV1** – AdV5 / 3-d24 (100 VP/mL), **AdV2** - AdV5 / 3-d24-ICOSL-CD40L (100 VP/mL), **AdV2** - AdV5 / 3-d24-WT (100 VP/mL), **Pseudovirus** - GeneCopoeia's Lentifect ™ SARS- CoV-2 Spike-pseudotyped lentivirus (100 VP/mL), **MIX1** - AdV1 + rRBD + pseudovirus (100 VP/mL+2.62 µg/mL+100 VP/mL), **MIX2** - AdV2 + rRBD + pseudovirus (100 VP/mL+2.62 µg/mL+100 VP/mL), **hCoV-OC43** - human coronavirus OC43 (100 VP/mL), **Pseudo+Ab** - pseudovirus + SARS-CoV-2 Spike Antibody '(GeneCopoeia; 100 VP/mL+ 2.62 µg/mL), **rRBD+Ab** (2.62 µg/mL +2.62 µg/mL).*

SUBPOPULATION OF LYMPHOCYTES	IMMUNOGENIC FACTORS												
	Untreated control	MOCK	rRBD	AdV1	AdV2	Pseudo-virus	MIX1	MIX2	hCoV-OC43	AdV1 +rRBD	AdV2 +rRBD	Pseudo +Ab	rRBD +Ab
CD19+	9.70 ±0.46	9.67 ±0.42	9.57 ±0.31	9.43 ±0.06	11.93 ±0.31	9.23 ±0.15	9.33 ±0.06	12.10 ±0.10	9.43 ±0.06	9.70 ±0.10	7.15 ±1.06	12.60 ±0.22	12.33 ±0.29
CD38- CD24+	84.93 ±1.10	82.33 ±0.45	81.87 ±1.45	82.30 ±0.96	94.60 ±0.30	82.47 ±0.93	82.43 ±0.50	95.03 ±0.38	82.30 ±0.96	82.00 ±0.44	94.60 ±0.14	84.13 ±0.82	83.80 ±0.08
TRANSITIONAL	0.27 ±0.06	0.93 ±0.06	1.27 ±0.15	1.00 ±0.35	0.03 ±0.06	1.10 ±0.10	1.20 ±0.10	0.03 ±0.06	1.00 ±0.35	1.33 ±0.06	0.05 ±0.07	0.17 ±0.05	0.20 ±0.08
CD38+ CD24-	0.03 ±0.06	0.17 ±0.06	0.17 ±0.06	0.17 ±0.06	0.00 ±0.00	0.20 ±0.00	0.13 ±0.06	0.00 ±0.00	0.17 ±0.06	0.17 ±0.06	0.00 ±0.00	0.00 ±0.00	0.07 ±0.05
CS	8.57 ±0.25	6.70 ±0.20	6.07 ±0.35	5.77 ±0.06	13.80 ±0.87	5.97 ±0.06	6.53 ±0.68	17.73 ±2.61	5.77 ±0.06	7.73 ±0.74	19.05 ±1.34	6.83 ±0.21	6.80 ±0.51
NCS	21.40 ±1.44	14.97 ±0.72	15.93 ±0.40	16.17 ±0.64	14.70 ±1.77	15.53 ±1.42	15.53 ±1.85	12.57 ±1.70	16.17 ±0.64	11.13 ±0.15	15.50 ±1.41	15.93 ±0.21	14.97 ±0.87
NAÏVE	50.33 ±0.15	54.83 ±0.55	54.50 ±1.05	54.83 ±1.10	49.10 ±1.85	55.00 ±0.82	54.13 ±0.23	45.17 ±2.25	54.83 ±1.10	54.97 ±1.16	38.20 ±0.85	56.33 ±0.54	57.20 ±0.86

Table 4A CD19+ B cells subpopulation after treatment with immunogenic factors for 24 h.

Note. *MOCK* - LPS-treated cells (1.25 μg/mL), *rRBD* – recombinant protein, receptor binding domain (2.62 μg/mL), *AdV1* - AdV5 / 3-d24-ICOSL-CD40L (100 VP/mL), *AdV2* - AdV5 / 3-d24-WT (100 VP/mL), *Pseudovirus* - GeneCopoeia's Lentiject ™ SARS- CoV-2 Spike-pseudotyped lentivirus (100 VP/mL), *MIX1* - AdV1 + rRBD + pseudovirus (100 VP/mL+2.62 μg/mL+100 VP/mL), *MIX2* - AdV2 + rRBD + pseudovirus (100 VP/mL+2.62 μg/mL+100 VP/mL), *hCoV-OC43* - human coronavirus OC43 (100 VP/mL), *Pseudo+Ab* - pseudovirus + SARS-CoV-2 Spike Antibody '(GeneCopoeia; 100 VP/mL+2.62 μg/mL), *rRBD+Ab* (2.62 μg/mL +2.62 μg/mL).

CLASS & IMMUNO-GLOB.	IMMUNOGENIC FACTORS											
	MOCK	AdV1	AdV2	rRBD	Pseudovirus	AdV1+rRBD	AdV2+rRBD	AdV1+rRBD+pseudo	AdV2+rRBD+pseudo	rRBD+Ab	Pseudo+Ab	hCoV-OC43
CS IgM+	32.50 ±3,04	29,83 ±2,26	31,80 ±3,13	20,32 ±3,27	29,81 ±1,55	36,18 ±0,31	32,13 ±1,08	23,50 ±2,50	29,49 ±1,77	9,69 ±1,41	40,40 ±2,46	30,77 ±1,90
CS IgG+IgM+	0.10 ±0,14	0.55 ±0,31	0,23 ±0,16	7,39 ±0,34	0.11 ±0,16	0,20 ±0,14	0,29 ±0,25	5,01 ±2,00	2,24 ±0,54	6,16 ±0,53	0,08 ±0,12	0.50 ±0,13
CS IgG-IgM-	51,04 ±1,96	49,47 ±1,27	48,48 ±3,26	34,20 ±1,80	51,50 ±1,30	51,07 ±0,90	50,35 ±3,64	40,78 ±7,36	48,25 ±0,27	34,17 ±0,95	53,29 ±0,21	51,34 ±1,44
CS IgG+	16,37 ±1,32	20,15 ±2,65	19,49 ±1,87	38,09 ±1,74	18,59 ±2,71	12,55 ±0,82	17,23 ±2,78	30,71 ±7,83	20,02 ±1,72	49,99 ±2,88	6,23 ±2,38	17,39 ±0,48
NCS IgM+	56,76 ±1,47	57,84 ±2,22	57,64 ±1,05	14,99 ±2,36	56,99 ±4,08	51,75 ±1,60	49,70 ±1,36	29,29 ±10,02	38,25 ±1,70	7,76 ±0,83	66,17 ±1,90	57,76 ±4,08
NCS IgG+IgM+	7,49 ±0,31	6,80 ±0,42	7,05 ±1,32	27,26 ±2,17	6,78 ±0,68	7,12 ±0,43	7,03 ±0,93	19,99 ±8,70	8,55 ±1,52	29,47 ±0,22	4,14 ±0,64	6,58 ±0,25
NCS IgG-IgM-	31,92 ±1,68	31,05 ±1,50	31,39 ±0,71	24,28 ±2,76	32,02 ±2,69	35,39 ±1,36	37,13 ±0,88	31,75 ±6,79	44,01 ±3,62	10,98 ±0,91	27,40 ±1,90	32,39 ±2,54
NCS IgG+	3,83 ±0,38	4,31 ±0,55	3,92 ±0,50	33,47 ±3,15	4,21 ±0,73	5,74 ±0,13	6,14 ±1,17	19,31 ±8,37	9,19 ±0,81	51,80 ±1,96	1,80 ±0,74	3,27 ±1,30
NAÏVE IgM+	21,49 ±2,01	23,14 ±0,97	24,30 ±1,07	11,64 ±0,33	24,28 ±0,92	13,88 ±0,41	13,82 ±0,63	16,17 ±3,08	20,05 ±1,16	11,75 ±0,94	30,11 ±2,71	24,97 ±1,89
NAÏVE IgG+IgM+	6,18 ±0,98	6,36 ±1,70	7,43 ±0,56	11,22 ±0,76	6,44 ±0,44	6,51 ±0,05	6,51 ±0,71	7,92 ±2,54	4,11 ±0,25	19,62 ±0,21	3,85 ±0,72	7,48 ±0,73
NAÏVE IgG-IgM-	65,13 ±3,41	62,82 ±1,45	61,95 ±1,29	60,58 ±2,15	63,14 ±1,48	67,99 ±0,26	67,41 ±0,42	65,98 ±3,84	71,85 ±0,87	44,26 ±2,81	63,59 ±1,64	62,00 ±0,18
NAÏVE IgG+	7,20 ±0,74	6,67 ±0,50	6,31 ±0,38	16,55 ±1,64	6,14 ±0,34	11,62 ±0,25	12,26 ±0,73	9,93 ±4,42	3,98 ±0,69	24,38 ±3,95	2,44 ±0,46	5,56 ±1,43

Table 5A Percentage of different classes of CD38⁻CD24⁺ lymphocytes after 24 h treatment with various immunogenic factors.